# Role of Adult-Born Neurons in Hippocampal Representations of Space

by Maria Agustina Frechou Schandy

Candidate:

Maria Frechou

Signature

*Maria Agustina Frechou Schandy*

Thesis Advisor:

Signature

J. Tiago Gonçalves, PhD
Assistant Professor
Department of Neuroscience and Stem Cell Institute

Submitted in partial fulfillment of the requirements for the degree of Doctor of Philosophy in the Graduate Division of Medical Sciences

Albert Einstein College of Medicine
New York

July 7th, 2023

**Acknowledgements**

I would like to express my gratitude to Dr. Tiago Goncalves for the remarkable opportunity to join his research laboratory, where I had the privilege of engaging in some of the most captivating scientific pursuits of my career. Tiago not only provided me with the space to explore and cultivate my interests and skills, but also welcomed me into a new research environment and guided me through the initial phases of the laboratory.

I extend my heartfelt appreciation to Dr. Ruben Coen-Cagli, who joined the project as collaborator in 2020. Ruben provided invaluable training that enabled me to employ novel data manipulation techniques and participate in prestigious events such as COSYNE, an opportunity I had never envisioned for myself.

I am deeply indebted to my remarkable colleagues in the laboratory, both past and present. Beginning with Kelsey, I am immensely grateful for the privilege of sharing the journey of pursuing a Ph.D. with her, through the highs and lows. Kelsey's intelligence, determination, and genuine friendship have been instrumental in my progress, and for this, I affectionately thank her.

Jake, Sunaina, and Elizabeth are not just colleagues but also dear friends and exceptionally talented scientists. Their unwavering support and friendship have been a constant source of motivation. The fond memories of our delicious summer barbecues remain some of my most cherished experiences during my PhD.

I would also like to thank our neighboring laboratory colleagues, who consistently extended their assistance without hesitation whenever I required it. Their enthusiastic planning of lab outings, including activities such as axe throwing, karting, ATV riding, and more, added a wonderful dimension to our research journey.

I would also like to extend my heartfelt gratitude to my family and friends, both from the Einstein community and back home. Having friends here with whom I could relate and share my daily experiences has been invaluable. Additionally, the unwavering support of my friends and loved

ones back home, who celebrated my triumphs and offered solace during challenging times, has been a source of immense strength and encouragement.

Lastly, but certainly not least, I want to extend my deepest gratitude to my family. To my husband, Alfonso, I am immensely grateful. Without your unwavering support, I wouldn’t be where I am today. Thank you for not only ensuring the well-being of our family but also for being my source of strength and stability, the most incredible partner and father to our daughter that I could ever have dreamed of. To my beloved daughter, Emilia, I cherish every moment we share in this journey of life, watching you grow. Your personality and kindness never cease to amaze me, and I am profoundly grateful to have you as my daughter. To Lola, your unique contributions to this process are unforgettable. Your loud snores, and your demand to ride in the stroller on our walks while stealing the spotlight everywhere we go – you've brought nothing but joy to our lives. Your presence has been a source of happiness beyond measure.

**Table of Contents**

**List of Figures:**

**Abstract**

Adult neurogenesis is a unique form of neuronal plasticity in which newly generated neurons are integrated into the adult dentate gyrus in a process modulated by environmental stimuli. Adult-born neurons can contribute to spatial memory, but it is unknown how they contribute to neural representations of space in the hippocampus. Using *in vivo* two-photon calcium imaging we recorded neuronal activity from three different areas of the hippocampus while animals were head-fixed under the microscope on a treadmill. We found that mice that were previously housed in an enriched environment, which triggers an increase in neurogenesis, had increased spatial information content in the hippocampal dentate gyrus during novel context exposure. Ablating adult neurogenesis by prior focal irradiation of the hippocampus blocked the effect of enrichment and lowered spatial information content, as did the chemogenetic silencing of adult-born neurons. Both ablating neurogenesis and silencing adult-born neurons decreased the calcium activity rates of dentate gyrus neurons, resulting in a decreased amplitude of place-specific responses. These findings contrast previous studies that suggested a predominantly inhibitory action for adult-born neurons. Additionally, animals with prior exposure to an enriched environment exhibited an increase in spatial information content the CA1 region of the hippocampus in animals exposed to an enriched environment. Ablating adult neurogenesis by prior focal irradiation resulted in a decrease in spatial information content potentially driven by an overall increase in noise in the tuning curves of pyramidal cells. Although we observed no change in the amplitude of the place-specific responses in animals with prior exposure to enriched environment, we did find a decrease in the width of these responses. The increase in overall noise could indicate additional mechanisms at play such as direct inputs from the entorhinal cortex influencing the overall firing patterns of CA1. In irradiated animals with prior exposure to an enriched environment, mossy cells showed a decrease in spatial information content when compared to their non-irradiated counterparts. Spatial tuning was also reduced as observed by a reduction in both unimodal and

bimodal place-specific responses. Conversely, animals housed in regular cage conditions with prior exposure to focal irradiation exhibited an increase spatial information content and complexity of the place-specific responses. These results suggest the role of mossy cells in the formation of neuronal representations of space may be partially dependent on adult neurogenesis and plasticity mechanisms induced by environmental enrichment. Overall, we propose that adult neurogenesis improves neural representations of space by modulating the shape of the tuning curves and therefore improving the ability of dentate gyrus neurons to tune to spatial features resulting in increased spatial information content in the hippocampus. These findings contribute to our understanding of how adult neurogenesis positively influences spatial learning and memory by elucidating the mechanisms by which adult-born neurons facilitate the formation of neuronal representations of space in the hippocampus.

## Chapter 1 – Introduction

### Adult neurogenesis in mammals

The adult brain was long thought to be unable to generate new neurons until the seminal findings of Joseph Altman in 1962 (Altman, 1962). Using autoradiographic images of brain sections from rats injected intracranially with thymidine-H3, Altman and colleagues showed for the first time the presence of labelled neurons and neuroblasts in hippocampal dentate gyrus. This finding was later confirmed by numerous studies (Altman, 1963; Altman & Das, 1965; Bayer et al., 1982; Kaplan & Hinds, 1977; Nottebohm, 1981) and gave rise to a new subfield in neuroscience. The first studies in primates confirming the presence of adult neurogenesis were published in 1999 (Gould, Reeves, et al., 1999) and in humans in 1998 (Eriksson et al., 1998) forcing the field to question preexisting concepts of the mechanisms of learning and memory as well as many neuropsychiatric disorders.

### The role of adult neurogenesis in learning and memory

The dentate gyrus (DG) of the hippocampus is one of very few regions where adult neurogenesis has been shown to take place in the mammalian brain (Altman & Das, 1965). Adult-born neurons in this area are thought to contribute to the role of the hippocampus in mediating learning and memory (Clelland et al., 2009; Danielson et al., 2016; Sahay et al., 2011). Two major contributions helped establish a theory on the function of the hippocampus. In 1957, patient H.M. underwent bilateral surgical removal of the hippocampal formation and the surrounding medial temporal lobe area, in an effort to alleviate epileptic seizures. The results of this procedure left patient H.M. unable to form new memories, an inability to recognize hospital staff or find his way to the bathroom (Scoville & Milner, 1957). H.M.'s memory impairment was studied and reproduced in animal models which pointed to a critical role for the hippocampus in declarative memory (Cohen & Squire, 1980; Corkin, 2002; Milner et al., 1968; Mishkin, 1978; Squire, 1992). Still, the mechanisms by which the hippocampus played this role were not understood. The first finding

that led to a more mechanistic understanding of memory formation in the hippocampus was the discovery of place cells, cells that fire selectively at one or more locations in space (O'Keefe, 1976). These are thought to support the formation of spatial memories in the hippocampus (Robinson et al., 2020). Furthermore, it was also found that these place cells are part of a group of spatially modulated neurons which include grid cells (Hafting et al., 2005), border cells (Solstad et al., 2008) and head directions cells (Taube et al., 1990). Place cell firing lacked location topography, which led to researchers at the time to propose the hippocampal cognitive map hypothesis (O'Keefe & Nadel, 1979; Tolman, 1948), where place cells act collectively as a cognitive representation of a physical location in space.

Anatomically, the hippocampus is composed of several regions broadly interconnected via a well-studied trisynaptic circuit. Incoming axons from the entorhinal cortex (EC) form the medial and lateral perforant pathways and synapse onto the DG (Amaral et al., 2007). Granule cells in the DG project to CA3 via their axons (known as mossy fibers) and CA3 pyramidal cells project via the Schaffer collaterals to CA1 (Amaral et al., 2007). Finally, CA1 projects back to EC (Amaral et al., 2007). CA1 neurons are critically involved in the formation, consolidation, and retrieval of hippocampus-dependent memories (Bartsch et al., 2011). They can also provide precise representations of specific locations in an environment and can code associations between objects and locations (Komorowski et al., 2009; Moser et al., 2015).

Other important neurons in hippocampal circuits are inhibitory interneurons that release GABA and play role in regulating cell excitability in the circuit by dictating the temporal window for synaptic excitation and shaping the afferent and efferent information flow (Pelkey et al., 2017). Mossy Cells are a major group of excitatory hilar neurons that are thought to regulate the activity of the dentate gyrus therefore contributing to processes of learning and memory (Jinde et al., 2012; Scharfman, 2016). They are unique in that they provide both longitudinal and commissural projections throughout the DG (Houser et al., 2021). Innervating both excitatory granule cells,

pyramidal neurons in CA3, and interneurons, exerting either excitatory or inhibitory influence on the DG (Scharfman, 1995; Wenzel et al., 1997). Still, much remains to be understood on the function of these cells and their contribution to the role of the DG. Overall, the hippocampal loop processes sensory information from specific cortical areas and returns this information back to EC (Amaral et al., 2007) (Fig 1).

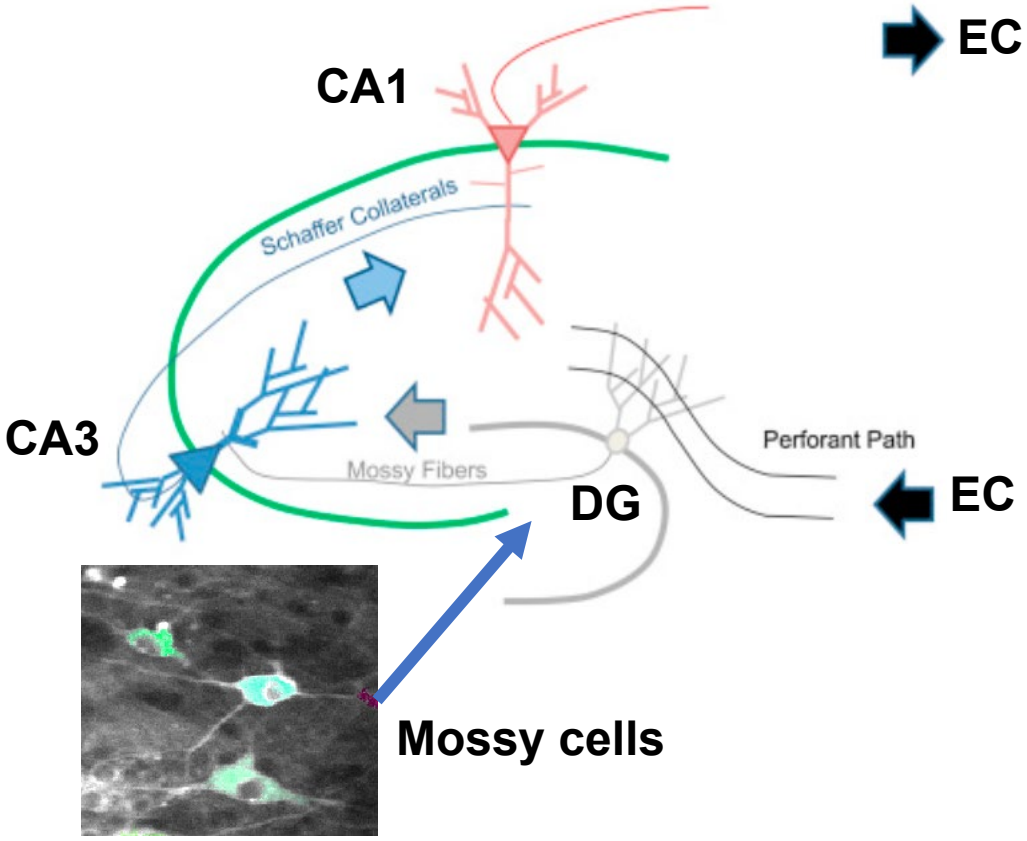


Figure 1. Diagram of hippocampal circuitry, adapted from Lopez-Rojas, et. al., 2016.

hippocampal circuit, while supporting a neurogenic niche that continuously introduces new neurons into this local network. So, the question remains, why is adult neurogenesis present in this region of the brain and what is its role in hippocampal function? Adult neurogenesis takes place in the subgranular zone (SGZ) of the hippocampal DG (Altman & Bayer, 1975; Altman & Das, 1965). This thin layer situated between the granule cell layer and the hilus provides the

appropriate microenvironment for neural stem cell (NSC) proliferation and differentiation into adult born neurons (Alvarez-Buylla & Lim, 2004; Ma et al., 2005). This process takes place through a series of steps that resemble embryonic neuronal development. Type 1 radial glia-like cells generate proliferating intermediate progenitor cells (IPCs, type 2 cells) with transient amplifying characteristics (Gonçalves et al., 2016). These IPCs differentiate into neuroblasts (type 3 cells) that then develop from immature neurons to mature DG granule cells (Gonçalves et al., 2016). Other cell types are present in this niche as well as a dense vascular network in association with NSCs (Gonçalves et al., 2016) (Fig. 2).

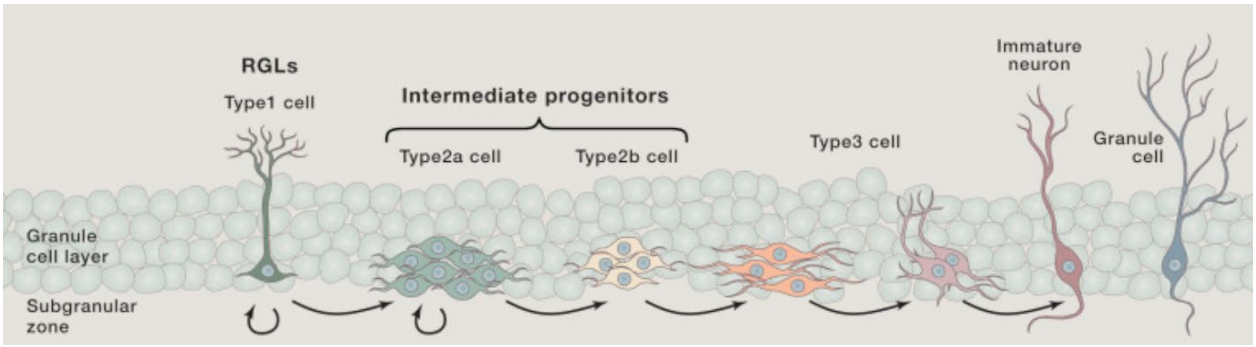


Figure 2. Adult neuronal development in the SGZ of the DG. Adapted from Goncalves, et. al., 2016.

To become functionally mature, adult-born neurons undergo developmental processes influenced by molecular networks, neuronal activity, and environmental factors (Toda et al., 2019). These factors provide adult-born neurons with unique and transient functional properties during their maturation period. The electrophysiological characteristics of adult-born neurons differ from those of mature neurons, including higher input resistance, lower threshold voltage, slower membrane time constant, and increased susceptibility to long-term potentiation (LTP) (Dieni et al., 2016; Ge et al., 2007; Marin-Burgin et al., 2012; Mu et al., 2011). As they mature, they become indistinguishable from mature DG cells (Espósito et al., 2005; Laplagne et al., 2006). Few argue when comparing mature adult born neurons to mature neurons born in infancy, the former present

larger presynaptic terminals, increased spine density and more putative efferent filopodial contacts onto inhibitory neurons suggesting potential unique functions of ABNs even after they matured (Cole et al., 2020). Between weeks two and three post-mitosis, gamma-aminobutyric acid (GABA) currents of adult-born neurons are excitatory, similarly to what occurs during development (Ge et al., 2006). GABA currents gradually become inhibitory as the Cl- transporter NKCC1 is replaced by KCC2, completing the switch by the 3rd week (Ge et al., 2006). The first synaptic inputs originating from inhibitory interneurons in the SGZ and hilus (Espósito et al., 2005; Ge et al., 2006), followed by glutamatergic mossy cells, are the first connections formed by adult-born neurons during the second week (Deshpande et al., 2013). Additionally, other inputs from the molecular layer, medial septum, nucleus of the diagonal band of Broca, entorhinal cortex, CA3, mature granule cells from DG and subiculum also appear during the second- and third-week post-mitosis (Vivar et al., 2012). The axons of adult-born neurons (mossy fibers), project to granule cell layer interneurons, as well as interneurons and mossy cells in the hilus and CA3. Glutamatergic projections to CA3 become functional at 17 days post-mitosis (Zhao, 2006). By the end of the first month, adult-born neurons are integrated into the hippocampal circuitry and possess unique electrophysiological properties (Dieni et al., 2016; Gu et al., 2012; Marin-Burgin et al., 2012). They exhibit increased excitability due to different excitation/inhibition balance (Marin-Burgin et al., 2012). Synaptic plasticity is enhanced due to reduced LTP induction thresholds and increased LTP amplitude, increased contribution of the NR2B-receptor subtype to NMDAR-mediated currents, and decreased feedforward inhibition (Ge et al., 2007; Li et al., 2013). These differences in excitability and plasticity in adult-born neurons last approximately between 4 to 6 weeks post mitosis, allowing these cells to respond to a wide range of input stimuli and rapidly strengthen active connections (Denny et al., 2012; Gu et al., 2012). This “critical period” is believed to play a crucial role in the function of adult-born neurons in the DG. As adult-born neurons continue to mature, they experience increased inhibitory control, leading to a narrower range of stimuli that can trigger their firing resulting in sparser activity, which is more characteristic

of mature dentate DG cells (Danielson et al., 2016; Marin-Burgin et al., 2012). Still, much is still unknown about the mechanisms by which these cells influence DG and hippocampal function during this transient period of unusual activity and plasticity. One of the ways in which the field investigates adult-born neuron function is by leveraging the influence of behavioral experiences on the connectivity profile of these neurons (Bergami et al., 2015). Exercise and exposure to an enriched environment during weeks 2-6 post-mitosis resulted in an increase in inputs from interneurons in CA3 and CA1, mammillary body, hippocampus, subiculum, and cortex (Bergami et al., 2015). These connections are otherwise rare in mice housed in regular cage conditions (Bergami et al., 2015). Both approaches result in an increase in the number of adult-born neurons (Bergami et al., 2015). Taken all together, it is important to understand how adult-born neurons influence the preexisting mature circuits of the DG and other areas of the hippocampus while transiently undergoing their developmental critical period. How this critical period is dependent on environmental stimuli is poorly understood and therefore important to identifying the impact of adult-born neurons in hippocampal circuit activity.

Numerous evidence shows that adult neurogenesis in the dentate gyrus of the hippocampus plays a role in learning and memory (Barnea & Nottebohm, 1994; Dupret et al., 2008; Gould et al., 1999; Sahay et al., 2011; Shors et al., 2001). Mice trained in associative learning tasks that require the hippocampus, such as spatial navigation learning in a Morris water maze, had a 2-fold increase in neurogenesis (Gould et al., 1999). Mice that were trained in a non-hippocampal dependent task such as cue training in a Morris water maze, did not present a significant increase in neurogenesis, suggesting an involvement of adult-born neurons in associative memory formation (Gould et al., 1999). Increasing the number of adult born neurons results in improved ability of animals to distinguish between similar context when exposed to a contextual fear conditioning paradigm (Sahay et al., 2011). Reducing the number of adult-born neurons resulted in an impairment in a trace conditioning paradigm in mice, but not in delay conditioning, which is a non-

hippocampal dependent task (Shors et al., 2001). These results suggest adult born neurons are necessary for the formation of trace memories associating stimuli that are separated in time (Shors et al., 2001). Ablating adult neurogenesis also resulted in a decrease in the ability of mice to learn the location of the platform in a Morris water maze task (Dupret et al., 2008). These results suggest adult neurogenesis is important for spatial relational memory, which supports a capacity for flexible, inferential memory expression (Dupret et al., 2008). These behavioral experiments established the relevance of adult neurogenesis in hippocampal dependent behaviors. The mechanisms underlying the relationship between adult neurogenesis and these functional dependencies are still mostly unexplored.

The unique properties of the Dentate Gyrus include strong inhibitory inputs that lead to sparse network activity (Coulter & Carlson, 2007; de Almeida et al., 2009; Rennó-Costa et al., 2010; Yu et al., 2013). Of the canonical tri-synaptic circuit of the hippocampus, the DG represents a "bottleneck" of processing information, receiving few projections from the entorhinal cortex and projecting even fewer projections to CA3 (Rolls & Treves, 1999; Treves & Rolls, 1994). Given the unique properties of DG, studies have proposed pattern separation as the potential mechanism by which the DG supports the encoding of both episodic and spatial memories (Yassa & Stark, 2011). Pattern separation is the process of transforming similar inputs of neuronal activity into non-overlapping output patterns, in this case non-overlapping memory traces, and it is thought to occur in the DG during memory formation (Marr, 1971). The perceptual process of pattern separation allows for the distinction of similar experiences or contexts, and studies have explored the potential role of adult neurogenesis in supporting this process (Sahay et al., 2011). Ablating adult neurogenesis in the hippocampus using gamma-ray irradiation or methylazoxymethanol acetate, resulted in the inhibition of the formation of contextual fear memory (Ko et al., 2009). Impaired neurogenesis also resulted in decreased spatial discrimination between contexts presented with little spatial separation, but not when stimuli where more separated in space

(Clelland et al., 2009) as well as the inability of mice to discriminate between two similar contexts after extensive training (Tronel et al., 2012). On the contrary, increasing the number of adult-born neurons by exposure to an enriched environment, resulted in an increase in the ability of mice to distinguish between similar contexts. Using a transgenic model to increase adult neurogenesis in the DG resulted in improved performance of mice in a contextual discrimination task (Sahay et al., 2011). Using a transgenic approach to silence granule cells in the DG showed enhanced or normal ability to distinguish between similar context when old GC were silenced but not young GCs. Suggesting that adult-born neurons are required for contextual pattern separation (Nakashiba et al., 2012).

A role for adult neurogenesis in the promotion of cognitive flexibility -the ability of an animal to change its behavior when the reward conditions change- has also been proposed (Anacker & Hen, 2017, p. 20; Garthe et al., 2009). An increase in the number of adult-born neurons using a transgenic approach resulted in an improvement in both memory precision and flexibility during a spatial navigation task (Berdugo-Vega et al., 2021). Separate genetic and focal X-irradiation approaches to ablate adult neurogenesis in the Dentate Gyrus showed that mice have a decreased ability to change a learned response to a stimulus-evoked memory (Burghardt et al., 2012). Adult-born neurons have also been proposed to have a role in the reduction of memory interference -between related or overlapping experiences (Appleby et al., 2011; Wiskott et al., 2006) in support of pattern separation (Miller & Sahay, 2019). A computational simulation study proposed that adult-born neurons improve recall by minimizing interference between similar items (Becker, 2005). Electrophysiological recordings in vivo revealed the existence of a neural code that is capable of separating events in time with the contribution of adult neurogenesis (Rangel et al., 2014). In another take on cognitive flexibility, some studies point out the importance of clearing memory systems of older information to allow for the input of new information and, potentially to distinguish older from newer events (Kempermann, 2008; Wiskott et al., 2006). There is some

evidence that adult neurogenesis may contribute to this process (Akers et al., 2014; Scott et al., 2021) and that an increase in adult-born neurons results in neurogenesis-mediated form of "forgetting" to facilitate new learning and reversal learning (Tran et al., 2019). Manipulating adult born neurons through exposure to experiences such as an enriched environment or exercise results in structural modifications of their dendritic arbors and connectivity as well as changes in the developmental timeline and integration into the mature preexisting circuits of the DG. (Bergami et al., 2015; Gonçalves et al., 2016; Piatti et al., 2011; Zhao, 2006). These findings suggest that experience could have an important impact on the contribution of adult-born neurons to memory formation.

Overall, these findings suggest adult-born neurons have a role in various mechanisms of memory processing and could selectively facilitate each of these different putative mechanisms, possibly by adopting different transcriptional programs, which is supported by reports of within-cell-type heterogeneity of the mature granule cells in the DG (Erwin et al., 2020). In addition, manipulating the number of adult-born neurons using both physiological, pathological, chemical, and genetic approaches result in effects on age related decline, stress, depression, and cognitive deficits when adult neurogenesis is decreased (Hollands et al., 2017; Planchez et al., 2021). When adult neurogenesis is increased findings show cognitive improvements, proposing this unique cell group as functionally relevant and a promising therapeutic target (Sahay et al., 2011).

Mechanisms of adult neurogenesis in the DG

Adult neurogenesis is a form of robust plasticity implicated in brain homeostasis and disease. Decreased number of adult-born neurons has been linked to various forms of disease such as depression (Sahay & Hen, 2007), stress (Snyder et al., 2011) and Alzheimer's disease (Babcock et al., 2021). Conversely, increasing the number of adult-born neurons results in improved cognition (Kempermann et al., 1997). Understanding the circuit mechanism by which adult

neurogenesis contributes to the function of the DG is crucial to uncover hippocampal dependent cognitive processes, pathophysiological brain states and potential therapeutics.

Adult-born neurons have been shown to have a role in cognitive processes related to learning, memory, such as behavioral pattern separation and cognitive flexibility. During their developmental critical period, they have been shown to provide a robust form of plasticity to hippocampal circuits. For example, several studies have shown that behavioral pattern separation is dependent on adult neurogenesis in hippocampal dependent memory tasks (Clelland et al., 2009; Clemenson et al., 2015; Nakashiba et al., 2012; Sahay et al., 2011). Yet, due to the sparsity of the DG network and the high neuronal density (Jung & McNaughton, 1993; Kempermann et al., 1997), the search for circuit mechanisms underlying behavioral outputs has been hindered by the inability to record from DG neurons during behavior. New techniques have been developed recently to overcome this.

Ex vivo electrophysiology and immediate early gene studies suggested adult-born neurons reduce excitability and increase sparsity of responses which could have beneficial effects on memory (Stone et al., 2011). Electrophysiological studies showed that long term potentiation can be induced more easily in adult-born neurons compared to mature neurons (Ge et al., 2007; Schmidt-Hieber et al., 2004). In addition, T-type Ca2+ channels generate Ca2+ spikes that increase fast Na+ action potentials, contributing to the induction of synaptic plasticity (Schmidt-Hieber et al., 2004). Long term potentiation and enhanced synaptic plasticity is dependent on NR2B-containing NMDA receptors (Ge et al., 2007). Calcium imaging and electrophysiological manipulations in acute slices revealed that weak afferent activity recruits a large proportion of adult-born neurons given their low input specificity, that then switches over time to highly specific responses with maturation (Marin-Burgin et al., 2012). Retroviral labeling of connectivity in mice with increased neurogenesis showed more adult-born neurons with excitatory synapse contacts onto hilar interneurons, which could serve as a potential mechanism by which adult-born neurons

modulate DG excitability (Ikrar et al., 2013). However, other studies propose that even though adult born neurons form synapses with interneurons at their critical period, they are less coupled than the connections formed directly between interneurons and mature granule cells (Temprana et al., 2015).

Modern electrophysiological methods have led to some of the most important breakthroughs in our understanding of brain function (Hubel & Wiesel, 1959; O'Keefe & Dostrovsky, 1971; Schwiening, 2012). Electrophysiological techniques provide high temporal resolution and precise information about the timing and dynamics of neuronal activity. However, these techniques are challenging when recording in vivo and during behavior. It's an invasive technique due to the insertion of electrodes, it is difficult to scale, and it is prone to movement related artifacts (Papaioannou & Medini, 2022). Other techniques can be used to indirectly study neuronal activity such as Immediate early genes, which provide a measure for gene expression, specific information about gene dynamics and have the potential for cell type specificity (Guzowski et al., 1999). Still, this technique fails to capture the dynamic nature of neuronal encoding. Optical imaging techniques such as 2-photon calcium imaging are being used in addition to the other techniques mentioned to record the activity of hippocampal neurons, including adult-born neurons, in vivo (Danielson et al., 2016; McHugh et al., 2022). This technique allows for the simultaneous recording of thousands of individual cells in awake behaving mice, including up to 1 million cells using light beads microscopy and calcium imaging in the mouse brain (Demas et al., 2021). This is a scalable system that allows for real time analysis of neuronal activity, increased imaging depth to reach deep regions of the hippocampus such as DG and less invasive at the region of interest (Andermann et al., 2013). It is worth noting that some of the disadvantages of using this methodology include lower temporal resolution compared to electrophysiological recordings because of the dependency to the dynamics of calcium itself and the calcium indicator utilized. The reliability on exogenous constructs such as AAV for the delivery of the calcium

encoders can have pathological consequences (Johnston et al., 2021; Papaioannou & Medini, 2022). Still, using in vivo calcium imaging and 2-photon microscopy is a reliable way to measure neuronal activity in the hippocampus maintaining this region intact by minimal invasiveness, depth of reach including DG and acquire data from a large number of cells. Using this approach a few studies managed to label, record from, and manipulate adult-born neurons in vivo. Long-term 2-photon imaging, combined with genetic labeling of neuronal stem/progenitor cells (NSPCs), is one of the strategies employed in mice. These mice express a Tamoxifen-regulable Cre recombinase under the control of the endogenous Achaete-scute homolog 1 (Ascl-1) promoter (Yang et al., 2015b). They are then crossed with a tdTomato reporter mouse line. This novel approach provided a new way to label adult-born neurons and study their long-term activity and morphology in vivo. The Ascl1 CreERT2 system allows the for the selective-age tagging of adult-born neurons, yet it is worth noting that a portion of the Ascl1+ cells in the subventricular zone of the Dentate Gyrus are Type-1 adult neural stem cells and they continue to produce neurons for approximately 1 month, mostly produced initially and then slowly tapering off (Pilz et al., 2018). An opto-tagging approach was also developed to study adult born neurons in vivo. Using either a retrovirus approach or a transgenic (Nestin-CreERT2) mouse line, the light-driven excitatory cation-channel Channelrhodopsin-2 (ChR2) (ChR2-eYFP) was expressed conditionally in adult-born neurons. This method resulted in low numbers of opto-tagged adult-born neurons (McHugh et al., 2022). It is worth mentioning that the Nestin-CreERT2 reporter strains label a wide range of adult-born neurons at different post-mitotic ages. Depending on the Nestin-CreERT2 line, they can either induce substantial expression of the reporter in other areas of the brain, which shows potential off target effects of this approach, or elicited inefficient labelling (Sun, 2014). Although a lot of progress has been made to develop techniques to label adult-born neurons mentioned, it is important to recognize their caveats, such as off target labelling. It is therefore still challenging to successfully label adult-born neurons.

The first functional *in vivo* characterization of mature granule cells and adult-born neurons in the DG (Danielson et al., 2016) revealed adult-born neurons have a higher firing rate and less spatial tuning when compared to mature granule cells. The same study found that mature granule cells undergo robust remapping of their spatial representations while adult-born neurons do not. Optogenetic silencing of adult-born neurons showed a direct involvement of adult-born neurons in context encoding and discrimination, consistent with their proposed role in pattern separation (Danielson et al., 2016; McHugh et al., 2022). Morphological in vivo characterization of adult born neurons using longitudinal in vivo 2 photon imaging showed initial over branching and later pruning of developing dendrites in adult-born neurons. Exposure to an enriched environment led to accelerated growth during branching, yet counteracted by more extensive pruning, suggesting a homeostatic control of dendritic morphology (Gonçalves et al., 2016). Overall, findings suggest adult-born neurons have a role in pattern separation and contribute to population sparsity, which helps support hippocampal function. It was also shown that environment plays a role in adult-born neuron development. Still, it is unknown how adult-born neurons contribute to spatial memory, and whether they alter neuronal representations of space in the hippocampus.

Effects of enriched environment and exercise on adult neurogenesis and the brain

The use of an enriched environment and exercise as manipulations to increase the number of adult-born neurons in the DG is widely used in the field (Bergami et al., 2015; Kempermann et al., 1997; Nilsson et al., 1999; Schloesser et al., 2010). It has been shown that exposure to an enriched environment and exercise increases both the survival and proliferation of adult born neurons (Liu & Nusslock, 2018; Nilsson et al., 1999; Olson et al., 2006). One of the strongest candidates mediating the effects of exercise in neurogenesis is the brain-derived neurotrophic factor (BDNF) signaling (Liu & Nusslock, 2018). BDNF is a growth factor widely expressed in the brain, a neurotrophin belonging to the family of polypepdide growth factors, which regulates proliferation and maturation of adult-born neurons in the DG (Vilar & Mira, 2016). BDNF

synthesizes primarily during exercise and functions by binding to tropomyosin receptor kinase B (TrkB), expressed in hippocampal neurons (Reichardt, 2006). The complex is internalized and functions as docking site for a variety of signaling cascades (Huang & Reichardt, 2003; Nykjaer et al., 2005; Yoshii & Constantine-Paton, 2010). Mice with voluntary access to a running wheel showed an increase in BDNF mRNA only after a few days of exercise (Neeper et al., 1995). Blocking TrkB resulted in a decrease in the benefits of exercise (Neeper et al., 1995). BDNF has also been shown to be required for the enhancement of hippocampal neurogenesis and the beneficial effect of enriched environment (Rossi et al., 2006). Bone morphogenic protein (BMP) signaling regulates cell proliferation and fate commitment in neurogenic niches in the brain during development (Gross et al., 1996). Inhibiting BMP signaling increases neurogenesis as it reduced the astroglial inductive effect in progenitor cells during differentiation and improves performance in a Y-maze spatial working memory task (Gobeske et al., 2009). Activation of BMP signaling results in a decrease in neurogenesis and these effects cannot be rescued by environmental stimuli (Gobeske et al., 2009). Recently, fibroblast growth factor (FGF) signaling pathway has been shown to mediate the effect of EE by inducing stem cell proliferation to increase hippocampal neurogenesis (Grońska-Pęski et al., 2021). In addition to the signaling pathways mentioned, it is important to consider that both EE and exercise have many other adult brain wide effects by which they could be mediating improvements in cognitive function regardless of their effects in neurogenesis. Some of the effects include increases in weight of the visual and somatosensory cortex (Diamond et al., 1964) and changes in auditory cortex (Engineer et al., 2004). At the dendritic level increased branching and increased number of dendritic spines (Diamond, 2001; Rosenzweig & Bennett, 1969). Alterations in glial cells (Hawrylak & Greenough, 1995) and in the number of blood capillaries in the brain as well as an increase in metabolic activity (Kolb & Whishaw, 1998). Given the wide range of effects environmental stimuli has in the brain, it is important to understand the specific mechanisms mediating the effects of environmental stimuli that lead to adult neurogenesis dependent improvements in cognition.

Functional characteristics of adult-born neurons in the hippocampus

The hippocampus plays an essential role in episodic and spatial memory (Morris et al., 1982; Scoville & Milner, 1957) by forming a 'cognitive map'—a neural representation of space to which objects and events can be bound. DG neurons achieve this in part by functioning as 'place cells', firing selectively to a single location in space (O'Keefe & Dostrovsky, 1971; O'Keefe & Nadel, 1979). But even neurons that are not selectively tuned to a single place can contribute to the spatial information encoded in neural populations, and neuronal activity recordings from large populations can be used to decode the position of an animal within an environment (Skaggs et al., 1993; Stefanini et al., 2020), with the decoding accuracy reflecting the spatial information content. This spatial code is essential for spatial memory, as was recently demonstrated (Robinson et al., 2020). Since ABNs contribute to spatial memory, one might expect that these cells would be sparsely active and finely tuned to a specific place. However, immature ABNs are highly excitable (Gu et al., 2012; Marin-Burgin et al., 2012; Schmidt-Hieber et al., 2004) and less spatially tuned than their mature granule cell counterparts (Danielson et al., 2016). Current models of DG function propose that ABNs contribute to memory function through the activation of local interneurons, resulting in a net increase in inhibition (Anacker et al., 2018; Drew et al., 2016; Ikrar et al., 2013; Lacefield et al., 2012). Yet it is unclear how this would affect neural representations of space in a novel environment, and how the net increase in inhibition would affect the DG and other areas of the hippocampus.

Effects of adult neurogenesis in CA1 and Mossy Cells

CA1 is a major output region of the hippocampus. CA1 pyramidal neurons play a crucial role in learning, memory formation and spatial navigation (Silva, Paylor, et al., 1992; Silva, Stevens, et al., 1992; Tsien et al., 1996). The first *in vivo* calcium imaging experiments in the hippocampus were done in CA1 (Dombeck et al., 2010) where mice were placed in virtual reality environments head-fixed to a modified 2-photon microscope. This setup allowed for the imaging of neuronal

activity paired with behavior experiments to study spatial information encoding in the CA1, thought to be involved in the encoding of episodic memories. Results demonstrated successful optical identification of place cells, their place fields in the virtual environment and their anatomical location in the tissue showing the role of CA1 in spatial navigation (Dombeck et al., 2010). Further functional characterization of CA1 revealed specific patterns of activity that are essential for memory encoding and retrieval (Ramirez et al., 2013). Some studies investigated the potential role of adult-neurogenesis in CA1 activity (McHugh et al., 2022; Rechavi et al., 2022). Optogenetically silencing adult-born neurons resulted in sparser hippocampal population activity in CA1 (McHugh et al., 2022). A study using miniature fluorescence microscopes (miniscopes) showed that exposure to exercise, known to increase the number of adult-born neurons in the DG, resulted in accelerated emergence of a stable spatial code in novel environments and increased code stability in CA1 across weeks (Rechavi et al., 2022). In addition, spatial codes were also more dynamic. When training a spatial decoder, its performance was better in runner mice compared to sedentary, suggesting more informative representations of space in mice with increase adult neurogenesis (Rechavi et al., 2022). Overall, these studies indicate that adult-born neurons indirectly influence CA1 activity and information encoding. In this study we sought to further investigate the role of adult-born neurons in CA1 and the potential circuit level mechanisms underlying these effects.

Another area of interest that is usually overlooked when establishing theories on the function of the DG is the hilus. This region contains another major glutamatergic principal cell, the Mossy Cell (Amaral et al., 2007; Scharfman, 2016). These cells receive major excitatory inputs from granule cells and provide both excitatory monosynaptic feedback and disynaptic inputs to granule cells (Scharfman, 1995, 2016). It has been shown these cells contribute to pattern separation in the DG (Jinde et al., 2012; Scharfman, 2016). Functional characterization of Mossy Cells *in vivo* revealed that these cells are significantly more active than dentate granule cells, they exhibit

spatial tuning during head-fixed spatial navigation and undergo robust remapping of their spatial representations in response to contextual manipulation (Danielson et al., 2017, p. 201). These results showed the active participation of Mossy Cells in the spatial coding. Therefore, follow up questions on the mechanisms behind this participation and potential role of adult-neurogenesis in the function of Mossy Cells are necessary to be addressed.

Is adult neurogenesis relevant to humans?

Adult hippocampal neurogenesis is a unique phenomenon that that occurs in many animals including in the mammalian brain, where new neurons are added throughout adulthood (Altman, 1962; Altman & Das, 1965). The presence of neurogenesis in humans was first demonstrated, (Eriksson et al., 1998) and later supported (Boldrini et al., 2018; Knoth et al., 2010; Spalding et al., 2005), by several studies. Conversely, other studies have questioned whether this process occurs in humans (Cipriani et al., 2018; Sorrells et al., 2018). Given the technical challenges that it imposes, this question remains highly discussed in the field.

Recent findings showed that the presence of immature neurons in the Dentate Gyrus region of the hippocampus can be observed well into the late stages of life if the experiments are performed in tightly controlled conditions and best-practices for tissue processing are utilized (Moreno-Jiménez et al., 2019). In addition, a decline in new neuron numbers with the progression of Alzheimer's disease was also observed in humans (Moreno-Jiménez et al., 2019). Studies using single-nucleus RNA-sequencing (snRNA-seq) identified newborn neurons in the human hippocampus of infant, child, adolescent, and adult aging stages (Y. Zhou et al., 2022). To identify newborn neurons, they used a supervised machine learning approach previously validated in a mouse model. They first trained the model in a human infant hippocampal dataset and then applied the model to all aging stages where newborn neurons were observed. They then repeated this analysis in other datasets previously published (Franjic et al., 2022), and identified newborn neurons were previously none have been found when applying standard methods in the field (Y.

Zhou et al., 2022). Overall, new techniques seem to further support the presence of newborn neurons across all developmental stages of the human brain. Further understanding of the function of these cells in the hippocampus will pose them as promising targets for therapeutic strategies.

Quantifying human adult neurogenesis

To determine whether neurogenesis in humans is of functional relevance, performing quantitative estimates across human developmental stages is important. Several studies quantified the number of cells containing neuroblast markers such as doublecortin (DCX) and polysialylated neuronal cell adhesion molecule (PSA-NCAM) in the human postmortem brain (Göritz & Frisén, 2012; Knoth et al., 2010; Sanai et al., 2011; Wang et al., 2011). Findings show neuroblasts numbers are highest during the perinatal period, then drop dramatically during the first postnatal months, and more slowly throughout life. Yet, this type of analysis is limited given that it is unclear if the cells containing neuroblast markers will differentiate and integrate to become functional mature neurons. One study made use of the aboveground nuclear tests conducted during the cold war, resulting in the increase in $^{14}C$ in the atmosphere (Spalding et al., 2013). $^{14}C$ integrates into the genomic DNA of cells during division (Spalding et al., 2013). Analyzing the amount of $^{14}C$ in cells and comparing it to the amount in the atmosphere, researchers were able to birth date cells in the human brain retrospectively. They found that 700 new neurons are added in each hippocampus each day with a modest decline during aging (Spalding et al., 2013).

The main factor limiting the quantification of adult-born neurons in humans is the difficulty of using labeling strategies currently used in other animals such as administering labeled nucleotides or genetic labeling with retroviruses or transgenic strategies. These strategies involve the administration of a marker in cells for later assessment postmortem. These markers are difficult to use in humans due to the risk of introducing DNA mutations or potential forms of toxicity

(Bergmann et al., 2015). In addition, analysis would have to occur after the research subject dies, therefore explaining the lack of studies in this area.

Neurogenesis is associated with improved memory performance in humans.

Regardless of the technical challenges to quantify adult neurogenesis in humas, many studies have shown a potential positive correlation between neurogenesis and memory performance. One study looked at whether morphological changes could be detected in the human brain after extensive experience in spatial navigation (Maguire et al., 2000). They analyzed the hippocampal structures of London taxi drivers and found they had larger hippocampi compared to control subjects. They also found a positive correlation between the posterior hippocampal volume and the amount of time spent as a taxi driver (Maguire et al., 2000). The understanding of the London map, and how routes and places relate to each other is increased in London taxi drivers compared to control subjects, suggesting that the posterior hippocampus plays a role in encoding this map (Maguire et al., 2000). This result suggests that the human brain is capable of local and robust plastic changes in response to environmental demands.

The role of the hippocampus in learning and memory in humans has been previously reported (Scoville & Milner, 1957; Squire, 1982). The mechanism by which adult neurogenesis contributes to hippocampal function has also been reported in mice and other animals (Aimone et al., 2009; Christian et al., 2014; Frankland et al., 2013; Kempermann, 2008). Environmental enrichment (EE) is known to influence hippocampal function in rodents, leading to an increase in the number of newborn neurons and subsequent improvement in spatial memory performance (Birch et al., 2013; Clemenson et al., 2015; Fabel, 2009; Freund et al., 2015; Kempermann et al., 1997; Olson et al., 2006; van Praag, Christie, et al., 1999; Z. Zhao et al., 2014). Studies have also shown that virtual environments serve as sources of enrichment in both humans and rodents (Harvey et al., 2009; Woollett et al., 2009). In humans, studies have shown that exposure to virtual environments in the form of video games that allow the exploration and virtual navigation of 3D spaces results

in an increase in recognition memory tasks, improved mnemonic discrimination ability and on a virtual water maze task (Clemenson et al., 2015). Another study has found that similar exposure results in an increase in the right hippocampal formation, an area of the brain important for spatial navigation (Kühn & Gallinat, 2014). Exercise is known to improve cognitive function and decrease the risk for age-related cognitive decline in rodents (van Praag, Christie, et al., 1999; van Praag, Kempermann, et al., 1999). Exposing human subjects to different forms of aerobic exercise resulted in an increase in the speed of vocabulary learning and an increase in BDNF and catecholamine levels which also correlated with faster learning and better retention (Winter et al., 2007). In rodents, the release of BDNF is increased in rats exposed to exercise (Neeper et al., 1996). In addition, BDNF is required for the increase in adult neurogenesis (Chan et al., 2008) mediated by enrichment (including exercise) (Rossi et al., 2006). Exercise also resulted in an increase in cerebral blood volume (CBV) as measured by MRI in the dentate gyrus of the human hippocampus and an improvement in cognitive function (Pereira et al., 2007). Increased CBV in the dentate gyrus of mice correlated with an increase in adult neurogenesis was observed (Pereira et al., 2007).

Summary

In summary, progress on the study of adult neurogenesis in humans has provided evidence for the role of neurogenesis in cognitive function. The positive effects of environmental enrichment on hippocampal function have long been thought to be mediated by adult neurogenesis, since enrichment leads to a strong increase in the number of adult-born neurons. Our study addresses the link between enrichment, adult neurogenesis, and circuit activity in the hippocampus. We first asked whether ABNs contribute to neural representations of space in the hippocampus. Using in vivo two-photon calcium imaging we recorded neuronal activity from three different areas of the hippocampus while animals were head-fixed under the microscope on a treadmill. We found that mice that were previously housed in an enriched environment, which triggers an increase in

neurogenesis, had increased spatial information content in the DG during novel context exposure. Ablating adult neurogenesis by prior focal irradiation of the hippocampus blocked the effect of enrichment and lowered spatial information content, as did the chemogenetic silencing of adult-born neurons. Both ablating neurogenesis and silencing adult-born neurons decreased the calcium activity rates of DG granule cells, resulting in a decreased amplitude of place-specific responses. These findings contrast with previous studies that suggested a predominantly inhibitory action of adult-born neurons. In CA1, animals with prior exposure to an enriched environment exhibited an increase in spatial information content. Ablating adult neurogenesis by prior focal irradiation resulted in a decrease in spatial information content potentially driven by an overall increase in noise in the tuning curves of pyramidal cells. We observed no change in the amplitude of place-specific responses in animals with prior exposure to enriched environment. We did find a decrease in the width of these responses, which suggests increased precision in activity at the tuned locations. The increase in overall noise could indicate additional mechanisms at play in CA1, such as direct inputs from the entorhinal cortex influencing the overall firing patterns of pyramidal cells. In mossy cells, irradiated animals with prior exposure to an enriched environment showed a decrease in spatial information content when compared to their non-irradiated counterparts. Spatial tuning was also reduced as observed by a reduction in both unimodal and bimodal place-specific responses. Conversely, animals housed in regular cage conditions with prior exposure to focal irradiation exhibited an increase in spatial information content and in the complexity of place-specific responses. These results suggest the role of mossy cells in the spatial information encoding may be partially dependent on adult neurogenesis and plasticity mechanisms induced by environmental enrichment. Overall, we propose that adult neurogenesis improves neural representations of space by modulating the shape of the tuning curves and therefore improving the ability of dentate gyrus neurons to tune to spatial features resulting in increased spatial information content in the hippocampus. These findings contribute to our understanding of how adult neurogenesis positively influences spatial learning and memory

by elucidating the mechanisms by which adult-born neurons facilitate the formation of neuronal representations of space in the hippocampus.

## Chapter 2 – Methods

### Animals

We used male and female C57BL6/J (Jackson Labs Stock #664) or, for chemogenetic silencing experiments, the offspring of hM4Di-Dreadd (Jackson Labs #26219) and Ascl1-Cre-ERT2 mice (Jackson Labs #12882). All mice were kept on a 12h light/dark cycle and had unrestricted access to chow and water. Animals were housed in groups of 3-5 and littermates were evenly distributed between experimental groups. Mice assigned to enriched environment (EE) housing were housed in groups of 5-10 in a large 121 × 61 cm enriched cage, containing a feeder, water dispenser, several running wheels, as well as plastic tubes, domes, and other structures. Mice assigned to EE experimental groups were housed in EE cages starting the day after the implantation surgery and for a period of 2 weeks, after which they were returned to RC conditions for the remainder of the experiment. Female and male mice were never mixed in the same cage, and all males were housed with littermates. Regular cage (RC) controls were housed in groups of up to 5 mice in standard mouse cages (dimensions 28 cm x 18 cm) containing a wire feeder and a water bottle. Experiments were carried out during the light phase of the cycle. All procedures were done in accordance with approval of the Institutional Animal Care and Use Committee (Protocol #: 00001197).

### Focal Irradiation

We permanently ablated adult neurogenesis in the dentate gyrus (DG) by bilateral focal irradiation of the hippocampus using opposed lateral fields (Fig. S2). We used 6 weeks old C57BL/6J mice (Jackson Labs #664). First, we traced the location of both hippocampi from a thin slice 9.4 T, T1 weighted MRI. Irradiation was performed using a small animal radiation device (SARRP, Xstrahl). To ensure a reproducible treatment setup, the mice were briefly anesthetized with isoflurane and immobilized using a custom fixation system prior to radiation delivery. Cone-beam computed

tomography was used to set up the irradiation fields and for calculating individual irradiation times, ensuring accurate and reproducible delivery of the intended irradiation. Hippocampal focusing irradiation was delivered using a 3 mm x 10 mm irradiation field positioned to cover the dorsal part of the brain, avoiding the olfactory bulb and subventricular zone (SVZ). A single dose of 10 Gy (at 2.5 Gy/min) was administered to trigger cell death within the hippocampus (Tomé et al., 2015). The administration of the single 10Gy dose was previously validated in mice (Tomé et al., 2015). With this approach irradiation was shown to limit neuronal damage exclusively to proliferating cells within the targeted area (Tomé et al., 2015). In addition, animals showed significant deficits in hippocampal dependent behaviors compared to sham-irradiated controls (Tomé et al., 2015). In addition, irradiated animals showed no impairment in non-hippocampal dependent behaviors (Tomé et al., 2015). Irradiated mice were allowed one month to recover prior to imaging.

Viral labeling and window implantation surgery

The right hemisphere dentate gyrus (DG) was labeled with an AAV vector that expressed the jRGECO1a genetically encoded calcium sensor (Dana et al., 2016) under the control of the CaMKIIα promoter (DJ serotype AAV-CaMKIIα.jRGECO1, University of North Carolina Vector Core, plasmid kindly donated by Dr. Fred Gage). 8-week-old mice were anesthetized with isoflurane (induction: 5%, maintenance: 2% in O2 vol/vol, via nose cone) and placed in a stereotaxic frame. The right DG was stereotactically targeted (Zhao et al., 2006) with a pulled-glass micropipette and 950nl of viral solution (5.4 ×1012 viral particles/mL) were injected with a microinjector (Drummond Nanoject III).

Mice also underwent surgery to implant an imaging ‘window’: a 3 mm craniotomy was drilled around the viral injection site and a custom-made titanium ring with a glass bottom was placed immediately above the dorsal surface of the hippocampus and anchored to the skull with dental cement (Mizrahi et al., 2004; Pilz et al., 2016). The alveus and all hippocampal structures were

left untouched during this procedure. A small titanium bar (9.5 × 3.1 × 1.3 mm) was also attached to the skull to attach the animal to the microscope stage. Mice were given carprofen (5 mg/kg) for inflammation and analgesic relief.

In vivo 2-photon calcium imaging

In vivo calcium imaging was performed 3-4 weeks after surgery, using a two-photon microscope (Thorlabs Bergamo) equipped with a 16x 0.8 NA objective (Nikon), using a Fidelity-2 1070 nm laser (Coherent) as a light source. The mice were head-fixed and placed on a treadmill belt. For optimum light transmission, the angle of the mouse's head was adjusted to ensure that the imaging window was perpendicular to the optical axis of the objective. Movies of calcium activity were acquired at 15 frames/s using an average laser power of ~120-180 mW, as measured in front of the objective.

Imaging Acquisition

We acquired 9 minutes of calcium activity recordings for each mouse, for each region of the hippocampus. The animals were imaged as they walked head-fixed on a previously described treadmill (Jordan et al., 2021) which was manually rotated at a speed of approximately 421±23 cm/min (Fig. S1B). The treadmill was comprised of a belt with 4 different textures each 45 cm length (velvet, smooth, 2.5 cm-diameter sandpaper disks of 100 and 60 grit) wrapped around two wheels of foam material. An optical rotary encoder was affixed to the axle of one of the wheels to gauge the belt's motion, thereby facilitating the calculation of the mouse's position along the belt. Four radio frequency identification (RFID) tags were placed on the belt at the transitions between different textures to rectify the positional estimation error that could accumulate from the rotary encoder data. Data from the treadmill was acquired using digitizer hardware (National Instruments) and the ThorSync software (Thorlabs). The treadmill and microscope setting were completely novel to the mice, which were allowed to sit still or freely move and explore the

treadmill during initial setup, but were required to walk during imaging, as the treadmill was rotated. Throughout the imaging session, the mice remained in the dark, in an enclosed box built around the microscope.

Silencing of adult-born neurons

To study the effects of adult neurogenesis on hippocampal circuits we recorded DG, CA1 and Mossy Cell activity (or contextual conditioning behavior) before and after silencing a cohort ABNs. We targeted ABNs by crossing Ascl1-CreERT2 transgenic mice (Kim et al., 2011) (Jackson Labs #12882) with a line expressing the inhibitory DREADD hM4Di (Roth, 2016; Zhu et al., 2016) in a Cre-dependent manner (Jackson Labs #26219). Mice with the two alleles allowed us to specifically target a cohort of newborn ABNs by injecting Tamoxifen (Tam) i.p. over the course of 3 days to express Cre in Ascl1+ cells, thereby inducing Cre expression. This approach resulted in hM4Di expression in both DG and SVZ newborn ABNs. We acutely silenced ABNs by administering the specific hM4Di ligand clozapine-N-oxide (CNO) (Roth, 2016) 30 minutes prior to imaging behavioral testing, as described above. CNO was dissolved in a saline solution (0.9% NaCl) at a concentration of 1 mg/mL and administered intraperitoneally at a dosage of 5 mg/kg (Varela et al., 2016). We used littermates lacking the Cre allele, and therefore hM4Di expression, as controls for the unspecific effects of CNO and Tam.

Analysis of calcium imaging data

Calcium imaging fluorescence intensity data was extracted from movies using the Suite2p opensource software suite (Pachitariu et al., 2016). Briefly, all movies were registered for motion correction, the cell contours of active cells were detected, and calcium traces extracted for each cell. Movement (rotary encoder) and texture (RFID) data were matched with the corresponding imaging frames. The position of the mouse on the treadmill was determined by calculating the cumulative sum of the treadmill rotation signal for every frame of the calcium imaging movie.

To decode the spatial position from the neuronal population activity, we used a logistic regression model (Kanitscheider et al., 2015), trained on 75% of the data and tested using the remaining 25%, cross-validating using 10 random splits of the data to prevent for overfitting. We did not employ regularization. We determined that decoding the position from unfiltered fluorescence traces yielded the best results and dynamic range, as either filtering, thresholding, or deconvolution results in consistently very high or very low decoding accuracy (Fig. S1 C, D, E). We also verified that decoder performance was similar on train and test data, indicating minimal overfitting (Fig. S1 F, G). The position data was segmented into 20 bins and ΔF/F unfiltered calcium traces were used as input data. Each bin is approximately the length of one mouse and contains an average of 400 frames. The population activity was projected onto the decoder weights to obtain a 1D signal and compute d-prime squared (which is equivalent to linear Fisher information) (Kanitscheider et al., 2015).

Single-cell Fisher Information (FI) was calculated using the ΔF/F unfiltered fluorescence calcium data using previously published methods (Kanitscheider et al., 2015). Briefly, a bias-corrected signal to noise ratio was computed, where the signal is the square of the difference of the mean activity at two locations on the treadmill, and the noise is the average variance of the activity at each location. The position data was segmented into 20 bins.

Tuning indices were calculated using deconvolved firing rates (Pachitariu et al., 2018), which were thresholded to 2 σ of the baseline, so that every point not significantly above that noise threshold is set to zero. The treadmill band was segmented into 100 position bins and the putative firing epochs were mapped to these bins according to the location of the mice on the treadmill to generate a tuning vector for each cell (Danielson et al., 2016). The mean thresholded firing rates at each location were calculated for every neuron and normalized to the time the mouse spent at that position. The tuning index was defined as the modulus of this normalized tuning vector.

Calcium activity was calculated on a per-cell basis: ΔF/F data was first filtered with a third order Butterworth lowpass filter by applying the filter to the data both forwards and backwards to compensate for phase shifts. Significant calcium transients were determined as the consecutive frames that start when the ΔF/F fluorescence signal rises 2 standard deviations (σ) above the rolling-mean baseline and end when the signal drops below 0.5 σ. The significant transients were then removed, and the remaining calcium trace was used to calculate a new rolling mean baseline, iterating through this process 3 times. The resulting significant calcium transient was used to determine the activity as the cumulative sum of the trace for each cell. The result was normalized to the total distance traveled by the mouse.

Curve Fitting Analysis

To study the properties of tuning of every cell, we first generated a tuning curve by mapping the unfiltered ΔF/F fluorescence data of each cell to one of 20 angular position bins on the treadmill belt. This fluorescence data was averaged over all laps. This circular tuning curve was fitted with Von Mises function:

$$B + Ae^{k(\cos(x-\varphi)-1)}$$

Where B is an offset parameter, A is the amplitude of the peak, k is a measure of concentration and φ is the location of the peak of tuning. The parameters of the function were optimized numerically by minimizing the sum of squared differences between data and model. The goodness of fit was calculated and cross validated as follows:

$$R^2 = 1 - (ss\_res/ss\_tot)$$

Where ss_res is equal to the sum of the squares of the residuals and ss_tot equals the sum of the squares of the differences from the mean. Note that this value of R2 is normalized between 0 (null model, i.e. ss_res_null = ss_tot) and 1 (oracle model, i.e. ss_res_oracle = 0): a R2 value of zero corresponds to a model where none of the variance can be explained by the Von Mises

function and 1 corresponds to an error equal to zero, predicting all of the data points. The crossvalidation was done using 75% of the data in each bin to train and 25% of the data to test the model. The width of the peak was determined as the circular variance using the function below:

$$V = 1 - (\frac{I_1(k)}{I_0(k)})$$

Where I1 is the Bessel function of order 1 and I0 is the Bessel function of order 0 (Swindale, 1998). To determine tuning bimodality in Mossy Cells, we utilized the same approach, and a bimodal circular tuning curve was fitted with Von Mises function:

$$B + Ae^{k(\cos(x-\varphi)-1)} + A_2 e^{k_2(\cos(x-\varphi_2)-1)}$$

Immunohistochemistry

To quantify the numbers of ABNs we labeled brain tissue with an antibody against Doublecortin (DCX) (CST, 1:800). To quantify hM4Di expression, we stained brain tissue with an antibody against HA-Tag (CST, 1:800). Briefly, animals were first infused with ice-cold 0.1M phosphate-buffered saline, followed by a 4% paraformaldehyde (PFA) solution. Brains were then post-fixed in 4% PFA for 24 hours and then cryoprotected in 30% sucrose. The hippocampus was sliced at 40 μm thickness on a freezing microtome and three slices within the implanted region of interest were stained for each mouse. Slices were rinsed three times in 0.1M PBS (pH = 7.4) and incubated in a blocking solution (10% goat serum, 0.3% Triton-X in 0.1M PBS) for one hour. The sectioned tissue was then incubated in a primary antibody in block for 48 hours, followed by three rinses in 0.1M PBS. The sections were then incubated in Alexa 488, Alexa 568, or Alexa 633, goat anti-rabbit secondary in 0.1M PBS (1:500; Invitrogen) for 2 hours, rinsed three times in 0.1M PBS, counterstained with 300nM DAPI in 0.1M PBS, rinsed again in 0.1M PBS, and then mounted and

cover-slipped with Fluoromount-G (Southern Biotech). The tissue was then imaged on a Zeiss Axio Imager.A2 fluorescence microscope. Animals in which there was no expression in the dorsal hippocampus were removed from analysis.

Contextual Discrimination Task

Mice were placed in a fear conditioning chamber within a sound-attenuating cubicle. For conditioning, mice were allowed 3 minutes of free exploration of a pre-cleaned cube-shaped chamber with a grid floor (context A) before receiving three mild foot-shocks (2s, 0.7 mA) spaced 60 seconds apart. Mice were returned to their home cage 30 seconds after the last shock. Contextual fear memory was tested 24 hours later by re-exposing mice to context A for 3 minutes of free exploration (no shocks). Forty-eight hours after conditioning, mice were tested on discrimination of a novel context B (plastic floor, A-frame geometry, and scented). In this session, mice were allowed 3 minutes of free exploration (no shocks). Context discrimination was measured as a discrimination index, DI: (Time freezing in A – Time freezing in B)/(Time freezing in A + Time freezing in B). In silencing experiments, we expressed hM4Di specifically in a cohort of immature ABNs so they could be silenced by the selective ligand CNO. Conditioning and re-exposure to context A took place without CNO but were injected with CNO 30-40 minutes prior to exposure to the novel context B. To control for unspecific effects of CNO we used mice that lacked a Cre allele, and therefore did not express hM4Di (hM4Di-).

Statistical analyses

A non-parametric Mann-Whitney test was used to compare between mouse groups. When pooling cell data from different mice into a single experimental group, significance testing was done using a muti-level bootstrapped approach that took data nesting into account, as follows. To assess a significant difference between two experimental conditions (e.g., EE and RC), the null distribution was constructed for each condition as follows: The data from both conditions was combined into

one group. The animal and data value were sampled in each condition, a total equivalent to the number of data values within the condition. The mean was then calculated. This process was repeated for each condition and the difference between the null distributions generated for each group was calculated. 100,000 bootstraps were generated. The empirically observed value of the difference between conditions was then compared to the null distribution. The statistical significance level (α) was set at 0.05. Bonferroni's correction for multiple comparisons was applied. One-sample t-tests with Bonferroni's correction for multiple comparisons were used to determine differences between group means and chance performance in contextual fear conditioning experiments.

## Chapter 3 - Adult neurogenesis improves spatial information encoding in the mouse DG.

### Environmental enrichment increases spatial information encoding in the DG.

Environmental enrichment and exercise have been found to improve cognitive performance, including spatial memory in humans (Vemuri et al., 2014) and rodents (Kempermann et al., 1997), as well as increase the number of ABNs in the DG (Kempermann et al., 1997). We asked whether this improvement in spatial memory could be due to improved neural representations of space in the hippocampus. To address this question, we imaged the granule cell layer of the DG of mice housed in regular cages (RC) or in an EE with running wheels. We labeled DG neurons of 8-week old C57Bl6/J mice with an AAV encoding the red calcium sensor jRGECO1a (Dana et al., 2016) and implanted them with a titanium imaging 'window' (Fig. 1A), resting above the surface of CA1 of the dorsal hippocampus (Pilz et al., 2016). After the implantation surgery, mice were housed in regular cages for 3.5 weeks or in an EE cage for 2 weeks, before being returned to a RC. A single calcium imaging session took place ~3.5 weeks after surgery (Fig. 1 A, B). Mice were head-fixed to a treadmill with a belt composed of different texture materials (Fig. 1A) and imaged unanesthetized as the treadmill was rotated at a mean speed of ~420 cm/min (Fig. S1 A, B, Movie S1). As expected, EE animals showed a ~2-fold increase in doublecortin (DCX) positive neurons (Fig. 1C). DG neuronal activity was sparse with an average of 86 neurons active during a 9 min recording session in a field of view of up to 343 μm x 343 μm, corresponding to 4.3 ± 0.8 % of all labeled putative neurons. To estimate spatial information content from the imaged neurons we trained a linear decoder to decode the position of the mouse on the treadmill from the calcium traces (trained on 75% and tested on 25% of the data, see Methods). Since numbers of imaged and active neurons were substantially different across mice, we subsampled our datasets (n = 42 cells) to compare decoding performance of equally sized populations across different mice. Exposure to EE resulted in a 10% increase in decoding accuracy compared to mice in RC (Fig.

1B, D, E), reflecting an increase in spatial information content in the DG. While multiple exposures to a single context are known to increase hippocampal spatial information within that same context (Cacucci et al., 2007; S. Kim et al., 2020), our findings show that 2-weeks of EE housing can increase spatial information in future exposures to a novel context.

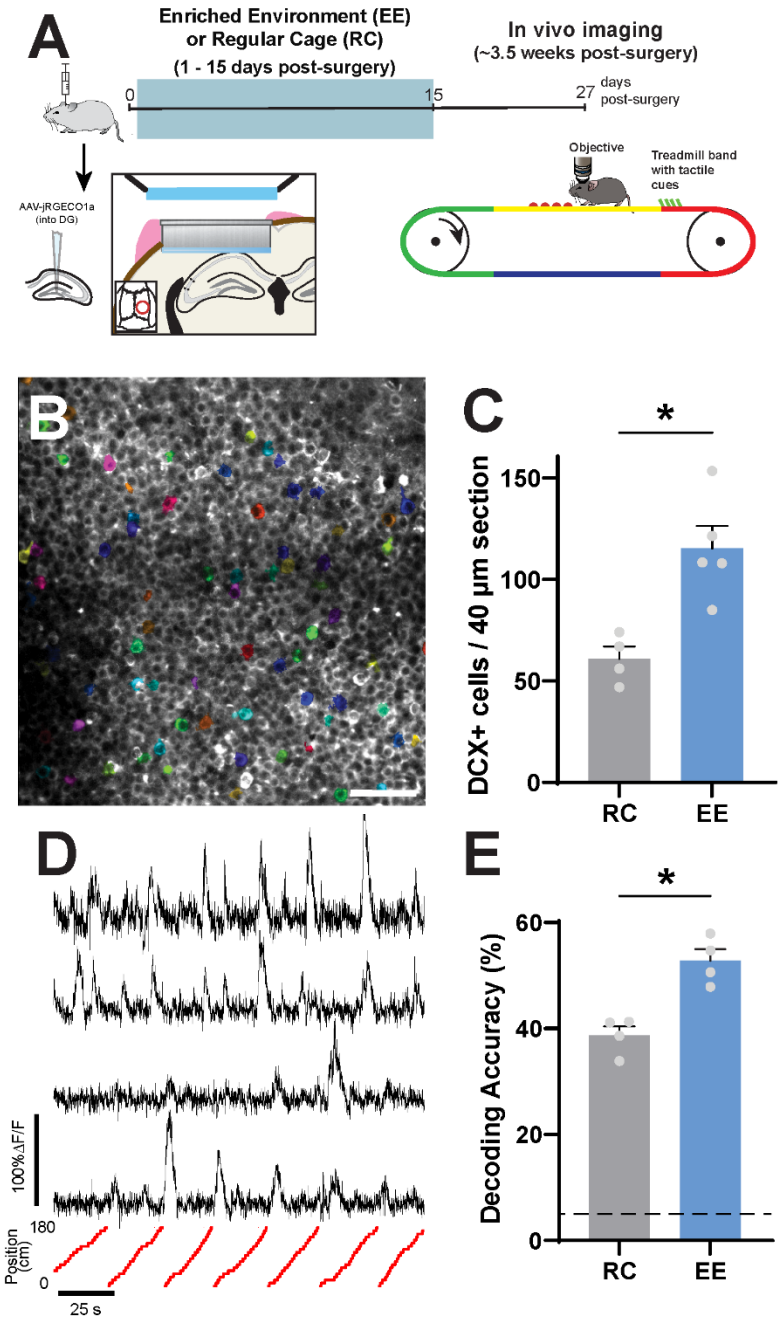

**Figure 1.** Environmental enrichment increases the spatial information encoding in the DG. A) Experimental timeline, including surgery, enriched environment, and in vivo imaging. B) Example of calcium imaging field of view. C) Number of DCX-expressing granule neurons in regular cage (RC) and enriched environment (EE) groups. (p = 0.026, nRC = 4 mice, nEE = 5 mice, average of three 40µm slices per mouse, Mann-Whitney U test) D) Example calcium traces (top) and respective position of animal on the treadmill (bottom). E) Accuracy in decoding position of mouse on treadmill from calcium traces (p = 0.0286, n = 4 mice, 42 cells subsampled per mouse, Mann-Whitney U test). Dotted line is chance performance level (5%). See also Figure S1.

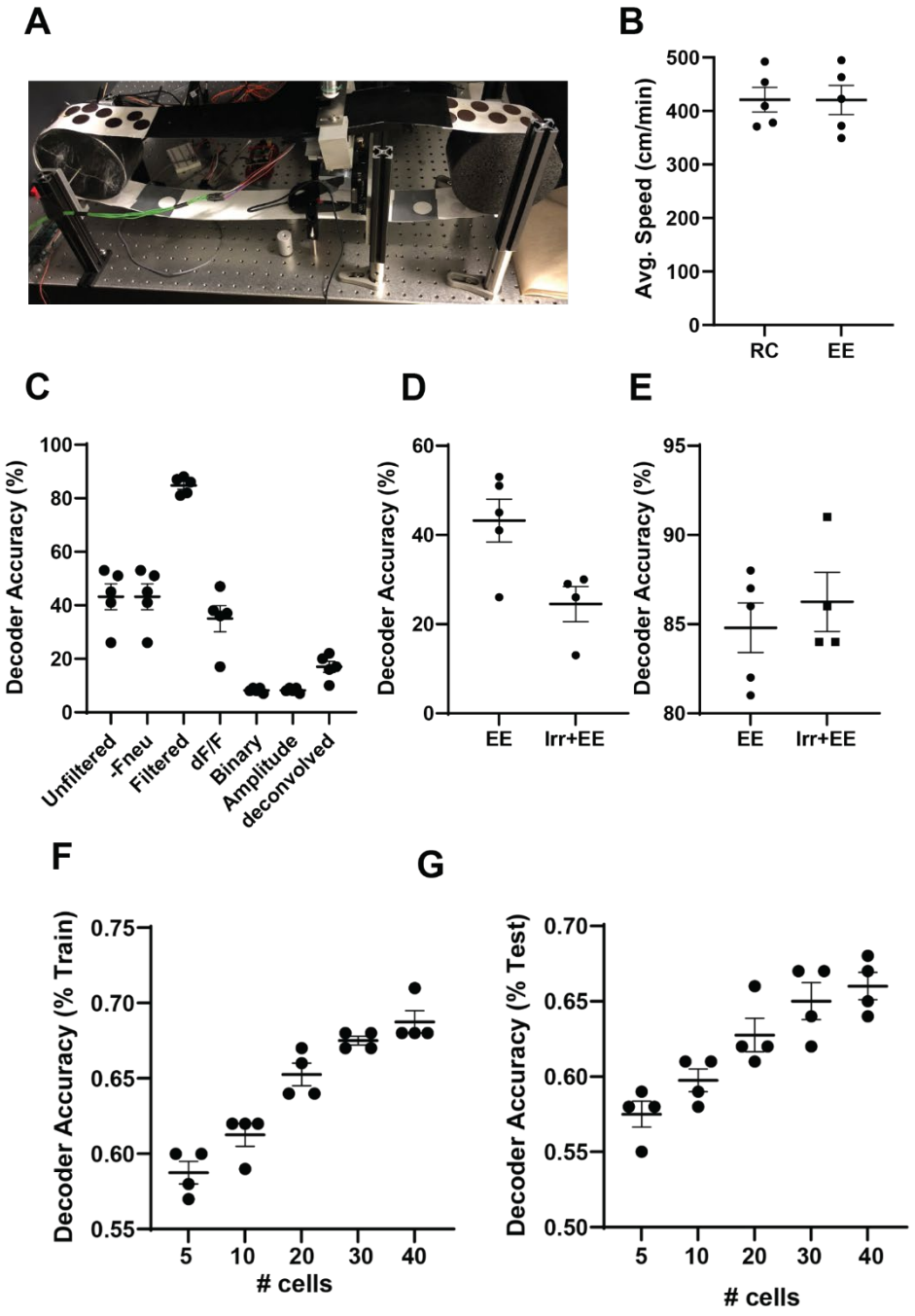

**Figure S1.** Optimization of decoder for calcium imaging analysis. A) Photograph of two-photon imaging treadmill with different textile cues. B) Average speed of RC and EE mice on treadmill during experimental sessions. C) Comparison of percentage of decoding accuracy using different methods for filtering calcium trace data. Unfiltered raw traces, raw traces with neuropil subtraction, filtered traces using a moving average approach and window size of 100, dF/F, binary data on the location of the deconvolved spikes on the trace, traces being represented by the amplitude of the deconvolved spikes on the trace and the deconvolved traces. Spike deconvolution was performed using suite2p based on the OASIS algorithm. D) Example of decoder accuracy using unfiltered calcium traces in EE and Irr+EE mice. E) Example of decoder accuracy using filtered calcium traces in EE and Irr+EE mice. F) Decoder accuracy on training data plotted by number of cells analyzed. G) Decoder accuracy on testing data plotted by number of cells analyzed. Related to Figure 1.

Prior focal irradiation of the hippocampus blocks the effects of EE on DG spatial encoding.

We then asked whether the changes in spatial encoding in EE mice were driven by an increase in the number of immature ABNs, rather than other systemic effects of EE housing. We recorded calcium activity in mice that had DG neurogenesis ablated by bilateral focal irradiation using opposing large fields (Tomé et al., 2015) at 6 weeks of age (Fig. 2A, Fig. S2A,B). Irradiation results in the permanent ablation of DG adult neurogenesis (Fig. 2 B, C), while preserving subventricular zone / olfactory bulb (OB) neurogenesis, as confirmed post hoc by the persistence of DCX immuno-reactive cells in the OB (Fig. S2C). A group of irradiated mice were housed under RC conditions (Irr+RC), whereas another group was exposed to EE (Irr+EE). EE exposure failed to increase decoding accuracy in irradiated mice, in contrast with non-irradiated mice (Fig. 2D). Additionally, irradiated animals had lower decoder accuracy than their non-irradiated counterparts (Fig. 2D). These results suggest that the effects of EE on spatial encoding in the DG are driven primarily by immature ABNs, and that decreasing adult neurogenesis results in a decrease in spatial information in the DG, which could explain why reducing neurogenesis results in memory encoding deficits.

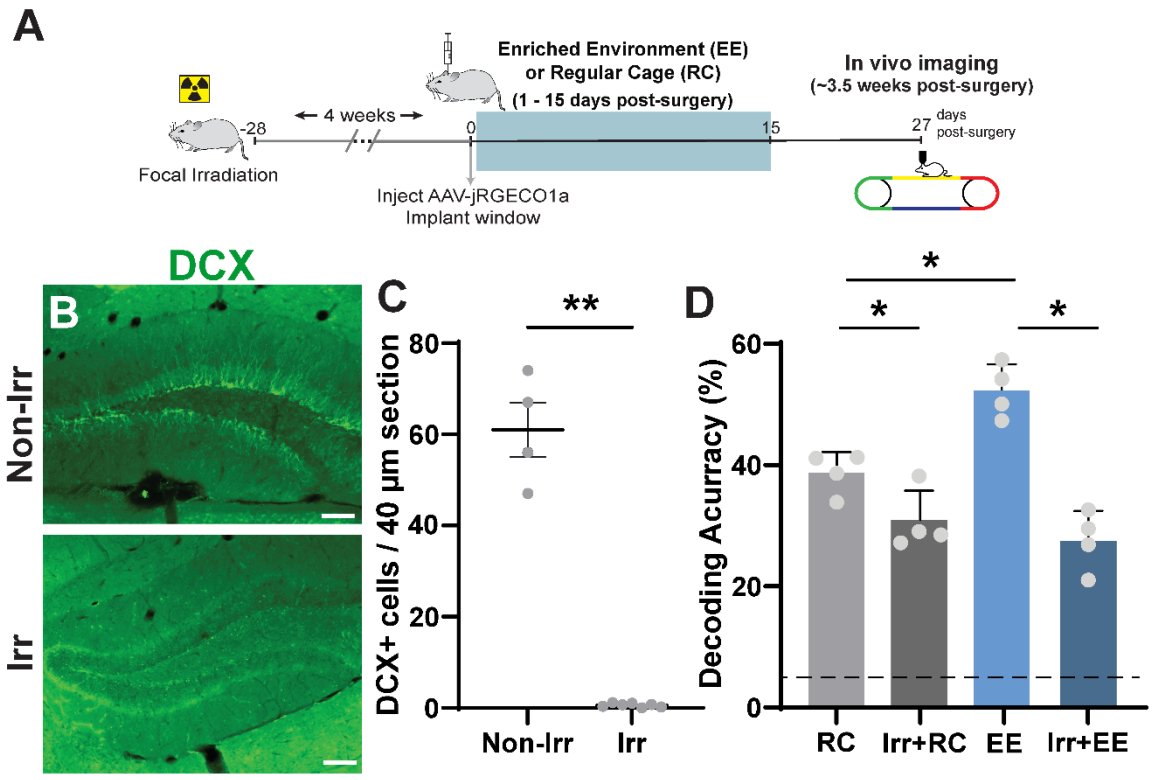


**Figure 2.** Prior focal irradiation of the hippocampus blocks the effects of EE on DG spatial encoding. A) Experimental timeline, including focal irradiation, surgery, and in vivo imaging. B) Immunofluorescence labelling of DCX positive neurons in the DG of non-irradiated (top) and irradiated (bottom) mice. C) Number of DCX-expressing granule neurons in non-irradiated and irradiated groups ($p = 0.0061$, nNon-Irr = 4 mice, nIrr = 9 mice, average of three 40µm slices per mouse, Mann-Whitney U test). D) Accuracy in decoding position of mouse on treadmill from calcium traces (RC vs Irr+RC: $p = 0.0288$, EE vs Irr+EE: $p = <0.0001$, RC vs EE: $p = 0.0031$, ANOVA, Holm-Sidak correction for multiple comparisons, n = 4 mice, 42 neurons subsampled per mouse). Dotted line is chance performance level (5%). See also Figure S2.

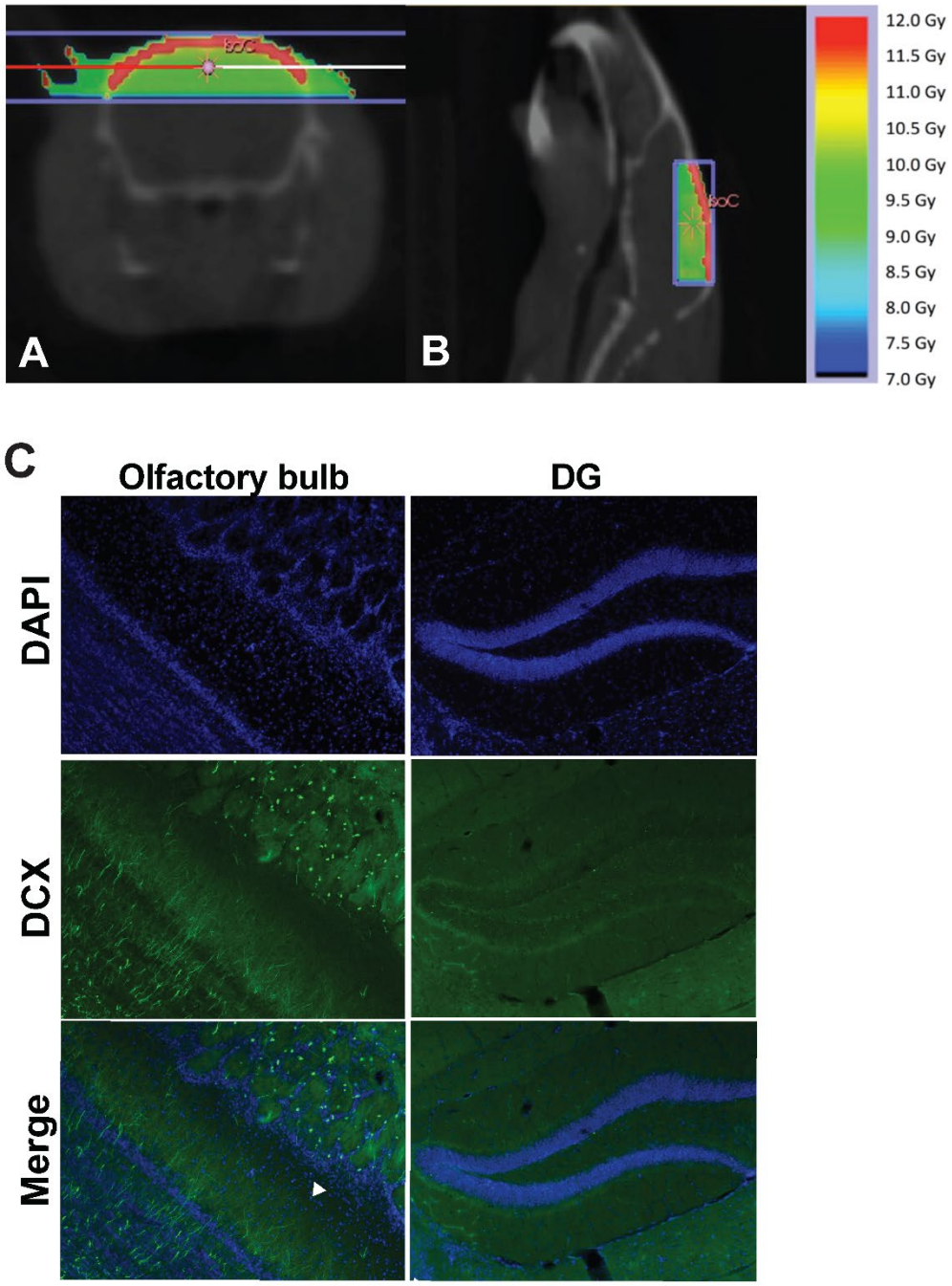


**Figure S2.** Olfactory bulb neurogenesis is preserved with hippocampal focal irradiation. Typical isodose distributions for hippocampal focusing irradiation employed in this study: A) coronal plane, B) sagittal plane. C) Immunofluorescence images of the DCX-positive neurons and DAPI labelled nuclei in the olfactory bulb (left) and dentate gyrus (right) of a mouse that has undergone focal irradiation. Related to Figure 2.

Ablating adult neurogenesis decreases single-cell spatial information content.

Next, we studied whether changes in spatial information in the DG were driven by changes at the population level or at single-cell level. The information content of neural populations is determined jointly by the response properties of individual neurons, i.e. their tuning and the variability of their activity when repeatedly presented with the same stimulus (in this case each location on the treadmill belt) and by the structure of noise correlations (NCs; (Cohen & Kohn, 2011)), i.e how this variability is correlated among pairs of neurons (Averbeck et al., 2006; Kohn et al., 2016).

We quantified spatial information using the linear Fisher Information (a measure of population sensitivity to spatial location, equivalent to d-prime; (Kanitscheider et al., 2015) because it allows us to assess population-wide effects more accurately than decoding performance (Kafashan et al., 2021) and because it allows us to express the sensitivity also in terms of discrimination thresholds. First, to test the contribution of noise correlations to spatial information encoding in the DG, we created surrogate datasets where we shuffled the trial order independently for each neuron. The response of each neuron is given by the response at the same location but on a different trial/timepoint. Therefore, noise correlations are destroyed, but the tuning of individual neurons is preserved. Our results show that spatial information in the shuffled datasets was generally increased although only marginally in some conditions (Fig. 3A-D), indicating that noise correlations are either detrimental or have no effect on decoding accuracy in the DG. This result suggests that the effect of ABNs on spatial information cannot be explained by changes in noise correlations. The weaker influence of noise correlations in the EE condition compared to RC (Fig. 3 A, B), raises the possibility that exposure to EE increases spatial information by reducing the detrimental effect of noise correlations, but testing this conclusively will require larger scale recordings.

Next, we calculated the spatial information of individual neurons (Fig. 3E). We found that ablating neurogenesis strongly reduced spatial information for single neurons and that this reduction was

present both among the neurons with most spatial information as well as neurons that had lower spatial encoding (Fig. 3F). As a more intuitive measurement, we also calculated a discrimination threshold, that is the minimum distance between two points on the treadmill that will be discriminated correctly 70% of the times (lower thresholds reflect a more precise spatial code; Fig. 3G). As expected, irradiated cohorts both in RC and EE conditions had increased discrimination thresholds. These findings indicate that the observed changes in DG spatial information occur primarily at single-cell level, which led us to study in greater detail how the activity single-cells changes with EE exposure and the ablation of adult neurogenesis.

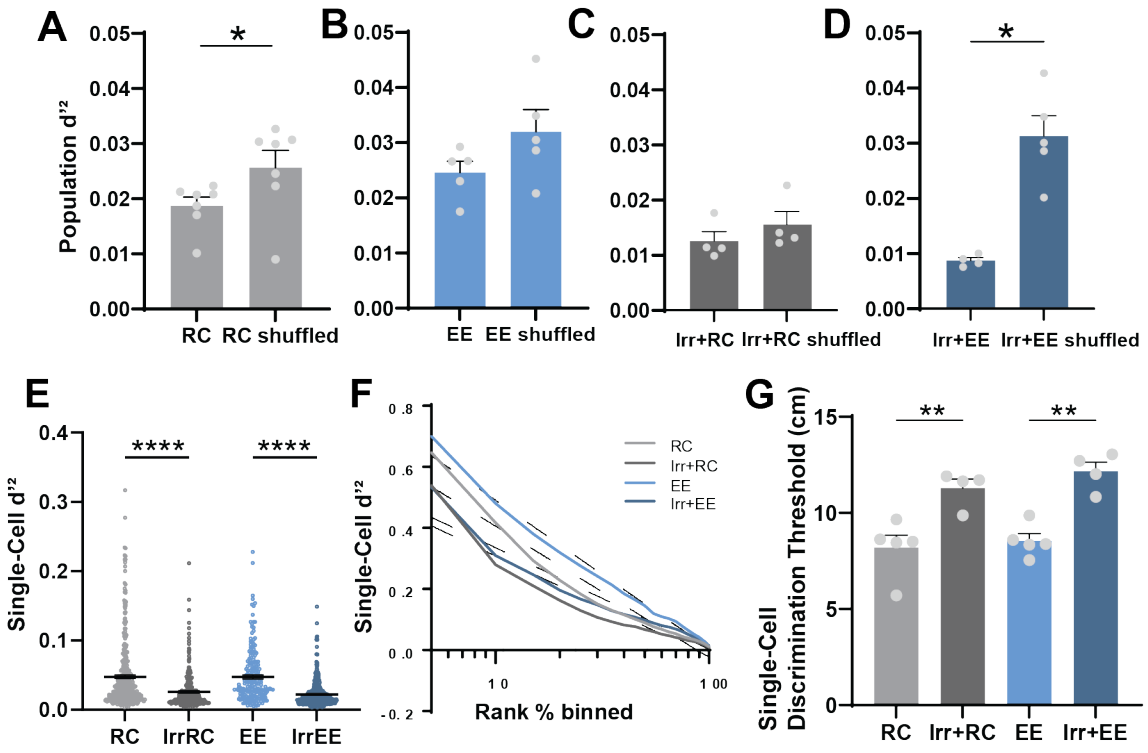

**Figure 3.** Ablating adult neurogenesis decreases spatial information content at the single cell level. A-D) Population Fisher information determined with noise correlations and after random shuffling to disrupt noise correlations (RC vs RC w/o NC: p = 0.0571 n.s, n = 5 mice per group, EE vs EE w/o NC: p = 0.1508 n.s, n = 5 mice per group, Irr+RC vs Irr+RC w/o NC: p= 0.2000 n.s., n = 4 mice per group, Irr+EE vs Irr+EE w/o NC: p = 0.0159, n = 5 mice per group, Mann-Whitney U test). E) Single-cell spatial information content determined using Fisher information (FI) (RC vs Irr+RC: p < 1/100000, nRC = 5 mice, 277 neurons, nIrr+RC = 4 mice, 253 neurons, EE vs Irr+EE: p < 1/100000, nEE = 5 mice, 201 neurons, nIrr+EE = 4 mice, 412 neurons). Statistical analysis: Bootstrap and Bonferroni correction for multiple comparisons (see methods). Error bars are mean ± SEM. F) Distribution of spatial information content across the imaged neurons. Linear fits showed in dotted lines. G) Distance between two positions that DG single-cells are able, on average, to discriminate correctly 70% of the time (RC vs Irr+RC: p = 0.0038 nRC = 5 mice, nIrr+RC = 4 mice, EE vs Irr+EE: p = 0.0012, nEE = 5 mice, nIrr+EE = 4 mice). Statistical analysis: ANOVA, Holm-Sidak correction for multiple comparisons).

Ablating adult neurogenesis reduces tuning specificity and single cell activity.

To assess how single cell information changes in the DG, we mapped the calcium activity traces to the position of the mouse on the treadmill to generate a tuning vector (Fig. 4 A, B). The mean calcium signal at each location was computed for every neuron and normalized to the time the mouse spent at that position. The modulus of the tuning vector was used as a spatial tuning index that reflects the place-specificity of activity (Danielson et al., 2016). Irradiated cohorts had significantly lower mean tuning indices than non-irradiated animals (Fig 4C). While both irradiated and non-irradiated groups had highly tuned cells, the distribution of tuning indices skewed lower in the irradiated cohorts, both for highly tuned cells as well as their low-tuning counterparts (Fig. S3A), suggesting that the lower information content in these mice could be caused by a decrease in the place-specificity of neuronal activity. This decrease in tuning could be caused by an overall change in the calcium activity levels of DG neurons or by changes in how this activity is distributed along the treadmill belt. Since adult neurogenesis is usually thought to contribute to a net decrease in DG activity through the increased activation of feedback inhibitory circuits by immature adult-born neurons, we hypothesized that the DG neurons of irradiated mice would be hyperactive in comparison with the non-irradiated cohorts. To test this, we computed the calcium activity rates of cells that were active during recording sessions by integrating their calcium signals over each session and normalizing this to the distance travelled (see methods). In contrast to our expectation, we found that irradiated groups, where neurogenesis was ablated, had significantly

reduced calcium activity (Fig. 4D). Keeping with this pattern, EE mice, which have increased neurogenesis, had significantly higher activity than their RC counterparts. Reduced calcium activity rates were found both among the most active neurons, as well as in the less-active quartiles (Fig. S3B), which is similar to our findings for tuning (Fig. S3A). To better determine how the tuning specificity changed in mice with ablated neurogenesis, we mapped the cumulative activity of each cell to create a tuning curve and fit a Von Mises function to the curves for every cell (Fig 4E). EE mice had significantly higher goodness-of-fit (R2) than RC mice, while both irradiated groups had significantly lower R2 than their non-irradiated counterparts (Fig. 4F). This could be a result of poorly fitted cells having flatter and/or noisier tuning, resulting in lower information content in irradiated animals (Dayan & Abbott, 2001). The peak width of fitted curves was not significantly different across experimental groups (Fig. 4G), indicating that differences in spatial information were not due to increased lap-to-lap variance in the location to which individual DG neurons are responsive. However, the peak amplitude of fitted cells was significantly lower in the irradiated cohorts (Fig. 4H), reflecting a dampened place-specific response of individual neurons. These results suggest that the reduction in spatial information content (Fig. 2D, 3E) is driven by two components at the single cell level: an overall reduction in tuning selectivity explained by a decreased number in well-tuned cells, and a reduction in the amplitude of the tuning curve with no change in the lap-to-lap variance of the location of the tuning maximum, as observed by the unchanged peak widths. These results suggest that integrating ABNs may be either directly or indirectly modulating the gain of DG neurons, increasing calcium activity rates in a multiplicative manner, which for well-fitted neurons ($R2 > 0.5$) reflects as a larger increase in calcium activity at the preferred location of each neuron than at non-preferred locations, thereby increasing tuning curve slope and spatial information. Furthermore, because gain modulation can also influence trial by trial variability (Coen-Cagli & Solomon, 2019; Hénaff et al., 2020), and variability limits single-neuron spatial information, our finding of increased spatial information indicates that the presence of immature ABNs leads to an increase response gain without

increasing variability as much. However, the changes we observed could also be due to non-specific side effects of irradiation. We therefore investigated whether the same circuit effects were present in mice where ABNs were silenced using a chemogenetic approach.

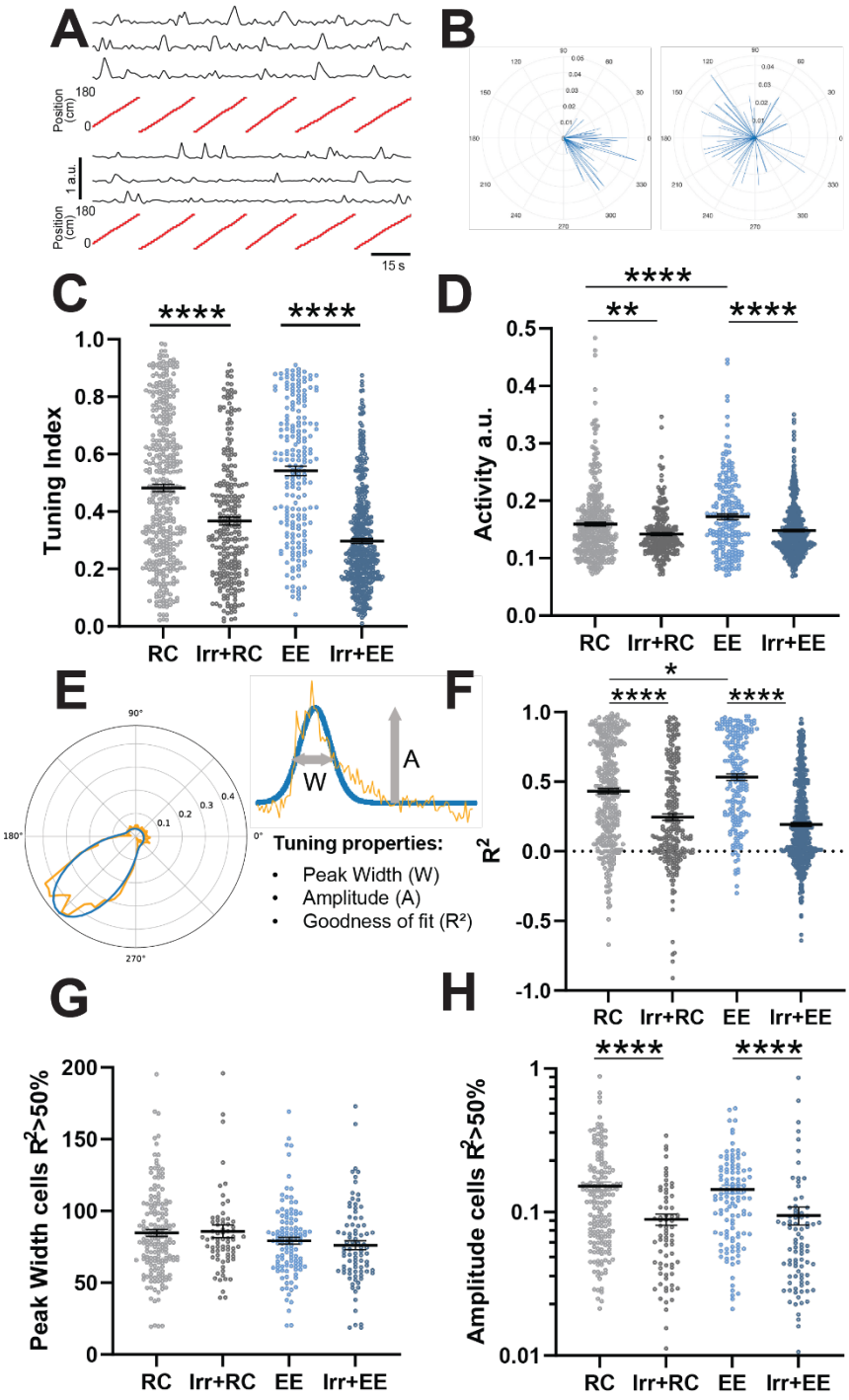

**Figure 4.** Ablating adult neurogenesis reduces tuning specificity and activity. A) Examples of cells with high (top) and low (bottom) tuning indices. B) Tuning vectors from cells in A plotted in polar coordinates. C) Tuning indices of cells in non-irradiated and irradiated groups (RC vs Irr+RC: $p < 1/100000$, nRC = 5 mice, 277 neurons, nIrr+RC = 4 mice, 253 neurons, EE vs Irr+EE: $p < 1/100000$, nEE = 5 mice, 201 neurons, nIrr+EE = 4 mice, 412 neurons). D) Activity measured as integrated calcium traces normalized to distance travelled (RC vs EE: $p < 1/100000$, nRC = 5 mice, 277 neurons, nEE = 5 mice, 201 neurons, RC vs Irr+RC: $p < 0.00228$, nRC = 5 mice, 277 neurons, nIrr+RC = 4 mice, 253 neurons, EE vs Irr+EE: $p < 1/100000$, nEE = 5 mice, 201 neurons, nIrr+EE = 4 mice, 412 neurons). E) Schematic of tuning curve properties of individual cells fitted with Von Mises function. F) Cross-validated goodness of fit (R2) of tuning curves (RC vs EE: $p = 0.01617$, nRC = 5 mice, 277 neurons, nEE = 5 mice, 201 neurons, RC vs Irr+RC: $p < 1/100000$, nRC = 5 mice, 277 neurons, nIrr+RC = 4, 253 neurons, EE vs Irr+EE: $p < 1/100000$, nEE = 5 mice, 201 neurons, nIrr+EE = 4 mice, 412). G) Peak width of tuning curves of well-fitted cells. H) Peak amplitude of well-fitted cells (RC vs Irr+RC: $p < 1/100000$, nRC = 5 mice, 173 neurons, nIrr+RC = 4 mice, 70 neurons, EE vs Irr+EE: $p = 0.00237$, nEE = 4 mice, 113 neurons, nIrr+EE = 4 mice, 85 neurons). See also Figure S3. Statistical analysis: Bootstrap and Bonferroni correction for multiple comparisons. Error bars are mean ± SEM.

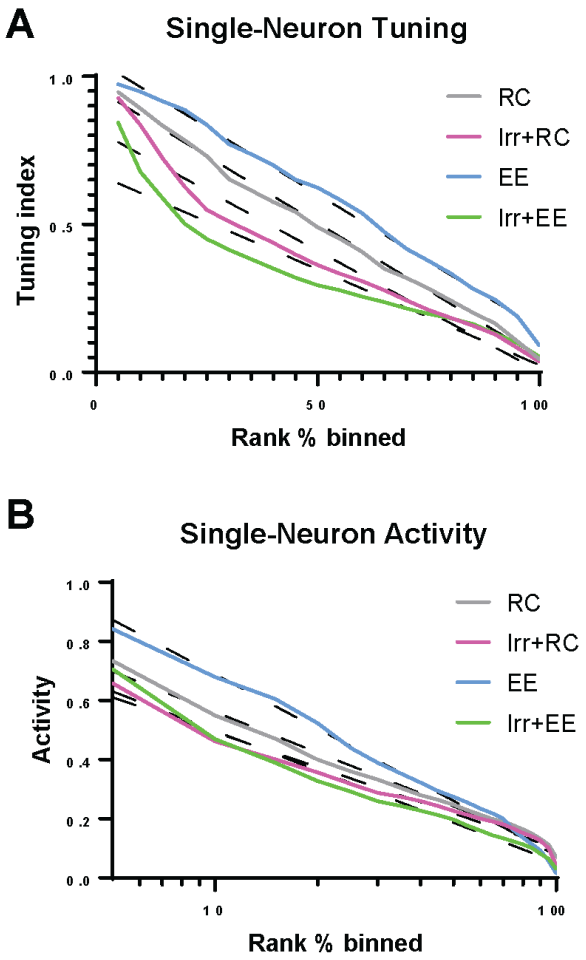


**Figure S3.** Ablating adult neurogenesis reduces single-cell tuning specificity and activity. A) Distribution of single-cell tuning indices between non-irradiated and irradiated cohorts. B) Distribution of single-cell activity rates between non-irradiated and irradiated cohorts. Related to Figure 4.

Acute chemogenetic silencing of ABNs decreases spatial information content in the DG.

Previous studies suggested that synaptic competition between ABNs and mature neurons plays a role in mediating the effects of adult neurogenesis on DG networks. By disrupting the synaptic connectivity of mature neurons, ABNs force the rewiring of the circuit (Adlaf et al., 2017; Toni et al., 2008; Toni & Schinder, 2016). We asked whether ABN-induced changes in spatial information content required ABN activity or were a product of their integration into the DG. To address this question, we acutely silenced a cohort of ABNs by crossing Ascl1-CreERT2 knockin mice (E. J. Kim et al., 2011) with a line expressing the inhibitory DREADD hM4Di (Roth, 2016; Zhu et al., 2016) in a Cre-dependent manner, allowing us to specifically target a cohort of newborn ABNs. Animals were injected daily with Tam for 3 days at 8 weeks of age (Fig. 5A) and housed in EE conditions. Littermates lacking hM4Di expression were used as controls for the unspecific effects of CNO. To assess the efficacy of ABN silencing, and since hM4Di can inhibit synaptic release independently from its effect on action potential firing (Roth, 2016), we testing the effects of CNO-induced silencing on mouse behavior. We used a context discrimination task where the animals are conditioned to associate a specific context with a foot shock (Fig. 5B). In line with previous studies (Clelland et al., 2009; Danielson et al., 2016; Sahay et al., 2011), silencing ABNs resulted in impaired discrimination between a Context A where the animals were shocked, and a novel Context B (Fig. 5C,D). All mice were injected with an AAV encoding jRGECO1a and implanted with an imaging window over the hippocampus 2 weeks after the end of Tam treatment, and imaged 3.5 weeks after implantation, both in baseline conditions and 30 minutes after an i.p. CNO injection (5 mg/kg). The exact same field of view was imaged in both sessions. Consistent with our previous results in irradiation experiments, single-cell Fisher information (Fig. 5G), Ca2+ activity (Fig. 5I) and tuning index (Fig. 5K) were significantly reduced after silencing ABNs with CNO but were unchanged in control animals that did not express hM4Di (Fig. 5 H, J, L). We also fit the tuning curves of DG neurons before and after CNO administration to a von Mises function.

The goodness-of-fit (R2) showed a trend for decrease as seen in the irradiated cohorts but no significant difference was found, including when only well-fit cells (R2>0.5) were considered (Fig. 5 M, N). Similar to our previous experiments, no significant change was seen in the width of the fitted tuning curves, while their amplitude was decreased upon CNO administration (Fig. 5 O, P). This difference was not present in control animals that did not express hM4Di, although we did see a significant increase in the peak width of controls following CNO administration, which could reflect an unspecific effect of CNO (Fig. S4). Given these findings, we conclude that the effect ABNs on the neural representations of space in the DG is dependent on their activity. Silencing ABNs generally replicated our results from the ablation experiments, suggesting that spatial information changes in the irradiated cohorts were not due to potential side effects of irradiation, such as increased inflammation. Taken together, these results indicate that ABNs increase spatial information in the DG by increasing the spatial selectivity of otherwise untuned DG granule cells and leading to an increase in the gain of DG granule neurons, either directly or through other circuit mechanisms.

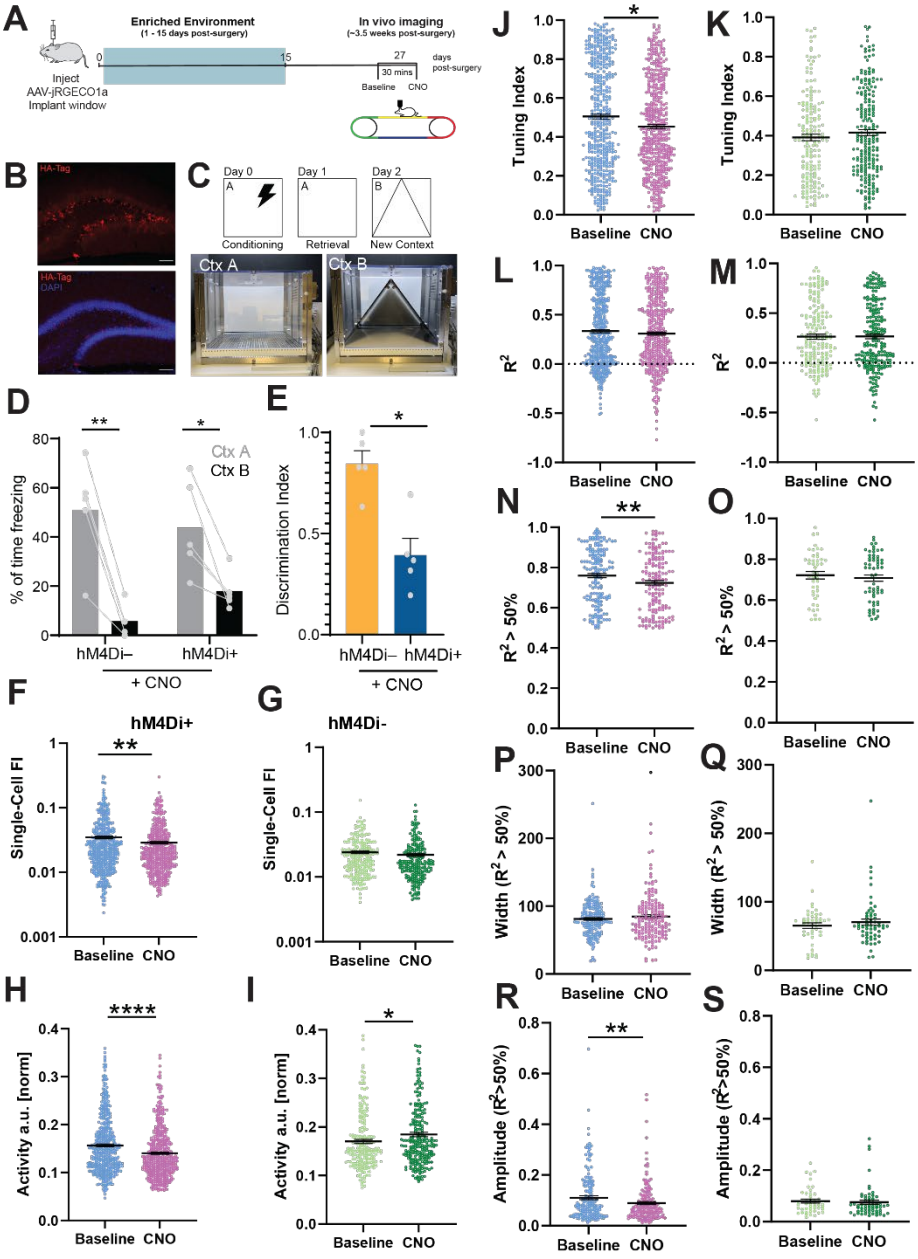
A
Enriched Environment
(1 - 15 days post-surgery)
In vivo imaging
(~3.5 weeks post-surgery)
Inject
AAV-jRGECO1a
Implant window
0
15
27
days
post-surgery
30 mins
Baseline
CNO
B
HA-Tag
HA-Tag
DAPI
C
Day 0
A
Day 1
A
Day 2
B
Conditioning
Retrieval
New Context
Ctx A
Ctx B
D
% of time freezing
Ctx A
Ctx B
hM4Di–
hM4Di+
+ CNO
E
Discrimination Index
hM4Di–
hM4Di+
+ CNO
F
hM4Di+
Single-Cell FI
Baseline
CNO
G
hM4Di-
Single-Cell FI
Baseline
CNO
H
Activity a.u. [norm]
Baseline
CNO
I
Activity a.u. [norm]
Baseline
CNO
J
Tuning Index
Baseline
CNO
K
Tuning Index
Baseline
CNO
L
R²
Baseline
CNO
M
R²
Baseline
CNO
N
R² > 50%
Baseline
CNO
O
R² > 50%
Baseline
CNO
P
Width (R² > 50%)
Baseline
CNO
Q
Width (R² > 50%)
Baseline
CNO
R
Amplitude (R²>50%)
Baseline
CNO
S
Amplitude (R²>50%)
Baseline
CNO

**Figure 5.** Acute chemogenetic silencing of ABNs decreases spatial information content in the DG. A) Experimental timeline, including surgery, enriched environment, and in vivo imaging with chemogenetic silencing. B) Immunofluorescence images of HA-tag positive neurons (red) and DAPI labelled nuclei (blue). C) Schematic of contextual fear conditioning (CFC) task. Images of boxes used as context A and context B during behavior experiment. D) Percentage of time spent freezing in shocked and novel contexts (hM4Di-Ctx A vs Ctx B: p = 0.0015, nCtx A = 5 mice, nCtx B = 5 mice, hM4Di+ Ctx A vs Ctx B, p = 0.0484, nCtx A = 5 mice, nCtx B = 5 mice). E) Discrimination index of freezing between contexts (hM4Di-(control) vs hM4Di+: p = 0.0159, nhM4Di- = 5 mice, nhM4Di+ = 5 mice). Statistical analysis: Mann-Whitney U test. F, G) Fisher information (Baseline vs CNO: p = 0.00345, $n_{Baseline}$ = 9 mice, 471 neurons, $n_{CNO}$ = 9 mice, 461 neurons, Baseline vs CNO (control): p = 0.08291, $n_{Baseline}$ = 5 mice, 228 neurons, $n_{CNO}$ = 5 mice, 217 neurons). H, I) Activity (Baseline vs CNO: p = 0.00005, $n_{Baseline}$ = 9 mice, 471 neurons, $n_{CNO}$ = 9 mice, 461 neurons, Baseline vs CNO (control): p = 0.01964, $n_{Baseline}$ = 5 mice, 228 neurons, $n_{CNO}$ = 5 mice, 217 neurons). J, K) Tuning indices (Baseline vs CNO: p 0.0173, $n_{Baseline}$ = 9 mice, 471 neurons, $n_{CNO}$ = 9 mice, 461 neurons, Baseline vs CNO (control): p = 0.13226, $n_{Baseline}$ = 5 mice, 228 neurons, $n_{CNO}$ = 5 mice, 217 neurons). L, M) Goodness-of-fit (R2) of the Von Mises function to the tuning curves of all cells (Baseline vs CNO: p 0.44973, $n_{Baseline}$ = 9 mice, 471 neurons, $n_{CNO}$ = 9 mice, 461 neurons, Baseline vs CNO (control): p = 0.47035, $n_{Baseline}$ = 5 mice, 228 neurons, $n_{CNO}$ = 5 mice, 217 neurons). N, O) Goodness-of-fit of well-fitted cells (R2>0.5). (Baseline vs CNO: p = 0.00776, $n_{Baseline}$ = 9 mice, 471 neurons, $n_{CNO}$ = 9 mice, 461 neurons, nCNO = 5 mice, 319 neurons, Baseline vs CNO (control): p = 0.47035, $n_{Baseline}$ = 5 mice, 228 neurons, $n_{CNO}$ = 5 mice, 217 neurons). P, Q) Peak width of well fitted cells (Baseline vs CNO: p = 0.49976, $n_{Baseline}$ = 9 mice, 471 neurons, $n_{CNO}$ = 9 mice, 461 neurons, Baseline vs CNO (control): p = 0.17618, $n_{Baseline}$ = 5 mice, 228 neurons, $n_{CNO}$ = 5 mice, 217 neurons). R, S) Peak amplitude of well-fitted cells (Baseline vs CNO: p = 0.00636, $n_{Baseline}$ = 9 mice, 471 neurons, $n_{CNO}$ = 9 mice, 461 neurons, Baseline vs CNO (control): p = 0.3244, $n_{Baseline}$ = 5 mice, 228 neurons, $n_{CNO}$ = 5 mice, 217 neurons). Statistical analysis: Bootstrap. Error bars are mean ± SEM.

## Discussion

Adult neurogenesis is a unique type of brain plasticity that involves the addition of new neurons in response to environmental factors and other stimuli. In the years since ABNs were first reported in the rodent DG (Altman & Das, 1965), several studies have confirmed their presence in humans (Eriksson et al., 1998; Moreno-Jiménez et al., 2019; Zhou et al., 2022) and other species, characterized their cellular and physiological properties, and identified their different contributions to memory tasks. Despite this progress, the processes mediating the contribution of ABNs to behavior remain poorly understood, partially due to the technical difficulties of recording population activity in DG circuits in vivo. More recently, several studies made use of in vivo calcium imaging to determine how the DG encodes space, finding that a portion of DG neurons are spatially selective, although immature ABNs were less selective than their mature counterparts (Danielson et al., 2016; Hainmueller & Bartos, 2018; Tuncdemir et al., 2022). In this work we used a similar in vivo imaging approach to determine how the DG spatial code changes when adult neurogenesis is upregulated with EE or, conversely, when neurogenesis is ablated, or ABNs are silenced. We imaged naïve mice during their first exposure to a moving treadmill. Our results showed that 2 weeks of EE housing prior to imaging increases spatial information content in the DG (Fig. 1), and that this increase requires ABNs (Fig. 2). This change in neural representations following EE is a novel phenotype that potentially explains why EE and similar environmental manipulations are beneficial to memory and learning. We also found that ablating ABNs decreases spatial information content in the DG (Fig. 2D, 3F). We then showed that these ABN-driven changes are mediated by an increase in spatially selective activity at the single cell level (Fig. 4D, 4H). Furthermore, we described a potential dual mode of action for ABNs: increasing overall tuning selectivity and response gain of DG neurons, which in well-tuned cells results in an increase in activity specifically at the tuning maximum. Finally, we showed that ABN activity is required to elicit the changes in information content in the DG, as both tuning selectivity and spatial information were reduced after acutely silencing a cohort of immature ABNs (Fig. 5G, 5K).

Overall, these findings amount to a novel role for ABNs in modulating information encoding in the DG.

ABNs are thought to have a net inhibitory effect on DG activity (Anacker et al., 2018; Ikrar et al., 2013; Lacefield et al., 2012), which is regarded as beneficial for tasks such as contextual memory discrimination since the resulting increase in sparsity reduces the overlap between neuronal populations responding to different stimuli. The mechanisms behind this inhibitory action are not entirely understood, as immature ABNs are only poorly coupled to feedback inhibitory circuits in the DG (Groisman et al., 2020; Temprana et al., 2015). Our results stand in contrast with mechanistic models that propose an inhibitory effect of ABNs: we found that increasing the number of ABNs modulates the gain of DG neurons, leading to higher single-cell calcium activity rates (Fig. 4D). In addition, this increase in activity was spatially selective: it conveyed spatial tuning to otherwise untuned cells and increased spatial information of tuned cells by increasing activity near the peak more than at other locations. Our results do not necessarily mean that the net effect of ABNs in the DG is excitatory, since our analyses only considered neurons that were active during each imaging session while other studies found differences in the fraction of active neurons. It is possible that ABNs act to reduce the fraction of active DG neurons while at the same time increasing the firing rate of those same active neurons. Of note, a recent calcium imaging study found that voluntary exercise, which also increases adult neurogenesis, leads to increased calcium activity and spatial information in CA1 (Rechavi et al., 2022). Conversely, another study, using single unit electrophysiology recordings, found that silencing ABNs reduces population sparsity throughout hippocampal subfields, without affecting single-neurons spatial information (McHugh et al., 2022).

Since our AAV labeling approach targets all excitatory DG neurons, both mature DG neurons and immature ABNs will express the calcium sensor. The increase in single-cell calcium activity with EE could potentially be due to more ABNs being present in the field of view, their higher excitability resulting in increased calcium activity. However, this is unlikely, first because immature ABNs comprise a very small proportion (< 1%, (Kempermann et al., 1997)) of the total DG granule cell population, but also because they are less spatially tuned (Danielson et al., 2016), whereas we observed a significant increase in tuning. To further verify this, we replicated our results using a labeling approach that targets mature DG neurons specifically (Fig. S5).

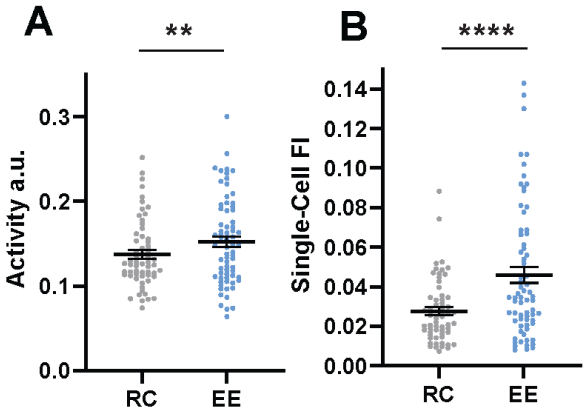


**Figure S5.** EE increases DG single-cell activity and spatial information in mice injected with a retro AAV virus in CA3. A) Activity (RC vs EE: p = 0.00143, nRC = 3 mice, 49 neurons, nEE = 3 mice, 69 neurons) and B) Fisher Information (RC vs EE: p < 1/100000, nRC = 3 mice, 49 neurons, nEE = 3 mice, 69 neurons) in mice injected with a retro AAV virus in CA3.

The positive correlation between neurogenesis and DG neuronal activity suggests that the contribution of ABNs to the DG neural code is not solely mediated by feedback inhibitory circuits. In addition to making weak connections to local interneurons, immature ABNs also form synapses with mossy cells, a population of excitatory neurons whose axonal arbors innervate large portions of the DG granule cell layer (Scharfman, 2016). It is possible that recurrent excitation through mossy cells may mediate the increase in tuning of DG neurons in mice with elevated adult neurogenesis. Our finding that ABNs act by modulating the gain of DG granule cells offers an additional clue about potential mechanisms. Gain modulation has been shown recently to

influence response variability in visual cortex (Coen-Cagli & Solomon, 2019) producing diverse effects depending on the stimulus and other factors (Verhoef & Maunsell, 2017). In our analysis, the gain increase induced by ABNs did not increase lap-by-lap variability of responses disproportionately, because if it did, then spatial information would decrease despite the higher response amplitude and tuning slope. ABNs may thus act by recruiting a network mechanism that simultaneously increases DG activity and stabilizes it by modulating the balance of recurrent excitation and inhibition (Echeveste et al., 2020; Heeger & Zemlianova, 2020; Ozeki et al., 2009).

In one set of experiments, we used irradiation as a method to ablate neurogenesis, which can result in increased inflammation and other side effects. We therefore resorted to a well-established method of focal irradiation (Tomé et al., 2015), and allowed a one-month period of recovery prior to imaging sessions to allow for inflammation to subside. Still, the side effects of irradiation (Chakraborti et al., 2012; Parihar & Limoli, 2013) could account for some of the changes observed in our study. To account for this, in separate experiments, we used a chemogenetic approach to acutely silence ABNs. We obtained similar results as in irradiated animals (Fig. 5), namely a loss of spatial information and reduction in neuronal activity when ABNs were silenced, although the effects of silencing were less pronounced than those of irradiation. This is likely because fewer neurons are targeted when using chemogenetics and, in addition, even neurons that express hM4Di will likely not be completely silenced by CNO administration. Our silencing approach used an inducible transgenic mouse line to express hM4Di in Ascl1 + progenitors that give origin to both DG and olfactory bulb (OB) ABNs. Silencing olfactory bulb ABNs could potentially result in decreased olfactory discrimination, which could in turn impact spatial tuning in the DG as the animals may also use olfaction to navigate the treadmill. However, our irradiation experiments showed a significant difference in spatial tuning when DG neurogenesis is selectively ablated and sub-ventricular zone neurogenesis is spared, therefore we do not expect that OB

ABNs contribute to DG spatial representations. Overall, our results are remarkably consistent across the two techniques used to induce a loss-of-function of immature ABNs.

Another potential caveat in our experiments is the use of the AAV vectors to deliver the jRGECO1a calcium sensor. Although AAVs have been widely used in a variety of neuroscience applications, including in-vivo calcium imaging, recent findings have demonstrated that intermediate progenitor cells and < 2-week-old ABNs can undergo apoptosis when targeted by AAVs (Johnston et al., 2021). To overcome this caveat, we optimized our protocol to limit the time between AAV injections and imaging. Nevertheless, we performed an additional control experiment using a retrograde AAV vector injected into hippocampal area CA3. The retrograde viral vectors were taken up by the axonal terminals of DG granule neurons, resulting in the expression of jRGECO1a in the ipsilateral granule layer while preserving similar numbers of ABNs in the injected and contralateral hemispheres. Using this approach, we were able to confirm that housing mice in EE elicited an increase in calcium activity and spatial information content in the DG (Fig. S5). Importantly, in this control experiment no immature (<6 weeks-old) ABNs were labeled, since their axons had not reached CA3 at the time of the viral injection. This confirms that the changes in neuronal activity leading to improved spatial coding occur in the mature granule cells, and not only in the immature ABNs.

In our analysis of the factors that contribute to spatial encoding, we found that noise correlations between neurons either had no effect on spatial information content or were even detrimental to it (Fig 3A-D). This suggests that noise correlations might limit the amount of spatial information encoded by the DG, similar to recent results in CA1 (Hazon et al., 2022), although one caveat is that we imaged a relatively low number of active cells when compared with the entirety of the DG

coding space, as DG activity is very sparse. Our result is different from, but not incompatible with, a related finding in DG (Stefanini et al., 2020), which showed that knowing the structure of noise correlations helps to correctly decode the available information (Averbeck et al., 2006; Kanitscheider et al., 2015). Furthermore, in our data the effects of noise correlation do not appear to be qualitatively modulated by adult neurogenesis, namely, the action of ABNs did not induce a switch from detrimental to beneficial noise correlations. Nonetheless, we observed some quantitative differences between the effects of correlations in RC and EE animals; larger population recordings will be needed to reveal how much this difference contributes to the overall effect of adult neurogenesis on spatial information.

While our work focused on spatial information, several types of neuronal coding modalities likely coexist in the DG. Neurons in the dorsal DG encode not only position, but also direction of motion, speed (Danielson et al., 2016; Stefanini et al., 2020), as well as other sensory cues (Hainmueller & Bartos, 2018; Tuncdemir et al., 2022), and a population of stress-responsive cells has also been found in the ventral DG (Anacker et al., 2018). It is therefore possible that ABNs have different effects on the encoding of different sensory features or contexts, so recordings in the ventral DG or during specific behavioral tasks may reveal different functional roles for ABNs. Alternatively, the gain amplification effect we identified could generalize beyond spatial information and improve encoding across other modalities.

In summary, our results indicate that adult neurogenesis leads to increased response gain in the DG, improving the ability of the granule cells to tune to spatial features and therefore improving spatial information encoding. Our findings demonstrate that the spatial information content in the DG can be modulated even by brief environmental manipulations, such as EE housing, that result

in changes in the number of ABNs. The increased spatial information and resulting improvement in the accuracy of neural representations of space in mice with elevated neurogenesis provide a novel mechanistic, circuit-level explanation for their improved performance at many spatial memory tasks (Garthe & Kempermann, 2013). Furthermore, our findings provide novel directions for the study of how ABNs contribute to memory, identifying new modes of action that could be harnessed as a therapeutic target for memory disorders.

## Chapter 4 – The role of ABNs in the hippocampal network

### Noise correlations limit spatial information encoding in CA1.

In chapter 3, we found that increasing hippocampal adult neurogenesis results in an increase of spatial information and calcium activity in the DG. We then asked whether the role of adult born neurons in neuronal representations of space is limited exclusively to local circuitry in the granule cell layer of the DG, or if broader effects can be observed across the hippocampus. To answer this question, we imaged calcium activity both in CA1 pyramidal cells and Mossy Cells of the hilus, in the same animals we imaged calcium activity in DG. Briefly, to manipulate the number of adult-born neurons we exposed 8-week-old mice to 2 weeks of environmental enrichment (EE), which is known to increase the number of adult-born neurons (Kempermann et al., 1997), or focal irradiation, to permanently ablate the number of adult-born neurons in the hippocampus (Chapter 3 Fig 2, C). We recorded calcium activity of pyramidal neurons in CA1 and Mossy Cells using in vivo 2-photon microscopy in awake moving animals head-fixed to a treadmill (Chapter 3 Fig. 1, A-C). As previously reported (Chapter 3 Fig. 1, C), EE animals exhibited a ~2-fold increase in doublecortin (DCX) positive neurons. CA1 activity rates were similar to previous findings (Dong et al., 2021) with an average of 269 cells active over a 9 min imaging session in a 343 μm x 343 μm field of view, resulting in 52.6% active of all putative labeled neurons. To determine the spatial information content in CA1 we trained a linear decoder to estimate the position of the animal on the treadmill base on the calcium traces recorded (75% - 25% train and tested to avoid overfitting). Data was subsampled to account for the variability in number of neurons per mouse. Due to the small number of Mossy Cells recorded per mouse within the field of view, the linear decoder was not trained in this dataset. We found no significant difference in the spatial information content in CA1 in animals exposed to EE or focal irradiation using our linear decoder (Fig. 1 D). The linear decoder captures the population coding of the firing neurons regardless of their spatial tuning capabilities, by considering the correlations between pairs of active neurons. We then asked

whether these noise correlations could be having a detrimental effect on the spatial information content in the DG. We removed noise correlation effects in the dataset by shuffling activity in each trial independently, preserving the tuning specificity of each individual neuron. We measured linear Fisher information (which is a measure of the population sensitivity to a spatial location, equivalent to d-prime (Kanitscheider et al., 2015) as a way to better assess population wide effects compared to the linear decoder (Kafashan et al., 2021). Upon removing noise correlations, we found a significant increase in population Fisher information in mice exposed to regular cage conditions, regular cage conditions with prior focal irradiation and EE (Fig. 1 E). Overall, these results suggest that manipulating the number of adult-born neurons results in no effects at the population level. This result may be driven by the information-limiting effects of noise correlations present in CA1 (Hazon et al., 2022).

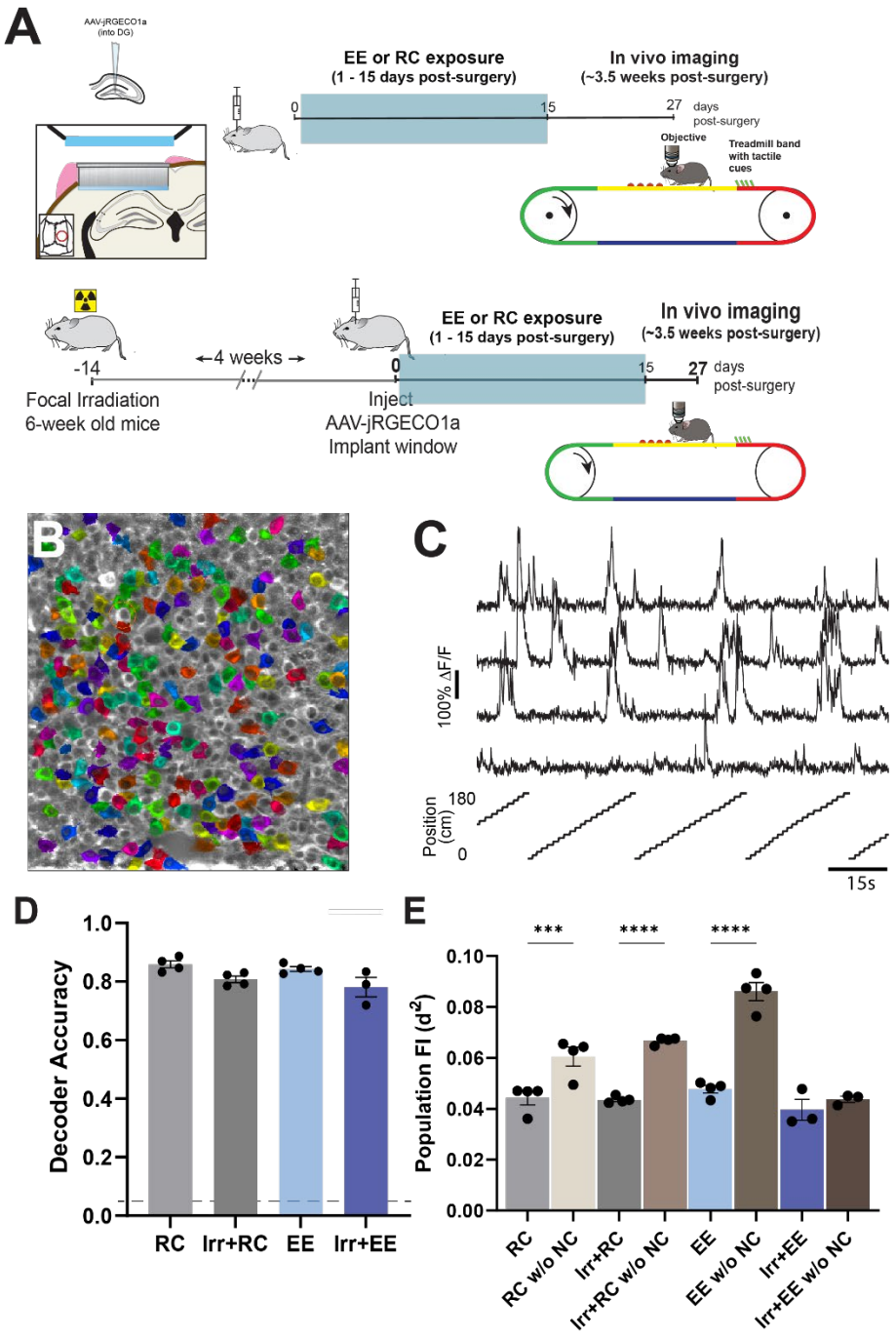


**Figure 1.** Removing noise correlations increases spatial information content in CA1. A) Experimental timeline, including surgery, enriched environment, and in vivo imaging for non-irradiated (top) and irradiated experiments (bottom). B) Example of calcium imaging field of view. C) Example calcium traces (top) and respective position of animal on the treadmill (bottom). D) Accuracy in decoding position of mouse on treadmill from calcium traces (RC vs EE: $p > 0.99$, RC vs Irr+RC, $p = 0.3776$, EE vs Irr+EE: $p = 0.5529$, ANOVA, Bonferroni correction for multiple comparisons, $n_{RC} = 4$ mice, $n_{Irr+RC} = 4$, $n_{EE} = 4$, $n_{Irr+EE} = 3$ mice, 56 cells subsampled per mouse), dotted line is chance performance level (0.05). E) Population Fisher information determined with noise correlations and after random shuffling to disrupt noise correlations (RC vs RC w/o NC: $p = 0.0010$, n = 4 mice per group, EE vs EE w/o NC: $p < 0.0001$, n = 4 mice per group, Irr+RC vs Irr+RC w/o NC: $p < 0.0001$, n = 4 mice per group, Irr+EE vs Irr+EE w/o NC: $p = 0.9338$, n = 3 mice per group, ANOVA, Bonferroni correction for multiple comparisons).

Ablating adult neurogenesis reduces spatial information content and tuning in CA1.

We then asked whether manipulation of adult-born neurons could result in changes at the single cell level. We first calculated single-cell Fisher information as a measure of spatial information content per neuron. Exposure to EE resulted in a significant increase in single-cell Fisher information compared to mice housed in regular caged conditions (Fig. 2 A). Conversely, exposure to focal irradiation resulted in a decrease in information content in mice housed in regular caged conditions compared to their non-irradiated counterparts (Fig. 2 A). Single-cell spatial information content was also significantly decreased in focally irradiated mice with prior exposure to EE, suggesting the effects in spatial information content in CA1 could be driven primarily by adult born neurons (Fig. 2 A). We next measured the tuning specificity of individual neurons in CA1. Exposure to focal irradiation resulted in a significant decrease in tuning in mice housed in regular cage conditions and EE compared to their non-irradiated counterparts. A decrease in tuning specificity was also observed in mice with prior exposure to EE (Fig. 2 B). To further understand how adult-born neurons affect spatial information content in CA1 we measured both the calcium activity rates and the tuning curve properties of each individual cell. We found a significant increase in activity in mice exposed to EE. A significant increase in activity was also observed in mice housed in regular cages, but not in EE, that received prior focal irradiation (Fig. 2 C, D). To analyze the tuning curve properties, we fit our data to a Von Mises function and analyzed the goodness of fit, width and amplitude of the tuning curves. Exposure to focal irradiation resulted in a significant decrease in both the goodness of fit of all individual neurons regardless of their tuning specificity and of the well-tuned cells defined by an R2 of 50% or above (Fig. 2 E, F). No changes were observed in either the amplitude or the width of the tuning curves (Fig. 2 G-H). Exposure to EE also resulted in a significant decrease in the goodness of fit overall as well as when comparing only well-tuned cells (Fig. 2 E-F). Yet, a significant decrease in the width of the tuning curve peaks was also observed (Fig. 2 G). Overall, we show that adult born neurons are necessary to maintain normal levels of spatial information content in CA1.

Mechanistically, we suggest that adult-born neurons mediate the levels of tuning specificity of CA1 pyramidal cells by regulating the signal to noise ratio of individual neurons. Increased numbers of adult born neurons resulted in an increase in spatial information content. This could be explained by the observed narrowing of the tuning curves. Yet, we also observed a decrease in tuning specificity and increase in noise which suggest additional mechanisms involved.

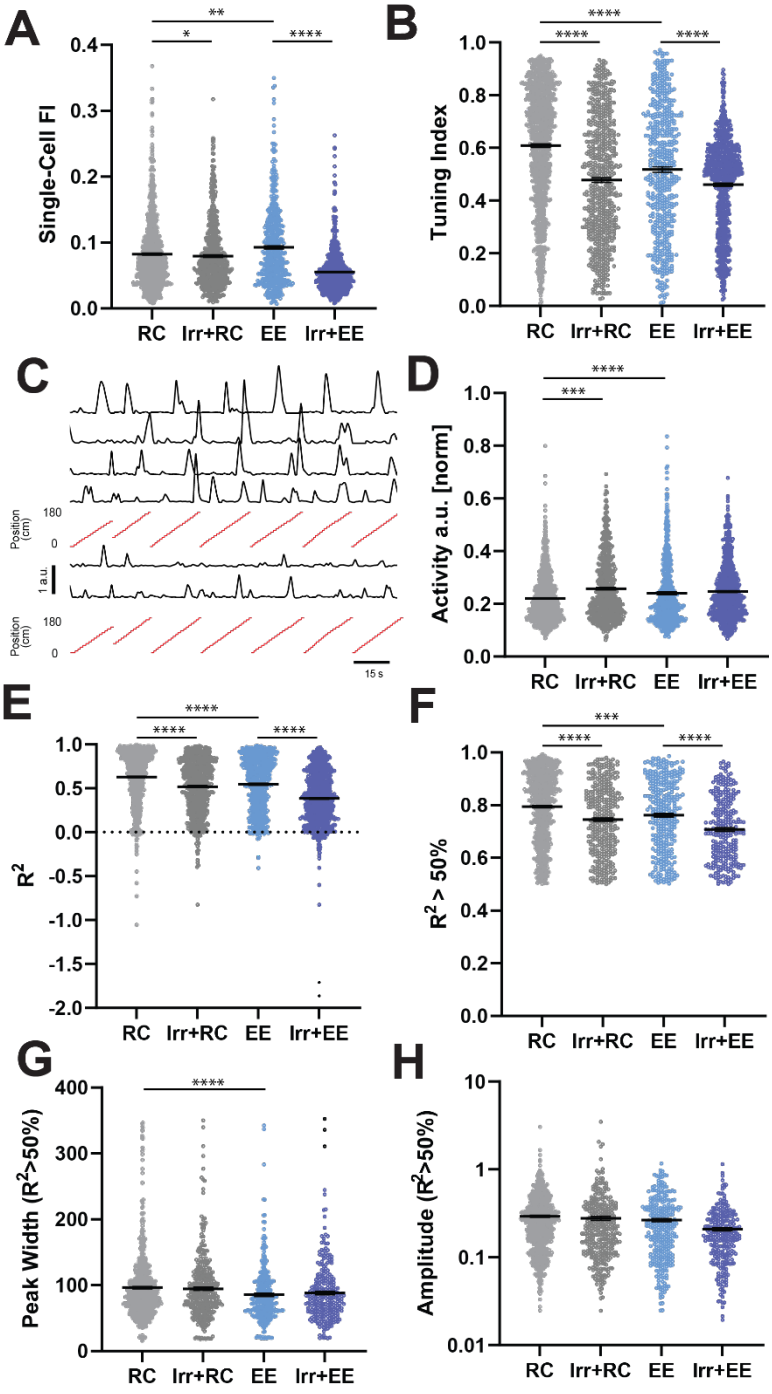

**Figure 2.** Ablating adult neurogenesis reduces spatial information content and tuning in CA1. A) Single-cell spatial information content determined using Fisher information (FI) (RC vs EE: p = 0.00123, $n_{RC}$ = 4 mice, 1075 neurons, $n_{EE}$ = 5 mice, 534 neurons, RC vs Irr+RC: p = 0.0267, $n_{RC}$ = 4 mice, 1075 neurons, $n_{Irr+RC}$ = 4 mice, 666 neurons, EE vs Irr+EE: p = < 1/100000, $n_{EE}$ = 5 mice, 534 neurons, $n_{Irr+EE}$ = 3 mice, 781 neurons). B) Tuning indices of cells in non-irradiated and irradiated groups (RC vs EE: p < 1/100000, $n_{RC}$ = 4 mice, 1075 neurons, $n_{EE}$ = 5 mice, 534 neurons, RC vs Irr+RC: p < 1/100000, $n_{RC}$ = 4 mice, 1075 neurons, $n_{Irr+RC}$ = 4 mice, 666 neurons, EE vs Irr+EE: p < 1/100000, $n_{EE}$ = 5 mice, 534 neurons, $n_{Irr+EE}$ = 3 mice, 781 neurons). C) Examples of cells with high (top) and low (bottom) tuning indices. D) Activity measured as integrated calcium traces normalized to distance travelled (RC vs EE: p = 0.00006, $n_{RC}$ = 4 mice, 1075 neurons, $n_{EE}$ = 5 mice, 534 neurons, RC vs Irr+RC: p < 1/100000, $n_{RC}$ = 4 mice, 1075 neurons, $n_{Irr+RC}$ = 4 mice, 666 neurons, EE vs Irr+EE: p > 0.9999, $n_{EE}$ = 5 mice, 534 neurons, $n_{Irr+EE}$ = 3 mice, 781 neurons). E) Cross-validated goodness of fit ($R^2$) of tuning curves (RC vs EE: p < 1/100000, $n_{RC}$ = 4 mice, 1075 neurons, $n_{EE}$ = 5 mice, 534 neurons, RC vs Irr+RC: p < 1/100000, $n_{RC}$ = 4 mice, 1075 neurons, $n_{Irr+RC}$ = 4 mice, 666 neurons, EE vs Irr+EE: p < 1/100000, $n_{EE}$ = 5 mice, 534 neurons, $n_{Irr+EE}$ = 3 mice, 781 neurons). F) Cross-validated goodness of fit ($R^2$) of tuning curves of well-fitted cells ($R^2$ > 50%) (RC vs EE: p = 0.00069, $n_{RC}$ = 4 mice, 757 neurons, $n_{EE}$ = 5 mice, 323 neurons, RC vs Irr+RC: p < 1/100000, $n_{RC}$ = 4 mice, 757 neurons, $n_{Irr+RC}$ = 4 mice, 375 neurons, EE vs Irr+EE: p < 1/100000, $n_{EE}$ = 5 mice, 323 neurons, $n_{Irr+EE}$ = 3 mice, 282 neurons). G) Peak width of tuning curves of well-fitted cells (RC vs EE: p = 0.00006, $n_{RC}$ = 4 mice, 757 neurons, $n_{EE}$ = 5 mice, 323 neurons). H) Peak amplitude of well-fitted cells. Statistical analysis: Bootstrap and Bonferroni correction for multiple comparisons (See Methods). Error bars: mean ± SEM. * p<0.1, ** p<0.001, *** p<0.0001, ****p<0.00001.

Effects of adult neurogenesis in Mossy Cells.

We next asked whether manipulating the number of adult-born neurons results in changes in spatial information content in Mossy Cells. Animals with prior focal irradiation and exposure to EE had a significant decrease in spatial information content, as measured using single-cell Fisher information, compared to their EE-exposed counterparts (Fig. 3 A-C). This cohort also presented no change in overall calcium activity rates (Fig. 3 D) and a significant decrease in the complexity of the tuning curves as shown by the decrease in goodness of fit of both unimodal and bimodal tuning curves (Fig. 3 E-F). Animals housed in regular cages exposed to prior focal irradiation had no change in spatial information content (Fig. 3 C), a significant increase in overall calcium activity rates (Fig. 3 D) and a significant increase in the complexity of their tuning properties (Fig. 3 E-F). Increasing the number of adult-born neurons resulted in a significant decrease in spatial information content compared to their regular caged counterparts (Fig. 3 C). Overall, these results either suggest a dependency on the number of adult-born neurons in DG prior to ablation or the presence of off target effects that were not measured. If there is an increased number of neurons prior to irradiation, the ablation had a negative role in the spatial function of mossy cells and the

loss of spatial information content may be driven by a loss in the complexity of the tuning curves. If the number of ABNs is lower prior to ablation, Mossy Cells present increased the complexity of their tuning curves potentially driven by an increase in the overall activity. It is worth noting this is the first study that attempted to manipulate ABNs and analyze mossy cell responses in vivo. Future studies refining the in vivo paradigm will be important to fully parse out these effects.

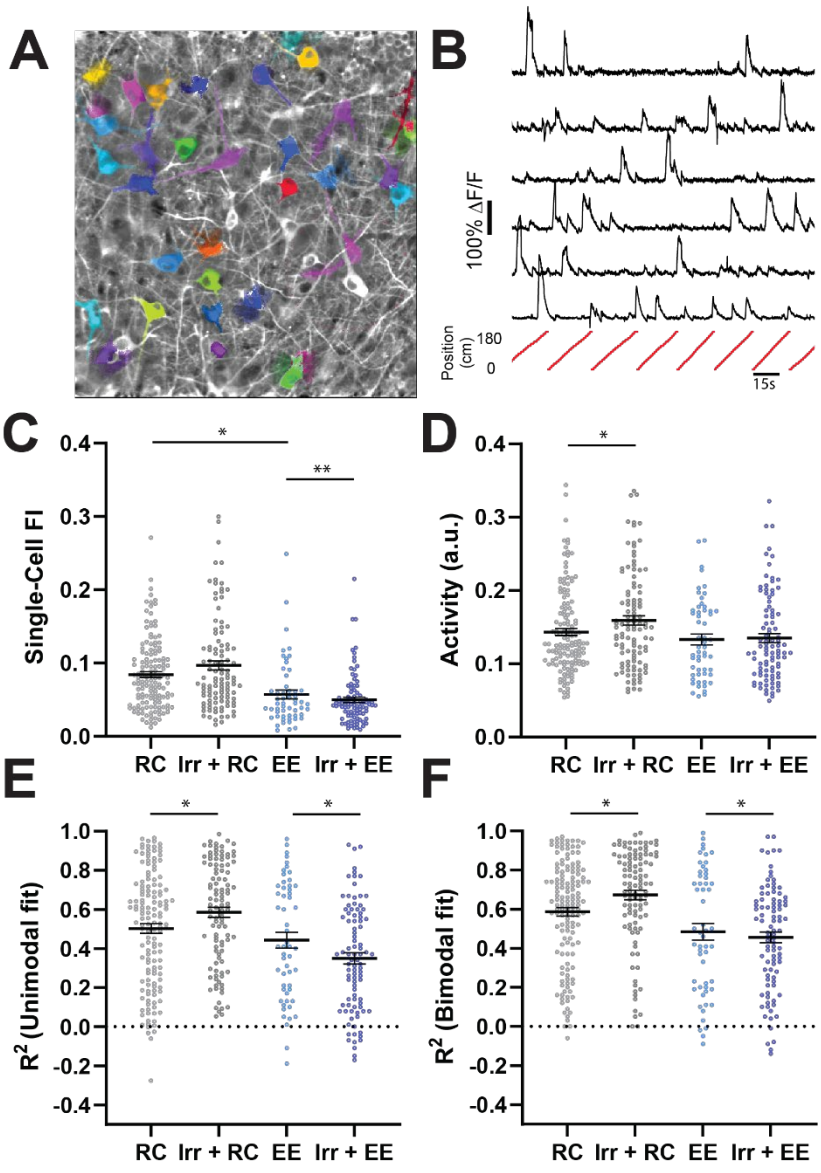

**Figure 3.** Ablating adult neurogenesis results in confounding effects in Mossy Cells. A) Example of Mossy Cell calcium imaging field of view. B) Example calcium traces (top) and respective position of animal on the treadmill (bottom). C) Single-cell spatial information content determined using Fisher information (FI) (RC vs EE: p = 0.03144, $n_{RC}$ = 5 mice, 143 neurons, $n_{EE}$ = 5 mice, 56 neurons, EE vs Irr+EE: p = 0.01599, $n_{EE}$ = 5 mice, 56 neurons, $n_{Irr+EE}$ = 3 mice, 94 neurons). D) Activity measured as integrated calcium traces normalized to distance travelled (RC vs Irr+RC: p = 0.01455, $n_{RC}$ = 5 mice, 143 neurons, $n_{Irr+RC}$ = 4 mice, 108 neurons). E) Unimodal Cross-validated goodness of fit ($R^2$) of tuning curves (RC vs Irr+RC: p = 0.0282, $n_{RC}$ = 5 mice, 143 neurons, $n_{Irr+RC}$ = 4 mice, 108 neurons, EE vs Irr+EE: p = 0.04482, $n_{EE}$ = 5 mice, 56 neurons, $n_{Irr+EE}$ = 3 mice, 94 neurons). F) Bimodal Cross-validated goodness of fit ($R^2$) of tuning curves of well-fitted cells ($R^2$ > 50%) (RC vs Irr+RC: p = 0.02811, $n_{RC}$ = 5 mice, 143 neurons, $n_{Irr+RC}$ = 4 mice, 108 neurons, EE vs Irr+EE: p = 0.04725, $n_{EE}$ = 5 mice, 56 neurons, $n_{Irr+EE}$ = 3 mice, 94 neurons). Statistical analysis: Bootstrap and Bonferroni correction for multiple comparisons (See Methods). Error bars: mean ± SEM. * p<0.1, ** p<0.001, *** p<0.0001, ****p<0.00001.

Acute chemogenetic silencing of ABNs and spatial information content in CA1 and Mossy Cells.

We next asked whether the changes in CA1 and mossy cells observed were dependent on adult-born neuron firing, rather than potential side effects or irradiation. To answer this question, we used an Ascl1-CreERT2 knock-in mouse line (E. J. Kim et al., 2011) crossed with a line expressing the inhibitory DREADD hM4Di (Roth, 2016; Zhu et al., 2016) in a Cre-dependent manner, which allows us to target adult-born neurons specifically for acute silencing. Animals were injected with tamoxifen for 3 days and later exposed to an EE (Fig. 4 A). Results show no significant difference in the parameters measured comparing the experimental cohort and hM4Di controls (Fig. 4 B-O). It is possible that due to experimental paradigm and exposure to a novel environment, significant development of place cell formation in CA1 may have been captured in the first session (J. D. Cohen et al., 2017) and therefore occluded any potential changes due to adult-born neuron silencing. Future analysis could include the use of familiar environments to bypass the initial spatial learning processes.

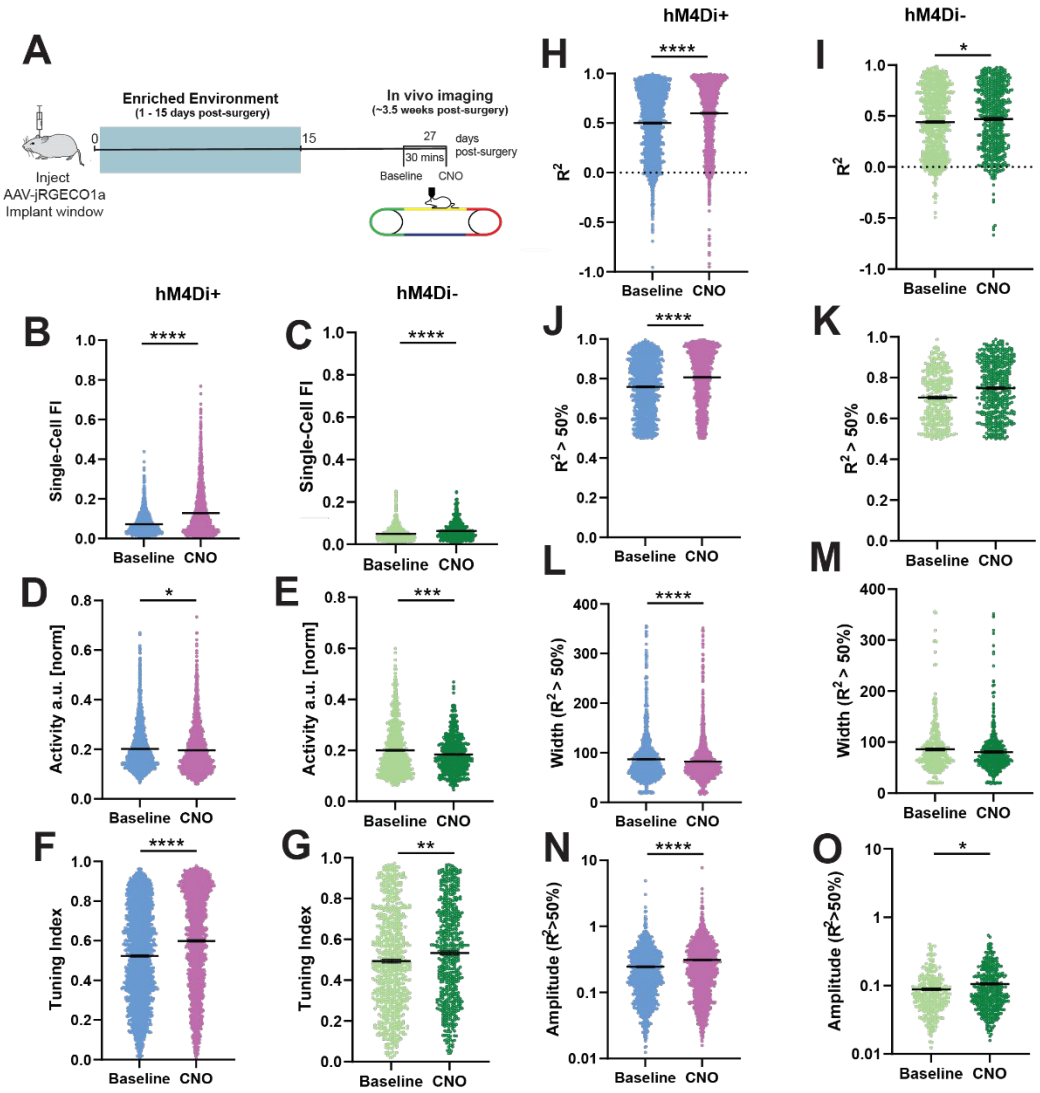


**Figure 4.** Acute chemogenetic silencing of ABNs has no effect on spatial information content in CA1 with this experimental paradigm. A) Experimental timeline, including surgery, enriched environment, and in vivo imaging with chemogenetic silencing. B, C) Single-cell Fisher information (Baseline vs CNO: $p < 1/100000$, $n_{Baseline}$ = 9 mice, 2242 neurons, $n_{CNO}$ = 9 mice, 2085 neurons, Baseline vs CNO (control): $p < 1/100000$, $n_{Baseline}$ = 3 mice, 744 neurons, $n_{CNO}$ = 3 mice, 578 neurons). D, E) Activity (Baseline vs CNO: $p = 0.0102$, $n_{Baseline}$ = 9 mice, 2242 neurons, $n_{CNO}$ = 9 mice, 2085 neurons, Baseline vs CNO (control): $p = 0.00087$, $n_{Baseline}$ = 3 mice, 744 neurons, $n_{CNO}$ = 3 mice, 578 neurons). F, G) Tuning indices (Baseline vs CNO: $p < 1/100000$, $n_{Baseline}$ = 9 mice, 2242 neurons, $n_{CNO}$ = 9 mice, 2085 neurons, Baseline vs CNO (control): $p = 0.0015$, $n_{Baseline}$ = 3 mice, 744 neurons, $n_{CNO}$ = 3 mice, 578 neurons). H, I)) Goodness-of-fit (R2) of the Von Mises function to the tuning curves of all cells (Baseline vs CNO: $p < 1/100000$, $n_{Baseline}$ = 9 mice, 2242 neurons, $n_{CNO}$ = 9 mice, 2085 neurons, Baseline vs CNO (control): $p = 0.05426$, $n_{Baseline}$ = 3 mice, 744 neurons, $n_{CNO}$ = 3 mice, 578 neurons). J, K) Goodness-of-fit of well-fitted cells (R2>0.5). (Baseline vs CNO: $p < 1/100000$, $n_{Baseline}$ = 9 mice, 1241 neurons, $n_{CNO}$ = 9 mice, 1384 neurons, Baseline vs CNO (control): $p = 0.27412$, $n_{Baseline}$ = 3 mice, 328 neurons, $n_{CNO}$ = 3 mice, 428 neurons). L, M) Peak width of well fitted cells (Baseline vs CNO: $p = 0.00938$, $n_{Baseline}$ = 9 mice, 1241 neurons, $n_{CNO}$ = 9 mice, 1384 neurons, Baseline vs CNO (control): $p = 0.02914$, $n_{Baseline}$ = 3 mice, 328 neurons, $n_{CNO}$ = 3 mice, 428 neurons). N, O) Peak amplitude of well-fitted cells (Baseline vs CNO: $p < 1/100000$, $n_{Baseline}$ = 9 mice, 1241 neurons, $n_{CNO}$ = 9 mice, 1384 neurons, Baseline vs CNO (control): $p = 0.37731$, $n_{Baseline}$ = 3 mice, 328 neurons, $n_{CNO}$ = 3 mice, 428 neurons). Statistical analysis: Bootstrap and Bonferroni correction for multiple comparisons (See Methods). Error bars: mean ± SEM. * $p<0.1$, ** $p<0.001$, *** $p<0.0001$, ****$p<0.00001$.

Overall, significant changes were not observed when we silenced adult born neurons and recorded the activity of Mossy Cells (Fig. 5 A-H). We conclude the paradigm used did not elicit the effects expected.

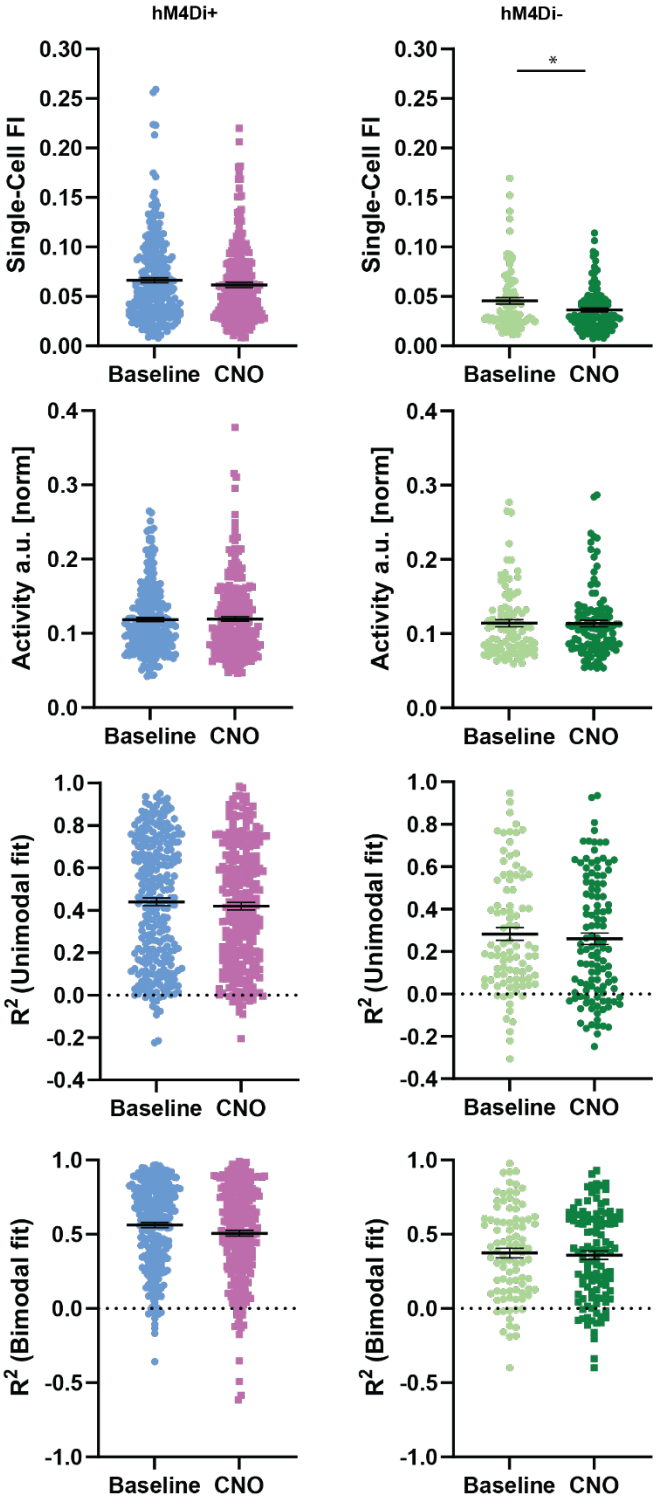

**Figure 5.** Acute chemogenetic silencing of ABNs has no effect on spatial information content in Mossy Cells in this experimental paradigm. A, B) Single-cell Fisher information (Baseline vs CNO: p = 0.10781, $n_{Baseline}$ = 9 mice, 270 neurons, $n_{CNO}$ = 9 mice, 263 neurons, Baseline vs CNO (control): p = 0.01241, $n_{Baseline}$ = 5 mice, 91 neurons, $n_{CNO}$ = 5 mice, 114 neurons). C, D) Activity (Baseline vs CNO: p = 0.43279, $n_{Baseline}$ = 9 mice, 270 neurons, $n_{CNO}$ = 9 mice, 263 neurons, Baseline vs CNO (control): p = 0.46389, $n_{Baseline}$ = 5 mice, 91 neurons, $n_{CNO}$ = 5 mice, 114 neurons). E, F) Unimodal Goodness-of-fit (R2) of the Von Mises function to the tuning curves of all cells (Baseline vs CNO: p = 0.21562, $n_{Baseline}$ = 9 mice, 270 neurons, $n_{CNO}$ = 9 mice, 263 neurons, Baseline vs CNO (control): p = 0.28661, $n_{Baseline}$ = 5 mice, 91 neurons, $n_{CNO}$ = 5 mice, 114 neurons). G, H) Bimodal Goodness-of-fit (R2) of the Von Mises function to the tuning curves of all cells (Baseline vs CNO: p = 0.21596, $n_{Baseline}$ = 9 mice, 270 neurons, $n_{CNO}$ = 9 mice, 263 neurons, Baseline vs CNO (control): p = 0.2860, $n_{Baseline}$ = 5 mice, 91 neurons, $n_{CNO}$ = 5 mice, 114 neurons). Statistical analysis: Bootstrap and Bonferroni correction for multiple comparisons (See Methods). Error bars: mean ± SEM. * p<0.1, ** p<0.001, *** p<0.0001, ****p<0.00001.

Chemogenetic silencing of Mossy Cells decreases tuning specificity in DG granule cells.

Previous studies suggested that Mossy Cells contribute to the maintenance of sparse DG activity, as well as to context discrimination and spatial memory (Danielson et al., 2017). Mossy cells synapse onto DG neurons as well as establish monosynaptic connections onto interneurons which then have an inhibitory effect in DG (Scharfman, 2016). We therefore asked whether Mossy Cells could have a role in neuronal representations of space in DG. To answer this question, we silenced Mossy Cells using a combination of Drd2-Cre mice and a retrograde Cre-dependent AAV to selectively express hM4Di in Mossy Cells injected in the contralateral hemisphere. This preliminary study shows that silenced Mossy Cells displayed a slight non-significant decrease in their overall calcium activity rates. In addition, calcium imaging in the DG revealed no difference in spatial information content, but a significant difference in tuning specificity (Fig. 6 A-D). The loss of Mossy Cells is a major characteristic of temporal lobe epilepsy (Blümcke et al., 2000). During the onset of an epileptic seizure, Mossy Cell activity increases significantly (Nasrallah et al., 2022). Silencing Mossy Cells results in a decrease in spatial context encoding in mice (Bui et al., 2018), which is in line with our preliminary finding showing decreased spatial tuning in DG (Fig. 6, C).

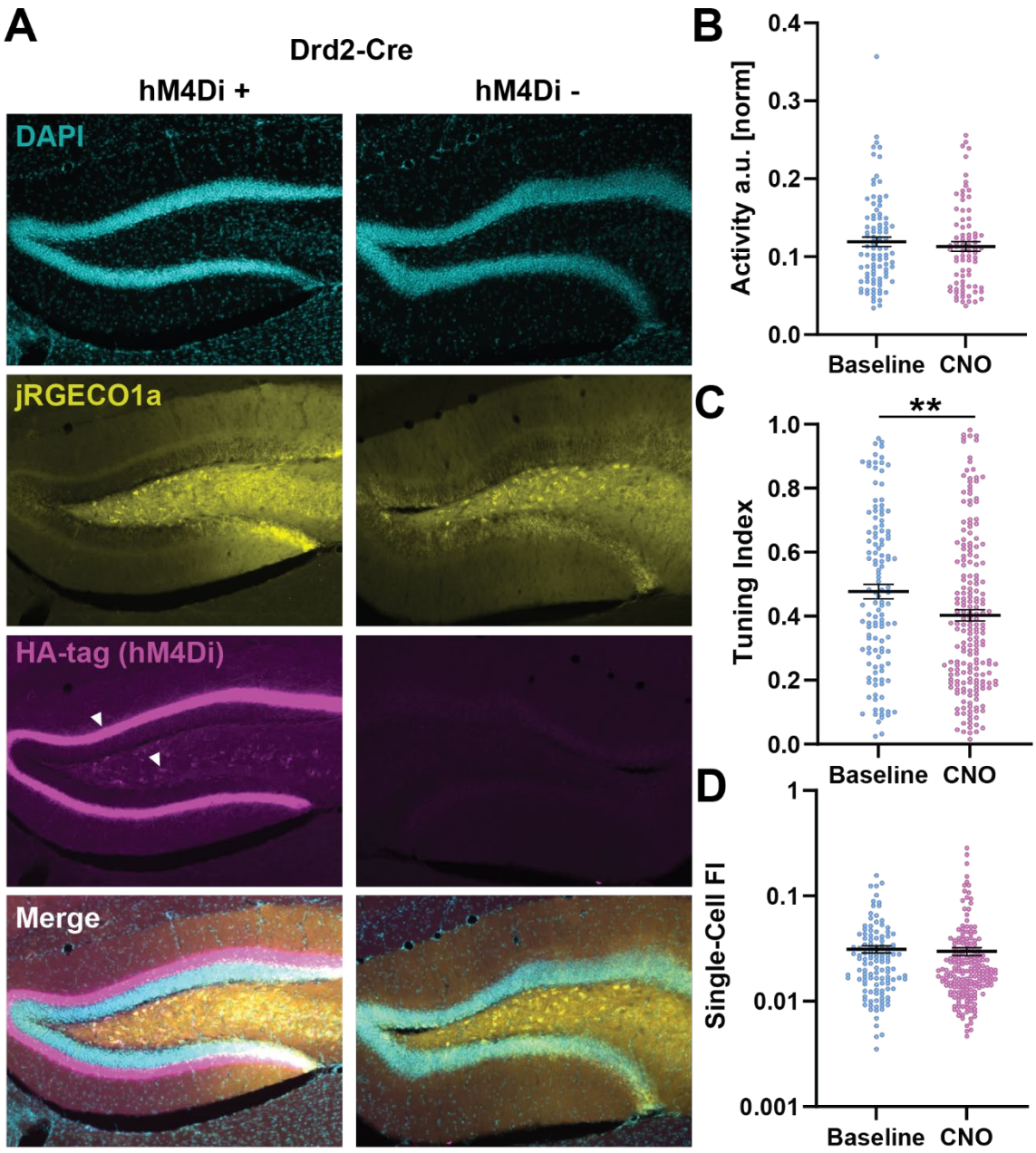


**Figure 6.** Chemogenetic silencing of Mossy Cells decreases tuning specificity in DG granule cells. A) Immunofluorescence images of HA-tag positive neurons (pink), jRGECO1a (yellow) and DAPI (blue) labelled nuclei (left: hM4Di +, right: hM4Di - (controls). B) Mossy Cell activity (Baseline vs CNO: p = 0.0755, $n_{Baseline}$ = 3 mice, 93 neurons, $n_{CNO}$ = 3 mice, 78 neurons). C) Single-cell Fisher information (Baseline vs CNO: p = 0.29702, $n_{Baseline}$ = 3 mice, 93 neurons, $n_{CNO}$ = 3 mice, 78 neurons). D) Tuning indices (Baseline vs CNO: p = 0.00256, $n_{Baseline}$ = 3 mice, 93 neurons, $n_{CNO}$ = 3 mice, 78 neurons). Statistical analysis: Bootstrap and Bonferroni correction for multiple comparisons (See Methods). Error bars: mean ± SEM. * p<0.1, ** p<0.001, *** p<0.0001, ****p<0.00001.

Taken all together, these results suggest that neuronal representations of space in CA1 are partially dependent on adult-born neurons. We showed that adult-born neurons are necessary to maintain normal levels of spatial information and a potential mechanism could include the mediation of adult-born neurons in the tuning specificity and noise in the network. To the extent that Mossy Cells themselves support the formation of neuronal representations of space, we found that adult-born neurons can influence the properties of these representations. Still, future studies will need to further elucidate its potential mechanisms. Finally, preliminary results suggest that DG excitatory feedback circuits via mossy cells may contribute to spatial information encoding in the DG supporting a potential role of Mossy Cells in neural representations of space in the DG.

Discussion

In chapter 1 we found adult neurogenesis leads to an increased response gain in the DG, improving the ability of the granule cells to tune to spatial features and therefore improving spatial information encoding. In this chapter we ask whether ABN's modulatory role extends into the hippocampal network. We focused our study on CA1, the output region of the hippocampus involved primarily in the integration of signals from CA3 and directly from EC (Van Strien et al., 2009). CA1 is involved in spatial processing and memory, it can tune is firing to specific locations in space and it can code associations between objects (Komorowski et al., 2009; Moser et al., 2015). We first asked whether ABNs have a role in the neuronal representations of space in CA1. Using in vivo 2-photon calcium imaging we recorded neuronal activity from CA1 while animals were head-fixed under the microscope on a treadmill. We found that mice that were previously housed in an enriched environment, which triggers an increase in neurogenesis, exhibited an increase in spatial information content. Ablating adult neurogenesis by prior focal irradiation resulted in a decrease in spatial information content potentially driven by the overall increase in noise in the tuning curves of pyramidal cells. Although we observed no change in the amplitude of the place-specific responses in animals with prior exposure to enriched environment, we did find a decrease in the width of these responses, which could point to a potential mechanism of modulation of the system by ABNs. Still, the increase in overall noise observed could indicate additional mechanisms at play in CA1 that have yet to be fully parsed out. In chapter 1, we also found that both ablating neurogenesis and silencing adult-born neurons decreased the calcium activity rates of DG granule cells, resulting in a decreased amplitude of place-specific responses. These findings contrast previous studies that suggested a predominantly inhibitory action of adult-born neurons. We therefore asked whether the contribution of ABNs to the hippocampal neural code is not solely mediated by feedback inhibitory circuits. In addition to making weak connections to local interneurons, immature ABNs also form synapses with mossy cells, a population of excitatory neurons whose axonal arbors innervate large portions of the DG granule cell layer

(Scharfman, 2016). It is possible that recurrent excitation through mossy cells may mediate the increase in tuning of DG neurons in mice with elevated adult neurogenesis. Ablating adult neurogenesis in animals with prior exposure to an enriched environment showed a decrease in spatial information content when compared to their non-irradiated counterparts. Spatial tuning was also reduced as observed by a reduction in both unimodal and bimodal place-specific responses. Conversely, animals housed in regular cage conditions with prior exposure to focal irradiation exhibited an increase in spatial information content and complexity of the place-specific responses. These results, together with the fact we were unable to elicit an observable effect in mossy cells using our chemogenetic approach, are inconclusive. Yet, preliminary studies silencing mossy cells, resulted in a significant decrease in spatial tuning in DG, suggesting a potential role of mossy cells in spatial information encoding in the hippocampus, but how ABNs are driving this effect remains to be understood.

Our findings show that ablation of ABNs results in a decrease in spatial information content in CA1, primarily driven by an increase in overall noise. These findings are in line with McHugh et. al. that showed silencing of ABNs resulted in a decrease in population sparsity in CA1 (McHugh et al., 2022), which is important to optimize capacity and reduce interference between co-existing representations of space (Denève & Machens, 2016). Another study that exposed animals to exercise, which increases adult neurogenesis, lead to increased calcium activity and spatial information in CA1 (Rechavi et al., 2022). In our study, we also observed an increase in calcium activity and single-cell spatial information content. We did not observe differences in population spatial information. Our decoder results in CA1 showed no significant difference by either ablation of adult neurogenesis or exposure to enriched environment. Future analysis of this data could be done by running the decoder and subsampling for different numbers of cells. Correlating number of cells subsampled with the accuracy of the decoder for each group could help us understand whether there are changes in the loss of accuracy between our ablated and exposed to EE mice.

An additional analysis could look at what is the contribution of the tuned and untuned cells by running the decoder separately for each group. This analysis could allow us to determine what are the cells that are contributing the most to the accuracy of the decoder and if there are any changes between experimental groups that could give us clue on how the hippocampus represents spatial information. Similar to the loss of CA1 untuned cells coding discrimination in Alzheimer's disease (Zhang et al., 2022). We would expect that the decoding accuracy of lower tuned CA1 pyramidal cells will decrease in mice with ablated neurogenesis.

Our analysis of population Fisher information also revealed the same results as our decoding accuracy. We saw no change in population Fisher information in mice with prior exposure to EE compared to regular cage or mice with prior neurogenesis ablation. Interestingly, when we removed noise correlations, we saw a significant increase in population Fisher information in all groups. The biggest increase in was observed in mice with prior exposure to EE. Therefore, noise correlations are most detrimental in mice with increased adult neurogenesis. We suggest that when adult neurogenesis is increased, correlations may then have an additional function in network information processing. One possible explanation is that an increase in robustness of the system takes place when adult neurogenesis is increased, making the readout of information onto EC easier to process because its more redundant (Nassar et al., 2018). Additional analysis is needed to further confirm this hypothesis.

CA1 single cell analysis in mice with prior exposure to EE resulted in some potential discrepancies. We observed a significant increase in single cell Fisher information in mice with prior exposure to EE accompanied by a narrowing of the tuning curves. Yet, we also observed a decrease in tuning index and an increase in noise. One possible explanation is that single cell Fisher information is a local measure of signal to noise ratio measured on a trial-by-trial basis. Tuning index and noise are both global measures. Therefore, the neurons' responses may exhibit more fine-grained differences or increased separability, allowing for better discrimination and thus

higher single cell Fisher information. Ablating neurogenesis resulted in a decrease in single cell Fisher information, a decrease in tuning specificity and an increase in noise. In line with previous findings (McHugh et al., 2022), we showed adult neurogenesis exerts its function in the hippocampal network including in neuronal representations of space in CA1.

The Silencing of ABNs using a chemogenetic approach resulted inconclusive in CA1. Both hM4DI+ animals and controls showed significant increase in single cell Fisher information, tuning specificity, and amplitude of the tuning curves. Both control and experimental mice also showed a decrease in nose and width of the tuning curves. These results show improvement in the neuronal representations of space, but it is inconclusive as to whether acute silencing of ABNs has any effects in CA1. These results are in line with previous findings that show that CA1 significantly develops stable spatial representations in the first minutes of the exposure to a novel environment (Frank et al., 2004; Priestley et al., 2022; Wilson & McNaughton, 1994). In our experiment, we are capturing that initial fast learning of the novel environment that masked any effects from ABNs, if present. Given that this paradigm was optimized for DG, we were unable to capture differences in CA1. Future analysis could include the comparison between the second halves of each session (Baseline and CNO). To compare our data post initial exposure to the novel environment, to allow the system to stabilize. In addition, future experiments could include familiarization of the mice to the treadmill prior to treatment.

Our mossy cell results showed a significant decrease in single cell Fisher information and tuning complexity of mossy cells in mice with ablated neurogenesis and previous exposure to EE. Conversely, mice with ablated neurogenesis with prior housing in regular cages had an increase in single cell Fisher information and tuning complexity of mossy cells. These results are difficult to interpret due to the presence of potential off target effects, from either exposure to irradiation or EE environment, and complexity of the function of mossy cells. Results from our chemogenetic approach were also inconclusive as our paradigm resulted in no significant differences in mossy

cells after silencing ABNs. One of the reasons for this is that the experimental approach may not have been sensitive enough to capture potential differences. Secondly, it may occur that the exposure of novelty in our chemogenetic approach was enough to elicit a response in DG, but not enough in mossy. It could be the case that Mossy Cells (and CA1) do not have the same role in novelty detection compared to DG. It would be interesting in future studies to repeat this chemogenetic approach while the animals are engaged in a task such as running for a reward. Many examples in studies show certain effects are observed exclusively under very specific conditions (Gonçalves et al., 2013), which open clues to underlying circuit mechanisms. Also, longer silencing of ABNs could be enough to trigger encoding differences in mossy cells.

Finally, our results suggested silencing mossy cells using a chemogenetic approach decreases spatial tuning in DG. In line with previous findings (Danielson et al., 2017), we also show mossy cells are spatially tuned (Fig. 3 E-F). Given that mossy cells are located downstream of DG, are innervated by DG and project back to the DG, mossy cells may be needed as an extra step to fine tune spatial information in DG. This preliminary finding is in line with previous reports with previous studies (Bui et al., 2018). Future studies should be included to increase the number of mice.

## Chapter 5 - General Discussion

Adult neurogenesis is a unique form of neuronal plasticity in which newly generated neurons are integrated into the adult dentate gyrus in a process modulated by environmental stimuli. Adult-born neurons have been found to contribute to spatial memory, but it is unknown how they do so. In this study, we asked whether adult-born neurons contribute to neural representations of space in the hippocampus. Using in vivo two-photon calcium imaging we recorded neuronal activity during exposure to a novel environment. We recorded from three different areas of the hippocampus (CA1, DG and Mossy Cells) while animals were head-fixed under the microscope on a manually moving treadmill. We found that mice that were previously housed in an enriched environment, which triggers an increase in neurogenesis, had increased spatial information content in the DG during novel context exposure. Ablating adult neurogenesis by prior focal irradiation of the hippocampus blocked the effect of enrichment and lowered spatial information, as did the chemogenetic silencing of adult-born neurons. Both ablating neurogenesis and silencing adult-born neurons decreased the calcium activity rates of DG granule cells, resulting in a decreased amplitude of place-specific responses. These findings contrast previous studies that suggested a predominantly inhibitory action of adult-born neurons. In CA1, animals with prior exposure to an enriched environment exhibited an increase in spatial information content. Ablating adult neurogenesis by prior focal irradiation resulted in a decrease in spatial information content potentially driven by an overall increase in noise in the tuning curves of pyramidal cells. We observed no change in the amplitude of the place-specific responses in animals with prior exposure to enriched environment. We did find a decrease in the width of these responses, which suggests increased precision in activity at the tuned locations. The increase in overall noise could indicate additional mechanisms at play such as direct inputs from the entorhinal cortex influencing the overall firing patterns of CA1. In mossy cells, irradiated animals with prior exposure to an enriched environment showed a decrease in spatial information content when compared to their

non-irradiated counterparts. Spatial tuning was also reduced as observed by a reduction in both unimodal and bimodal place-specific responses. Conversely, animals housed in regular cage conditions with prior exposure to focal irradiation exhibited an increase in spatial information content and complexity of the place-specific responses. These results suggest the role of mossy cells in the spatial information encoding may be partially dependent on adult neurogenesis, but future studies are needed to confirm these results. Overall, we propose that under novel contexts, adult neurogenesis improves neural representations of space through mechanisms that modulate the shape of the tuning curves. In turn, this modulation improves the ability of dentate gyrus neurons to tune to spatial features resulting in increased spatial information content in the hippocampus. These findings contribute to our understanding of how adult neurogenesis positively influences spatial learning and memory by elucidating the mechanisms by which adult-born neurons facilitate the formation of neuronal representations of space in the hippocampus.

The role of adult-born neurons in the hippocampus

The hippocampus has been shown to have a role in spatial information encoding and episodic memories (Barnea & Nottebohm, 1994; Dupret et al., 2008; Gould, Beylin, et al., 1999; Sahay et al., 2011; Shors et al., 2001). Accurately encoding this information requires the hippocampus to discriminate the features of overlapping sensory features to accurately encode the memory (Leutgeb et al., 2007). Studies show that the area of the hippocampus involved in the discrimination of similar features is the DG (Leutgeb et al., 2007). Anatomically, the DG has a neuronal population significantly larger than both EC and CA3 (Amaral et al., 2007). Given this anatomical feature, the DG has been proposed to perform patter separation, decorrelating similar inputs and to prevent the interference of information (Marr, 1971). The theory proposed as to how adult-born neurons contribute to pattern separation in the DG is by modulating the activity of the mature GCs, recruiting inhibitory interneurons or competing for synaptic connections and

therefore increasing the sparseness of the DG (Anacker et al., 2018; Drew et al., 2016; Lacefield et al., 2012; Sahay et al., 2011).

Recent studies have shown adult-born neurons can inhibit mature granule cells via GABAergic interneurons in the hilus during hippocampal dependent tasks (Burghardt et al., 2012; Drew et al., 2016; Temprana et al., 2015). One study found adult-born neurons recruit GABAergic feedback loops that restrict spiking of neighboring GCs (Temprana et al., 2015). Another study found that ablating adult-born neurons results in an increase in the immediate early gene Arc in the dorsal DG, suggesting adult-born neurons modulate network excitability in the DG (Burghardt et al., 2012). Finally, Optogenetic stimulation of adult-born neurons in awake behaving animals resulted in a decrease in the number of active mature GCs in the DG (Drew et al., 2016).

Our findings showed that an increase in the number of adult-born neurons resulted in an increase in the activity of the GCs. Conversely, a decrease in the number of adult-born neurons resulted in a significant decrease in the activity of the GCs. These findings may seemingly oppose those of previous studies, yet they can be explained in line with existing literature. We primarily focused on the activity of the active cells in the network, we did not quantify the overall number of active cells. Therefore, as previous findings suggest, increasing the number of adult-born neurons could result in an increase in the recruitment of feedback inhibitory loops (Temprana et al., 2015), increase in the expression of Arc (Burghardt et al., 2012) and a decrease in the overall number of active cells in the DG (Drew et al., 2016). Yet, our study could suggest that of the cells that remain active, these present increased activity and improved spatial information content. A sparse DG network with increased activity within the cells that carry the highly distinctive hippocampal representations could result in an improvement in information processing within the DG, potentially improving contextual discrimination in spatial memory tasks.

Imaging quality may impair accurate quantification of fraction of active cells.

Although we intended to quantify the overall changes in number of active cells in the different subregions of the hippocampus studied, we encountered several caveats related to the technological challenges of the approach. During our analysis we asked whether we were able to measure both changes in the calcium activity rates of individual cells and changes in the fraction of cells that are active. For the latter we employed Cellpose (Stringer et al., 2021), an anatomical segmentation algorithm that can be used to quantify the number of cells present in a FOV based on their morphology. Using this analysis our goal was to measure the fraction of active cells present in the FOV and compare across the different experimental conditions. However, there are also some caveats to this approach: Cellpose detects the total number of cells from mean projections of calcium imaging movies, which can introduce several biases, for example active cells will tend to be brighter and therefore more visible. We found a correlation between the percentage of active cells and the total number of cells in the imaging field (McDermott et al., 2023), as fields of view with fewer detected cells had much higher variance of the fraction of active cells. Fields with more total cells generally had more cells that were dimmer and less active but were still counted in the total. In contrast, in fields with few cells due to areas of lower viral expression or obscured by blood vessels, there are likely more cells present than can be quantified in the mean projection image. These differences in imaging fields across animals make it difficult to calculate the exact fraction of active cells, limiting the usefulness of this approach.

Our inability to accurately estimate the fraction of active cells is ultimately due to the limitations of the technique: 2-photon microscopy allows for deeper imaging into the brain due to the reduction of optical scattering that can degrade the image quality. 2-photon excitation of fluorophores is non-linear. This nonlinearity restricts excitation to the focal point reducing the out of focus background fluorescence and minimizing photodamage (Denk et al., 1990; Svoboda & Yasuda, 2006). However, even with this methodology, and the removal of a portion of the cortex to allow

access to the hippocampus (Mizrahi et al., 2004), we are still at the limit of the imaging depth that this technology can provide, since we are imaging through 600-750 μm of tissue, primarily in the DG and hilus. Given the technical challenges of imaging at this depth, we did observe some variability in the quality of the FOV imaged. Reasons why this variability occurred could be due to light scattering as expected at this imaging depth, as well as other potential factors such as the presence of blood vessels above the FOV that can overshadow some cells preventing the acquisition of the calcium transients.

Any decrease in signal to noise ratio due to background noise can influence the image quality and therefore diminish our ability to record calcium activity. Even though 2-photon microscopy is better at reducing background fluorescence compared to other traditional fluorescence microscopes, the tissue column above the DG or hilus containing fluorescent cells could still be a source of background noise, partially through light absorption. In addition, an inconsistent viral expression could lead to variability in fluorescence across the tissue. Given the above mentioned, we focused our analysis on the activity properties of the active cells within our FOVs.

Labelling adult-born neurons in a temporally specific manner presents challenges.

Adult-born neurons in the DG undergo various stages of maturation, and their properties differ from those of mature neurons. This heterogeneity in cellular characteristics, including morphology and molecular markers, can make the process of specifically targeting and labeling adult-born neurons challenging. It is known that adult-born neurons contribute to DG function at approximately 4 to 6 weeks of age post mitosis. Therefore, it is important to appropriately label adult-born neurons at the maturational time point of interest.

We attempted to ask how spatial information content changed in adult-born neurons when animals are exposed to an enriched environment. We employed several distinct techniques to label adult-born neurons with calcium sensors but were unsuccessful in appropriately detecting

calcium activity in these cells. Our first approach was the use of genetic labelling of neuronal stem/progenitor cells (NSPCs) using mice expressing a Tamoxifen-inducible Cre recombinase under the control of the endogenous Achaete-scute homolog 1 (Ascl-1) promoter (Yang et al., 2015a), crossed with a tdTomato reporter mouse line, where the fluorescent reporter is flanked by LoxP sites (Pilz et al., 2018). Using the Ascl1 CreERT2 system allowed to selectively tag a cohort of adult-born neurons with a relatively well-defined age range and to study their activity *in vivo* long term. One of the previously known drawbacks of this technique when focusing on selectively-age tagging is that the Ascl1+ cells in the subventricular zone of the DG are not only transiently amplifying progenitors (Type-2a cells) but also include a small portion of adult neural stem cells (Type-1), which continue to produce a decreasing number of adult-born neurons for approximately 1 month after induction (Pilz et al., 2018). In our study, this method was unsuccessful given that we detected Ascl1+ cells or jRGECO1a+ cells but no colocalization. We were therefore unable to record the activity of these cells. In addition, we observed low quantities of adult-born neurons labelled *in vivo*.

We used a similar approach by genetically labelling adult-born neurons using Tbr2-CreER T2 mice crossed with a tdTomato reporter mouse line. This approach allows for the labelling of Tbr2-expressing progenitor cells in the adult hippocampus *in vivo*. Tbr2-CreER T2 labeled progenitor cells are neuronal precursors that under conditions of homeostasis were shown not to generate astrocytes or radial glia-like neural stem cells. They do however generate immature neurons and do not undergo a significant amount of amplification which makes them potential candidates to record calcium activity in adult-born neurons. We were unsuccessful imaging ABN activity due to the low levels of adult born neurons labelled *in vivo* and lack of colocalization with jRGECO1a.

Other approaches also tested included using different viruses such as RV-GFP virus, RVjRGECO1a that were also unsuccessful. Finally, an alternative method we did not use was the Nestin-Cre ERT2 transgenic mouse line crossed with a reporter as a tamoxifen-inducible way to

label ABNs. Nestin-CreERT2 reporter strains label a wide range of adult-born neurons at different post-mitotic ages. Depending on the Nestin-CreERT2 line, they can either induce substantial expression of the reporter in other areas of the brain, which shows potential off target effects of this approach, or elicited inefficient labelling (Sun et al., 2014).

Our results show that the techniques available to label adult-born neurons for in vivo calcium imaging still present many challenges. Aside from the challenges mentioned specifically from the use of these labelling techniques there are additional problems with the use of the viral vectors employed to deliver the calcium sensors to ABNs and potential calcium sensor toxicity (RV-jRGECO1a, RV-GCaMP6, etc.). The use of AAV vectors to deliver the jRGECO1a calcium sensor to hippocampal neurons has been widely reported in a variety of neuroscience applications, including in vivo calcium imaging, but recent findings have demonstrated that intermediate progenitor cells and <2-week-old ABNs can undergo apoptosis when targeted by AAVs (Johnston et al., 2021). In our study, we employed several strategies to address this issue, including additional control experiments. The design optimization of the protocol allows the ABNs that were targeted for manipulation to develop for two weeks post-mitosis before injection of the calcium indicator. This is the maximum amount of time we can separate the birth of the targeted ABNs to the AAV injection as to allow viral expression by the imaging session at 3.5 weeks post AAV injection. This method allows us to maximize survival of ABNs while still being able to image at the time the targeted neurons are at their developmental critical period between 4–6-week post-mitosis.

We included post hoc analysis and quantification of adult neurogenesis in our injected and imaged animals to confirm the presence of ABNs (Chapter 3, Fig. 1 C). Even though we do see a decrease in the quantity of ABNs compared to mice that did not receive an AAV injection and surgery, we are still able to capture the effects of ABNs in the hippocampus using this approach. To further address this point, we also performed an additional experiment using a retrograde AAV vector

injected into hippocampal area CA3. The retrograde viral vector was taken up by the axonal terminals of DG granule neurons, resulting in the expression of jRGECO1a in the ipsilateral granule layer while preserving similar numbers of ABNs in the injected and contralateral hemispheres. Using this approach, we were able to confirm that housing mice in EE elicited an increase in calcium activity and single-cell spatial information content in the DG (Chapter 3, Fig S5). We couldn't confirm all our results including the decoder, given the low number of cells detected. We observed sparser activity when using this approach which could be due to fewer copies of the retrograde AAV present in DG cells leading to lower amounts of jRGECO1a. In addition, the sparser activity detected could be due to a potential increase in the number of ABNs compared to the use of AAV-CaMKIIα.jRGECO1.

Imaging mature granule cells in the DG

A caveat to be addressed when using both AAV and retrograde AAV vectors when studying the effects of ABNs on hippocampal neuronal representations of space is the need to differentiate between ABNs and mature neurons in the imaging recordings, particularly in the DG. It is possible that using our methodology we image both mature cells and ABNs, which could then be all included in the analysis due to the lack of ability to differentiate them, creating potential problems with the interpretability of the results.

AAV vectors deliver the calcium indicator jRGECO1a under the control of the CaMKIIα promoter, which allows for the expression of the calcium sensor in excitatory cells regardless of whether they are mature neurons or ABNs. The increase in single-cell calcium activity with EE could potentially be due to more ABNs being present in the field of view, their higher excitability resulting in increased calcium activity. However, this is unlikely, first because immature ABNs comprise a very small proportion (< 1%, (Kempermann et al., 1997)) of the total DG granule cell population, but also because they are less spatially tuned (Danielson et al., 2016), whereas we observed a significant increase in tuning.

We replicated our results using a labeling approach that specifically targets the axons mature DG neurons using a retrograde AAV injection in hippocampal area CA3 (Chapter 3, Fig S5). Importantly, in this control experiment no immature (<6 weeks-old) ABNs were labeled, since their axons had not reached CA3 at the time of the viral injection. This confirms that the changes in neuronal activity leading to improved spatial coding occur in the mature granule cells, and not only in the immature ABNs. With this approach, we were not able to use our population wide approaches due to the small number of granule cells detected with this methodology. The observed low power with this strategy may be attributed to lower expression of jRGECO1a in the retrograde AAV approach. In addition, an increased number of ABNs in the network leading to increased sparsity (Ikrar et al., 2013) could lead to lower number of cells detected. Our current data is not enough to accurately demonstrate this.

So far, we know of only another study that manipulated ABNs in vivo and recorded hippocampal activity and neural representations of space. Using multiarray electrode recordings and opto-tagging of ABNs with excitatory or inhibitory rhodopsins, the Dupret group studied the properties of ABNs and their effects on the hippocampal network (McHugh et al., 2022). As was previously found using calcium imaging (Danielson et al., 2016), activity was increased in ABNs compared to granule cells in DG. ABNs also carried less single-cell spatial information, which was determined with a commonly used measure (Skaggs et al., 1993) that is derived from mutual information (Shannon, 1948). They also found that ABNs discharge high-rate spikes that are temporally structured with respect to network oscillations, suggesting that ABNs could exert strong influence on downstream hippocampal activity. Finally, they showed that ABNs promote population sparsity in the hippocampus, and silencing ABNs reduces population sparsity without affecting single-cell spatial information. It is worth noting that this methodology performed parallel recordings of DG, CA1 and CA3 which is an advantage because it allows for the manipulation of ABNs while recording in all regions simultaneously to better understand distributed network

dynamics in the hippocampus. Recording simultaneously from all three regions using multiphoton microscopy would be very challenging. The use of multi electrode arrays results in the acquisition of spiking activity instead of calcium transients, which need to be deconvolved to estimate the underlying spiking activity. Nevertheless, data acquired from electrode arrays requires identification of the firing units to infer the type of neurons and number of neurons present in the recording such as CA1 pyramidal neurons, DG mature granule cells, etc. When using calcium imaging this step is not required due to the visualization of cell morphology and fluorescent labelling. The authors were able to detect ABNs exclusively with their opto-tagging strategy, yet no considerations were taken to prevent ABN ablation with the use of AAV vectors to deliver the opto-tagging ChR2 into the DG. No post hoc analysis was provided to show the colocalization of ABN markers and ChR2 in previously recorded mice or to quantify the number of ABNs. The spatial information analysis was done based on single firing unit analysis potentially missing higher dimensional relationships among the populations. Normal distribution of the data was assumed and not tested. Bootstrapping was done 5000 times which may be low. This study suggests ABNs exert their effects downstream of the hippocampus promoting population sparsity potentially supporting discriminative responses to mnemonic stimuli, minimizing interference between memories. In our study, we also found that manipulating ABNs has downstream effects in the hippocampal network. In mice housed in regular cages, ablating neurogenesis significantly increases calcium activity rates in CA1 and decreases single-cell spatial information content and spatial tuning, in line with the findings of McHugh et. al. supporting the role of ABNs in information processing downstream of the DG (McHugh et al., 2022). In addition, we also show that ABNs contribute to DG spatial information encoding and that they do so by modulating the gain of the tuning curves of DG granule cells. No change in population sparsity was observed in the McHugh, et. al, study. One of the reasons why these differences were observed could relate to the low numbers of ABNs opto-tagged (33 ABNs out of 920 principal cells), potentially due to loss of neurogenesis because of viral toxicity as previously described (Johnston et al., 2021). Still, given

these low ABNs numbers manipulated, it is interesting that they observed significant effects in the hippocampal network, which points to the reach ABNs have over the function of the hippocampus during their critical period.

Calcium indicators as a measure of neuronal activity

The use of calcium indicators such as the one employed in this study, provide an indirect measurement of neuronal activity (Grynkiewicz et al., 1985). Reporting changes in intracellular calcium concentration may not correlate exactly with the action potentials fired by the neuron (Yuste et al., 2011). Therefore, caution must be taken when analyzing data and interpreting results with this approach. The use of 2-photon microscopy and calcium imaging provides the opportunity to record from larger number of neurons when compared to other methods such as electrophysiology (Kerlin et al., 2010). Yet, the temporal resolution is limited by the dynamics of the calcium indicator, in some cases unable to capture the precise timing of the rapid neuronal firing events (Tay et al., 2007). Different GCaMP calcium sensors were developed presenting different kinetics, sensitivity, and brightness, depending on the application for which they are needed (Y. Zhang et al., 2023). Fast calcium sensors present rapid response kinetics and detect fast neuronal events such as action potentials (Y. Zhang et al., 2023). The downside is they have lower calcium binding affinity leading to low signal to noise ratio (Y. Zhang et al., 2023). Slow calcium sensors have slower response kinetics and are less likely to saturate in response to rapid calcium fluctuations, but they present less temporal resolution (Y. Zhang et al., 2023). Selecting the right calcium sensor depends on the application intended, the firing properties of the neuronal population and the experimental goals. In this study we utilized jRGECO1a, which would be consistent with the kinetics of a medium GCAMP6 sensor, providing good temporal resolution to capture burst firing in CA1 and the average firing in the DG of 3-7 action potentials per burst (Dana et al., 2016; Neubrandt et al., 2018).

Neurons employ intricate calcium buffering mechanisms which can vary between cell types (Matthews & Dietrich, 2015). The use of calcium indicators may perturb these natural calcium buffering mechanisms potentially leading to inaccurate measures of neuronal activity (McMahon & Jackson, 2018). In our study, we employed the use of an AAV to deliver the calcium sensor. This methodology results in neuronal overexpression of the calcium sensor and potential variability of viral expression between neurons (Rose et al., 2014). This could result in variability in the temporal resolution between neurons. Overall, although this methodology is being widely employed (Danielson et al., 2016; Kumar et al., 2020; McHugh et al., 2022; Tuncdemir et al., 2022), it is still understudied how the calcium sensors expressed both genetically or with the use of AAVs affect neuronal activity.

Place cells of texture cells?

In this study, we employ the use of a treadmill-based paradigm to study spatial representations of space in the mouse hippocampus. This approach involves analyzing neuronal activity data in relation to the animal's position on the treadmill, which allows us to gain insights into hippocampal spatial coding. With this tool, we can precisely measure the animal's movement and location on the treadmill, which we can then correlate with the imaging data. It is possible that with this methodology, some of the neuronal activity recorded on the treadmill may not represent true spatial coding but rather a response to specific features or textures on the treadmill. Neurons, including place cells, can exhibit responses to a variety of different sensory cues beyond spatial information alone (Alexander et al., 2020; Tuncdemir et al., 2022). These cues may include tactile sensations, motor locomotion and odors among others (Alexander et al., 2020). This may result in some cells imaged that are being considered tuned to location, to be in fact tuned to texture on the treadmill. Given our study is centered in the hippocampus, it is more likely that the cells we image are cells tuned to the location of the animal on the treadmill. We would expect a higher concentration of treadmill texture cells in the somatosensory cortex, responsible for processing

tactile information (Y.-D. Zhou & Fuster, 2000). A recent study argues that the hippocampal response to nonspatial stimuli is almost invariably dependent on the animal's location (O'Keefe & Krupic, 2021). This supports the cognitive map theory where these nonspatially tuned cells carry a spatial component that is not apparent, because the nonspatial event took place when the animal was in one location (O'Keefe & Krupic, 2021). In our study, we found that non spatially tuned cells also carried spatial information content which goes in line with this finding.

Other set ups used to study spatial encoding in the hippocampus include virtual reality environments (Leinweber et al., 2014). These environments offer a highly customizable platform that allows for the precise control of the layout, landmarks and sensory cues in the environment (Leinweber et al., 2014). The environmental designs utilized vary widely such as the use of mazes or more depictions of more natural environments. Different cues such as landmarks can be selectively added or removed to understand their influence in the encoding of space. Yet, given the virtual nature of the environment, it may not fully replicate the sensory experience which in turn could result in inaccurate measurements of spatial encoding. The use of open field environments where animals freely explore allows for the study of spatial encoding in more naturalistic behaviors compared to the other methods (Ghosh et al., 2011). Mice can engage in unconstrained behaviors including exploration and navigation (Ghosh et al., 2011). A wide range of behaviors can be recorded, and spatial encoding can be studied in the context of foraging, social interactions and territorial exploration (Ghosh et al., 2011). Yet, this setup requires the use of miniscopes and 1 photon microscopy which present reduced spatial resolution and potential inflammation due to the insertion of the lens into the tissue (Cai et al., 2016).

Some of the caveats of our setup include spatial constraints. Animals can only move in one direction without visual stimuli, which restricts the environment and therefore limits the amount of sensory stimuli available to encode space. The cognitive demand of navigating a treadmill in the dark may not fully capture the cognitive processes involved in hippocampal spatial encoding. The

lack of variability and distinct landmarks in the setup can limit the diversity of the neural representations observed. In addition, the treadmill setup might increase stress levels in mice that could affect neuronal activity.

Quantifying information in the hippocampus

The use of high-throughput techniques to record brain activity in vivo, such as calcium imaging, allows for the recording of neuronal activity from a growing number of neurons simultaneously, in behaving mice (Chen et al., 2013; Ghosh et al., 2011; Ziv et al., 2013). Estimating information content from calcium imaging data and other large neuronal activity datasets enables the study of the neural code. This paradigm shift advances our understanding of how neurons store information and cooperate to process information. These processes have been based on the principles of information theory, where several theories of brain function have been proposed and ways of quantifying information in the brain have been developed (Koren et al., 2023). One of the ways to quantify information in the brain is to quantify mutual information (MI) between the neuronal activity and the stimulus (Brunel & Nadal, 1998; Optican & Richmond, 1987; Puchalla et al., 2005; Shannon, 1948). Calculating MI involves estimating the conditional probability distributions of firing rates given each stimulus. This estimation process requires a substantial amount of data to accurately capture the relationship between firing rates and stimuli. However, in practical experiments, researchers are limited by the finite number of trials or stimulus repetitions they can record. Because of this limitation, estimations of MI often present a significant positive error or upward bias. This means that the calculated MI values tend to be higher than the true MI values that would be obtained with an infinite amount of data. The upward bias occurs because the limited data sample may not fully represent the underlying distribution, leading to inaccurate estimations of the conditional probability distributions (Optican et al., 1991; Panzeri et al., 2007; Sheintuch et al., 2022; Treves & Panzeri, 1995, p. 199).

An adaptation of MI that has been widely used to quantify information is the Skaggs information index (Skaggs et al., 1993). It estimates the amount of information conveyed by the activity of a neuron about a given experimental variable. When expressed in bits/spike, it quantifies tuning specificity and when it is expressed in bits/sec it quantifies the rate at which information about the stimulus is conveyed by the neuronal activity. This approach has been widely used in the study of neuronal representations of space with the animal's position being the variable of interest (Deshmukh & Knierim, 2011; Esteves et al., 2021; Mankin et al., 2015; Nakashiba et al., 2008; Sheintuch et al., 2022; Skaggs & McNaughton, 1996; Stefanini et al., 2020; Tanaka et al., 2018). One of the main advantages of this methodology is that it performs better than MI when the number of samples is limited (Bezzi et al., 2002). Still, the Skaggs information index exhibits an upwards bias. Specifically in calcium imaging, this bias can be more problematic due to the temporally sparser neuronal activity compared to electrophysiological techniques. Even though bias-correction methods have been adapted for Skaggs information index and proposed recently, most of the studies present their Skaggs index data in its potential biased form (Deshmukh & Knierim, 2011; Esteves et al., 2021; Mankin et al., 2015; Nakashiba et al., 2008; Sheintuch et al., 2022; Skaggs & McNaughton, 1996; Tanaka et al., 2018). Specifically in hippocampal *in vivo* calcium imaging in more recent studies which include DG imaging, nearly all use the Skaggs index to quantify information (Danielson et al., 2016; Hainmueller & Bartos, 2018; Tuncdemir et al., 2022). This analysis presents two challenges, the potential bias in the data and the use of single cell approaches to quantify information, which do not consider the cooperative nature of neuronal information processing. Other studies that include DG calcium data used linear decoders to infer the position of the animal in space based on its neuronal calcium activity.

The use of decoding algorithms in hippocampal data is recent and has been adapted from other regions of the brain that have been using this technique longer, such as in the visual cortex. For example, In the primary visual cortex (V1), results show visual discrimination accuracy exceeds

what would be expected based on the responses of individual neurons (Paradiso, 1988). Different algorithms have been used to determine how much information can be decoded from neuronal activity including linear decoders (Ni et al., 2022). These decoders are computationally simplistic, involving linear transformations that are easy to implement. Decoding weights correspond directly to the contribution of individual neurons to the population activity being decoded which results in interpretable results. Linear decoders are also robust and generalizable which makes them ideal candidates to implement in different hippocampal applications. Linear decoders have also been employed in calcium imaging data from visual cortex, where they demonstrate long term quantitative monitoring of neural and behavioral responses (Andermann, 2010). The accuracy of decoding provides an indirect method of quantifying information. In the hippocampus, Stefanini et.al. used linear decoders to decode the animal's position, direction of motion and speed from DG and CA1 (Stefanini et al., 2020). It is worth noting that in this study, the calcium imaging data was deconvolved to estimate spiking activity. These deconvolving algorithms are common when manipulating calcium imaging data but are estimations and whether there is a good relationship between calcium imaging and spiking activity is still debated in the field (Friedrich et al., 2017; Huang et al., 2021; Lütcke et al., 2013). It is worth noting they did compare the performance of the decoder when feeding it the raw data and the deconvolved data and reported no significant differences (Stefanini et al., 2020). In conclusion, the ways to quantify information in the hippocampus are still in development and there are currently limited resources on how to estimate information based on calcium activity (Sheintuch et al., 2022). In our study, we performed extensive testing during the development of the novel methodology employed. We employed different strategies to quantify information including the use of single cell and population wide approaches. We characterized different ways to condition the signals to feed into information estimators and found that raw data conveyed the most information compared to deconvolved traces. We are the first to use a linear decoder using calcium traces and not deconvolved estimations, since we found the signal carries the most information. In addition to the use of the

linear decoder, we also included Fisher information as another way of defining the decoder's performance. Fisher information measures the amount of information that an observed data sample provides about an unknown parameter or variable of interest. When applied to neural activity, it quantifies how much information the neural responses carry about a specific stimulus or parameter (Berens et al., 2012; Graf et al., 2011; Kanitscheider et al., 2015; Moreno-Bote et al., 2014). One of the advantages of this approach is the increased resolution compared to the accuracy of the decoder, because it avoids the compression of the detection being the fraction of correct trials out of 100. In addition, Fisher information also allows us to calculate total information per neuron and the sum of each is the total amount of Fisher information in the population (If they are uncorrelated). It is worth noting that one of the disadvantages of this method is that it is less intuitive compared to the decoder. To quantify Fisher information, considerations are needed. If there are more trials than neurons, an analytical estimator should be used. If there are more neurons than trials, such is our case, a decoder should be used (Moreno-Bote et al., 2014). The information content of neural populations is determined jointly by the response properties of individual neurons, i.e. their tuning and the variability of their activity when repeatedly presented with the same stimulus (in this case each location on the treadmill belt) and by the structure of noise correlations (M. R. Cohen & Kohn, 2011), i.e how this variability is correlated among pairs of neurons (Averbeck et al., 2006; Kohn et al., 2016). In our study, we found that noise correlations have either no effects or detrimental effects on spatial information encoding in the hippocampus. This suggests noise correlations might limit the amount of spatial information encoded by DG and CA1. Recent studies in CA1 have shown similar results (Hazon et al., 2022). They concluded that maximal accuracy in spatial coding was achieved with 300 or more depending on the animal, which is more neurons than the amount we were able to subsample in CA1 (69 neurons). Another study found that noise correlations were beneficial to spatial coding in CA1 (Stefanini et al., 2020). Yet, it is worth noting that this study contained very few tuned cells in CA1 (4%), which has been previously shown to be approximately 30 – 50% (Dong et al., 2021; Hainmueller & Bartos, 2018).

In conclusion, part of the contribution of this study is the innovative methods employed to further learn how to use calcium signals to estimate information in the brain.

Cognition and adult-neurogenesis

Cognitive health, which refers to the ability to think clearly, learn and memorize, is an important component of performing everyday activities. Still, there are few known ways to preserve and improve cognitive ability and little understanding of the mechanisms that promote long-term cognitive health. Cognitive decline is a normal side effect of aging, so finding ways to maintain cognitive health is very relevant in a society that is now able to live longer than ever before. The currently known ways to improve and preserve cognition in humans are physical exercise (Cassilhas et al., 2007), exposure to enriched environments (Arai & Feig, 2011), adequate sleep (Diekelmann, 2014), stress reduction (Blankespoor et al., 2017), healthy diet (Klimova et al., 2020), and social engagement (Z. Zhou et al., 2018). They have all been linked to adult neurogenesis at least partially. Extensive study is underway to understand the mechanisms mediating these processes in the brain. At the molecular level, several factors have been identified to mediate the increase in adult neurogenesis after exposure to an enriched environment such as the brain-derived neurotrophic factor (BDNF) via its receptor TrkB (Liu & Nusslock, 2018), BMPs (Gobeske et al., 2009), CX3CR1 fractalkine receptor (Vukovic et al., 2012) and the fibroblast growth factor FGF (Grońska-Pęski et al., 2021). At the systemic level, exposing aged mice to young blood through heterochronic parabiosis has been shown to reverse the effects of brain aging and improve cognitive function in behavioral tasks such as contextual fear conditioning and spatial learning and memory (Villeda et al., 2014). In the reverse experiment, exposing young mice to blood serum from aged mice decreased synaptic plasticity, and impaired contextual learning and memory. This also leads to reduced neurogenesis, with chemokines such as CCL11 identified as potential mediators of these effects. Increasing CCL11 in young mice results in decreased adult neurogenesis and cognitive impairments (Horowitz et al., 2020; Villeda et al.,

2011). The localization of the neurogenic niche around blood vessels together with these recent findings suggests cues extrinsic to the CNS delivered by the blood could also mediate the effects of adult neurogenesis and improvement in brain cognition. Adult neurogenesis is affected by several different factors such as morphogens, growth factors, transcription factors neurotransmitters, etc. It is also at least partially responsible for the benefits exercise and enrichment among others in improving brain cognition. Although progress has been made in understanding adult neurogenesis at the molecular, cellular, and behavioral levels, few studies have shown the role of ABNs at the circuit level. Our study questioned the mechanisms by which adult neurogenesis could potentially mediate the effects of enriched environment in improved cognition at the network level.

Overview of findings

Our study revealed that ABNs exert a network modulatory role in the DG and suggest potential hippocampal network effects influencing both CA1 and mossy cells. Our study also found that mossy cells are required for spatial information encoding in the DG. In brief, results indicate that adult neurogenesis leads to increased response gain in the DG, improving the ability of the granule cells to tune to spatial features and therefore improving spatial information encoding. Adult-neurogenesis also leads to increased single-cell spatial information via modulation of the variance of the place-specific responses of CA1 pyramidal neurons. Additional confounding results suggest off target effects present that need further interpretation. Manipulation of ABNs resulted in contrasting effects in mossy cells where methods such as irradiation and other brain wide effects could be occluding the effects of adult neurogenesis. Still, our findings demonstrate that the spatial information content in the hippocampus can be modulated even by brief environmental manipulations, such as EE housing, that result in changes in the number of ABNs. The increased spatial information and resulting improvement in the accuracy of neural representations of space in mice with elevated neurogenesis provide a novel mechanistic, circuit-

level explanation for their improved performance at many spatial memory tasks (Garthe & Kempermann, 2013). Furthermore, our findings provide novel directions for the study of how ABNs contribute to memory, identifying new modes of action that could be harnessed as a therapeutic target for memory disorders.

Summary

Exposure to an enriched environment and exercise resulted in an increase in adult born neurons in the hippocampal DG. This increase in the number of adult-born neurons has been shown to be the result of an increase in proliferation and cell survival of this cell pool. The addition of an increased number of neurons into the preexisting circuits of the DG results in an increase in the complexity of the system and its computational strength. As more neurons are incorporated, these present distinct synaptic connections and excitability properties that may support improved pattern separation in the DG. The circuit-level mechanism by which adult-born neurons achieve this could be both by increasing the sparseness of activity in the DG and improving the response to changing spatial cues of the active GCs. By modulating the gain of the active DG GCs, adult born neurons improve the encoding of the neuronal representation of space in the DG. This improved ability to encode space has downstream effects within the hippocampus. In CA1, the incoming inputs benefit spatial encoding in this area by increasing the amount of spatial information these pyramidal neurons carry. Mossy cells on the other hand, although understudied, could provide a supportive role in pattern separation, through their excitatory monosynaptic feedback and disynaptic inputs to GCs, Mossy cells could be proposed as an additional avenue by which adult born neurons exert their effects in the GC layer. Behaviorally, the improvements in spatial information encoding in the hippocampus as a result of the increase in adult-born neurons,

could explain the improvement in hippocampal dependent tasks such as contextual fear conditioning and Morris water maze. The improvement in spatial encoding could explain the improvements in spatial navigation and spatial memory tasks.

**Bibliography**

Adlaf, E. W., Vaden, R. J., Niver, A. J., Manuel, A. F., Onyilo, V. C., Araujo, M. T., Dieni, C. V., Vo, H. T., King, G. D., Wadiche, J. I., & Overstreet-Wadiche, L. (2017). Adult-born neurons modify excitatory synaptic transmission to existing neurons. *ELife*, *6*, e19886. https://doi.org/10.7554/eLife.19886

Aimone, J. B., Wiles, J., & Gage, F. H. (2009). Computational Influence of Adult Neurogenesis on Memory Encoding. *Neuron*, *61*(2), 187–202. https://doi.org/10.1016/j.neuron.2008.11.026

Akers, K. G., Martinez-Canabal, A., Restivo, L., Yiu, A. P., De Cristofaro, A., Hsiang, H.-L. (Liz), Wheeler, A. L., Guskjolen, A., Niibori, Y., Shoji, H., Ohira, K., Richards, B. A., Miyakawa, T., Josselyn, S. A., & Frankland, P. W. (2014). Hippocampal Neurogenesis Regulates Forgetting During Adulthood and Infancy. *Science*, *344*(6184), 598–602. https://doi.org/10.1126/science.1248903

Alexander, A. S., Robinson, J. C., Dannenberg, H., Kinsky, N. R., Levy, S. J., Mau, W., Chapman, G. W., Sullivan, D. W., & Hasselmo, M. E. (2020). Neurophysiological coding of space and time in the hippocampus, entorhinal cortex, and retrosplenial cortex. *Brain and Neuroscience Advances*, *4*, 2398212820972871. https://doi.org/10.1177/2398212820972871

Altman, J. (1962). Are New Neurons Formed in the Brains of Adult Mammals? *Science*, *135*(3509), 1127–1128. https://doi.org/10.1126/science.135.3509.1127

Altman, J. (1963). Autoradiographic investigation of cell proliferation in the brains of rats and cats. *The Anatomical Record*, *145*(4), 573–591. https://doi.org/10.1002/AR.1091450409

Altman, J., & Bayer, S. (1975). Postnatal Development of the Hippocampal Dentate Gyrus Under Normal and Experimental Conditions. In R. L. Isaacson & K. H. Pribram (Eds.),

*The Hippocampus: Volume 1: Structure and Development* (pp. 95–122). Springer US. https://doi.org/10.1007/978-1-4684-2976-3_5

Altman, J., & Das, G. D. (1965). Autoradiographic and histological evidence of postnatal hippocampal neurogenesis in rats. *The Journal of Comparative Neurology*, *124*(3), 319–335. https://doi.org/10.1002/cne.901240303

Alvarez-Buylla, A., & Lim, D. A. (2004). For the long run: Maintaining germinal niches in the adult brain. *Neuron*, *41*(5), 683–686. https://doi.org/10.1016/s0896-6273(04)00111-4

Amaral, D. G., Scharfman, H. E., & Lavenex, P. (2007). *The dentate gyrus: Fundamental neuroanatomical organization (dentate gyrus for dummies)* (pp. 3–790). https://doi.org/10.1016/S0079-6123(07)63001-5

Anacker, C., & Hen, R. (2017). Adult hippocampal neurogenesis and cognitive flexibility—Linking memory and mood. *Nature Reviews Neuroscience*, *18*(6), 335–346. https://doi.org/10.1038/nrn.2017.45

Anacker, C., Luna, V. M., Stevens, G. S., Millette, A., Shores, R., Jimenez, J. C., Chen, B., & Hen, R. (2018). Hippocampal neurogenesis confers stress resilience by inhibiting the ventral dentate gyrus. *Nature*, *559*(7712), 98–102. https://doi.org/10.1038/s41586-018-0262-4

Andermann, M. L. (2010). Chronic cellular imaging of mouse visual cortex during operant behavior and passive viewing. *Frontiers in Cellullar Neuroscience*. https://doi.org/10.3389/fncel.2010.00003

Andermann, M. L., Gilfoy, N. B., Goldey, G. J., Sachdev, R. N. S., Wölfel, M., McCormick, D. A., Reid, R. C., & Levene, M. J. (2013). Chronic Cellular Imaging of Entire Cortical Columns in Awake Mice Using Microprisms. *Neuron*, *80*(4), 900–913. https://doi.org/10.1016/j.neuron.2013.07.052

Appleby, P. A., Kempermann, G., & Wiskott, L. (2011). The Role of Additive Neurogenesis and Synaptic Plasticity in a Hippocampal Memory Model with Grid-Cell Like Input. *PLoS Computational Biology*, *7*(1), e1001063. https://doi.org/10.1371/journal.pcbi.1001063

Arai, J. A., & Feig, L. A. (2011). Long-lasting and transgenerational effects of an environmental enrichment on memory formation. *Brain Research Bulletin*, *85*(1–2), 30–35. https://doi.org/10.1016/j.brainresbull.2010.11.003

Averbeck, B. B., Latham, P. E., & Pouget, A. (2006). Neural correlations, population coding and computation. *Nature Reviews Neuroscience*, *7*(5), 358–366. https://doi.org/10.1038/nrn1888

Babcock, K. R., Page, J. S., Fallon, J. R., & Webb, A. E. (2021). Adult Hippocampal Neurogenesis in Aging and Alzheimer's Disease. *Stem Cell Reports*, *16*(4), 681–693. https://doi.org/10.1016/j.stemcr.2021.01.019

Barnea, A., & Nottebohm, F. (1994). Seasonal recruitment of hippocampal neurons in adult free-ranging black-capped chickadees. *Proceedings of the National Academy of Sciences*, *91*(23), 11217–11221. https://doi.org/10.1073/pnas.91.23.11217

Bartsch, T., Döhring, J., Rohr, A., Jansen, O., & Deuschl, G. (2011). CA1 neurons in the human hippocampus are critical for autobiographical memory, mental time travel, and autonoetic consciousness. *Proceedings of the National Academy of Sciences*, *108*(42), 17562–17567. https://doi.org/10.1073/pnas.1110266108

Bayer, S. A., Yackel, J. W., & Puri, P. S. (1982). Neurons in the Rat Dentate Gyrus Granular Layer Substantially Increase During Juvenile and Adult Life. *Science*, *216*(4548), 890–892. https://doi.org/10.1126/SCIENCE.7079742

Becker, S. (2005). A computational principle for hippocampal learning and neurogenesis. *Hippocampus*, *15*(6), 722–738. https://doi.org/10.1002/hipo.20095

Berdugo-Vega, G., Lee, C., Garthe, A., Kempermann, G., & Calegari, F. (2021). Adult-born neurons promote cognitive flexibility by improving memory precision and indexing. *Hippocampus*, *31*(10), 1068–1079. https://doi.org/10.1002/hipo.23373

Berens, P., Ecker, A. S., Cotton, R. J., Ma, W. J., Bethge, M., & Tolias, A. S. (2012). A Fast and Simple Population Code for Orientation in Primate V1. *Journal of Neuroscience*, *32*(31), 10618–10626. https://doi.org/10.1523/JNEUROSCI.1335-12.2012

Bergami, M., Masserdotti, G., Temprana, S. G., Motori, E., Eriksson, T. M., Göbel, J., Yang, S. M., Conzelmann, K. K., Schinder, A. F., Götz, M., & Berninger, B. (2015). A Critical Period for Experience-Dependent Remodeling of Adult-Born Neuron Connectivity. *Neuron*, *85*(4), 710–717. https://doi.org/10.1016/j.neuron.2015.01.001

Bergmann, O., Spalding, K. L., & Frisén, J. (2015). Adult Neurogenesis in Humans. *Cold Spring Harbor Perspectives in Biology*, *7*(7), a018994. https://doi.org/10.1101/cshperspect.a018994

Bezzi, M., Diamond, M. E., & Treves, A. (2002). Redundancy and Synergy Arising from Pairwise Correlations in Neuronal Ensembles. *Journal of Computational Neuroscience*, *12*(3), 165–174. https://doi.org/10.1023/A:1016531312091

Birch, A. M., McGarry, N. B., & Kelly, Á. M. (2013). Short-term environmental enrichment, in the absence of exercise, improves memory, and increases NGF concentration, early neuronal survival, and synaptogenesis in the dentate gyrus in a time-dependent manner. *Hippocampus*, *23*(6), 437–450. https://doi.org/10.1002/hipo.22103

Blankespoor, R. J., Schellekens, M. P. J., Vos, S. H., Speckens, A. E. M., & De Jong, B. A. (2017). The Effectiveness of Mindfulness-Based Stress Reduction on Psychological Distress and Cognitive Functioning in Patients with Multiple Sclerosis: A Pilot Study. *Mindfulness*, *8*(5), 1251–1258. https://doi.org/10.1007/s12671-017-0701-6

Blümcke, I., Suter, B., Behle, K., Kuhn, R., Schramm, J., Elger, C. E., & Wiestler, O. D. (2000). Loss of hilar mossy cells in Ammon's horn sclerosis. *Epilepsia*, *41 Suppl 6*, S174-180. https://doi.org/10.1111/j.1528-1157.2000.tb01577.x

Boldrini, M., Fulmore, C. A., Tartt, A. N., Simeon, L. R., Pavlova, I., Poposka, V., Rosoklija, G. B., Stankov, A., Arango, V., Dwork, A. J., Hen, R., & Mann, J. J. (2018). Human Hippocampal Neurogenesis Persists throughout Aging. *Cell Stem Cell*, *22*(4), 589-599.e5. https://doi.org/10.1016/j.stem.2018.03.015

Brunel, N., & Nadal, J.-P. (1998). Mutual Information, Fisher Information, and Population Coding. *Neural Computation*, *10*(7), 1731–1757. https://doi.org/10.1162/089976698300017115

Bui, A. D., Nguyen, T. M., Limouse, C., Kim, H. K., Szabo, G. G., Felong, S., Maroso, M., & Soltesz, I. (2018). Dentate gyrus mossy cells control spontaneous convulsive seizures and spatial memory. *Science*, *359*(6377), 787–790. https://doi.org/10.1126/science.aan4074

Burghardt, N. S., Park, E. H., Hen, R., & Fenton, A. A. (2012). Adult-born hippocampal neurons promote cognitive flexibility in mice. *Hippocampus*, *22*(9), 1795–1808. https://doi.org/10.1002/hipo.22013

Cacucci, F., Wills, T. J., Lever, C., Giese, K. P., & O'Keefe, J. (2007). Experience-Dependent Increase in CA1 Place Cell Spatial Information, But Not Spatial Reproducibility, Is Dependent on the Autophosphorylation of the α-Isoform of the Calcium/Calmodulin-Dependent Protein Kinase II. *The Journal of Neuroscience*, *27*(29), 7854–7859. https://doi.org/10.1523/JNEUROSCI.1704-07.2007

Cai, D. J., Aharoni, D., Shuman, T., Shobe, J., Biane, J., Song, W., Wei, B., Veshkini, M., La-Vu, M., Lou, J., Flores, S. E., Kim, I., Sano, Y., Zhou, M., Baumgaertel, K., Lavi, A., Kamata, M., Tuszynski, M., Mayford, M., … Silva, A. J. (2016). A shared neural ensemble links

distinct contextual memories encoded close in time. *Nature*, *534*(7605), Article 7605. https://doi.org/10.1038/nature17955

Cassilhas, R. C., Viana, V. A. R., Grassmann, V., Santos, R. T., Santos, R. F., Tufik, S., & Mello, M. T. (2007). The Impact of Resistance Exercise on the Cognitive Function of the Elderly. *Medicine & Science in Sports & Exercise*, *39*(8), 1401–1407. https://doi.org/10.1249/mss.0b013e318060111f

Chakraborti, A., Allen, A., Allen, B., Rosi, S., & Fike, J. R. (2012). Cranial Irradiation Alters Dendritic Spine Density and Morphology in the Hippocampus. *PLOS ONE*, *7*(7), e40844. https://doi.org/10.1371/journal.pone.0040844

Chan, K. L., Tong, K. Y., & Yip, S. P. (2008). Relationship of serum brain-derived neurotrophic factor (BDNF) and health-related lifestyle in healthy human subjects. *Neuroscience Letters*, *447*(2–3), 124–128. https://doi.org/10.1016/j.neulet.2008.10.013

Chen, T.-W., Wardill, T. J., Sun, Y., Pulver, S. R., Renninger, S. L., Baohan, A., Schreiter, E. R., Kerr, R. A., Orger, M. B., Jayaraman, V., Looger, L. L., Svoboda, K., & Kim, D. S. (2013). Ultrasensitive fluorescent proteins for imaging neuronal activity. *Nature*, *499*(7458), 295–300. https://doi.org/10.1038/nature12354

Christian, K. M., Song, H., & Ming, G. (2014). Functions and Dysfunctions of Adult Hippocampal Neurogenesis. *Annual Review of Neuroscience*, *37*(1), 243–262. https://doi.org/10.1146/annurev-neuro-071013-014134

Cipriani, S., Ferrer, I., Aronica, E., Kovacs, G. G., Verney, C., Nardelli, J., Khung, S., Delezoide, A.-L., Milenkovic, I., Rasika, S., Manivet, P., Benifla, J.-L., Deriot, N., Gressens, P., & Adle-Biassette, H. (2018). Hippocampal Radial Glial Subtypes and Their Neurogenic Potential in Human Fetuses and Healthy and Alzheimer's Disease Adults. *Cerebral Cortex*, *28*(7), 2458–2478. https://doi.org/10.1093/cercor/bhy096

Clelland, C. D., Choi, M., Romberg, C., Clemenson, G. D., Fragniere, A., Tyers, P., Jessberger, S., Saksida, L. M., Barker, R. A., Gage, F. H., & Bussey, T. J. (2009). A Functional Role

for Adult Hippocampal Neurogenesis in Spatial Pattern Separation. *Science*, *325*(5937), 210–213. https://doi.org/10.1126/science.1173215

Clemenson, G. D., Lee, S. W., Deng, W., Barrera, V. R., Iwamoto, K. S., Fanselow, M. S., & Gage, F. H. (2015). Enrichment rescues contextual discrimination deficit associated with immediate shock. *Hippocampus*, *25*(3), 385–392. https://doi.org/10.1002/hipo.22380

Coen-Cagli, R., & Solomon, S. S. (2019). Relating Divisive Normalization to Neuronal Response Variability. *The Journal of Neuroscience*, *39*(37), 7344–7356. https://doi.org/10.1523/JNEUROSCI.0126-19.2019

Cohen, J. D., Bolstad, M., & Lee, A. K. (2017). Experience-dependent shaping of hippocampal CA1 intracellular activity in novel and familiar environments. *ELife*, *6*, e23040. https://doi.org/10.7554/eLife.23040

Cohen, M. R., & Kohn, A. (2011). Measuring and interpreting neuronal correlations. *Nature Neuroscience*, *14*(7), 811–819. https://doi.org/10.1038/nn.2842

Cohen, N. J., & Squire, L. R. (1980). Preserved Learning and Retention of Pattern-Analyzing Skill in Amnesia: Dissociation of Knowing How and Knowing That. *Science*, *210*(4466), 207–210. https://doi.org/10.1126/science.7414331

Cole, J. D., Espinueva, D. F., Seib, D. R., Ash, A. M., Cooke, M. B., Cahill, S. P., O'Leary, T. P., Kwan, S. S., & Snyder, J. S. (2020). Adult-Born Hippocampal Neurons Undergo Extended Development and Are Morphologically Distinct from Neonatally-Born Neurons. *The Journal of Neuroscience*, *40*(30), 5740–5756. https://doi.org/10.1523/JNEUROSCI.1665-19.2020

Corkin, S. (2002). What's new with the amnesic patient H.M.? *Nature Reviews. Neuroscience*, *3*(2), 153–160. https://doi.org/10.1038/NRN726

Coulter, D. A., & Carlson, G. C. (2007). Functional regulation of the dentate gyrus by GABA-mediated inhibition. *Progress in Brain Research*, *163*, 235–243. https://doi.org/10.1016/S0079-6123(07)63014-3

Dana, H., Mohar, B., Sun, Y., Narayan, S., Gordus, A., Hasseman, J. P., Tsegaye, G., Holt, G. T., Hu, A., Walpita, D., Patel, R., Macklin, J. J., Bargmann, C. I., Ahrens, M. B., Schreiter, E. R., Jayaraman, V., Looger, L. L., Svoboda, K., & Kim, D. S. (2016). Sensitive red protein calcium indicators for imaging neural activity. *ELife*, *5*, e12727. https://doi.org/10.7554/eLife.12727

Danielson, N. B. B., Kaifosh, P., Zaremba, J. D. D., Lovett-Barron, M., Tsai, J., Denny, C. A. A., Balough, E. M. M., Goldberg, A. R. R., Drew, L. J. J., Hen, R., Losonczy, A., & Kheirbek, M. A. A. (2016). Distinct Contribution of Adult-Born Hippocampal Granule Cells to Context Encoding. *Neuron*, *90*(1), 101–112. https://doi.org/10.1016/j.neuron.2016.02.019

Danielson, N. B., Turi, G. F., Ladow, M., Chavlis, S., Petrantonakis, P. C., Poirazi, P., & Losonczy, A. (2017). In Vivo Imaging of Dentate Gyrus Mossy Cells in Behaving Mice. *Neuron*, *93*(3), 552-559.e4. https://doi.org/10.1016/j.neuron.2016.12.019

Dayan, P., & Abbott, L. F. (2001). *Theoretical Neuroscience: Computational and Mathematical Modeling of Neural Systems*. The MIT Press.

de Almeida, L., Idiart, M., & Lisman, J. E. (2009). The Input–Output Transformation of the Hippocampal Granule Cells: From Grid Cells to Place Fields. *The Journal of Neuroscience*, *29*(23), 7504–7512. https://doi.org/10.1523/JNEUROSCI.6048-08.2009

Demas, J., Manley, J., Tejera, F., Barber, K., Kim, H., Traub, F. M., Chen, B., & Vaziri, A. (2021). High-speed, cortex-wide volumetric recording of neuroactivity at cellular resolution using light beads microscopy. *Nature Methods*, *18*(9), 1103–1111. https://doi.org/10.1038/s41592-021-01239-8

Denève, S., & Machens, C. K. (2016). Efficient codes and balanced networks. *Nature Neuroscience*, *19*(3), Article 3. https://doi.org/10.1038/nn.4243

Denk, W., Strickler, J. H., & Webb, W. W. (1990). Two-Photon Laser Scanning Fluorescence Microscopy. *Science*, *248*(4951), 73–76. https://doi.org/10.1126/science.2321027

Denny, C. A., Burghardt, N. S., Schachter, D. M., Hen, R., & Drew, M. R. (2012). 4- to 6-week-old adult-born hippocampal neurons influence novelty-evoked exploration and contextual fear conditioning. *Hippocampus*, *22*(5), 1188–1201. https://doi.org/10.1002/hipo.20964

Deshmukh, S. S., & Knierim, J. J. (2011). Representation of Non-Spatial and Spatial Information in the Lateral Entorhinal Cortex. *Frontiers in Behavioral Neuroscience*, *5*. https://doi.org/10.3389/fnbeh.2011.00069

Deshpande, A., Bergami, M., Ghanem, A., Conzelmann, K.-K., Lepier, A., Götz, M., & Berninger, B. (2013). Retrograde monosynaptic tracing reveals the temporal evolution of inputs onto new neurons in the adult dentate gyrus and olfactory bulb. *Proceedings of the National Academy of Sciences*, *110*(12). https://doi.org/10.1073/pnas.1218991110

Diekelmann, S. (2014). Sleep for cognitive enhancement. *Frontiers in Systems Neuroscience*, *8*. https://doi.org/10.3389/fnsys.2014.00046

Dieni, C. V., Panichi, R., Aimone, J. B., Kuo, C. T., Wadiche, J. I., & Overstreet-Wadiche, L. (2016). Low excitatory innervation balances high intrinsic excitability of immature dentate neurons. *Nature Communications*, *7*, 11313. https://doi.org/10.1038/ncomms11313

Dombeck, D. A., Harvey, C. D., Tian, L., Looger, L. L., & Tank, D. W. (2010). Functional imaging of hippocampal place cells at cellular resolution during virtual navigation. *Nature Neuroscience*, *13*(11), 1433–1440. https://doi.org/10.1038/nn.2648

Dong, C., Madar, A. D., & Sheffield, M. E. J. (2021). Distinct place cell dynamics in CA1 and CA3 encode experience in new environments. *Nature Communications*, *12*(1), 2977. https://doi.org/10.1038/s41467-021-23260-3

Drew, L. J., Kheirbek, M. A., Luna, V. M., Denny, C. A., Cloidt, M. A., Wu, M. V., Jain, S., Scharfman, H. E., & Hen, R. (2016). Activation of local inhibitory circuits in the dentate gyrus by adult-born neurons. *Hippocampus*, *26*(6), 763–778. https://doi.org/10.1002/hipo.22557

Dupret, D., Revest, J.-M., Koehl, M., Ichas, F., De Giorgi, F., Costet, P., Abrous, D. N., & Piazza, P. V. (2008). Spatial Relational Memory Requires Hippocampal Adult Neurogenesis. *PLoS ONE*, *3*(4), e1959. https://doi.org/10.1371/journal.pone.0001959

Echeveste, R., Aitchison, L., Hennequin, G., & Lengyel, M. (2020). Cortical-like dynamics in recurrent circuits optimized for sampling-based probabilistic inference. *Nature Neuroscience*, *23*(9), 1138–1149. https://doi.org/10.1038/s41593-020-0671-1

Eriksson, P. S., Perfilieva, E., Bjork-Eriksson, T., Alborn, A. M., Nordborg, C., Peterson, D. A., & Gage, F. H. (1998). Neurogenesis in the adult human hippocampus. *Nat Med*, *4*(11), 1313–1317. https://doi.org/10.1038/3305

Erwin, S. R., Sun, W., Copeland, M., Lindo, S., Spruston, N., & Cembrowski, M. S. (2020). A Sparse, Spatially Biased Subtype of Mature Granule Cell Dominates Recruitment in Hippocampal-Associated Behaviors. *Cell Reports*, *31*(4), 107551. https://doi.org/10.1016/j.celrep.2020.107551

Espósito, M. S., Piatti, V. C., Laplagne, D. A., Morgenstern, N. A., Ferrari, C. C., Pitossi, F. J., & Schinder, A. F. (2005). Neuronal Differentiation in the Adult Hippocampus Recapitulates Embryonic Development. *The Journal of Neuroscience*, *25*(44), 10074–10086. https://doi.org/10.1523/jneurosci.3114-05.2005

Esteves, I. M., Chang, H., Neumann, A. R., Sun, J., Mohajerani, M. H., & McNaughton, B. L. (2021). Spatial Information Encoding across Multiple Neocortical Regions Depends on an Intact Hippocampus. *The Journal of Neuroscience*, *41*(2), 307–319. https://doi.org/10.1523/JNEUROSCI.1788-20.2020

Fabel, K. (2009). Additive effects of physical exercise and environmental enrichment on adult hippocampal neurogenesis in mice. *Frontiers in Neuroscience*. https://doi.org/10.3389/neuro.22.002.2009

Franjic, D., Skarica, M., Ma, S., Arellano, J. I., Tebbenkamp, A. T. N., Choi, J., Xu, C., Li, Q., Morozov, Y. M., Andrijevic, D., Vrselja, Z., Spajic, A., Santpere, G., Li, M., Zhang, S., Liu,

Y., Spurrier, J., Zhang, L., Gudelj, I., … Sestan, N. (2022). Transcriptomic taxonomy and neurogenic trajectories of adult human, macaque, and pig hippocampal and entorhinal cells. *Neuron*, *110*(3), 452-469.e14. https://doi.org/10.1016/j.neuron.2021.10.036

Frank, L. M., Stanley, G. B., & Brown, E. N. (2004). Hippocampal Plasticity across Multiple Days of Exposure to Novel Environments. *Journal of Neuroscience*, *24*(35), 7681–7689. https://doi.org/10.1523/JNEUROSCI.1958-04.2004

Frankland, P. W., Köhler, S., & Josselyn, S. A. (2013). Hippocampal neurogenesis and forgetting. *Trends in Neurosciences*, *36*(9), 497–503. https://doi.org/10.1016/j.tins.2013.05.002

Freund, J., Brandmaier, A. M., Lewejohann, L., Kirste, I., Kritzler, M., Krüger, A., Sachser, N., Lindenberger, U., & Kempermann, G. (2015). Association between exploratory activity and social individuality in genetically identical mice living in the same enriched environment. *Neuroscience*, *309*, 140–152. https://doi.org/10.1016/j.neuroscience.2015.05.027

Friedrich, J., Zhou, P., & Paninski, L. (2017). Fast online deconvolution of calcium imaging data. *PLOS Computational Biology*, *13*(3), e1005423. https://doi.org/10.1371/journal.pcbi.1005423

Garthe, A., Behr, J., & Kempermann, G. (2009). Adult-Generated Hippocampal Neurons Allow the Flexible Use of Spatially Precise Learning Strategies. *PLoS ONE*, *4*(5), e5464. https://doi.org/10.1371/journal.pone.0005464

Garthe, A., & Kempermann, G. (2013). An old test for new neurons: Refining the Morris water maze to study the functional relevance of adult hippocampal neurogenesis. *Frontiers in Neuroscience*, *7*. https://doi.org/10.3389/fnins.2013.00063

Ge, S., Goh, E. L. K., Sailor, K. a, Kitabatake, Y., Ming, G., & Song, H. (2006). GABA regulates synaptic integration of newly generated neurons in the adult brain. *Nature*, *439*(7076), 589–593. https://doi.org/10.1038/nature04404

Ge, S., Yang, C., Hsu, K., Ming, G., & Song, H. (2007). A Critical Period for Enhanced Synaptic Plasticity in Newly Generated Neurons of the Adult Brain. *Neuron*, *54*(4), 559–566. https://doi.org/10.1016/j.neuron.2007.05.002

Ghosh, K. K., Burns, L. D., Cocker, E. D., Nimmerjahn, A., Ziv, Y., Gamal, A. E., & Schnitzer, M. J. (2011). Miniaturized integration of a fluorescence microscope. *Nature Methods*, *8*(10), 871–878. https://doi.org/10.1038/nmeth.1694

Gobeske, K. T., Das, S., Bonaguidi, M. A., Weiss, C., Radulovic, J., Disterhoft, J. F., & Kessler, J. A. (2009). BMP Signaling Mediates Effects of Exercise on Hippocampal Neurogenesis and Cognition in Mice. *PLoS ONE*, *4*(10), e7506. https://doi.org/10.1371/journal.pone.0007506

Gonçalves, J. T., Anstey, J. E., Golshani, P., & Portera-Cailliau, C. (2013). Circuit level defects in the developing neocortex of Fragile X mice. *Nature Neuroscience*, *16*(7), 903–909. https://doi.org/10.1038/nn.3415

Gonçalves, J. T., Bloyd, C. W., Shtrahman, M., Johnston, S. T., Schafer, S. T., Parylak, S. L., Tran, T., Chang, T., & Gage, F. H. (2016). In vivo imaging of dendritic pruning in dentate granule cells. *Nature Neuroscience*, *19*(6), 788–791. https://doi.org/10.1038/nn.4301

Göritz, C., & Frisén, J. (2012). Neural Stem Cells and Neurogenesis in the Adult. *Cell Stem Cell*, *10*(6), 657–659. https://doi.org/10.1016/j.stem.2012.04.005

Gould, E., Beylin, A., Tanapat, P., Reeves, A., & Shors, T. J. (1999). Learning enhances adult neurogenesis in the hippocampal formation. *Nature Neuroscience*, *2*(3), 260–265. https://doi.org/10.1038/6365

Gould, E., Reeves, A. J., Fallah, M., Tanapat, P., Gross, C. G., & Fuchs, E. (1999). Hippocampal neurogenesis in adult Old World primates. *Proceedings of the National Academy of Sciences of the United States of America*, *96*(9), 5263–5267. https://doi.org/10.1073/pnas.96.9.5263

Graf, A. B. A., Kohn, A., Jazayeri, M., & Movshon, J. A. (2011). Decoding the activity of neuronal populations in macaque primary visual cortex. *Nature Neuroscience*, *14*(2), 239–245. https://doi.org/10.1038/nn.2733

Groisman, A. I., Yang, S. M., & Schinder, A. F. (2020). Differential Coupling of Adult-Born Granule Cells to Parvalbumin and Somatostatin Interneurons. *Cell Reports*, *30*(1), 202-214.e4. https://doi.org/10.1016/j.celrep.2019.12.005

Grońska-Pęski, M., Gonçalves, J. T., & Hébert, J. M. (2021). Enriched Environment Promotes Adult Hippocampal Neurogenesis through FGFRs. *The Journal of Neuroscience*, *41*(13), 2899–2910. https://doi.org/10.1523/JNEUROSCI.2286-20.2021

Grynkiewicz, G., Poenie, M., & Tsien, R. Y. (1985). A new generation of Ca2+ indicators with greatly improved fluorescence properties. *The Journal of Biological Chemistry*, *260*(6), 3440–3450.

Gu, Y., Arruda-Carvalho, M., Wang, J., Janoschka, S. R., Josselyn, S. A., Frankland, P. W., & Ge, S. (2012). Optical controlling reveals time-dependent roles for adult-born dentate granule cells. *Nature Neuroscience*. https://doi.org/10.1038/nn.3260

Guzowski, J. F., McNaughton, B. L., Barnes, C. A., & Worley, P. F. (1999). Environment-specific expression of the immediate-early gene Arc in hippocampal neuronal ensembles. *Nature Neuroscience*, *2*(12), 1120–1124. https://doi.org/10.1038/16046

Hafting, T., Fyhn, M., Molden, S., Moser, M.-B., & Moser, E. I. (2005). Microstructure of a spatial map in the entorhinal cortex. *Nature*, *436*(7052), 801–806. https://doi.org/10.1038/nature03721

Hainmueller, T., & Bartos, M. (2018). Parallel emergence of stable and dynamic memory engrams in the hippocampus. *Nature*, *558*(7709), 292–296. https://doi.org/10.1038/s41586-018-0191-2

Harvey, C. D., Collman, F., Dombeck, D. A., & Tank, D. W. (2009). Intracellular dynamics of hippocampal place cells during virtual navigation. *Nature*, *461*(7266), 941–946. https://doi.org/10.1038/nature08499

Hazon, O., Minces, V. H., Tomàs, D. P., Ganguli, S., Schnitzer, M. J., & Jercog, P. E. (2022). Noise correlations in neural ensemble activity limit the accuracy of hippocampal spatial representations. *Nature Communications*, *13*(1), Article 1. https://doi.org/10.1038/s41467-022-31254-y

Heeger, D. J., & Zemlianova, K. O. (2020). A recurrent circuit implements normalization, simulating the dynamics of V1 activity. *Proceedings of the National Academy of Sciences*, *117*(36), 22494–22505. https://doi.org/10.1073/pnas.2005417117

Hénaff, O. J., Boundy-Singer, Z. M., Meding, K., Ziemba, C. M., & Goris, R. L. T. (2020). Representation of visual uncertainty through neural gain variability. *Nature Communications*, *11*(1), Article 1. https://doi.org/10.1038/s41467-020-15533-0

Hollands, C., Tobin, M. K., Hsu, M., Musaraca, K., Yu, T.-S., Mishra, R., Kernie, S. G., & Lazarov, O. (2017). Depletion of adult neurogenesis exacerbates cognitive deficits in Alzheimer's disease by compromising hippocampal inhibition. *Molecular Neurodegeneration*, *12*(1), 64. https://doi.org/10.1186/s13024-017-0207-7

Horowitz, A. M., Fan, X., Bieri, G., Smith, L. K., Sanchez-Diaz, C. I., Schroer, A. B., Gontier, G., Casaletto, K. B., Kramer, J. H., Williams, K. E., & Villeda, S. A. (2020). Blood factors transfer beneficial effects of exercise on neurogenesis and cognition to the aged brain. *Science*, *369*(6500), 167–173. https://doi.org/10.1126/science.aaw2622

Houser, C. R., Peng, Z., Wei, X., Huang, C. S., & Mody, I. (2021). Mossy Cells in the Dorsal and Ventral Dentate Gyrus Differ in Their Patterns of Axonal Projections. *The Journal of Neuroscience*, *41*(5), 991–1004. https://doi.org/10.1523/JNEUROSCI.2455-20.2020

Huang, L., Ledochowitsch, P., Knoblich, U., Lecoq, J., Murphy, G. J., Reid, R. C., De Vries, S. E., Koch, C., Zeng, H., Buice, M. A., Waters, J., & Li, L. (2021). Relationship between

simultaneously recorded spiking activity and fluorescence signal in GCaMP6 transgenic mice. *ELife*, *10*, e51675. https://doi.org/10.7554/eLife.51675

Hubel, D. H., & Wiesel, T. N. (1959). Receptive fields of single neurones in the cat's striate cortex. *The Journal of Physiology*, *148*(3), 574–591. https://doi.org/10.1113/jphysiol.1959.sp006308

Ikrar, T., Guo, N., He, K., Besnard, A., Levinson, S., Hill, A., Lee, H.-K., Hen, R., Xu, X., & Sahay, A. (2013). Adult neurogenesis modifies excitability of the dentate gyrus. *Frontiers in Neural Circuits*, *7*. https://doi.org/10.3389/fncir.2013.00204

Jinde, S., Zsiros, V., Jiang, Z., Nakao, K., Pickel, J., Kohno, K., Belforte, J. E., & Nakazawa, K. (2012). Hilar Mossy Cell Degeneration Causes Transient Dentate Granule Cell Hyperexcitability and Impaired Pattern Separation. *Neuron*, *76*(6), 1189–1200. https://doi.org/10.1016/j.neuron.2012.10.036

Johnston, S., Parylak, S. L., Kim, S., Mac, N., Lim, C., Gallina, I., Bloyd, C., Newberry, A., Saavedra, C. D., Novak, O., Gonçalves, J. T., Gage, F. H., & Shtrahman, M. (2021). AAV ablates neurogenesis in the adult murine hippocampus. *ELife*, *10*, e59291. https://doi.org/10.7554/eLife.59291

Jordan, J. T., McDermott, K. D., Frechou, M. A., Shtrahman, M., & Gonçalves, J. T. (2021). Treadmill-based task for assessing spatial memory in head-fixed mice. *STAR Protocols*, *2*(3), 100770. https://doi.org/10.1016/j.xpro.2021.100770

Jung, M. W., & McNaughton, B. L. (1993). Spatial Selectivity of Unit-Activity in the Hippocampal Granular Layer. *Hippocampus*, *3*(2), 165–182. https://doi.org/10.1002/hipo.450030209

Kafashan, M., Jaffe, A. W., Chettih, S. N., Nogueira, R., Arandia-Romero, I., Harvey, C. D., Moreno-Bote, R., & Drugowitsch, J. (2021). Scaling of sensory information in large neural populations shows signatures of information-limiting correlations. *Nature Communications*, *12*(1), 473. https://doi.org/10.1038/s41467-020-20722-y

Kanitscheider, I., Coen-Cagli, R., & Pouget, A. (2015). Origin of information-limiting noise correlations. *Proceedings of the National Academy of Sciences*, *112*(50). https://doi.org/10.1073/pnas.1508738112

Kaplan, M. S., & Hinds, J. W. (1977). Neurogenesis in the Adult Rat: Electron Microscopic Analysis of Light Radioautographs. *Science*, *197*(4308), 1092–1094. https://doi.org/10.1126/SCIENCE.887941

Kempermann, G. (2008). The neurogenic reserve hypothesis: What is adult hippocampal neurogenesis good for? *Trends in Neurosciences*, *31*(4), 163–169. https://doi.org/10.1016/j.tins.2008.01.002

Kempermann, G., Kuhn, H. G., & Gage, F. H. (1997). More hippocampal neurons in adult mice living in an enriched environment. *Nature*, *386*(6624), 493–495. https://doi.org/10.1038/386493a0

Kerlin, A. M., Andermann, M. L., Berezovskii, V. K., & Reid, R. C. (2010). Broadly tuned response properties of diverse inhibitory neuron subtypes in mouse visual cortex. *Neuron*, *67*(5), 858–871. https://doi.org/10.1016/j.neuron.2010.08.002

Kim, E. J., Ables, J. L., Dickel, L. K., Eisch, A. J., & Johnson, J. E. (2011). Ascl1 (Mash1) Defines Cells with Long-Term Neurogenic Potential in Subgranular and Subventricular Zones in Adult Mouse Brain. *PLOS ONE*, *6*(3), e18472. https://doi.org/10.1371/journal.pone.0018472

Kim, S., Jung, D., & Royer, S. (2020). Place cell maps slowly develop via competitive learning and conjunctive coding in the dentate gyrus. *Nature Communications*, *11*(1), Article 1. https://doi.org/10.1038/s41467-020-18351-6

Klimova, B., Dziuba, S., & Cierniak-Emerych, A. (2020). The Effect of Healthy Diet on Cognitive Performance Among Healthy Seniors – A Mini Review. *Frontiers in Human Neuroscience*, *14*, 325. https://doi.org/10.3389/fnhum.2020.00325

Knoth, R., Singec, I., Ditter, M., Pantazis, G., Capetian, P., Meyer, R. P., Horvat, V., Volk, B., & Kempermann, G. (2010). Murine Features of Neurogenesis in the Human Hippocampus across the Lifespan from 0 to 100 Years. *PLoS ONE*, *5*(1), e8809. https://doi.org/10.1371/journal.pone.0008809

Ko, H.-G., Jang, D.-J., Son, J., Kwak, C., Choi, J.-H., Ji, Y.-H., Lee, Y.-S., Son, H., & Kaang, B.-K. (2009). Effect of ablated hippocampal neurogenesis on the formation and extinction of contextual fear memory. *Molecular Brain*, *2*(1), 1. https://doi.org/10.1186/1756-6606-2-1

Kohn, A., Coen-Cagli, R., Kanitscheider, I., & Pouget, A. (2016). Correlations and Neuronal Population Information. *Annual Review of Neuroscience*, *39*(1), 237–256. https://doi.org/10.1146/annurev-neuro-070815-013851

Komorowski, R. W., Manns, J. R., & Eichenbaum, H. (2009). Robust Conjunctive Item–Place Coding by Hippocampal Neurons Parallels Learning What Happens Where. *The Journal of Neuroscience*, *29*(31), 9918–9929. https://doi.org/10.1523/JNEUROSCI.1378-09.2009

Koren, V., Bondanelli, G., & Panzeri, S. (2023). Computational methods to study information processing in neural circuits. *Computational and Structural Biotechnology Journal*, *21*, 910–922. https://doi.org/10.1016/j.csbj.2023.01.009

Kühn, S., & Gallinat, J. (2014). Segregating cognitive functions within hippocampal formation: A quantitative meta-analysis on spatial navigation and episodic memory: A Meta-analysis on Navigation and Episodic Memory. *Human Brain Mapping*, *35*(4), 1129–1142. https://doi.org/10.1002/hbm.22239

Kumar, D., Koyanagi, I., Carrier-Ruiz, A., Vergara, P., Srinivasan, S., Sugaya, Y., Kasuya, M., Yu, T.-S., Vogt, K. E., Muratani, M., Ohnishi, T., Singh, S., Teixeira, C. M., Chérasse, Y., Naoi, T., Wang, S.-H., Nondhalee, P., Osman, B. A. H., Kaneko, N., … Sakaguchi, M. (2020). Sparse Activity of Hippocampal Adult-Born Neurons during REM Sleep Is Necessary for Memory Consolidation. *Neuron*, *107*(3), 552-565.e10. https://doi.org/10.1016/j.neuron.2020.05.008

Lacefield, C. O., Itskov, V., Reardon, T., Hen, R., & Gordon, J. A. (2012). Effects of adult-generated granule cells on coordinated network activity in the dentate gyrus. *Hippocampus*, *22*(1), 106–116. https://doi.org/10.1002/hipo.20860

Laplagne, D. A., Espósito, M. S., Piatti, V. C., Morgenstern, N. A., Zhao, C., Van Praag, H., Gage, F. H., & Schinder, A. F. (2006). Functional convergence of neurons generated in the developing and adult hippocampus. *PLoS Biology*. https://doi.org/10.1371/journal.pbio.0040409

Leinweber, M., Zmarz, P., Buchmann, P., Argast, P., Hübener, M., Bonhoeffer, T., & Keller, G. B. (2014). Two-photon calcium imaging in mice navigating a virtual reality environment. *Journal of Visualized Experiments: JoVE*, *84*, e50885. https://doi.org/10.3791/50885

Leutgeb, J. K., Leutgeb, S., Moser, M.-B., & Moser, E. I. (2007). Pattern Separation in the Dentate Gyrus and CA3 of the Hippocampus. *Science*, *315*(5814), 961–966. https://doi.org/10.1126/science.1135801

Li, Z., Zhang, H., & Tang, N. (2013). Influences of NR2B-containing NMDA receptors knockdown on neural activity in hippocampal newborn neurons. *Journal of Huazhong University of Science and Technology [Medical Sciences]*, *33*(4), 457–462. https://doi.org/10.1007/s11596-013-1142-7

Liu, P. Z., & Nusslock, R. (2018). Exercise-Mediated Neurogenesis in the Hippocampus via BDNF. *Frontiers in Neuroscience*, *12*, 52. https://doi.org/10.3389/fnins.2018.00052

Lütcke, H., Gerhard, F., Zenke, F., Gerstner, W., & Helmchen, F. (2013). Inference of neuronal network spike dynamics and topology from calcium imaging data. *Frontiers in Neural Circuits*, *7*. https://doi.org/10.3389/fncir.2013.00201

Ma, D. K., Ming, G.-L., & Song, H. (2005). Glial influences on neural stem cell development: Cellular niches for adult neurogenesis. *Current Opinion in Neurobiology*, *15*(5), 514–520. https://doi.org/10.1016/j.conb.2005.08.003

Maguire, E. A., Gadian, D. G., Johnsrude, I. S., Good, C. D., Ashburner, J., Frackowiak, R. S. J., & Frith, C. D. (2000). Navigation-related structural change in the hippocampi of taxi drivers. *Proceedings of the National Academy of Sciences*, *97*(8), 4398–4403. https://doi.org/10.1073/pnas.070039597

Mankin, E. A., Diehl, G. W., Sparks, F. T., Leutgeb, S., & Leutgeb, J. K. (2015). Hippocampal CA2 Activity Patterns Change over Time to a Larger Extent than between Spatial Contexts. *Neuron*, *85*(1), 190–201. https://doi.org/10.1016/j.neuron.2014.12.001

Marin-Burgin, A., Mongiat, L. A., Pardi, M. B., & Schinder, A. F. (2012). Unique Processing During a Period of High Excitation/Inhibition Balance in Adult-Born Neurons. *Science*, *335*(6073), 1238–1242. https://doi.org/10.1126/science.1214956

Marr, D. (1971). Simple Memory: A Theory for Archicortex. *Philosophical Transactions of the Royal Society B: Biological Sciences*, *262*(841), 23–81. https://doi.org/10.1098/rstb.1971.0078

Matthews, E. A., & Dietrich, D. (2015). Buffer mobility and the regulation of neuronal calcium domains. *Frontiers in Cellular Neuroscience*, *9*, 48. https://doi.org/10.3389/fncel.2015.00048

McDermott, K. D., Frechou, M. A., Jordan, J. T., Martin, S. S., & Gonçalves, J. T. (2023). Delayed formation of neural representations of space in aged mice. *BioRxiv*.

McHugh, S. B., Lopes-dos-Santos, V., Gava, G. P., Hartwich, K., Tam, S. K. E., Bannerman, D. M., & Dupret, D. (2022). Adult-born dentate granule cells promote hippocampal population sparsity. *Nature Neuroscience*, *25*(11), 1481–1491. https://doi.org/10.1038/s41593-022-01176-5

McMahon, S. M., & Jackson, M. B. (2018). An Inconvenient Truth: Calcium Sensors Are Calcium Buffers. *Trends in Neurosciences*, *41*(12), 880–884. https://doi.org/10.1016/j.tins.2018.09.005

Miller, S. M., & Sahay, A. (2019). Functions of adult-born neurons in hippocampal memory interference and indexing. *Nature Neuroscience*, *22*(10), 1565–1575. https://doi.org/10.1038/s41593-019-0484-2

Milner, B., Corkin, S., & Teuber, H.-L. (1968). Further analysis of the hippocampal amnesic syndrome: 14-year follow-up study of H.M. *Neuropsychologia*, *6*(3), 215–234. https://doi.org/10.1016/0028-3932(68)90021-3

MISHKIN, M. (1978). Memory in monkeys severely impaired by combined but not by separate removal of amygdala and hippocampus. *Nature*, *273*(5660), 297–298. https://doi.org/10.1038/273297a0

Mizrahi, A., Crowley, J. C., Shtoyerman, E., & Katz, L. C. (2004). High-Resolution *In Vivo* Imaging of Hippocampal Dendrites and Spines. *The Journal of Neuroscience*, *24*(13), 3147–3151. https://doi.org/10.1523/JNEUROSCI.5218-03.2004

Moreno-Bote, R., Beck, J., Kanitscheider, I., Pitkow, X., Latham, P., & Pouget, A. (2014). Information-limiting correlations. *Nature Neuroscience*, *17*(10), 1410–1417. https://doi.org/10.1038/nn.3807

Moreno-Jiménez, E. P., Flor-García, M., Terreros-Roncal, J., Rábano, A., Cafini, F., Pallas-Bazarra, N., Ávila, J., & Llorens-Martín, M. (2019). Adult hippocampal neurogenesis is abundant in neurologically healthy subjects and drops sharply in patients with Alzheimer's disease. *Nature Medicine*. https://doi.org/10.1038/s41591-019-0375-9

Morris, R. G. M., Garrud, P., Rawlins, J. N. P., & O'Keefe, J. (1982). Place navigation impaired in rats with hippocampal lesions. *Nature*, *297*(5868), 681–683. https://doi.org/10.1038/297681a0

Moser, M.-B., Rowland, D. C., & Moser, E. I. (2015). Place Cells, Grid Cells, and Memory. *Cold Spring Harbor Perspectives in Biology*, *7*(2), a021808. https://doi.org/10.1101/cshperspect.a021808

Mu, Y., Zhao, C., & Gage, F. H. (2011). Dopaminergic Modulation of Cortical Inputs during Maturation of Adult-Born Dentate Granule Cells. *The Journal of Neuroscience*, *31*(11), 4113–4123. https://doi.org/10.1523/JNEUROSCI.4913-10.2011

Nakashiba, T., Cushman, J. D., Pelkey, K. A., Renaudineau, S., Buhl, D. L., McHugh, T. J., Barrera, V. R., Chittajallu, R., Iwamoto, K. S., McBain, C. J., Fanselow, M. S., & Tonegawa, S. (2012). Young dentate granule cells mediate pattern separation, whereas old granule cells facilitate pattern completion. *Cell*. https://doi.org/10.1016/j.cell.2012.01.046

Nakashiba, T., Young, J. Z., McHugh, T. J., Buhl, D. L., & Tonegawa, S. (2008). Transgenic Inhibition of Synaptic Transmission Reveals Role of CA3 Output in Hippocampal Learning. *Science*, *319*(5867), 1260–1264. https://doi.org/10.1126/science.1151120

Nasrallah, K., Frechou, M. A., Yoon, Y. J., Persaud, S., Gonçalves, J. T., & Castillo, P. E. (2022). Seizure-induced strengthening of a recurrent excitatory circuit in the dentate gyrus is proconvulsant. *Proceedings of the National Academy of Sciences of the United States of America*, *119*(32), e2201151119. https://doi.org/10.1073/pnas.2201151119

Nassar, M., Simonnet, J., Huang, L.-W., Mathon, B., Cohen, I., Bendels, M. H. K., Beraneck, M., Miles, R., & Fricker, D. (2018). Anterior Thalamic Excitation and Feedforward Inhibition of Presubicular Neurons Projecting to Medial Entorhinal Cortex. *The Journal of Neuroscience: The Official Journal of the Society for Neuroscience*, *38*(28), 6411–6425. https://doi.org/10.1523/JNEUROSCI.0014-18.2018

Neeper, S. A., Gómez-Pinilla, F., Choi, J., & Cotman, C. W. (1996). Physical activity increases mRNA for brain-derived neurotrophic factor and nerve growth factor in rat brain. *Brain Research*, *726*(1–2), 49–56. https://doi.org/10.1016/0006-8993(96)00273-9

Neubrandt, M., Oláh, V. J., Brunner, J., Marosi, E. L., Soltesz, I., & Szabadics, J. (2018). Single Bursts of Individual Granule Cells Functionally Rearrange Feedforward Inhibition. *The*

*Journal of Neuroscience*, *38*(7), 1711–1724. https://doi.org/10.1523/JNEUROSCI.1595-17.2018

Ni, A. M., Huang, C., Doiron, B., & Cohen, M. R. (2022). A general decoding strategy explains the relationship between behavior and correlated variability. *ELife*, *11*, e67258. https://doi.org/10.7554/eLife.67258

Nottebohm, F. (1981). A Brain for All Seasons: Cyclical Anatomical Changes in Song Control Nuclei of the Canary Brain. *Science*, *214*(4527), 1368–1370. https://doi.org/10.1126/SCIENCE.7313697

O'Keefe, J. (1976). Place units in the hippocampus of the freely moving rat. *Experimental Neurology*. https://doi.org/10.1016/0014-4886(76)90055-8

O'Keefe, J., & Dostrovsky, J. (1971). The hippocampus as a spatial map. Preliminary evidence from unit activity in the freely-moving rat. *Brain Research*, *34*(1), 171–175. https://doi.org/10.1016/0006-8993(71)90358-1

O'Keefe, J., & Krupic, J. (2021). Do hippocampal pyramidal cells respond to nonspatial stimuli? *Physiological Reviews*, *101*(3), 1427–1456. https://doi.org/10.1152/physrev.00014.2020

O'Keefe, J., & Nadel, L. (1979). Précis of O'Keefe & Nadel's *The hippocampus as a cognitive map*. *Behavioral and Brain Sciences*, *2*(4), 487–494. https://doi.org/10.1017/S0140525X00063949

Olson, I. R., Page, K., Moore, K. S., Chatterjee, A., & Verfaellie, M. (2006). Working Memory for Conjunctions Relies on the Medial Temporal Lobe. *The Journal of Neuroscience*, *26*(17), 4596–4601. https://doi.org/10.1523/JNEUROSCI.1923-05.2006

Optican, L. M., Gawne, T. J., Richmond, B. J., & Joseph, P. J. (1991). Unbiased measures of transmitted information and channel capacity from multivariate neuronal data. *Biological Cybernetics*, *65*(5), 305–310. https://doi.org/10.1007/BF00216963

Optican, L. M., & Richmond, B. J. (1987). Temporal encoding of two-dimensional patterns by single units in primate inferior temporal cortex. III. Information theoretic analysis. *Journal of Neurophysiology*, *57*(1), 162–178. https://doi.org/10.1152/jn.1987.57.1.162

Ozeki, H., Finn, I. M., Schaffer, E. S., Miller, K. D., & Ferster, D. (2009). Inhibitory Stabilization of the Cortical Network Underlies Visual Surround Suppression. *Neuron*, *62*(4), 578–592. https://doi.org/10.1016/j.neuron.2009.03.028

Pachitariu, M., Stringer, C., Schröder, S., Dipoppa, M., Rossi, L. F., Carandini, M., & Harris, K. D. (2016). Suite2p: Beyond 10,000 neurons with standard two-photon microscopy. *BioRxiv*, 061507. https://doi.org/10.1101/061507

Panzeri, S., Senatore, R., Montemurro, M. A., & Petersen, R. S. (2007). Correcting for the Sampling Bias Problem in Spike Train Information Measures. *Journal of Neurophysiology*, *98*(3), 1064–1072. https://doi.org/10.1152/jn.00559.2007

Papaioannou, S., & Medini, P. (2022). Advantages, Pitfalls, and Developments of All Optical Interrogation Strategies of Microcircuits in vivo. *Frontiers in Neuroscience*, *16*. https://doi.org/10.3389/fnins.2022.859803

Paradiso, M. A. (1988). A theory for the use of visual orientation information which exploits the columnar structure of striate cortex. *Biological Cybernetics*, *58*(1), 35–49. https://doi.org/10.1007/BF00363954

Parihar, V. K., & Limoli, C. L. (2013). Cranial irradiation compromises neuronal architecture in the hippocampus. *Proceedings of the National Academy of Sciences*, *110*(31), 12822–12827. https://doi.org/10.1073/pnas.1307301110

Pelkey, K. A., Chittajallu, R., Craig, M. T., Tricoire, L., Wester, J. C., & McBain, C. J. (2017). Hippocampal GABAergic Inhibitory Interneurons. *Physiological Reviews*, *97*(4), 1619–1747. https://doi.org/10.1152/physrev.00007.2017

Pereira, A. C., Huddleston, D. E., Brickman, A. M., Sosunov, A. A., Hen, R., McKhann, G. M., Sloan, R., Gage, F. H., Brown, T. R., & Small, S. A. (2007). An *in vivo* correlate of

exercise-induced neurogenesis in the adult dentate gyrus. *Proceedings of the National Academy of Sciences*, *104*(13), 5638–5643. https://doi.org/10.1073/pnas.0611721104

Piatti, V. C., Davies-Sala, M. G., Esposito, M. S., Mongiat, L. A., Trinchero, M. F., & Schinder, A. F. (2011). The Timing for Neuronal Maturation in the Adult Hippocampus Is Modulated by Local Network Activity. *Journal of Neuroscience*, *31*(21), 7715–7728. https://doi.org/10.1523/JNEUROSCI.1380-11.2011

Pilz, G.-A., Bottes, S., Betizeau, M., Jörg, D. J., Carta, S., Simons, B. D., Helmchen, F., & Jessberger, S. (2018). Live imaging of neurogenesis in the adult mouse hippocampus. *Science*, *359*(6376), 658–662. https://doi.org/10.1126/science.aao5056

Pilz, G.-A., Carta, S., Stauble, A., Ayaz, A., Jessberger, S., & Helmchen, F. (2016). Functional Imaging of Dentate Granule Cells in the Adult Mouse Hippocampus. *Journal of Neuroscience*, *36*(28), 7407–7414. https://doi.org/10.1523/JNEUROSCI.3065-15.2016

Planchez, B., Lagunas, N., Le Guisquet, A.-M., Legrand, M., Surget, A., Hen, R., & Belzung, C. (2021). Increasing Adult Hippocampal Neurogenesis Promotes Resilience in a Mouse Model of Depression. *Cells*, *10*(5), 972. https://doi.org/10.3390/cells10050972

Priestley, J. B., Bowler, J. C., Rolotti, S. V., Fusi, S., & Losonczy, A. (2022). Signatures of rapid plasticity in hippocampal CA1 representations during novel experiences. *Neuron*, *110*(12), 1978-1992.e6. https://doi.org/10.1016/j.neuron.2022.03.026

Puchalla, J. L., Schneidman, E., Harris, R. A., & Berry, M. J. (2005). Redundancy in the Population Code of the Retina. *Neuron*, *46*(3), 493–504. https://doi.org/10.1016/j.neuron.2005.03.026

Ramirez, S., Liu, X., Lin, P.-A., Suh, J., Pignatelli, M., Redondo, R. L., Ryan, T. J., & Tonegawa, S. (2013). Creating a False Memory in the Hippocampus. *Science*, *341*(6144), 387–391. https://doi.org/10.1126/science.1239073

Rangel, L. M., Alexander, A. S., Aimone, J. B., Wiles, J., Gage, F. H., Chiba, A. A., & Quinn, L. K. (2014). Temporally selective contextual encoding in the dentate gyrus of the hippocampus. *Nature Communications*, *5*(1), 3181. https://doi.org/10.1038/ncomms4181

Rechavi, Y., Rubin, A., Yizhar, O., & Ziv, Y. (2022). Exercise increases information content and affects long-term stability of hippocampal place codes. *Cell Reports*, *41*(8), 111695. https://doi.org/10.1016/j.celrep.2022.111695

Rennó-Costa, C., Lisman, J., & Verschure, P. (2010). The Mechanism of Rate Remapping in the Dentate Gyrus. *Neuron*, *68*(6), 1051–1058. https://doi.org/10.1016/j.neuron.2010.11.024

Robinson, N. T. M., Descamps, L. A. L., Russell, L. E., Buchholz, M. O., Bicknell, B. A., Antonov, G. K., Lau, J. Y. N., Nutbrown, R., Schmidt-Hieber, C., & Häusser, M. (2020). Targeted Activation of Hippocampal Place Cells Drives Memory-Guided Spatial Behavior. *Cell*, *183*(7), 2041–2042. https://doi.org/10.1016/j.cell.2020.12.010

Rolls, E. T., & Treves, A. (1999). *Neural networks and brain function* (Reprint). Oxford Univ. Press.

Rose, T., Goltstein, P. M., Portugues, R., & Griesbeck, O. (2014). Putting a finishing touch on GECIs. *Frontiers in Molecular Neuroscience*, *7*, 88. https://doi.org/10.3389/fnmol.2014.00088

Rossi, C., Angelucci, A., Costantin, L., Braschi, C., Mazzantini, M., Babbini, F., Fabbri, M. E., Tessarollo, L., Maffei, L., Berardi, N., & Caleo, M. (2006). Brain-derived neurotrophic factor (BDNF) is required for the enhancement of hippocampal neurogenesis following environmental enrichment. *European Journal of Neuroscience*, *24*(7), 1850–1856. https://doi.org/10.1111/j.1460-9568.2006.05059.x

Roth, B. L. (2016). DREADDs for Neuroscientists. *Neuron*, *89*(4), 683–694. https://doi.org/10.1016/j.neuron.2016.01.040

Sahay, A., & Hen, R. (2007). Adult hippocampal neurogenesis in depression. *Nature Neuroscience*, *10*(9), 1110–1115. https://doi.org/10.1038/nn1969

Sahay, A., Scobie, K. N., Hill, A. S., O'Carroll, C. M., Kheirbek, M. A., Burghardt, N. S., Fenton, A. A., Dranovsky, A., & Hen, R. (2011). Increasing adult hippocampal neurogenesis is sufficient to improve pattern separation. *Nature*, *472*(7344), 466–470. https://doi.org/10.1038/nature09817

Sanai, N., Nguyen, T., Ihrie, R. A., Mirzadeh, Z., Tsai, H.-H., Wong, M., Gupta, N., Berger, M. S., Huang, E., Garcia-Verdugo, J.-M., Rowitch, D. H., & Alvarez-Buylla, A. (2011). Corridors of migrating neurons in the human brain and their decline during infancy. *Nature*, *478*(7369), 382–386. https://doi.org/10.1038/nature10487

Scharfman, H. E. (1995). Electrophysiological evidence that dentate hilar mossy cells are excitatory and innervate both granule cells and interneurons. *Journal of Neurophysiology*, *74*(1), 179–194. https://doi.org/10.1152/jn.1995.74.1.179

Scharfman, H. E. (2016). The enigmatic mossy cell of the dentate gyrus. *Nature Reviews Neuroscience*, *17*(9), 562–575. https://doi.org/10.1038/nrn.2016.87

Schmidt-Hieber, C., Jones, P., & Bischofberger, J. (2004). Enhanced synaptic plasticity in newly generated granule cells of the adult hippocampus. *Nature*, *429*(6988), 184–187. https://doi.org/10.1038/nature02553

Schwiening, C. J. (2012). A brief historical perspective: Hodgkin and Huxley. *The Journal of Physiology*, *590*(11), 2571–2575. https://doi.org/10.1113/jphysiol.2012.230458

Scott, G. A., Terstege, D. J., Roebuck, A. J., Gorzo, K. A., Vu, A. P., Howland, J. G., & Epp, J. R. (2021). Adult neurogenesis mediates forgetting of multiple types of memory in the rat. *Molecular Brain*, *14*(1), 97. https://doi.org/10.1186/s13041-021-00808-4

Scoville, W. B., & Milner, B. (1957). LOSS OF RECENT MEMORY AFTER BILATERAL HIPPOCAMPAL LESIONS. *Journal of Neurology, Neurosurgery & Psychiatry*, *20*(1), 11–21. https://doi.org/10.1136/jnnp.20.1.11

Shannon, C. E. (1948). A Mathematical Theory of Communication. *Bell System Technical Journal*, *27*(3), 379–423. https://doi.org/10.1002/j.1538-7305.1948.tb01338.x

Sheintuch, L., Rubin, A., & Ziv, Y. (2022). Bias-free estimation of information content in temporally sparse neuronal activity. *PLOS Computational Biology*, *18*(2), e1009832. https://doi.org/10.1371/journal.pcbi.1009832

Shors, T. J., Miesegaes, G., Beylin, A., Zhao, M., Rydel, T., & Gould, E. (2001). Neurogenesis in the adult is involved in the formation of trace memories. *Nature*, *410*(6826), 372–376. https://doi.org/10.1038/35066584

Silva, A. J., Paylor, R., Wehner, J. M., & Tonegawa, S. (1992). Impaired Spatial Learning in α-Calcium-Calmodulin Kinase II Mutant Mice. *Science*, *257*(5067), 206–211. https://doi.org/10.1126/science.1321493

Silva, A. J., Stevens, C. F., Tonegawa, S., & Wang, Y. (1992). Deficient hippocampal long-term potentiation in alpha-calcium-calmodulin kinase II mutant mice. *Science (New York, N.Y.)*, *257*(5067), 201–206. https://doi.org/10.1126/science.1378648

Skaggs, W. E., & McNaughton, B. L. (1996). Replay of Neuronal Firing Sequences in Rat Hippocampus During Sleep Following Spatial Experience. *Science*, *271*(5257), 1870–1873. https://doi.org/10.1126/science.271.5257.1870

Skaggs, W. E., McNaughton, B. L., Gothard, K. M., & Markus, E. J. (1993). An information-theoretic approach to deciphering the hippocampal code. *In Advances in Neural Information Processing Systems*, 1030–1037.

Snyder, J. S., Soumier, A., Brewer, M., Pickel, J., & Cameron, H. A. (2011). Adult hippocampal neurogenesis buffers stress responses and depressive behaviour. *Nature*. https://doi.org/10.1038/nature10287

Solstad, T., Boccara, C. N., Kropff, E., Moser, M.-B., & Moser, E. I. (2008). Representation of Geometric Borders in the Entorhinal Cortex. *Science*, *322*(5909), 1865–1868. https://doi.org/10.1126/science.1166466

Sorrells, S. F., Paredes, M. F., Cebrian-Silla, A., Sandoval, K., Qi, D., Kelley, K. W., James, D., Mayer, S., Chang, J., Auguste, K. I., Chang, E. F., Gutierrez, A. J., Kriegstein, A. R.,

Mathern, G. W., Oldham, M. C., Huang, E. J., Garcia-Verdugo, J. M., Yang, Z., & Alvarez-Buylla, A. (2018). Human hippocampal neurogenesis drops sharply in children to undetectable levels in adults. *Nature*, *555*(7696), 377–381. https://doi.org/10.1038/nature25975

Spalding, K. L., Bergmann, O., Alkass, K., Bernard, S., Salehpour, M., Huttner, H. B., Boström, E., Westerlund, I., Vial, C., Buchholz, B. A., Possnert, G., Mash, D. C., Druid, H., & Frisén, J. (2013). Dynamics of Hippocampal Neurogenesis in Adult Humans. *Cell*, *153*(6), 1219–1227. https://doi.org/10.1016/j.cell.2013.05.002

Spalding, K. L., Bhardwaj, R. D., Buchholz, B. A., Druid, H., & Frisén, J. (2005). Retrospective birth dating of cells in humans. *Cell*, *122*(1), 133–143. https://doi.org/10.1016/j.cell.2005.04.028

Squire, L. R. (1982). The Neuropsychology of Human Memory. *Annual Review of Neuroscience*, *5*(1), 241–273. https://doi.org/10.1146/annurev.ne.05.030182.001325

Squire, L. R. (1992). Memory and the hippocampus: A synthesis from findings with rats, monkeys, and humans. *Psychological Review*, *99*(2), 195–231. https://doi.org/10.1037/0033-295X.99.2.195

Stefanini, F., Kushnir, L., Jimenez, J. C., Jennings, J. H., Woods, N. I., Stuber, G. D., Kheirbek, M. A., Hen, R., & Fusi, S. (2020). A Distributed Neural Code in the Dentate Gyrus and in CA1. *Neuron*, *107*(4), 703-716.e4. https://doi.org/10.1016/j.neuron.2020.05.022

Stone, S. S. D., Teixeira, C. M., Zaslavsky, K., Wheeler, A. L., Martinez-Canabal, A., Wang, A. H., Sakaguchi, M., Lozano, A. M., & Frankland, P. W. (2011). Functional convergence of developmentally and adult-generated granule cells in dentate gyrus circuits supporting hippocampus-dependent memory. *Hippocampus*. https://doi.org/10.1002/hipo.20845

Stringer, C., Wang, T., Michaelos, M., & Pachitariu, M. (2021). Cellpose: A generalist algorithm for cellular segmentation. *Nature Methods*, *18*(1), 100–106. https://doi.org/10.1038/s41592-020-01018-x

Sun, M.-Y., Yetman, M. J., Lee, T.-C., Chen, Y., & Jankowsky, J. L. (2014). Specificity and efficiency of reporter expression in adult neural progenitors vary substantially among nestin-CreER $^{T2}$ lines. *Journal of Comparative Neurology*, *522*(5), 1191–1208. https://doi.org/10.1002/cne.23497

Svoboda, K., & Yasuda, R. (2006). Principles of Two-Photon Excitation Microscopy and Its Applications to Neuroscience. *Neuron*, *50*(6), 823–839. https://doi.org/10.1016/j.neuron.2006.05.019

Tanaka, K. Z., He, H., Tomar, A., Niisato, K., Huang, A. J. Y., & McHugh, T. J. (2018). The hippocampal engram maps experience but not place. *Science*, *361*(6400), 392–397. https://doi.org/10.1126/science.aat5397

Taube, J. S., Muller, R. U., & Ranck, J. B. (1990). Head-direction cells recorded from the postsubiculum in freely moving rats. I. Description and quantitative analysis. *The Journal of Neuroscience : The Official Journal of the Society for Neuroscience*, *10*(2), 420–435. https://doi.org/10.1523/JNEUROSCI.10-02-00420.1990

Tay, L. H., Griesbeck, O., & Yue, D. T. (2007). Live-cell transforms between Ca2+ transients and FRET responses for a troponin-C-based Ca2+ sensor. *Biophysical Journal*, *93*(11), 4031–4040. https://doi.org/10.1529/biophysj.107.109629

Temprana, S. G., Mongiat, L. A., Yang, S. M., Trinchero, M. F., Alvarez, D. D., Kropff, E., Giacomini, D., Beltramone, N., Lanuza, G. M., & Schinder, A. F. (2015). Delayed Coupling to Feedback Inhibition during a Critical Period for the Integration of Adult-Born Granule Cells. *Neuron*, *85*(1), 116–131. https://doi.org/10.1016/j.neuron.2014.11.023

Toda, T., Parylak, S., Linker, S. B., & Gage, F. H. (2019). The role of adult hippocampal neurogenesis in brain health and disease. *Molecular Psychiatry*, *24*(1), 67–87. https://doi.org/10.1038/s41380-018-0036-2

Tolman, E. C. (1948). Cognitive maps in rats and men. *Psychological Review*, *55*(4), 189–208. https://doi.org/10.1037/h0061626

Tomé, W. A., Gökhan, Ş., Brodin, N. P., Gulinello, M. E., Heard, J., Mehler, M. F., & Guha, C. (2015). A mouse model replicating hippocampal sparing cranial irradiation in humans: A tool for identifying new strategies to limit neurocognitive decline. *Scientific Reports*, *5*, 14384. https://doi.org/10.1038/srep14384

Toni, N., Laplagne, D. A., Zhao, C., Lombardi, G., Ribak, C. E., Gage, F. H., & Schinder, A. F. (2008). Neurons born in the adult dentate gyrus form functional synapses with target cells. *Nature Neuroscience*, *11*(8), 901–907. https://doi.org/10.1038/nn.2156

Toni, N., & Schinder, A. F. (2016). Maturation and Functional Integration of New Granule Cells into the Adult Hippocampus. *Cold Spring Harbor Perspectives in Biology*, *8*(1), a018903. https://doi.org/10.1101/cshperspect.a018903

Tran, L. M., Josselyn, S. A., Richards, B. A., & Frankland, P. W. (2019). Forgetting at biologically realistic levels of neurogenesis in a large-scale hippocampal model. *Behavioural Brain Research*, *376*, 112180. https://doi.org/10.1016/j.bbr.2019.112180

Treves, A., & Panzeri, S. (1995). The Upward Bias in Measures of Information Derived from Limited Data Samples. *Neural Computation*, *7*(2), 399–407. https://doi.org/10.1162/neco.1995.7.2.399

Treves, A., & Rolls, E. T. (1994). Computational analysis of the role of the hippocampus in memory. *Hippocampus*, *4*(3), 374–391. https://doi.org/10.1002/hipo.450040319

Tronel, S., Belnoue, L., Grosjean, N., Revest, J. M., Piazza, P. V., Koehl, M., & Abrous, D. N. (2012). Adult-born neurons are necessary for extended contextual discrimination. *Hippocampus*. https://doi.org/10.1002/hipo.20895

Tsien, J. Z., Huerta, P. T., & Tonegawa, S. (1996). The essential role of hippocampal CA1 NMDA receptor-dependent synaptic plasticity in spatial memory. *Cell*, *87*(7), 1327–1338. https://doi.org/10.1016/s0092-8674(00)81827-9

Tuncdemir, S. N., Grosmark, A. D., Turi, G. F., Shank, A., Bowler, J. C., Ordek, G., Losonczy, A., Hen, R., & Lacefield, C. O. (2022). Parallel processing of sensory cue and spatial

information in the dentate gyrus. *Cell Reports*, *38*(3), 110257. https://doi.org/10.1016/j.celrep.2021.110257

van Praag, H., Christie, B. R., Sejnowski, T. J., & Gage, F. H. (1999). Running enhances neurogenesis, learning, and long-term potentiation in mice. *Proceedings of the National Academy of Sciences*, *96*(23), 13427–13431. https://doi.org/10.1073/pnas.96.23.13427

van Praag, H., Kempermann, G., & Gage, F. H. (1999). Running increases cell proliferation and neurogenesis in the adult mouse dentate gyrus. *Nat Neurosci*, *2*(3), 266–270. https://doi.org/10.1038/6368

Van Strien, N. M., Cappaert, N. L. M., & Witter, M. P. (2009). The anatomy of memory: An interactive overview of the parahippocampal–hippocampal network. *Nature Reviews Neuroscience*, *10*(4), 272–282. https://doi.org/10.1038/nrn2614

Vemuri, P., Lesnick, T. G., Przybelski, S. A., Machulda, M., Knopman, D. S., Mielke, M. M., Roberts, R. O., Geda, Y. E., Rocca, W. A., Petersen, R. C., & Jack, C. R. (2014). Association of lifetime intellectual enrichment with cognitive decline in the older population. *JAMA Neurology*, *71*(8), 1017–1024. https://doi.org/10.1001/jamaneurol.2014.963

Verhoef, B.-E., & Maunsell, J. H. R. (2017). Attention-related changes in correlated neuronal activity arise from normalization mechanisms. *Nature Neuroscience*, *20*(7), 969–977. https://doi.org/10.1038/nn.4572

Villeda, S. A., Luo, J., Mosher, K. I., Zou, B., Britschgi, M., Bieri, G., Stan, T. M., Fainberg, N., Ding, Z., Eggel, A., Lucin, K. M., Czirr, E., Park, J.-S., Couillard-Després, S., Aigner, L., Li, G., Peskind, E. R., Kaye, J. A., Quinn, J. F., … Wyss-Coray, T. (2011). The ageing systemic milieu negatively regulates neurogenesis and cognitive function. *Nature*, *477*(7362), 90–94. https://doi.org/10.1038/nature10357

Villeda, S. A., Plambeck, K. E., Middeldorp, J., Castellano, J. M., Mosher, K. I., Luo, J., Smith, L. K., Bieri, G., Lin, K., Berdnik, D., Wabl, R., Udeochu, J., Wheatley, E. G., Zou, B.,

Simmons, D. A., Xie, X. S., Longo, F. M., & Wyss-Coray, T. (2014). Young blood reverses age-related impairments in cognitive function and synaptic plasticity in mice. *Nature Medicine*, *20*(6), 659–663. https://doi.org/10.1038/nm.3569

Vivar, C., Potter, M. C., Choi, J., Lee, J.-Y., Stringer, T. P., Callaway, E. M., Gage, F. H., Suh, H., & van Praag, H. (2012). Monosynaptic inputs to new neurons in the dentate gyrus. *Nature Communications*, *3*, 1107. https://doi.org/10.1038/ncomms2101

Vukovic, J., Colditz, M. J., Blackmore, D. G., Ruitenberg, M. J., & Bartlett, P. F. (2012). Microglia Modulate Hippocampal Neural Precursor Activity in Response to Exercise and Aging. *The Journal of Neuroscience*, *32*(19), 6435–6443. https://doi.org/10.1523/JNEUROSCI.5925-11.2012

Wang, C., Liu, F., Liu, Y.-Y., Zhao, C.-H., You, Y., Wang, L., Zhang, J., Wei, B., Ma, T., Zhang, Q., Zhang, Y., Chen, R., Song, H., & Yang, Z. (2011). Identification and characterization of neuroblasts in the subventricular zone and rostral migratory stream of the adult human brain. *Cell Research*, *21*(11), 1534–1550. https://doi.org/10.1038/cr.2011.83

Wenzel, H. J., Buckmaster, P. S., Anderson, N. L., Wenzel, M. E., & Schwartzkroin, P. A. (1997). Ultrastructural localization of neurotransmitter immunoreactivity in mossy cell axons and their synaptic targets in the rat dentate gyrus. *Hippocampus*, *7*(5), 559–570. https://doi.org/10.1002/(SICI)1098-1063(1997)7:5<559::AID-HIPO11>3.0.CO;2-#

Wilson, M. A., & McNaughton, B. L. (1994). Reactivation of hippocampal ensemble memories during sleep. *Science (New York, N.Y.)*, *265*(5172), 676–679. https://doi.org/10.1126/science.8036517

Winter, B., Breitenstein, C., Mooren, F. C., Voelker, K., Fobker, M., Lechtermann, A., Krueger, K., Fromme, A., Korsukewitz, C., Floel, A., & Knecht, S. (2007). High impact running improves learning. *Neurobiology of Learning and Memory*, *87*(4), 597–609. https://doi.org/10.1016/j.nlm.2006.11.003

Wiskott, L., Rasch, M. J., & Kempermann, G. (2006). A functional hypothesis for adult hippocampal neurogenesis: Avoidance of catastrophic interference in the dentate gyrus. *Hippocampus*, *16*(3), 329–343. https://doi.org/10.1002/hipo.20167

Woollett, K., Spiers, H. J., & Maguire, E. A. (2009). Talent in the taxi: A model system for exploring expertise. *Philosophical Transactions of the Royal Society B: Biological Sciences*, *364*(1522), 1407–1416. https://doi.org/10.1098/rstb.2008.0288

Yang, S. M., Alvarez, D. D., & Schinder, A. F. (2015a). Reliable Genetic Labeling of Adult-Born Dentate Granule Cells Using *Ascl1* $^{CreERT2}$ and *Glast* $^{CreERT2}$ Murine Lines. *The Journal of Neuroscience*, *35*(46), 15379–15390. https://doi.org/10.1523/JNEUROSCI.2345-15.2015

Yang, S. M., Alvarez, D. D., & Schinder, A. F. (2015b). Reliable Genetic Labeling of Adult-Born Dentate Granule Cells Using Ascl1 CreERT2 and Glast CreERT2 Murine Lines. *Journal of Neuroscience*, *35*(1529-2401 (Electronic)), 15379–15390. https://doi.org/10.1523/JNEUROSCI.2345-15.2015

Yassa, M. A., & Stark, C. E. L. (2011). Pattern separation in the hippocampus. *Trends in Neurosciences*, *34*(10), 515–525. https://doi.org/10.1016/j.tins.2011.06.006

Yu, E. P., Dengler, C. G., Frausto, S. F., Putt, M. E., Yue, C., Takano, H., & Coulter, D. A. (2013). Protracted Postnatal Development of Sparse, Specific Dentate Granule Cell Activation in the Mouse Hippocampus. *The Journal of Neuroscience*, *33*(7), 2947–2960. https://doi.org/10.1523/JNEUROSCI.1868-12.2013

Yuste, R., MacLean, J., Vogelstein, J., & Paninski, L. (2011). Imaging Action Potentials with Calcium Indicators. *Cold Spring Harbor Protocols*, *2011*(8), pdb.prot5650. https://doi.org/10.1101/pdb.prot5650

Zhang, L., Prince, S. M., Paulson, A. L., & Singer, A. C. (2022). Goal discrimination in hippocampal nonplace cells when place information is ambiguous. *Proceedings of the*

*National Academy of Sciences of the United States of America*, *119*(11), e2107337119. https://doi.org/10.1073/pnas.2107337119

Zhang, Y., Rózsa, M., Liang, Y., Bushey, D., Wei, Z., Zheng, J., Reep, D., Broussard, G. J., Tsang, A., Tsegaye, G., Narayan, S., Obara, C. J., Lim, J.-X., Patel, R., Zhang, R., Ahrens, M. B., Turner, G. C., Wang, S. S.-H., Korff, W. L., … Looger, L. L. (2023). Fast and sensitive GCaMP calcium indicators for imaging neural populations. *Nature*, *615*(7954), Article 7954. https://doi.org/10.1038/s41586-023-05828-9

Zhao, C. (2006). Distinct Morphological Stages of Dentate Granule Neuron Maturation in the Adult Mouse Hippocampus. *Journal of Neuroscience*, *26*(1), 3–11. https://doi.org/10.1523/JNEUROSCI.3648-05.2006

Zhao, Z., Liu, H., Xiao, K., Yu, M., Cui, L., Zhu, Q., Zhao, R., Li, G.-D., & Zhou, Y. (2014). Ghrelin administration enhances neurogenesis but impairs spatial learning and memory in adult mice. *Neuroscience*, *257*, 175–185. https://doi.org/10.1016/j.neuroscience.2013.10.063

Zhou, Y., Su, Y., Li, S., Kennedy, B. C., Zhang, D. Y., Bond, A. M., Sun, Y., Jacob, F., Lu, L., Hu, P., Viaene, A. N., Helbig, I., Kessler, S. K., Lucas, T., Salinas, R. D., Gu, X., Chen, H. I., Wu, H., Kleinman, J. E., … Song, H. (2022). Molecular landscapes of human hippocampal immature neurons across lifespan. *Nature*, *607*(7919), 527–533. https://doi.org/10.1038/s41586-022-04912-w

Zhou, Y.-D., & Fuster, J. M. (2000). Visuo-tactile cross-modal associations in cortical somatosensory cells. *Proceedings of the National Academy of Sciences*, *97*(17), 9777–9782. https://doi.org/10.1073/pnas.97.17.9777

Zhou, Z., Wang, P., & Fang, Y. (2018). Social Engagement and Its Change are Associated with Dementia Risk among Chinese Older Adults: A Longitudinal Study. *Scientific Reports*, *8*(1), 1551. https://doi.org/10.1038/s41598-017-17879-w

Zhu, H., Aryal, D. K., Olsen, R. H. J., Urban, D. J., Swearingen, A., Forbes, S., Roth, B. L., & Hochgeschwender, U. (2016). Cre-dependent DREADD (Designer Receptors Exclusively Activated by Designer Drugs) mice. *Genesis (New York, N.Y.: 2000)*, *54*(8), 439–446. https://doi.org/10.1002/dvg.22949

Ziv, Y., Burns, L. D., Cocker, E. D., Hamel, E. O., Ghosh, K. K., Kitch, L. J., Gamal, A. E., & Schnitzer, M. J. (2013). Long-term dynamics of CA1 hippocampal place codes. *Nature Neuroscience*, *16*(3), 264–266. https://doi.org/10.1038/nn.3329

## Appendix A

1) **Frechou M. A.**, Martin S. S., McDermott K., Gökhan S., Tomé W. A., Coen-Cagli R., Gonçalves J. T. Adult neurogenesis improves spatial information encoding in the mouse hippocampus. bioRxiv. Dec 2022.

   First author manuscript submitted to Nature Communications. Currently addressing revisions.

2) Nasrallah K., **Frechou M.A.**, Yoon Y. J., Persaud S., Gonçalves J.T., Castillo P. E. Seizure-induced strengthening of a recurrent excitatory circuit in the dentate gyrus is proconvulsant. Proc Natl Acad Sci. Aug 2022.

   Second author. Paper published. Performed in vivo experiments, data analysis, experimental design, and discussions.

3) McDermott K., **Frechou M.A.**, Jordan J.T., Martin S. S., Gonçalves J. T. Delayed formation of neural representations of space in aged mice. bioRxiv. Mar 2023.

   Second author. Paper accepted at Aging Cell. Contributions: Conceptualization and Methodology (data analysis).

4) Jordan J.T., McDermott K. D., **Frechou M. A.**, Shtrahman M., Gonçalves J. T. Treadmill-based task for assessing spatial memory in head-fixed mice. STAR Protoc. Aug 2021.

Third Author. Contributed to setting up and validating 2-photon microscope. Built initial version of the treadmill.

# Adult neurogenesis improves spatial information encoding in the mouse hippocampus

**M. Agustina Frechou[1,2], Sunaina S. Martin[1,3], Kelsey D. McDermott[1,2], Şölen Gökhan[4], Wolfgang A. Tomé[4,5], Ruben Coen-Cagli[1,6], J. Tiago Gonçalves[1,2]***

**[1] Dominick P. Purpura Department of Neuroscience, Albert Einstein College of Medicine, Bronx, NY**

**[2]Gottesmann Institute for Stem Cell Biology and Regenerative Medicine, Albert Einstein College of Medicine, Bronx, NY**

**[3] Current address: Department of Psychology, University of California San Diego, La Jolla, CA**

**[4] Saul R. Korey Department of Neurology, Albert Einstein College of Medicine, Bronx, NY**

**[5] Department of Radiation Oncology, Albert Einstein College of Medicine, Bronx, NY**

**[6] Department of Systems and Computational Biology and Department of Ophthalmology and Visual Sciences, Albert Einstein College of Medicine, Bronx, NY**

***Lead author. Correspondence: tiago.goncalves@einsteinmed.edu**

## ABSTRACT

Adult neurogenesis is a unique form of neuronal plasticity in which newly generated neurons are integrated into the adult dentate gyrus in a process that is modulated by environmental stimuli. Adult-born neurons can contribute to spatial memory but it is unknown whether they alter neural representations of space in the hippocampus. Using *in vivo* two-photon calcium imaging, we found that mice that were previously housed in an enriched environment, which triggers an increase in neurogenesis, had increased spatial information encoding in the hippocampal dentate gyrus during novel context exposure. Ablating adult neurogenesis by prior focal irradiation of the hippocampus blocked the effect of enrichment and lowered spatial information content, as did the chemogenetic silencing of adult-born neurons. Both ablating neurogenesis and silencing adult-born neurons decreased the calcium activity rates of dentate gyrus neurons, resulting in a decreased amplitude of place-specific responses. These findings are in contrast to previous studies that suggested a predominantly inhibitory action for adult-born neurons. We propose that adult neurogenesis improves neural representations of space by increasing the gain of dentate gyrus neurons and thereby improving their ability to tune to spatial features. This mechanism may mediate the beneficial effects of environmental enrichment on spatial learning and memory.

## INTRODUCTION

Environmental factors such as cognitive stimulation and exercise can lead to memory improvements and are associated with a lower incidence of aging-related cognitive decline [1,2], as well as protection against neurodegeneration [3–5]. While the effects of these environmental manipulations are complex and systemic, in the mouse hippocampal dentate gyrus (DG)

environmental enrichment increases adult neurogenesis [6], resulting in the addition of adult-born neurons (ABNs) that contribute to DG-mediated memory [7]. Several studies have found that increasing ABN numbers generally enhances memory and cognition. ABNs have been found to contribute to diverse cognitive tasks such as spatial memory [8], cognitive flexibility [9], discrimination between memories of similar events [10–13], and memory elimination/forgetting [14]. However, the field still lacks a unified conceptual framework for how ABNs influence hippocampal function to mediate these different behavioral phenotypes. In mice, ABNs primarily contribute to DG-dependent memory, during a critical period at 4-6 weeks post mitosis [15,16], when the still-immature neurons are already synaptically integrated into DG circuits but remain more plastic and excitable than mature DG granule neurons [17,18]. Nevertheless, it is unclear how these properties change DG circuits to improve memory.

The DG and other areas of the hippocampus play an essential role in episodic and spatial memory [19,20] by forming a 'cognitive map'—a neural representation of space to which objects and events can be bound. DG neurons achieve this in part by functioning as 'place cells', firing selectively to a single location in space [21,22]. But even neurons that are not selectively tuned to a single place can contribute to the spatial information encoded in neural populations, and neuronal activity recordings from large populations can be used to decode the position of an animal within an environment [23,24], with the decoding accuracy reflecting the spatial information content. This spatial code is essential for spatial memory, as was recently demonstrated [25]. Since ABNs contribute to spatial memory, one might expect that these cells would be sparsely active and finely tuned to a specific place. However, immature ABNs are highly excitable [15,17,26,27] and less spatially tuned than their mature granule cell counterparts [28]. Current models of DG function propose that ABNs contribute to memory through the activation of local interneurons, resulting in a net increase in inhibition [29–33]. Yet it is unclear how this would affect neural representations of space in a novel environment. To address these open questions, we investigated whether increasing adult neurogenesis by housing mice in an enriched environment (EE) for 2 weeks would change the

DG spatial code. We recorded activity from granule neurons in the DG using two-photon calcium imaging, as the mice walked on a moving treadmill with spatial cues. This allowed us to estimate spatial information in a population composed almost entirely of mature DG neurons, since fewer than 1% of all the neurons of the DG are immature ABNs [34]. Then, in order to directly and causally demonstrate the role of adult neurogenesis in the DG neural code, we either chronically ablated DG neurogenesis by focal irradiation of the hippocampus, or acutely silenced immature ABNs using chemogenetics, and assessed the effect of these manipulations on DG spatial information content. We found that EE-exposure resulted in increased spatial information content in the DG, and that this increase requires immature ABNs. Moreover, our results show that ABNs act to increase the mean activity rates of all individual DG granule neurons, and the spatially-selective activity of neurons that are tuned to a single location on the treadmill. These findings provide a novel understanding of the action of ABNs on the encoding of information in the DG.

## RESULTS

### *Environmental enrichment increases spatial information encoding in the DG*

Environmental enrichment and exercise have been found to improve cognitive performance, including spatial memory in humans [2] and rodents [6], as well as increase the number of ABNs in the DG. We asked whether this improvement in spatial memory could be due to improved neural representations of space in the hippocampus. To address this question, we imaged the granule cell layer of the DG of mice housed in regular cages (RC) or in an EE with running wheels. We labeled DG neurons of 8-week old C57Bl6/J mice with an AAV encoding the red calcium sensor jRGECO1a [35] and implanted them with a titanium imaging 'window' (Fig. 1A), resting above the surface of CA1 of the dorsal hippocampus [36]. After the implantation surgery, mice were housed in regular cages for 3.5 weeks or in an EE cage for 2 weeks, before being returned to a RC. A single calcium imaging session took place ~3.5 weeks after surgery (Fig. 1A,B). Mice were head-

fixed to a treadmill with a belt composed of different texture materials (Fig. 1A), and imaged unanesthetized as the treadmill was rotated at a mean speed of ~420 cm/min (Fig. S1A,B, Movie S1). As expected, EE animals showed a ~2-fold increase in doublecortin (DCX) positive neurons (Fig. 1C). DG neuronal activity was sparse with an average of 86 neurons active during a 9 min recording session in a field of view of up to 343 μm x 343 μm, corresponding to 4.3 ± 0.8 % of all labeled putative neurons. To estimate spatial information content from the imaged neurons we trained a linear decoder to decode the position of the mouse on the treadmill from the calcium traces (trained on 75% and tested on 25% of the data to avoid overfitting). Since numbers of imaged and active neurons were substantially different across mice, we subsampled our datasets to compare decoding performance of equally-sized populations across different mice. Exposure to EE resulted in an increase in decoding accuracy compared to mice in RC (Fig. 1B, D, E), reflecting an increase in spatial information content in the DG. While multiple exposures to a single context are known to increase hippocampal spatial information within that same context [37,38], our findings show that 2-weeks of EE housing can increase spatial information in future exposures to a novel context.

***Prior focal irradiation of the hippocampus blocks the effects of EE on DG spatial encoding***

We then asked whether the changes in spatial encoding in EE mice were driven by an increase in the number of immature ABNs, rather than other systemic effects of EE housing. We recorded calcium activity in mice that had DG neurogenesis ablated by bilateral focal irradiation using opposing large fields [39] at 6 weeks of age (Fig. 2A, Fig. S2A,B). Irradiation results in the permanent ablation of DG adult neurogenesis (Fig. 2B,C), while preserving subventricular zone / olfactory bulb (OB) neurogenesis, as confirmed post hoc by the persistence of DCX immuno-reactive cells in the OB (Fig. S2C). A group of irradiated mice were housed under RC conditions (Irr+RC), whereas another group was exposed to EE (Irr+EE). EE exposure failed to increase decoding accuracy in irradiated mice, in contrast with non-irradiated mice (Fig. 2D). Additionally,

irradiated animals had lower decoder accuracy than their non-irradiated counterparts (Fig. 2D). These results suggest that the effects of EE on spatial encoding in the DG are driven primarily by immature ABNs, and that decreasing adult neurogenesis results in a decrease in spatial information in the DG, which could explain why reducing neurogenesis results in memory encoding deficits.

***Ablating adult neurogenesis decreases single-cell spatial information content***

Next, we studied whether changes in spatial information in the DG were driven by changes at the population level or at single-cell level. The information content of neural populations is determined jointly by the response properties of individual neurons, i.e. their tuning and the variability of their activity when repeatedly presented with the same stimulus (in this case each location on the treadmill belt) and by the structure of noise correlations (NCs; Cohen and Kohn, 2011), i.e how this variability is correlated among pairs of neurons [41,42]

We quantified spatial information using the linear Fisher Information (a measure of population sensitivity to spatial location, equivalent to d-prime; Kanitscheider et al., 2015) because it allows us to assess population-wide effects more accurately than decoding performance [44] and because it allows us to express the sensitivity also in terms of discrimination thresholds. First, to test the contribution of noise correlations to spatial information encoding in the DG, we created surrogate datasets where we shuffled the trial order independently for each neuron. The response of each neuron is given by the response at the same location but on a different trial/timepoint. Therefore, noise correlations are destroyed, but the tuning of individual neurons is preserved. Our results show that spatial information in the shuffled datasets was slightly increased although this difference was not significant (Fig. 3A-D), indicating that noise correlations have no effect on decoding accuracy in the DG or are may be even detrimental. This result suggests that the effect of ABNs on spatial information cannot be explained by a qualitative change in the structure of

noise correlations from detrimental to helpful for coding (see Discussion for the relation with two other recent studies of how noise correlations impact spatial information in DG and CA1; Stefanini et al., 2020; Hazon et al., 2022).

Next, we calculated the spatial information of individual neurons (Fig. 3E). We found that ablating neurogenesis strongly reduced spatial information for single neurons and that this reduction was present both among the neurons with most spatial information as well as neurons that had lower spatial encoding (Fig. 3F). As a more intuitive measurement, we also calculated a discrimination threshold, that is the minimum distance between two points on the treadmill that will be discriminated correctly 70% of the times (lower thresholds reflect a more precise spatial code; Fig. 3G). As expected, irradiated cohorts both in RC and EE conditions had increased discrimination thresholds. These findings indicate that the observed changes in DG spatial information occur primarily at single-cell level, which led us study in greater detail how the activity single-cells changes with EE exposure and the ablation of adult neurogenesis.

***Ablating adult neurogenesis reduces tuning specificity and single-cell activity***

To assess how single cell information changes in the DG, we mapped the calcium activity traces to the position of the mouse on the treadmill to generate a tuning vector (Fig. 4A,B). The mean calcium signal at each location was computed for every neuron and normalized to the time the mouse spent at that position. The modulus of the tuning vector was used as a spatial tuning index that reflects the place-specificity of activity [28]. Irradiated cohorts had significantly lower mean tuning indices than non-irradiated animals (Fig 4C). While both irradiated and non-irradiated groups had highly tuned cells, the distribution of tuning indices skewed lower in the irradiated cohorts, both for highly tuned cells as well as their low-tuning counterparts (Fig. S3A), suggesting that the lower information content in these mice could be caused by a decrease in the place-specificity of neuronal activity. This decrease in tuning could be caused by an overall change in

the calcium activity levels of DG neurons or by changes in how this activity is distributed along the treadmill belt. Since adult neurogenesis is usually thought to contribute to a net decrease in DG activity through the increased activation of feedback inhibitory circuits by immature adult-born neurons, we hypothesized that the DG neurons of irradiated mice would be hyperactive in comparison with the non-irradiated cohorts. To test this, we computed the calcium activity rates of cells that were active during recording sessions by integrating their calcium signals over each session and normalizing this to the distance travelled (see methods). In contrast to our expectation, we found that irradiated groups, where neurogenesis was ablated, had significantly reduced calcium activity (Fig. 4D). Keeping with this pattern, EE mice, which have increased neurogenesis, had significantly higher activity than their RC counterparts. Reduced calcium activity rates were found both among the most active neurons, as well as in the less-active quartiles (Fig. S3B), which is similar to our findings for tuning (Fig. S3A). To better determine how the tuning specificity changed in mice with ablated neurogenesis, we mapped the cumulative activity of each cell to create a tuning curve and fit a Von Mises function to the curves for every cell (Fig 4E). EE mice had significantly higher goodness-of-fit ($R^2$) than RC mice, while both irradiated groups had significantly lower $R^2$ than their non-irradiated counterparts (Fig. 4F). This could be a result of poorly fitted cells having flatter and/or noisier tuning, resulting in lower information content in irradiated animals [47]. The peak width of fitted curves was not significantly different across experimental groups (Fig. 4G), indicating that differences in spatial information were not due to increased lap-to-lap variance in the location to which individual DG neurons are responsive. However, the peak amplitude of fitted cells was significantly lower in the irradiated cohorts (Fig. 4H), reflecting a dampened place-specific response of individual neurons. These results suggest that the reduction in spatial information content (Fig. 2D, 3E) is driven by two components at the single cell level: an overall reduction in tuning selectivity explained by a decreased number in well-tuned cells, and a reduction in the amplitude of the tuning curve with no change in the lap-to-lap variance of the location of the tuning maximum, as observed by the

unchanged peak widths. These results suggest that integrating ABNs may be either directly or indirectly modulating the gain of DG neurons, increasing calcium activity rates in a multiplicative manner, which for well-fitted neurons ($R^2 > 0.5$) reflects as a larger increase in calcium activity at the preferred location of each neuron than at non-preferred locations, thereby increasing tuning curve slope and spatial information. Furthermore, because gain modulation can also influence trial by trial variability [48,49], and variability limits single-neuron spatial information, our finding of increased spatial information indicates that the presence of immature ABNs leads to an increase response gain without increasing variability as much. However, the changes we observed could also be due to a non-specific side effect of irradiation. We therefore investigated whether the same circuit effects were present in mice where ABNs were silenced using a chemogenetic approach.

***Acute chemogenetic silencing of ABNs decreases spatial information content in the DG***

Previous studies suggested that synaptic competition between ABNs and mature neurons plays a role in mediating the effects of adult neurogenesis on DG networks. By disrupting the synaptic connectivity of mature neurons, ABNs force the rewiring of the circuit[50–52]. We asked whether ABN-induced changes in spatial information content required ABN activity or were a product of their integration into the DG. To address this question, we acutely silenced a cohort of ABNs by crossing Ascl1-CreERT2 knock-in mice[53] with a line expressing the inhibitory DREADD hM4Di[54,55] in a Cre-dependent manner, allowing us to specifically target a cohort of newborn ABNs. Animals were injected daily with Tam for 3 days at 8 weeks of age (Fig. 5A) and housed in EE conditions. Littermates lacking hM4Di expression were used as controls for the unspecific effects of CNO. To assess the efficacy of ABN silencing, and since hM4Di can inhibit synaptic release independently from its effect on action potential firing [54], we testing the effects of CNO-induced silencing on mouse behavior. We used a context discrimination task where the animals are conditioned to associate a specific context with a foot shock (Fig. 5B). In line with previous studies[10,11,28],

silencing ABNs resulted in impaired discrimination between a Context A where the animals were shocked, and a novel Context B (Fig. 5C,D). All mice were injected with an AAV encoding jRGECO1a and implanted with an imaging window over the hippocampus 2 weeks after the end of Tam treatment, and imaged 3.5 weeks after implantation, both in baseline conditions and 30 minutes after an i.p. CNO injection (5 mg/kg). The exact same field of view was imaged in both sessions. Consistent with our previous results in irradiation experiments, single-cell Fisher information (Fig. 5G), $Ca^{2+}$ activity (Fig. 5I) and tuning index (Fig. 5K) were significantly reduced after silencing ABNs with CNO, but were unchanged in control animals that did not express hM4Di (Fig. 5H,J,L). We also fit the tuning curves of DG neurons before and after CNO administration to a von Mises function. The goodness-of-fit ($R^2$) showed a trend for decrease as seen in the irradiated cohorts but no significant difference was found, including when only well-fit cells ($R^2$>0.5) were considered (Fig. 5M,N). Similar to our previous experiments, no significant change was seen in the width of the fitted tuning curves, while their amplitude was decreased upon CNO administration (Fig. 5O,P). This difference was not present in control animals that did not express hM4Di, although we did see a significant increase in the peak width of controls following CNO administration, which could reflect an unspecific effect of CNO (Fig. S4). Given these findings, we conclude that the effect ABNs on the neural representations of space in the DG is dependent on their activity. Silencing ABNs generally replicated our results from the ablation experiments, suggesting that spatial information changes in the irradiated cohorts were not due to potential side effects of irradiation, such as increased inflammation. Taken together, these results indicate that ABNs increase spatial information in the DG by increasing the spatial selectivity of otherwise untuned DG granule cells, and leading to an increase in the gain of DG granule neurons, either directly or through other circuit mechanisms.

## DISCUSSION

Adult neurogenesis is a unique type of brain plasticity that involves the addition of new neurons in response to environmental factors and other stimuli. In the years since ABNs were first reported in the rodent DG[56], several studies have confirmed their presence in humans [57–59] and other species, characterized their cellular and physiological properties, and identified their different contributions to memory tasks. Despite this progress, the processes mediating the contribution of ABNs to behavior remain poorly understood, partially due to the technical difficulties of recording population activity in DG circuits *in vivo*. More recently, several studies made use of *in vivo* calcium imaging to determine how the DG encodes space, finding that a portion of DG neurons are spatially selective, although immature ABNs were less selective than their mature counterparts [28,60,61]. In this work we used a similar *in vivo* imaging approach to determine how the DG spatial code changes when adult neurogenesis is upregulated with EE or, conversely, when neurogenesis is ablated, or ABNs are silenced. We imaged naïve mice during their first exposure to a moving treadmill. Our results showed that 2 weeks of EE housing prior to imaging increases spatial information content in the DG (Fig. 1), and that this increase requires ABNs (Fig. 2). This change in neural representations following EE is a novel phenotype that potentially explains why EE and similar environmental manipulations are beneficial to memory and learning. We also found that ablating ABNs decreases spatial information content in the DG (Fig. 2D, 3F). We then showed that these ABN-driven changes are mediated by an increase in spatially selective activity at the single cell level (Fig. 4D, 4H). Furthermore, we described a potential dual mode of action for ABNs: increasing overall tuning selectivity and response gain of DG neurons, which in well-tuned cells results in an increase in activity specifically at the tuning maximum. Finally, we showed that ABN activity is required to elicit the changes in information content in the DG, as both tuning selectivity and spatial information were reduced after acutely silencing a cohort of immature ABNs (Fig. 5G, 5K). Overall, these findings amount to a novel role for ABNs in modulating information encoding in the DG.

ABNs are thought to have a net inhibitory effect on DG activity [29–31], which is regarded as beneficial for tasks such as contextual memory discrimination since the resulting increase in sparsity reduces the overlap between neuronal populations responding to different stimuli. The mechanisms behind this inhibitory action are not entirely understood, as immature ABNs are only poorly coupled to feedback inhibitory circuits in the DG [62,63]. Our results stand in contrast with mechanistic models that propose an inhibitory effect of ABNs: we found that increasing the number of ABNs modulates the gain of DG neurons, leading to higher single-cell calcium activity rates (Fig. 4D). In addition, this increase in activity was spatially selective: it conveyed spatial tuning to otherwise untuned cells, and increased spatial information of tuned cells by increasing activity near the peak more than at other locations. Our results do not necessarily mean that the net effect of ABNs in the DG is excitatory, since our analyses only considered neurons that were active during each imaging session while other studies found differences in the fraction of active neurons. It is possible that ABNs act to reduce the fraction of active DG neurons while at the same time increasing the firing rate of those same active neurons. Of note, a recent calcium imaging study found that voluntary exercise, which also increases adult neurogenesis, leads to increased calcium activity and spatial information in CA1 [64]. Conversely, another study, using single unit electrophysiology recordings, found that silencing ABNs reduces population sparsity throughout hippocampal subfields, without affecting single-neurons spatial information [65].

Since our AAV labeling approach targets all excitatory DG neurons, both mature DG neurons and immature ABNs will express the calcium sensor. The increase in single-cell calcium activity with EE could potentially be due to more ABNs being present in the field of view, their higher excitability resulting in increased calcium activity. However, this is unlikely, first because immature ABNs comprise a very small proportion (< 1%, Kempermann et al., 1997) of the total DG granule cell population, but also because they are less spatially tuned [28], whereas we observed a significant

increase in tuning. In order to further verify this, we replicated our main results using a labeling approach that targets mature DG neurons specifically (Fig. S5).

The positive correlation between neurogenesis and DG neuronal activity suggests that the contribution of ABNs to the DG neural code is not solely mediated by feedback inhibitory circuits. In addition to making weak connections to local interneurons, immature ABNs also form synapses with mossy cells, a population of excitatory neurons whose axonal arbors innervate large portions of the DG granule cell layer [66]. It is possible that recurrent excitation through mossy cells may mediate the increase in tuning of DG neurons in mice with elevated adult neurogenesis. Our finding that ABNs act by modulating the gain of DG granule cells offers an additional clue about potential mechanisms. Gain modulation has been shown recently to influence response variability in visual cortex [48] producing diverse effects depending on the stimulus and other factors [67]. In our analysis, the gain increase induced by ABNs did not increase lap-by-lap variability of responses disproportionately, because if it did, then spatial information would decrease despite the higher response amplitude and tuning slope. ABNs may thus act by recruiting a network mechanism that simultaneously increases DG activity and stabilizes it by modulating the balance of recurrent excitation and inhibition [68–71].

In one set of experiments we used irradiation as a method to ablate neurogenesis, which can result in increased inflammation and other side effects. We therefore resorted to a well-established method of focal irradiation [39], and allowed a one-month period of recovery prior to imaging sessions to allow for inflammation to subside. Still, the side effects of irradiation [72,73] could account for some of the changes observed in our study. To account for this, in separate experiments, we used a chemogenetic approach to acutely silence ABNs. We obtained similar results as in irradiated animals (Fig. 5), namely a loss of spatial information and reduction in neuronal activity when ABNs were silenced, although the effects of silencing were less

pronounced than those of irradiation. This is likely because fewer neurons are targeted when using chemogenetics and, in addition, even neurons that express hM4Di will likely not be completely silenced by CNO administration. Our silencing approach used an inducible transgenic mouse line to express hM4Di in Ascl1+ progenitors that give origin to both DG and olfactory bulb (OB) ABNs. Silencing olfactory bulb ABNs could potentially result in decreased olfactory discrimination, which could in turn impact spatial tuning in the DG as the animals may also use olfaction to navigate the treadmill. However, our irradiation experiments showed a significant difference in spatial tuning when DG neurogenesis is selectively ablated and sub-ventricular zone neurogenesis is spared, therefore we do not expect that OB ABNs contribute to DG spatial representations. Overall, our results are remarkably consistent across the two techniques used to induce a loss-of-function of immature ABNs.

Another potential caveat in our experiments is the use the AAV vectors to deliver the jRGECO1a calcium sensor. Although AAVs have been widely used in a variety of neuroscience applications, including *in-vivo* calcium imaging, recent findings have demonstrated that intermediate progenitor cells and < 2-week-old ABNs can undergo apoptosis when targeted by AAVs [74]. To overcome this caveat, we optimized our protocol to limit the time between AAV injections and imaging. Nevertheless, we performed an additional control experiment using a retrograde AAV vector injected into hippocampal area CA3. The retrograde viral vectors were taken up by the axonal terminals of DG granule neurons, resulting in the expression of jRGECO1a in the ipsilateral granule layer while preserving similar numbers of ABNs in the injected and contralateral hemispheres. Using this approach, we were able to confirm that housing mice in EE elicited an increase in calcium activity and spatial information content in the DG (Fig. S5). Although tuning trended higher in EE mice, this difference was not significant with our sample size. Importantly, in this control experiment no immature (<6 weeks-old) ABNs were labeled, since their axons had not reached CA3 at the time of the viral injection. This confirms that the changes in neuronal

activity leading to improved spatial coding occur in the mature granule cells, and not only in the immature ABNs.

In our analysis of the factors that contribute to spatial encoding, we found that noise correlations between neurons had no effect on spatial information content or were even detrimental to it (Fig 3A-D), although spatial information in the shuffled datasets was not significantly different. This suggests that noise correlations might limit the amount of spatial information encoded by the DG, similar to recent results in CA1 [46], although one caveat is that we imaged a relatively low number of active cells when compared with the entirety of the DG coding space, as DG activity is very sparse. Our result is different from, but not incompatible with, a related finding in DG [45], which showed that knowing the structure of noise correlations helps to correctly decode the available information [41,43]. Furthermore, in our data the effects of noise correlation do not appear to be qualitatively modulated by adult neurogenesis, namely, the action of ABNs did not induce a switch from detrimental to beneficial noise correlations.

While our work focused on spatial information, several types of neuronal coding modalities likely coexist in the DG. Neurons in the dorsal DG encode not only position, but also direction of motion, speed [28,45], as well as other sensory cues [60,61], and a population of stress-responsive cells has also been found in the ventral DG [29]. It is therefore possible that ABNs have different effects on the encoding of different sensory features or contexts, so recordings in the ventral DG or during specific behavioral tasks may reveal different functional roles for ABNs. Alternatively, the gain amplification effect we identified could generalize beyond spatial information and improve encoding across other modalities.

In summary, our results indicate that adult neurogenesis leads to increased response gain in the DG, improving the ability of the granule cells to tune to spatial features and therefore improving spatial information encoding. Our findings demonstrate that the spatial information content in the

DG can be modulated even by brief environmental manipulations, such as EE housing, that result in changes in the number of ABNs. The increased spatial information and resulting improvement in the accuracy of neural representations of space in mice with elevated neurogenesis provide a novel mechanistic, circuit-level explanation for their improved performance at many spatial memory tasks [8]. Furthermore, our findings provide novel directions for the study of how ABNs contribute to memory, identifying new modes of action that could be harnessed as a therapeutic target for memory disorders.

## ACKNOWLEDGEMENTS

We would like to thank Jake Jordan, Roland Ferger, Elizabeth Wood, Maria Gulinello and Sacha Sokoloski for technical advice, assistance and discussions. M.A.F. was supported by a Fulbright Scholarship. M.A.F. and K.D.M. were funded by The Einstein Training Program in Stem Cell Research from the Empire State Stem Cell Fund through New York State Department of Health Contract C34874GG. J.T.G. acknowledges the support of the Whitehall Foundation (Research Grant 2019-05-71) and the National Institutes of Health (NINDS R01NS125252-01A1). R.C.C. acknowledges the support of the National Institutes of Health (NEI R01EY030578, NIDA RF1DA056400). This article is dedicated to the memory of Dr. Paul S. Frenette (1965-2021) who provided invaluable encouragement and support for this project.

## AUTHOR CONTRIBUTIONS

Project conceptualization: M.A.F., J. T. G.; Experimental design and data acquisition:, M.A.F., S.S.M. S.G., W.A.T., J.T.G.; Data analysis: M.A.F., R.C.C, J.T.G,; Writing, editing and discussion:, M.A.F., K.D.M., R.C.C., J.T.G.

## DECLARATION OF INTERESTS

The authors declare no competing interests.

## ONLINE METHODS

### Animals

We used male and female C57BL6/J (Jackson Labs Stock #664) or, for chemogenetic silencing experiments, the offspring of hM4Di-Dreadd (Jackson Labs #26219) and Ascl1-Cre-ERT2 mice (Jackson Labs #12882). All mice were kept on a 12h light/dark cycle and were allowed standard chow and water ad libitum. Animals were housed in groups of 3-5 and littermates were divided between experimental groups. Mice assigned to enriched environment (EE) housing were housed in groups of 5-10 in a large 121 x 61 cm enriched cage, containing a feeder, water dispenser, several running wheels, as well as plastic tubes, domes and other structures. Mice assigned to EE experimental groups were housed in EE cages starting the day after the implantation surgery and for a period of 2 weeks, after which they were returned to RC conditions for the remainder of the experiment. Female and male mice were never mixed in the same cage, and all males were housed with littermates. Regular cage (RC) controls were housed in groups of up to 5 mice in standard mouse cages (dimensions 28 cm x 18 cm) containing a wire feeder and a water bottle. Experiments were carried out during the light phase of the cycle. All procedures were done in accordance with a protocol approved by the Institutional Animal Care and Use Committee (Protocol #: 00001197).

### Focal Irradiation

We permanently ablated adult neurogenesis in the dentate gyrus (DG) by bilateral focal irradiation of the hippocampus using opposed lateral fields (Fig. S2) in C57BL/6J mice (Jackson Labs #664).

First, we traced the location of both hippocampi from a thin slice 9.4 T, T1 weighted MRI. Irradiation was performed using a small animal radiation device (SARRP, Xstrahl). To ensure a reproducible treatment setup, the mice were briefly anesthetized with isoflurane and immobilized using a custom fixation system prior to radiation delivery. Cone-beam computed tomography was used to setup the irradiation fields and for calculating individual irradiation times, ensuring accurate and reproducible delivery of the intended irradiation. Hippocampal focusing irradiation was delivered using a 3 mm x 10 mm irradiation field positioned to cover the dorsal part of the brain, avoiding the olfactory bulb and subventricular zone (SVZ). A single dose of 10 Gy (at 2.5 Gy/min) was administered to trigger cell death within the hippocampus [39]. Irradiated mice were allowed one month to recover prior to imaging.

**Viral labeling and window implantation surgery**

The right hemisphere dentate gyrus (DG) was labeled with an AAV vector that expressed the jRGECO1a genetically encoded calcium sensor [35] under the control of the CaMKIIα promoter (DJ serotype AAV-CaMKIIα.jRGECO1, University of North Carolina Vector Core, plasmid kindly donated by Dr. Fred Gage). Mice were anesthetized with isoflurane (induction: 5%, maintenance: 2% in $O_2$ vol/vol, via nose cone) and placed in a stereotaxic frame. The right DG was stereotactically targeted[75] with a pulled-glass micropipette and 950 nl of viral solution (5.4 $x10^{12}$ viral particles/mL) were injected with a microinjector (Drummond Nanoject III).

Mice also underwent surgery to implant an imaging 'window': a 3 mm craniotomy was drilled around the viral injection site and a custom-made titanium ring with a glass bottom was placed immediately above the dorsal surface of the hippocampus and anchored to the skull with dental cement [36,76] . The alveus and all hippocampal structures were left untouched during this procedure. A small titanium bar (9.5 x 3.1 x 1.3 mm) was also attached to the skull in order to

attach the animal to the microscope stage. Mice were given carprofen (5 mg/kg) for inflammation and analgesic relief.

### *In vivo* 2-photon calcium imaging

*In vivo* calcium imaging was performed 3 to 4 weeks after surgery when mice were 11.5 – 13.5 weeks of age. We used a two-photon microscope (Thorlabs Bergamo) equipped with a 16x 0.8 NA objective (Nikon) and a Fidelity-2 1070 nm laser (Coherent) as a light source. The mice were head-fixed and placed on a treadmill belt. For optimum light transmission, the angle of the mouse's head was adjusted to ensure that the imaging window was perpendicular to the optical axis of the objective. Movies of calcium activity were acquired at 15 frames/s using an average laser power of ~120-180 mW, as measured in front of the objective.

### Imaging Acquisition

We acquired 9 minutes of calcium activity recordings for each mouse. The animals were imaged as they walked head-fixed on a previously described treadmill [77] which was manually rotated at a speed of approximately 421±23 cm/min (Fig. S1B). The treadmill consisted of a belt with 4 different textures each 45 cm length (velvet, smooth, 2.5 cm-diameter sandpaper disks of 100 and 60 grit) wound around two wheels. An optical rotary encoder was attached to the axel of one wheel to measure the movement of the belt, enabling the estimation of the position of the mouse along the belt. Four radio frequency identification (RFID) tags were attached to the belt at transition zones between textures to correct the accumulating error of position estimation by the rotary encoder data. Data from the treadmill was acquired using digitizer hardware (National Instruments) and the ThorSync software (Thorlabs). The treadmill and microscope setting were completely novel to the mice, which were allowed to sit still or freely move and explore the

treadmill during initial setup, but were required to walk during imaging, as the treadmill was rotated. Throughout the imaging session, the mice remained in the dark, in an enclosed box built around the microscope.

**Silencing of adult-born neurons**

To study the effects of adult neurogenesis on hippocampal circuits we recorded DG activity (or contextual conditioning behavior) before and after silencing a cohort ABNs. We targeted ABNs by crossing Ascl1-CreERT2 transgenic mice[53] (Jackson Labs #12882) with a line expressing the inhibitory DREADD hM4Di[54,55] in a Cre-dependent manner (Jackson Labs #26219). Mice with the two alleles allowed us to specifically target a cohort of newborn ABNs by injecting Tamoxifen (Tam) i.p. over the course of 3 days to express Cre in Ascl1+ cells, thereby inducing Cre expression. This approach resulted in hM4Di expression in both DG and SVZ newborn ABNs. We acutely silenced ABNs by administering the specific hM4Di ligand clozapine-N-oxide (CNO)[54] 30 minutes prior to imaging behavioral testing, as described above. CNO was dissolved at a concentration of 1 mg/mL in saline solution (0.9% NaCl) and was injected intraperitoneally at a dose of 5 mg/kg [78]. We used littermates lacking the Cre allele, and therefore hM4Di expression, as controls for the unspecific effects of CNO and Tam.

**Analysis of calcium imaging data**

Calcium imaging fluorescence intensity data was extracted from movies using the Suite2p open-source software suite [79]. Briefly, all movies were registered for motion correction, the cell contours of active cells were detected and calcium traces extracted for each cell. Movement (rotary encoder) and texture (RFID) data were matched with the corresponding imaging frames. The position of the mouse on the treadmill was determined by calculating the cumulative sum of the treadmill rotation signal for every frame of the calcium imaging movie.

To decode the spatial position from the neuronal population activity, we used a logistic regression model [43], trained on 75% of the data and tested using the remaining 25%, cross-validating using 10 random splits of the data to account for overfitting. We determined that decoding the position from unfiltered fluorescence traces yielded the best results and dynamic range, as either filtering, thresholding or deconvolution results in consistently very high or very low decoding accuracy (Fig. S1C,D,E). We also verified that decoder performance was similar on train and test data, indicating minimal overfitting (Fig. S1F,G). The position data was segmented into 20 bins and ΔF/F unfiltered calcium traces were used as input data. The population activity was projected onto the decoder weights to obtain a 1D signal and compute d-prime squared (which is equivalent to linear Fisher information).

Single-cell Fisher Information (FI) was calculated using the ΔF/F unfiltered fluorescence calcium data using previously published methods [43]. Briefly, a bias-corrected signal to noise ratio was computed, where the signal is the square of the difference of the mean activity at two locations on the treadmill, and the noise is the average variance of the activity at each location. The position data was segmented into 20 bins.

Tuning indices were calculated using deconvolved firing rates [80], which were thresholded to 2 $\sigma$ of the baseline, so that every point not significantly above that noise threshold is set to zero. The treadmill band was segmented into 100 position bins and the putative firing epochs were mapped to these bins according to the location of the mice on the treadmill in order to generate a tuning vector for each cell [28]. The mean of the thresholded firing rates at each location was calculated for every neuron and normalized to the time the mouse spent at that position. The tuning index was defined as the modulus of this normalized tuning vector.

Calcium activity was calculated on a per-cell basis: ΔF/F data was first filtered with a third order Butterworth lowpass filter by applying the filter to the data both forwards and backwards to compensate for phase shifts. Significant calcium transients were determined as the consecutive frames that start when the ΔF/F fluorescence signal rises 2 standard deviations ($\sigma$) above the

rolling-mean baseline and end when the signal drops below 0.5 $\sigma$. The significant transients were then removed, and the remaining calcium trace was used to calculate a new rolling mean baseline, iterating through this process 3 times. The resulting significant calcium transient was used to determine the activity as the cumulative sum of the trace for each cell. The result was normalized to the total distance traveled by the mouse.

**Curve Fitting Analysis**

To study the properties of tuning of every cell, we first generated a tuning curve by mapping the unfiltered ΔF/F fluorescence data of each cell to one of 20 angular position bins on the treadmill belt. This fluorescence data was averaged over all laps. This circular tuning curve was fitted with Von Mises function:

$$B + Ae^{k(\cos(x-\varphi)-1)}$$

Where B is an offset parameter, A is the amplitude of the peak, $k$ is a measure of concentration and $\varphi$ is the location of the peak of tuning. The parameters of the function were optimized numerically by minimizing the sum of squared differences between data and model. The goodness of fit was calculated and cross validated as follows:

$$R^2 = 1 - (ss\_res / ss\_tot)$$

Where *ss_res* is equal to the sum of the squares of the residuals and *ss_tot* equals the sum of the squares of the differences from the mean. Note that this value of $R^2$ is normalized between 0 (null model, i.e. *ss_res_null* = *ss_tot*) and 1 (oracle model, i.e. *ss_res_oracle* = 0): a $R^2$ value of zero corresponds to a model where none of the variance can be explained by the Von Mises function and 1 corresponds to an error equal to zero, predicting all of the data points. The cross-validation was done using 75% of the data in each bin to train and 25% of the data to test the model. The width of the peak was determined as the circular variance using the function below:

$$V = 1 - \frac{I_1(k)}{I_0(k)}$$

Where $I_1$ is the Bessel function of order 1 and $I_0$ is the Bessel function of order 0 [81].

**Immunohistochemistry**

In order to quantify the numbers of ABNs we labeled brain tissue with an antibody against Doublecortin (DCX) (CST 14802S, 1:800). To quantify hM4Di expression, we stained brain tissue with an antibody against HA-Tag (CST 37224S, 1:800). Briefly, animals were perfused with ice cold 0.1M phosphate buffer saline followed by 4% paraformaldehyde (PFA) and were then post-fixed in 4% PFA for 24 hours. Brains were then cryoprotected in 30% sucrose and the hippocampus was sectioned at 40 μm thickness on a freezing microtome, three sections were stained for each mouse, all within the implanted region of the hippocampus. Sections were rinsed three times in 0.1M PBS (pH = 7.4) and incubated in a blocking solution (10% goat serum, 0.3% Triton-X in 0.1M PBS) for one hour. The sectioned tissue was then incubated in a primary antibody in block for 48 hours, followed by three rinses in 0.1M PBS. The sections were then incubated for 2 hours in Alexa 488 (A11034), Alexa 568 (A11011), or Alexa 633 (A21070) goat anti-rabbit secondary antibodies (Invitrogen) diluted at 1:500 in 0.1M PBS, rinsed three times in 0.1M PBS, counterstained with 300nM DAPI in 0.1M PBS, rinsed again in 0.1M PBS, and then mounted and cover-slipped with Fluoromount-G (Southern Biotech). The tissue was then imaged on a Zeiss Axio Imager.A2 fluorescence microscope. Animals in which there was no expression in the dorsal hippocampus were removed from analysis.

**Contextual Discrimination Task**

Mice were placed in a fear conditioning chamber within a sound-attenuating cubicle (Med Associates VideoFreeze). For conditioning, mice were allowed 3 minutes of free exploration of a pre-cleaned cube-shaped chamber with a grid floor (context A) before receiving three mild foot-shocks (2s, 0.7 mA) spaced 60 seconds apart. Mice were returned to their home cage 30 seconds after the last shock. Contextual fear memory was tested 24 hours later by re-exposing mice to context A for 3 minutes of free exploration (no shocks). Forty-eight hours after conditioning, mice were tested on discrimination of a novel context B (plastic floor, A-frame geometry, and scented). In this session, mice were allowed 3 minutes of free exploration (no shocks). Context discrimination was measured as a discrimination index, DI: (Time freezing in A – Time freezing in B)/(Time freezing in A + Time freezing in B). In silencing experiments, we expressed hM4Di specifically in a cohort of immature ABNs so they could be silenced by the selective ligand CNO. Conditioning and re-exposure to context A took place without CNO but were injected with CNO 30-40 minutes prior to exposure to the novel context B. To control for unspecific effects of CNO we used mice that lacked a Cre allele, and therefore did not express hM4Di (hM4Di-).

**Statistical analyses**

A non-parametric two-tailed Mann-Whitney test was used to compare between mouse groups. When pooling cell data from different mice into a single experimental group, significance testing was done using a muti-level bootstrapped approach that took data nesting into account, as follows. To assess a significant difference between two experimental conditions (e.g. EE and RC), the null distribution was constructed for each condition as follows: The data from both conditions was combined into one group. The animal and data value were sampled in each condition, a total equivalent to the number of data values within the condition. The mean was then calculated. This process was repeated for each condition and the difference between the null distributions generated for each group was calculated. 100,000 bootstraps were generated. The empirically

observed value of the difference between conditions was then compared to the null distribution. The statistical significance level ($\alpha$) was set at 0.05. Bonferroni's correction for multiple comparisons was applied. One-sample t-tests with Bonferroni's correction for multiple comparisons were used to determine differences between group means and chance performance in contextual fear conditioning experiments.

**Data and code availability**

The analysis code used in this study is openly available at https://github.com/GoncalvesLab/Frechou-et-al-Neurogenesis .

[*All the imaging data used in this study, consisting of calcium traces for every active cell and the position of the mouse on the treadmill, will be made openly available on a repository site before final publication. Due to their large size, raw calcium imaging movies will be made available upon request.*]

**REFERENCES**

1. Lövdén, M. *et al.* Spatial navigation training protects the hippocampus against age-related changes during early and late adulthood. *Neurobiol Aging* **33**, 620.e9-620.e22 (2012).
2. Vemuri, P. *et al.* Association of Lifetime Intellectual Enrichment With Cognitive Decline in the Older Population. *JAMA Neurol* **71**, 1017–1024 (2014).
3. Ngandu, T. *et al.* A 2 year multidomain intervention of diet, exercise, cognitive training, and vascular risk monitoring versus control to prevent cognitive decline in at-risk elderly people (FINGER): a randomised controlled trial. *The Lancet* **385**, 2255–2263 (2015).
4. Norton, S., Matthews, F. E., Barnes, D. E., Yaffe, K. & Brayne, C. Potential for primary prevention of Alzheimer's disease: an analysis of population-based data. *The Lancet Neurology* **13**, 788–794 (2014).
5. Verghese, J. *et al.* Leisure activities and the risk of dementia in the elderly. *N Engl J Med* **348**, 2508–2516 (2003).

6. Kempermann, G., Kuhn, H. G. & Gage, F. H. More hippocampal neurons in adult mice living in an enriched environment. *Nature* **386**, 493–495 (1997).
7. Shors, T. J. *et al.* Neurogenesis in the adult is involved in the formation of trace memories. *Nature* **410**, 372–376 (2001).
8. Garthe, A. & Kempermann, G. An old test for new neurons: refining the Morris water maze to study the functional relevance of adult hippocampal neurogenesis. *Front Neurosci* **7**, 63 (2013).
9. Burghardt, N. S., Park, E. H., Hen, R. & Fenton, A. A. Adult-born hippocampal neurons promote cognitive flexibility in mice. *Hippocampus* **22**, 1795–1808 (2012).
10. Clelland, C. D. *et al.* A Functional Role for Adult Hippocampal Neurogenesis in Spatial Pattern Separation. *Science* **325**, 210–213 (2009).
11. Sahay, A. *et al.* Increasing adult hippocampal neurogenesis is sufficient to improve pattern separation. *Nature* **472**, 466–470 (2011).
12. Nakashiba, T. *et al.* Young Dentate Granule Cells Mediate Pattern Separation, whereas Old Granule Cells Facilitate Pattern Completion. *Cell* **149**, 188–201 (2012).
13. Niibori, Y. *et al.* Suppression of adult neurogenesis impairs population coding of similar contexts in hippocampal CA3 region. *Nat Commun* **3**, 1253 (2012).
14. Akers, K. G. *et al.* Hippocampal Neurogenesis Regulates Forgetting During Adulthood and Infancy. *Science* **344**, 598–602 (2014).
15. Gu, Y. *et al.* Optical controlling reveals time-dependent roles for adult-born dentate granule cells. *Nat Neurosci* **15**, 1700–1706 (2012).
16. Denny, C. A., Burghardt, N. S., Schachter, D. M., Hen, R. & Drew, M. R. 4- to 6-week-old adult-born hippocampal neurons influence novelty-evoked exploration and contextual fear conditioning. *Hippocampus* **22**, 1188–1201 (2012).
17. Marín-Burgin, A., Mongiat, L. A., Pardi, M. B. & Schinder, A. F. Unique Processing During a Period of High Excitation/Inhibition Balance in Adult-Born Neurons. *Science* **335**, 1238–1242 (2012).
18. Overstreet-Wadiche, L. S. & Westbrook, G. L. Functional maturation of adult-generated granule cells. *Hippocampus* **16**, 208–215 (2006).
19. Scoville, W. B. & Milner, B. Loss of recent memory after bilateral hippocampal lesions. *J. Neurol. Neurosurg. Psychiatr.* **20**, 11–21 (1957).
20. Morris, R. G. M., Garrud, P., Rawlins, J. N. P. & O'Keefe, J. Place navigation impaired in rats with hippocampal lesions. *Nature* **297**, 681–683 (1982).
21. O'Keefe, J. & Dostrovsky, J. The hippocampus as a spatial map. Preliminary evidence from unit activity in the freely-moving rat. *Brain Research* **34**, 171–175 (1971).
22. O'Keefe, J. & Nadel, L. *The hippocampus as a cognitive map*. (Clarendon Press ; Oxford University Press, 1978).
23. Skaggs, W. E., McNaughton, B. L., Gothard, K. M. & Markus, E. J. An information-theoretic approach to deciphering the hippocampal code. in *Proceedings of the 5th International Conference on Neural Information Processing Systems* 1030–1037 (Morgan Kaufmann Publishers Inc., 1992).
24. Stefanini, F. *et al.* A Distributed Neural Code in the Dentate Gyrus and in CA1. *Neuron* (2020) doi:10.1016/j.neuron.2020.05.022.
25. Robinson, N. T. M. *et al.* Targeted Activation of Hippocampal Place Cells Drives Memory-Guided Spatial Behavior. *Cell* **183**, 1586-1599.e10 (2020).
26. Snyder, J. S., Kee, N. & Wojtowicz, J. M. Effects of Adult Neurogenesis on Synaptic Plasticity in the Rat Dentate Gyrus. *Journal of Neurophysiology* **85**, 2423–2431 (2001).
27. Schmidt-Hieber, C., Jonas, P. & Bischofberger, J. Enhanced synaptic plasticity in newly generated granule cells of the adult hippocampus. *Nature* **429**, 184–187 (2004).
28. Danielson, N. B. *et al.* Distinct Contribution of Adult-Born Hippocampal Granule Cells to Context Encoding. *Neuron* **90**, 101–112 (2016).

29. Anacker, C. *et al.* Hippocampal neurogenesis confers stress resilience by inhibiting the ventral dentate gyrus. *Nature* **559**, 98 (2018).
30. Ikrar, T. *et al.* Adult neurogenesis modifies excitability of the dentate gyrus. *Front. Neural Circuits* **7**, 204 (2013).
31. Lacefield, C. O., Itskov, V., Reardon, T., Hen, R. & Gordon, J. A. Effects of adult-generated granule cells on coordinated network activity in the dentate gyrus. *Hippocampus* **22**, 106–116 (2012).
32. Singer, B. H. *et al.* Compensatory network changes in the dentate gyrus restore long-term potentiation following ablation of neurogenesis in young-adult mice. *PNAS* **108**, 5437–5442 (2011).
33. Drew, L. J. *et al.* Activation of local inhibitory circuits in the dentate gyrus by adult-born neurons. *Hippocampus* **26**, 763–778 (2016).
34. Kempermann, G., Kuhn, H. G. & Gage, F. H. Genetic influence on neurogenesis in the dentate gyrus of adult mice. *PNAS* **94**, 10409–10414 (1997).
35. Dana, H. *et al.* Sensitive red protein calcium indicators for imaging neural activity. *eLife* **5**, e12727 (2016).
36. Pilz, G.-A. *et al.* Functional Imaging of Dentate Granule Cells in the Adult Mouse Hippocampus. *J. Neurosci.* **36**, 7407–7414 (2016).
37. Cacucci, F., Wills, T. J., Lever, C., Giese, K. P. & O'Keefe, J. Experience-dependent increase in CA1 place cell spatial information, but not spatial reproducibility, is dependent on the autophosphorylation of the alpha-isoform of the calcium/calmodulin-dependent protein kinase II. *J Neurosci* **27**, 7854–7859 (2007).
38. Kim, S., Jung, D. & Royer, S. Place cell maps slowly develop via competitive learning and conjunctive coding in the dentate gyrus. *Nat Commun* **11**, 4550 (2020).
39. Tomé, W. A. *et al.* A mouse model replicating hippocampal sparing cranial irradiation in humans: A tool for identifying new strategies to limit neurocognitive decline. *Scientific Reports* **5**, 14384 (2015).
40. Cohen, M. R. & Kohn, A. Measuring and interpreting neuronal correlations. *Nat Neurosci* **14**, 811–819 (2011).
41. Averbeck, B. B., Latham, P. E. & Pouget, A. Neural correlations, population coding and computation. *Nat Rev Neurosci* **7**, 358–366 (2006).
42. Kohn, A., Coen-Cagli, R., Kanitscheider, I. & Pouget, A. Correlations and Neuronal Population Information. *Annu Rev Neurosci* **39**, 237–256 (2016).
43. Kanitscheider, I., Coen-Cagli, R., Kohn, A. & Pouget, A. Measuring Fisher Information Accurately in Correlated Neural Populations. *PLOS Computational Biology* **11**, e1004218 (2015).
44. Kafashan, M. *et al.* Scaling of sensory information in large neural populations shows signatures of information-limiting correlations. *Nat Commun* **12**, 473 (2021).
45. Stefanini, F. *et al.* A Distributed Neural Code in the Dentate Gyrus and in CA1. *Neuron* **107**, 703-716.e4 (2020).
46. Hazon, O. *et al.* Noise correlations in neural ensemble activity limit the accuracy of hippocampal spatial representations. *Nat Commun* **13**, 4276 (2022).
47. Dayan, P. & Abbott, L. F. *Theoretical Neuroscience: Computational and Mathematical Modeling of Neural Systems*. (The MIT Press, 2005).
48. Coen-Cagli, R. & Solomon, S. S. Relating Divisive Normalization to Neuronal Response Variability. *J Neurosci* **39**, 7344–7356 (2019).
49. Hénaff, O. J., Boundy-Singer, Z. M., Meding, K., Ziemba, C. M. & Goris, R. L. T. Representation of visual uncertainty through neural gain variability. *Nat Commun* **11**, 2513 (2020).
50. Toni, N. *et al.* Neurons born in the adult dentate gyrus form functional synapses with target cells. *Nat Neurosci* **11**, 901–907 (2008).

51. Toni, N. & Schinder, A. F. Maturation and Functional Integration of New Granule Cells into the Adult Hippocampus. *Cold Spring Harb Perspect Biol* **8**, a018903 (2016).
52. Adlaf, E. W. *et al.* Adult-born neurons modify excitatory synaptic transmission to existing neurons. *eLife* **6**, e19886 (2017).
53. Kim, E. J., Ables, J. L., Dickel, L. K., Eisch, A. J. & Johnson, J. E. Ascl1 (Mash1) Defines Cells with Long-Term Neurogenic Potential in Subgranular and Subventricular Zones in Adult Mouse Brain. *PLOS ONE* **6**, e18472 (2011).
54. Roth, B. L. DREADDs for Neuroscientists. *Neuron* **89**, 683–694 (2016).
55. Zhu, H. *et al.* Cre-dependent DREADD (Designer Receptors Exclusively Activated by Designer Drugs) mice. *genesis* **54**, 439–446 (2016).
56. Altman, J. & Das, G. D. Autoradiographic and histological evidence of postnatal hippocampal neurogenesis in rats. *J. Comp. Neurol.* **124**, 319–335 (1965).
57. Eriksson, P. S. *et al.* Neurogenesis in the adult human hippocampus. *Nat Med* **4**, 1313–1317 (1998).
58. Moreno-Jiménez, E. P. *et al.* Adult hippocampal neurogenesis is abundant in neurologically healthy subjects and drops sharply in patients with Alzheimer's disease. *Nature Medicine* **25**, 554 (2019).
59. Zhou, Y. *et al.* Molecular landscapes of human hippocampal immature neurons across lifespan. *Nature* **607**, 527–533 (2022).
60. Hainmueller, T. & Bartos, M. Parallel emergence of stable and dynamic memory engrams in the hippocampus. *Nature* **558**, 292–296 (2018).
61. Tuncdemir, S. N. *et al.* Parallel processing of sensory cue and spatial information in the dentate gyrus. *Cell Rep* **38**, 110257 (2022).
62. Temprana, S. G. *et al.* Delayed Coupling to Feedback Inhibition during a Critical Period for the Integration of Adult-Born Granule Cells. *Neuron* **85**, 116–130 (2015).
63. Groisman, A. I., Yang, S. M. & Schinder, A. F. Differential Coupling of Adult-Born Granule Cells to Parvalbumin and Somatostatin Interneurons. *Cell Reports* **30**, 202-214.e4 (2020).
64. Rechavi, Y., Rubin, A., Yizhar, O. & Ziv, Y. Exercise increases information content and affects long-term stability of hippocampal place codes. *Cell Reports* **41**, 111695 (2022).
65. McHugh, S. B. *et al.* Adult-born dentate granule cells promote hippocampal population sparsity. *Nat Neurosci* **25**, 1481–1491 (2022).
66. Scharfman, H. E. The enigmatic mossy cell of the dentate gyrus. *Nature Reviews Neuroscience* **17**, 562–575 (2016).
67. Verhoef, B.-E. & Maunsell, J. H. R. Attention-related changes in correlated neuronal activity arise from normalization mechanisms. *Nat Neurosci* **20**, 969–977 (2017).
68. Ozeki, H., Finn, I. M., Schaffer, E. S., Miller, K. D. & Ferster, D. Inhibitory stabilization of the cortical network underlies visual surround suppression. *Neuron* **62**, 578–592 (2009).
69. Hennequin, G., Ahmadian, Y., Rubin, D. B., Lengyel, M. & Miller, K. D. The Dynamical Regime of Sensory Cortex: Stable Dynamics around a Single Stimulus-Tuned Attractor Account for Patterns of Noise Variability. *Neuron* **98**, 846-860.e5 (2018).
70. Echeveste, R., Aitchison, L., Hennequin, G. & Lengyel, M. Cortical-like dynamics in recurrent circuits optimized for sampling-based probabilistic inference. *Nat Neurosci* **23**, 1138–1149 (2020).
71. Heeger, D. J. & Zemlianova, K. O. A recurrent circuit implements normalization, simulating the dynamics of V1 activity. *Proc Natl Acad Sci U S A* **117**, 22494–22505 (2020).
72. Chakraborti, A., Allen, A., Allen, B., Rosi, S. & Fike, J. R. Cranial irradiation alters dendritic spine density and morphology in the hippocampus. *PLoS One* **7**, e40844 (2012).
73. Parihar, V. K. & Limoli, C. L. Cranial irradiation compromises neuronal architecture in the hippocampus. *Proc Natl Acad Sci U S A* **110**, 12822–12827 (2013).
74. Johnston, S. *et al.* AAV ablates neurogenesis in the adult murine hippocampus. *Elife* **10**, e59291 (2021).

75. Zhao, C., Teng, E. M., Summers, R. G., Ming, G. & Gage, F. H. Distinct Morphological Stages of Dentate Granule Neuron Maturation in the Adult Mouse Hippocampus. *J. Neurosci.* **26**, 3–11 (2006).
76. Mizrahi, A., Crowley, J. C., Shtoyerman, E. & Katz, L. C. High-Resolution In Vivo Imaging of Hippocampal Dendrites and Spines. *J. Neurosci.* **24**, 3147–3151 (2004).
77. Jordan, J. T., McDermott, K. D., Frechou, M. A., Shtrahman, M. & Gonçalves, J. T. Treadmill-based task for assessing spatial memory in head-fixed mice. *STAR Protoc* **2**, 100770 (2021).
78. Varela, C. *et al.* Tracking the Time-Dependent Role of the Hippocampus in Memory Recall Using DREADDs. *PLOS ONE* **11**, e0154374 (2016).
79. Pachitariu, M. *et al.* Suite2p: beyond 10,000 neurons with standard two-photon microscopy. *bioRxiv* 061507 (2017) doi:10.1101/061507.
80. Pachitariu, M., Stringer, C. & Harris, K. D. Robustness of Spike Deconvolution for Neuronal Calcium Imaging. *J. Neurosci.* **38**, 7976–7985 (2018).
81. Swindale, N. V. Orientation tuning curves: empirical description and estimation of parameters. *Biol Cybern* **78**, 45–56 (1998).

## Figure legends

**Figure 1. Environmental enrichment increases the spatial information encoding in the DG.** A) Experimental timeline, including surgery, enriched environment, and in vivo imaging. B) Example of calcium imaging field of view. C) Number of DCX-expressing granule neurons in regular cage (RC) and enriched environment (EE) groups. ($p = 0.026$, $n_{RC} = 4$ mice, $n_{EE} = 5$ mice, average of three 40µm slices per mouse, Mann-Whitney U test) D) Example calcium traces (top) and respective position of animal on the treadmill (bottom). E) Accuracy in decoding position of mouse on treadmill from calcium traces ($p = 0.0286$, $n = 4$ mice, 42 cells subsampled per mouse, Mann-Whitney U test). Dotted line is change performance level (5%). See also Figure S1.

**Figure 2. Prior focal irradiation of the hippocampus blocks the effects of EE on DG spatial encoding.** A) Experimental timeline, including focal irradiation, surgery, and in vivo imaging. B) Immunofluorescence labelling of DCX positive neurons in the DG of non-irradiated (top) and irradiated (bottom) mice. C) Number of DCX-expressing granule neurons in non-irradiated and irradiated groups ($p = 0.0061$, $n_{Non\text{-}Irr} = 4$ mice, $n_{Irr} = 9$ mice, average of three 40µm slices per mouse, Mann-Whitney U test). D) Accuracy in decoding position of mouse on treadmill from

calcium traces (RC vs Irr+RC: p = 0.0288, EE vs Irr+EE: p = <0.0001, RC vs EE: p = 0.0031, ANOVA, Holm-Sidak correction for multiple comparisons, n = 4 mice, 42 neurons subsampled per mouse). Dotted line is chance performance level (5%). See also Figure S2.

**Figure 3. Ablating adult neurogenesis decreases spatial information content at the single cell level.** A-D) Population Fisher information determined with noise correlations and after random shuffling to disrupt noise correlations (RC vs RC w/o NC: p = 0.0571 n.s, n = 5 mice per group, EE vs EE w/o NC: p = 0.1508 n.s, n = 5 mice per group, Irr+RC vs Irr+RC w/o NC: p= 0.2000 n.s., n = 4 mice per group, Irr+EE vs Irr+EE w/o NC: p = 0.0143, n = 5 mice per group, Mann-Whitney U test). E) Single-cell spatial information content determined using Fisher information (FI) (RC vs Irr+RC: p < 1/100000, $n_{RC}$ = 5 mice, 277 neurons, $n_{Irr+RC}$ = 4 mice, 253 neurons, EE vs Irr+EE: p < 1/100000, $n_{EE}$ = 5 mice, 201 neurons, $n_{Irr+EE}$ = 4 mice, 412 neurons). Statistical analysis: Bootstrap and Bonferroni correction for multiple comparisons (see methods). Error bars are mean ± SEM. F) Distribution of spatial information content across the imaged neurons. G) Distance between two positions that DG single-cells are able, on average, to discriminate correctly 70% of the time (RC vs Irr+RC: p = 0.0038 $n_{RC}$ = 5 mice, $n_{Irr+RC}$ = 4 mice, EE vs Irr+EE: p = 0.0012, $n_{EE}$ = 5 mice, $n_{Irr+EE}$ = 4 mice). Statistical analysis: ANOVA, Holm-Sidak correction for multiple comparisons).

**Figure 4. Ablating adult neurogenesis reduces tuning specificity and activity.** A) Examples of cells with high (top) and low (bottom) tuning indices. B) Tuning vectors from cells in A plotted in polar coordinates. C) Tuning indices of cells in non-irradiated and irradiated groups (RC vs Irr+RC: p < 1/100000, $n_{RC}$ = 5 mice, 277 neurons, $n_{Irr+RC}$ = 4 mice, 253 neurons, EE vs Irr+EE: p < 1/100000, $n_{EE}$ = 5 mice, 201 neurons, $n_{Irr+EE}$ = 4 mice, 412 neurons). D) Activity measured as integrated calcium traces normalized to distance travelled (RC vs EE: p < 1/100000, $n_{RC}$ = 5 mice, 277 neurons, $n_{EE}$ = 5 mice, 201 neurons, RC vs Irr+RC: p < 0.00228, $n_{RC}$ = 5 mice, 277 neurons, $n_{Irr+RC}$ = 4 mice, 253 neurons, EE vs Irr+EE: p < 1/100000, $n_{EE}$ = 5 mice, 201 neurons, $n_{Irr+EE}$ = 4 mice, 412 neurons). E) Schematic of tuning curve properties of individual cells fitted with Von

Mises function. F) Cross-validated goodness of fit ($R^2$) of tuning curves (RC vs EE: $p = 0.01617$, $n_{RC} = 5$ mice, 277 neurons, $n_{EE} = 5$ mice, 201 neurons, RC vs Irr+RC: $p < 1/100000$, $n_{RC} = 5$ mice, 277 neurons, $n_{Irr+RC} = 4$, 253 neurons, EE vs Irr+EE: $p < 1/100000$, $n_{EE} = 5$ mice, 201 neurons, $n_{Irr+EE} = 4$ mice, 412). G) Peak width of tuning curves of well-fitted cells. H) Peak amplitude of well-fitted cells (RC vs Irr+RC: $p < 1/100000$, $n_{RC} = 5$ mice, 173 neurons, $n_{Irr+RC} = 4$ mice, 70 neurons, EE vs Irr+EE: $p = 0.00237$, $n_{EE} = 4$ mice, 113 neurons, $n_{Irr+EE} = 4$ mice, 85 neurons). See also Figure S3. Statistical analysis: Bootstrap and Bonferroni correction for multiple comparisons. Error bars are mean ± SEM.

**Figure 5. Acute chemogenetic silencing of ABNs decreases spatial information content in the DG.** A) Experimental timeline, including surgery, enriched environment, and in vivo imaging with chemogenetic silencing. B) Immunofluorescence images of HA-tag positive neurons (red) and DAPI labelled nuclei (blue). C) Schematic of contextual fear conditioning (CFC) task. D) Images of boxes used as context A and context B during behavior experiment. E) Percentage of time spent freezing in shocked and novel contexts (hM4Di- Ctx A vs Ctx B: $p = 0.0015$, $n_{Ctx\ A} = 5$ mice, $n_{Ctx\ B} = 5$ mice, hM4Di+ Ctx A vs Ctx B, $p = 0.0484$, $n_{Ctx\ A} = 5$ mice, $n_{Ctx\ B} = 5$ mice). F) Discrimination index of freezing between contexts (hM4Di- (control) vs hM4Di+: $p = 0.0159$, $n_{hM4Di-} = 5$ mice, $n_{hM4Di+} = 5$ mice). Statistical analysis: Mann-Whitney U test. G,H) Fisher information (Baseline vs CNO: $p < 1/100000$, $n_{Baseline} = 5$ mice, 317 neurons, $n_{CNO} = 5$ mice, 319 neurons, Baseline vs CNO (control): $p = 0.14337$, $n_{Baseline} = 2$ mice, 118 neurons, $n_{CNO} = 2$ mice, 202 neurons). I, J) Activity (Baseline vs CNO: $p = 0.00004$, $n_{Baseline} = 5$ mice, 317 neurons, $n_{CNO} = 5$ mice, 319 neurons, Baseline vs CNO (control): $p = 0.2541$, $n_{Baseline} = 2$ mice, 118 neurons, $n_{CNO} = 2$ mice, 202 neurons). K,L) Tuning indices (Baseline vs CNO: $p < 0.02163$, $n_{Baseline} = 5$ mice, 317 neurons, $n_{CNO} = 5$ mice, 319 neurons, Baseline vs CNO (control): $p = 0.3069$, $n_{Baseline} = 2$ mice, 118 neurons, $n_{CNO} = 2$ mice, 202 neurons) in baseline and CNO conditions. M) Goodness-of-fit ($R^2$) of the Von Mises function to the tuning curves of all cells (Baseline vs CNO: $p < 0.2501$, $n_{Baseline} = 5$ mice, 317 neurons, $n_{CNO} = 5$ mice, 319 neurons). N) Goodness-of-fit of well-fitted cells

($R^2$>0.5). (Baseline vs CNO: p < 0.47548, $n_{Baseline}$ = 5 mice, 317 neurons, $n_{CNO}$ = 5 mice, 319 neurons) O) Peak width of well fitted cells (Baseline vs CNO: p <0.0834, $n_{Baseline}$ = 5 mice, 317 neurons, $n_{CNO}$ = 5 mice, 319 neurons) P) Peak amplitude of well-fitted cells (Baseline vs CNO: p = 0.04801, $n_{mice}$ = 5/5, $n_{cells}$ = 317/319, bootstrap). See also Figure S4. Statistical analysis: Bootstrap. Error bars are mean ± SEM.

**Movie S1. Example DG calcium imaging movie**

Example excerpt of calcium imaging movie recorded from the DG of a mouse that is walking head-fixed on a treadmill. Movie was registered and every 10 frames were averaged for display purposes. Field of view is 343.6 x 343.6 µm, total duration is 250 s.

**Figure S1. Optimization of decoder for calcium imaging analysis.** A) Photograph of two-photon imaging treadmill with different textile cues. B) Average speed of RC and EE mice on treadmill during experimental sessions. C) Comparison of percentage of decoding accuracy using different methods for filtering calcium trace data. Unfiltered raw traces, raw traces with neuropil subtraction, filtered traces using a moving average approach and window size of 100, dF/F, binary data on the location of the deconvolved spikes on the trace, traces being represented by the amplitude of the deconvolved spikes on the trace and the deconvolved traces. Spike deconvolution was performed using suite2p based on the OASIS algorithm. D) Example of decoder accuracy using unfiltered calcium traces in EE and Irr+EE mice. E) Example of decoder accuracy using filtered calcium traces in EE and Irr+EE mice. F) Decoder accuracy on training data plotted by number of cells analyzed. G) Decoder accuracy on testing data plotted by number of cells analyzed. Related to Figure 1.

**Figure S2. Olfactory bulb neurogenesis is preserved with hippocampal focal irradiation.** Typical isodose distributions for hippocampal focusing irradiation employed in this study: A)

coronal plane, B) sagittal plane. C) Immunofluorescence images of the DCX-positive neurons and DAPI labelled nuclei in the olfactory bulb (left) and dentate gyrus (right) of a mouse that has undergone focal irradiation. Related to Figure 2.

**Figure S3. Ablating adult neurogenesis reduces single-cell tuning specificity and activity.** A) Distribution of single-cell tuning indices between non-irradiated and irradiated cohorts. B) Distribution of single-cell activity rates between non-irradiated and irradiated cohorts. Related to Figure 4.

**Figure S4. Curve-fitting in hM4Di- control mice**

A) Goodness-of-fit ($R^2$) of the Von Mises function to the tuning curves of all cells (Baseline vs CNO (control): p = 0.17012, $n_{Baseline}$ = 2 mice, 118 neurons, $n_{CNO}$ = 2 mice, 202 neurons). B) Goodness-of-fit of well-fitted cells ($R^2$>0.5) (Baseline vs CNO (control): p = 0.17025, $n_{Baseline}$ = 2 mice, 48 neurons, $n_{CNO}$ = 2 mice, 66 neurons) C) Peak width of well fitted cells (Baseline vs CNO (control): p = 0.03993, $n_{Baseline}$ = 2 mice, 48 neurons, $n_{CNO}$ = 2 mice, 66 neurons). D) Peak amplitude of well-fitted cells (Baseline vs CNO (control): p = 0.10972, $n_{Baseline}$ = 2 mice, 48 neurons, $n_{CNO}$ = 2 mice, 66 neurons). Related to Figure 5.

**Figure S5. EE increases DG single-cell activity and spatial information in mice injected with a retro AAV virus in CA3 .** A) Activity (RC vs EE: p = 0.00143, $n_{RC}$ = 3 mice, 49 neurons, $n_{EE}$ = 3 mice, 69 neurons) and B) Fisher Information (RC vs EE: p < 1/100000, $n_{RC}$ = 3 mice, 49 neurons, $n_{EE}$ = 3 mice, 69 neurons) in mice injected with a retro AAV virus in CA3.

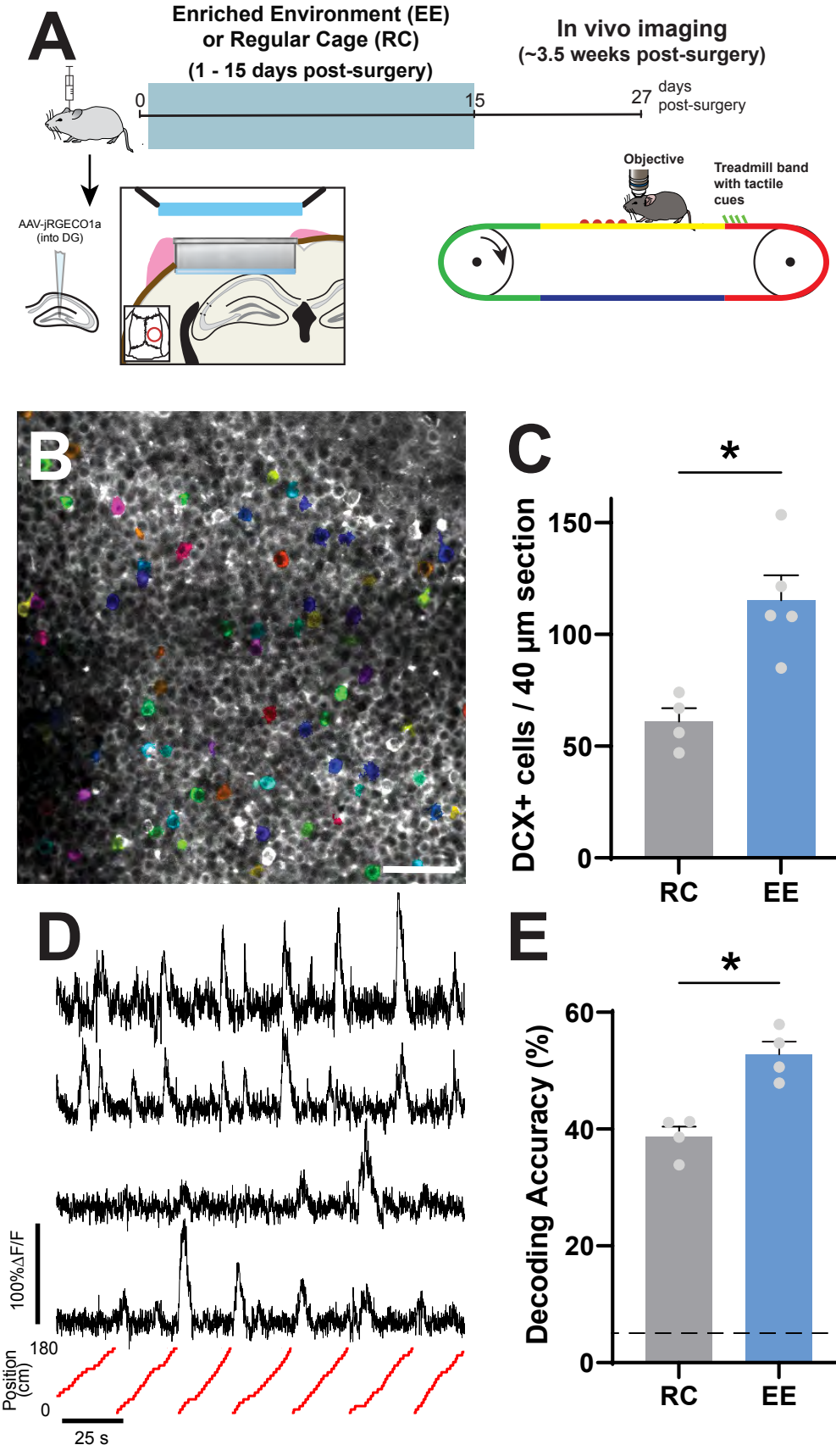


**Figure 1**

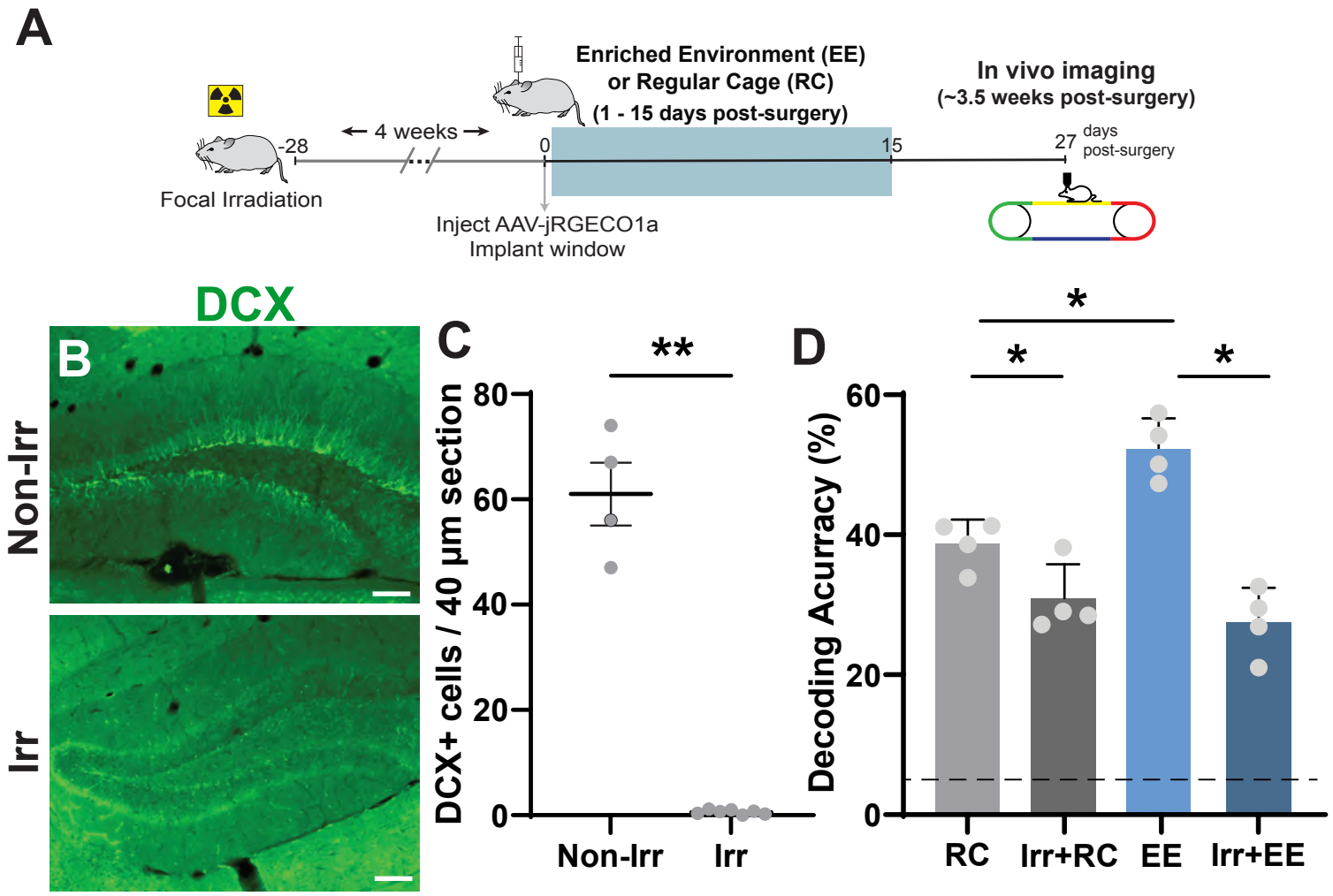


# Figure 2

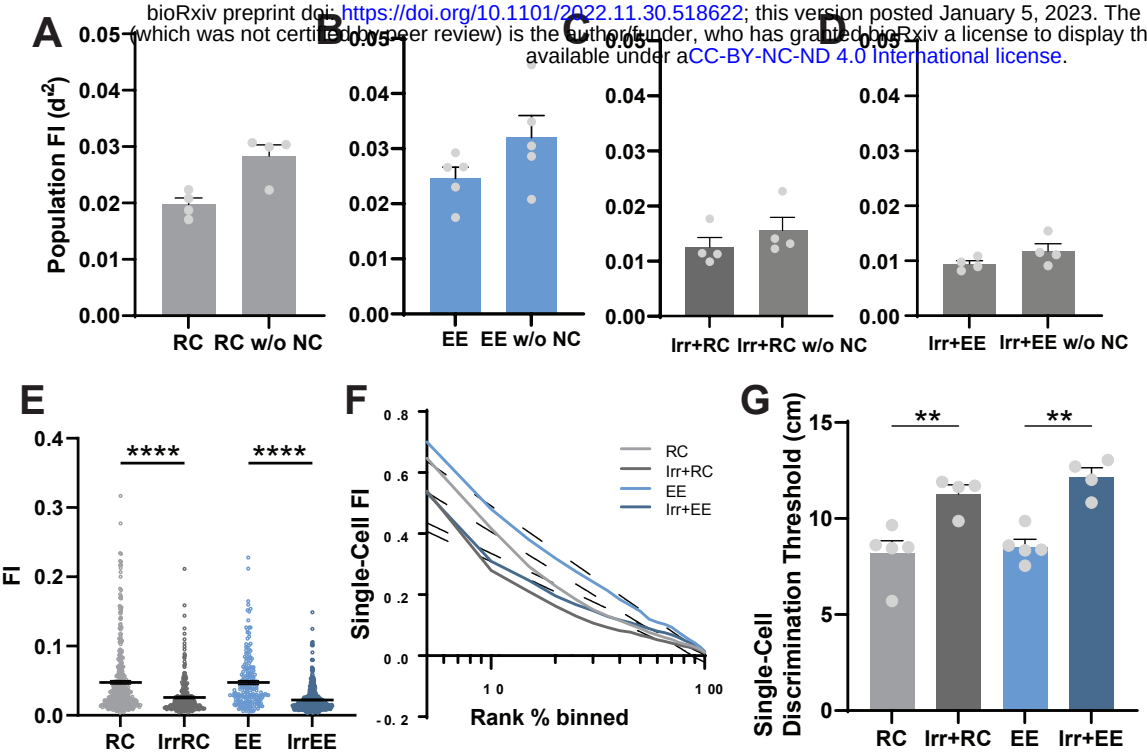





# Figure 3

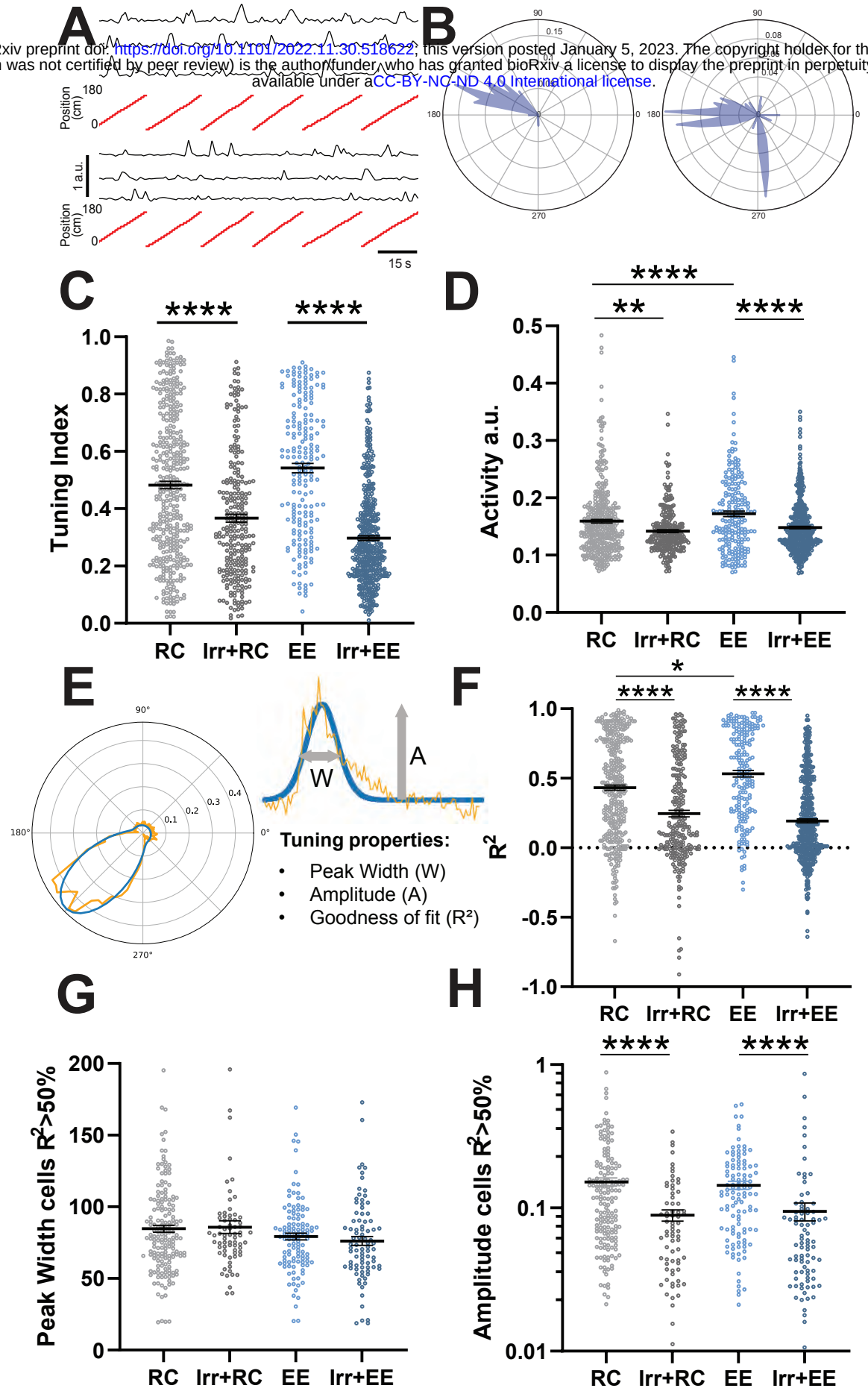




# Figure 4

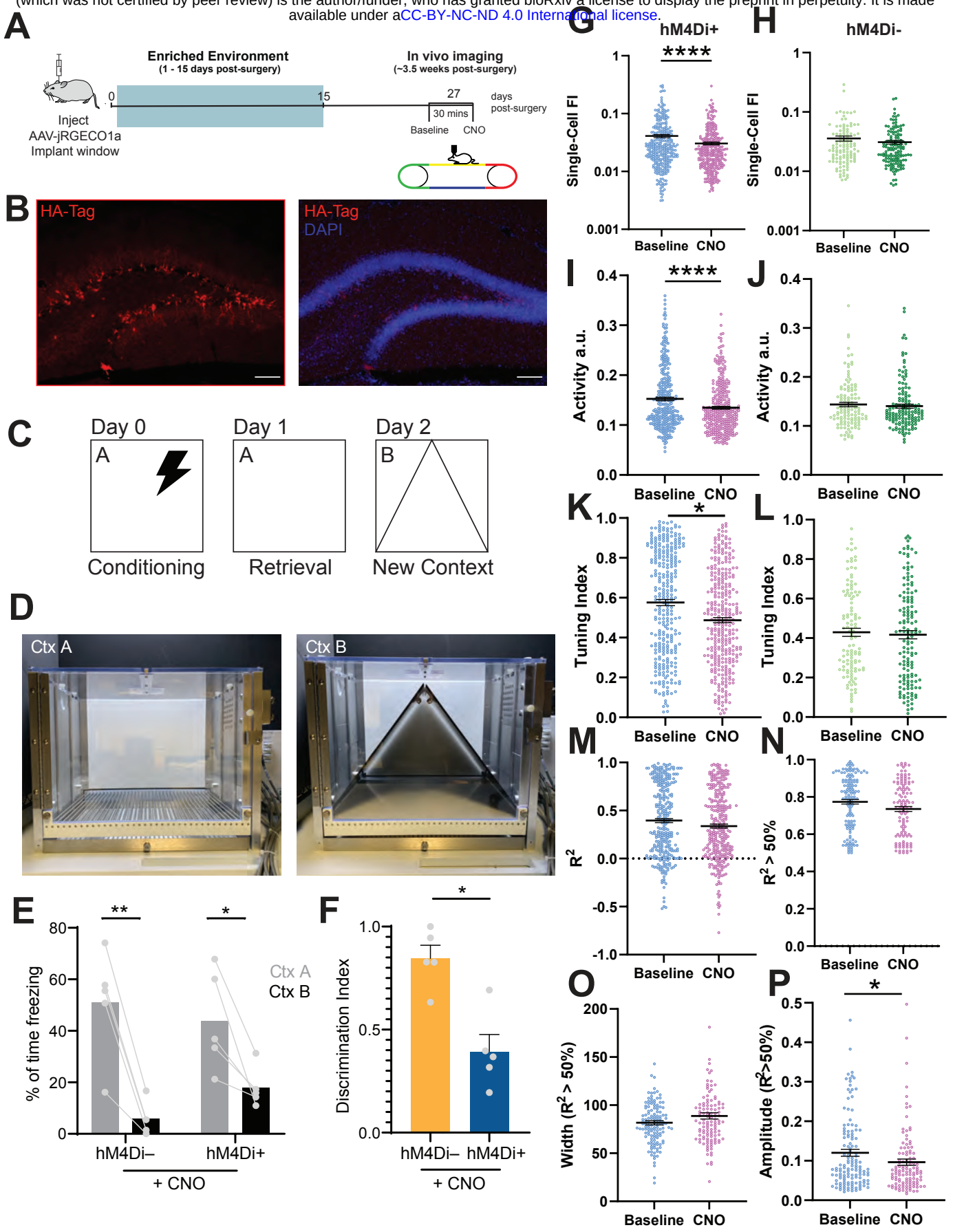


**Figure 5**

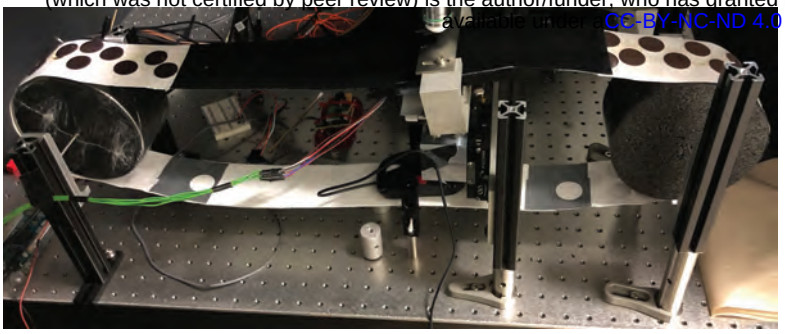

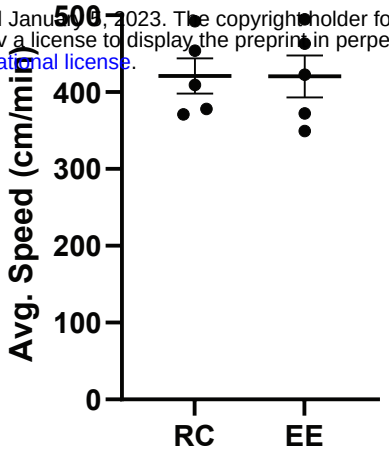


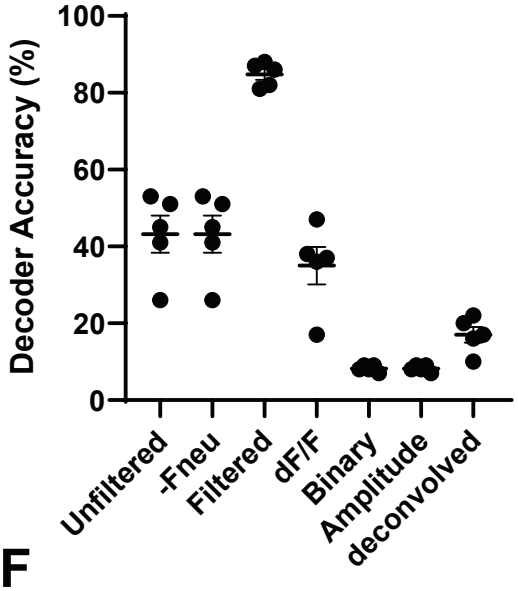


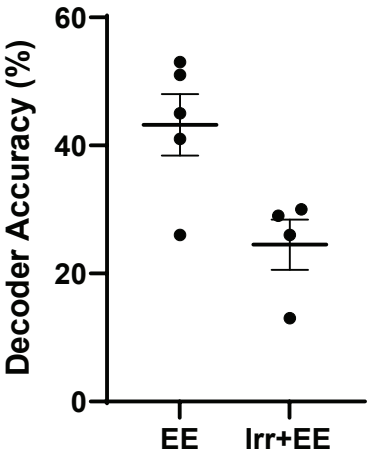


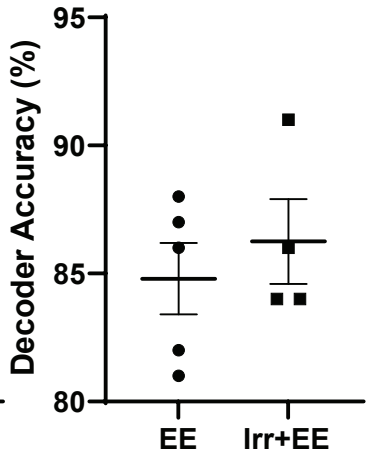


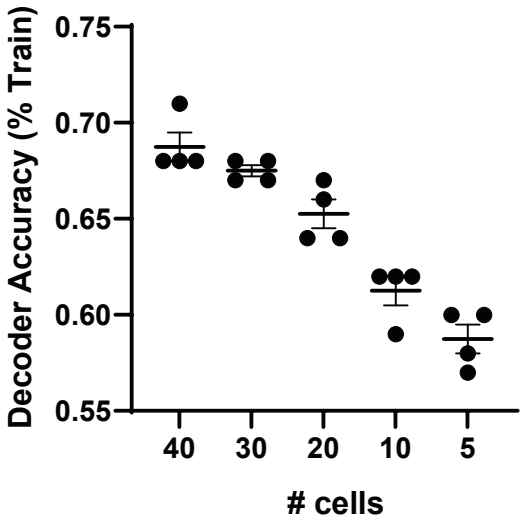


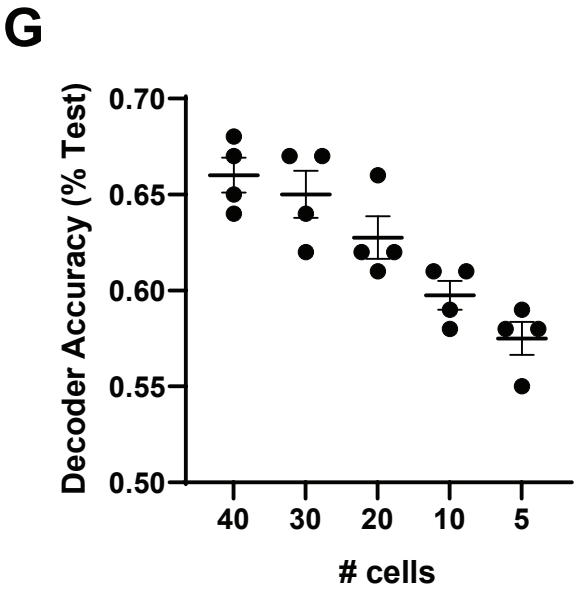


# Figure S1

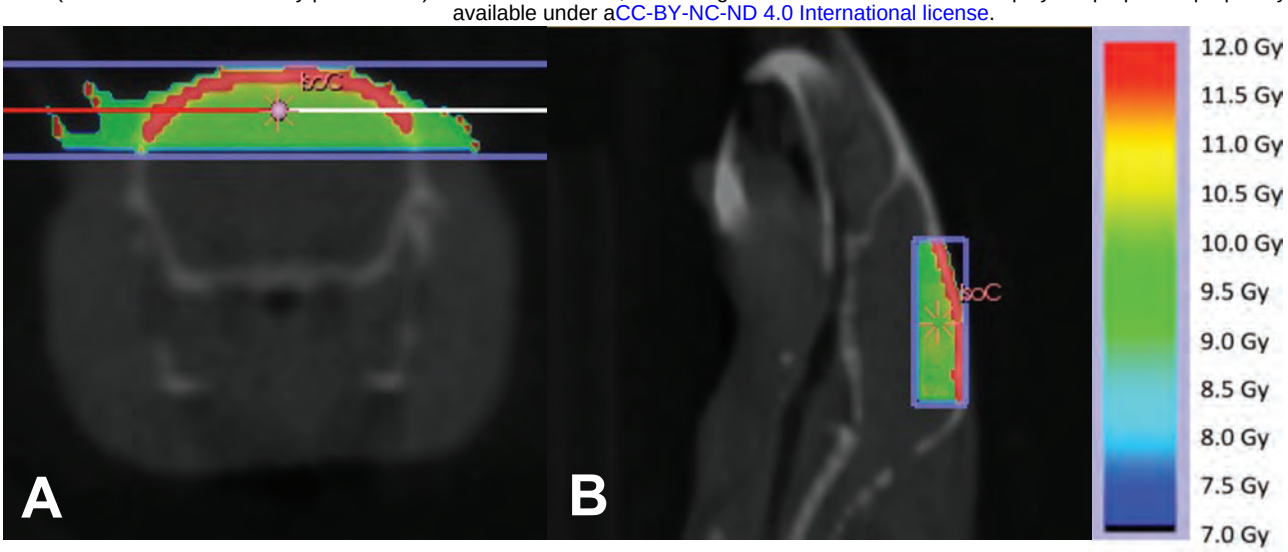


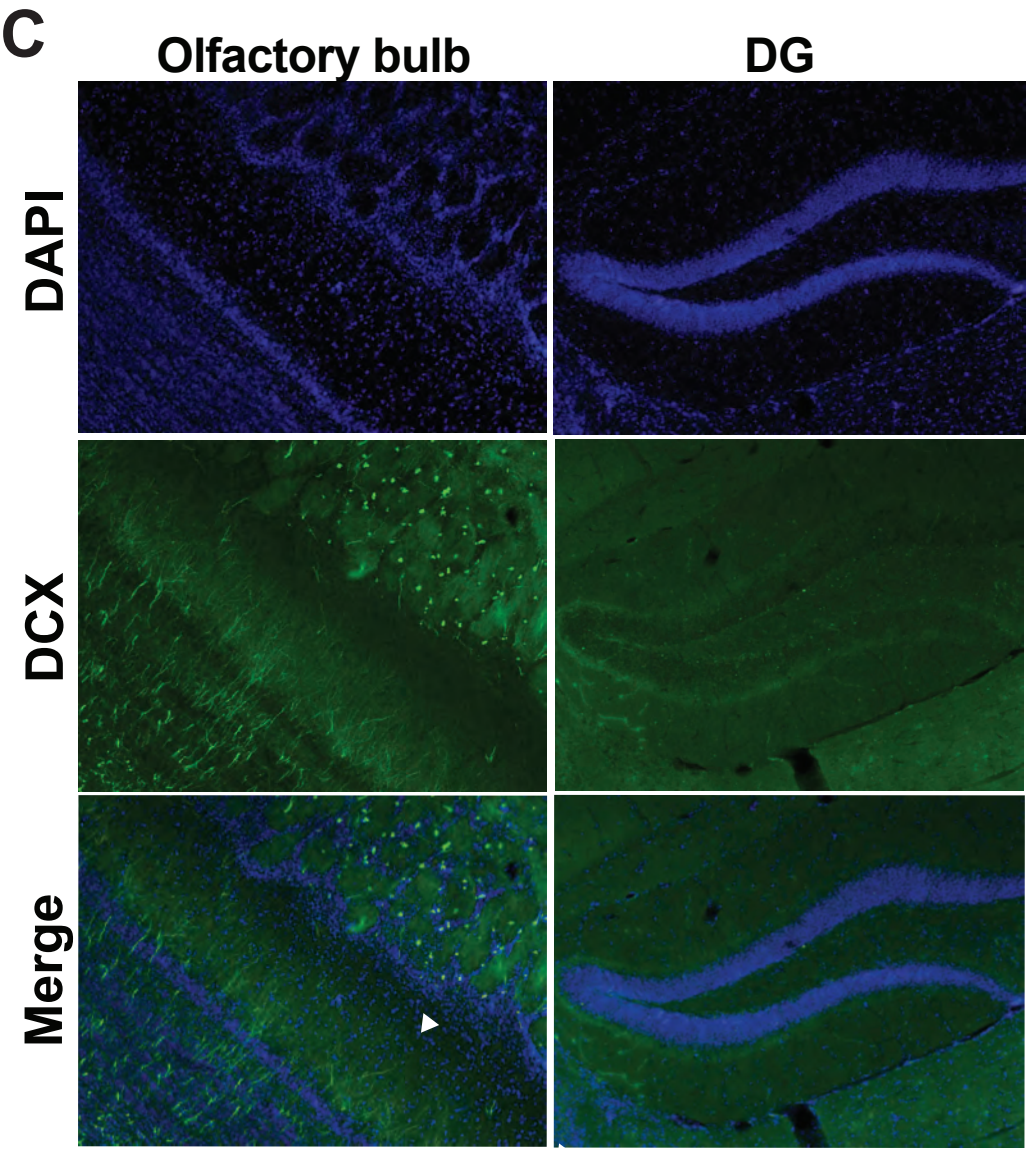


**Figure S2**

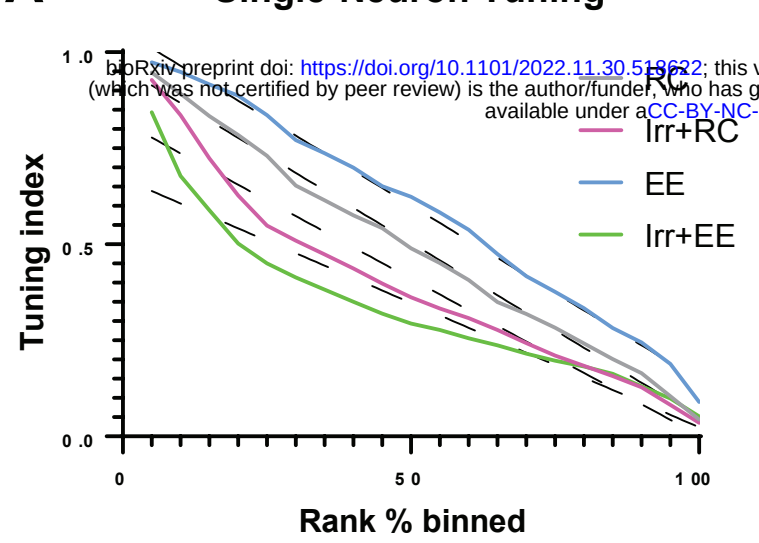


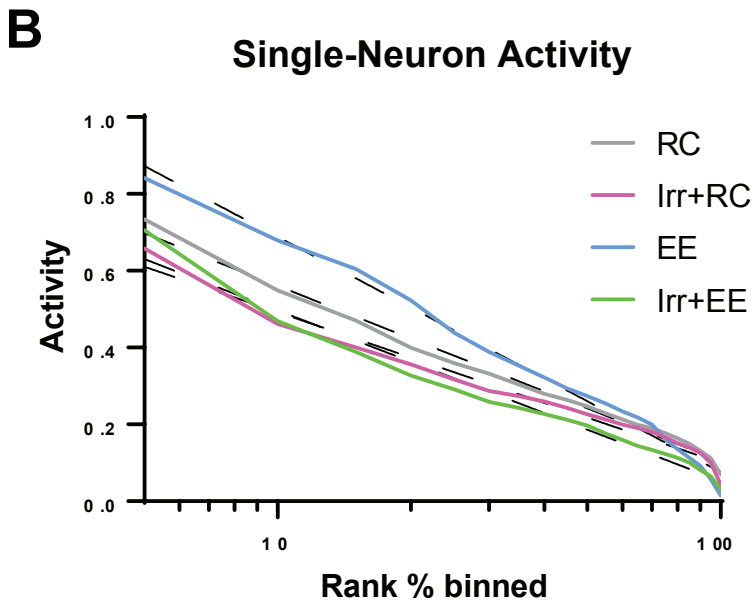


# Figure S3

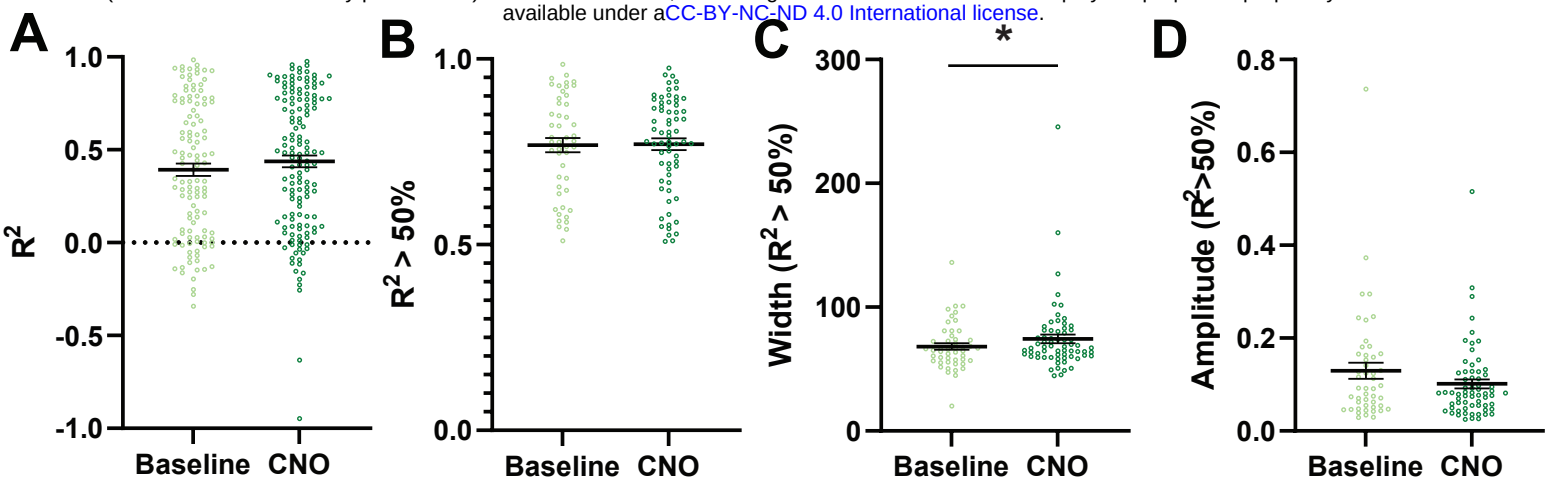


# Figure S4

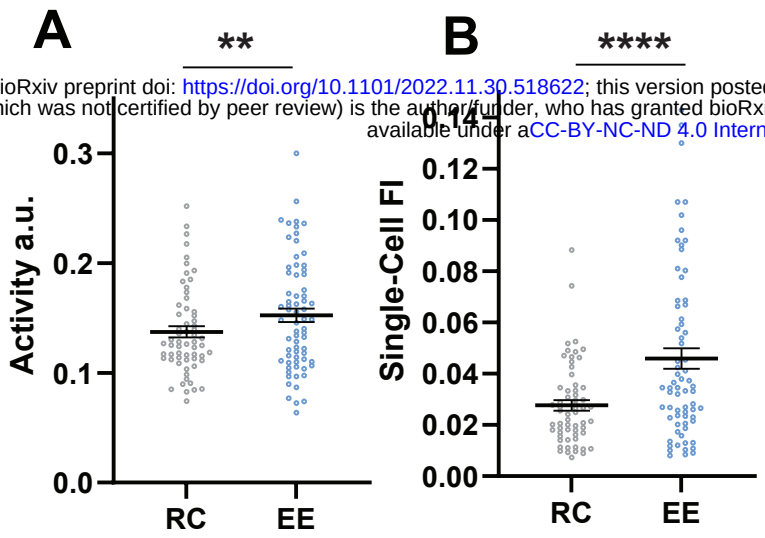


# Figure S5

PNAS RESEARCH ARTICLE | NEUROSCIENCE

# Seizure-induced strengthening of a recurrent excitatory circuit in the dentate gyrus is proconvulsant

Kaoutsar Nasrallah[a,1], M. Agustina Frechou[a,b], Young J. Yoon[a,c], Subrina Persaud[a], J. Tiago Gonçalves[a,b], and Pablo E. Castillo[a,d,1]

Edited by Thomas Südhof, Stanford University, Stanford, CA; received January 20, 2022; accepted June 27, 2022

**Epilepsy is a devastating brain disorder for which effective treatments are very limited. There is growing interest in early intervention, which requires a better mechanistic understanding of the early stages of this disorder. While diverse brain insults can lead to epileptic activity, a common cellular mechanism relies on uncontrolled recurrent excitatory activity. In the dentate gyrus, excitatory mossy cells (MCs) project extensively onto granule cells (GCs) throughout the hippocampus, thus establishing a recurrent MC-GC-MC excitatory loop. MCs are implicated in temporal lobe epilepsy, a common form of epilepsy, but their role during initial seizures (i.e., before the characteristic MC loss that occurs in late stages) is unclear. Here, we show that initial seizures acutely induced with an intraperitoneal kainic acid (KA) injection in adult mice, a well-established model that leads to experimental epilepsy, not only increased MC and GC activity in vivo but also triggered a brain-derived neurotrophic factor (BDNF)–dependent long-term potentiation (LTP) at MC-GC excitatory synapses. Moreover, in vivo induction of MC-GC LTP using MC-selective optogenetic stimulation worsened KA-induced seizures. Conversely, *Bdnf* genetic removal from GCs, which abolishes LTP, and selective MC silencing were both anticonvulsant. Thus, initial seizures are associated with MC-GC synaptic strengthening, which may promote later epileptic activity. Our findings reveal a potential mechanism of epileptogenesis that may help in developing therapeutic strategies for early intervention.**

hippocampus | mossy cell | epilepsy | granule cell | BDNF

## Significance

Better understanding of the initial molecular and cellular processes implicated in epileptogenesis is essential for early therapeutic intervention (i.e., before brain damage becomes irreversible). Uncontrolled activity of recurrent excitatory circuits is a common mechanism that promotes epileptic activity. In the dentate gyrus, mossy and granule cells form a recurrent excitatory circuit that can be strengthened upon activity and whose dysregulation has been implicated in temporal lobe epilepsy. Here, we found that acute induction of seizures triggers robust brain-derived neurotrophic factor (BDNF)–dependent strengthening of mossy cell–granule cell synapses that promotes further convulsive seizures. Moreover, blocking this synaptic strengthening prevents seizure activity. Together, our findings provide a potential mechanism for early epileptogenesis involving BDNF within a recurrent hippocampal excitatory network.

Epilepsy is a common neurological disorder characterized by recurrent epileptic seizures, often associated with profound cognitive, psychological, and social deleterious consequences (1). About 30% of patients are resistant to antiseizure drugs (2). To develop more effective treatments, a better understanding of the cellular and molecular processes implicated in the early stages of epilepsy, before brain damage becomes irreversible, is required. Mossy cells (MCs), excitatory neurons in the dentate gyrus (DG) of the hippocampus, play a critical role in temporal lobe epilepsy (TLE) (3–5), the most common form of focal epilepsy in adults (6). However, whether MC activity can be pro- or antiepileptic has been a subject of debate for several decades (3–5, 7, 8). MC loss is a hallmark feature of chronic TLE in both human and animal models (9–13). Recent studies reported that while surviving MCs in a mouse model of chronic TLE play an antiepileptic role (4), these cells could be proepileptic early during initial experimental seizures (5, 14).

Aberrant recurrent excitatory activity is a core mechanism in epilepsy (15). In the DG, glutamatergic MCs and granule cells (GCs) are reciprocally connected, thus forming an intrinsic excitatory loop. Remarkably, a single MC makes more than 30,000 synaptic contacts onto GCs, locally, contralaterally, and along the longitudinal axis of the hippocampus (16, 17). Furthermore, repetitive stimulation of MC axons in vitro induces robust long-term potentiation (LTP) at MC-GC excitatory synapses (MC-GC LTP). The DG is characterized by very sparse GC activity (18–20), and it is believed to act as a gate that opens during epileptic seizures (21, 22). The long-lasting strengthening of MC-GC synaptic transmission is sufficient to overcome the basal strong GC inhibition, thereby allowing MCs to drive GCs and presumably open the DG gate (23). MC-GC LTP is mediated by brain-derived neurotrophic factor (BDNF)/tropomyosin receptor kinase B (TrkB) signaling (23, 24), which is known to promote TLE (25). Therefore, activity-dependent strengthening of MC-GC synapses may promote epilepsy through the extensive MC projections onto GCs. While an episode of prolonged seizures (e.g., status epilepticus) can result in TLE (26–28), it is unknown whether and how initial seizures can impact MC-GC synaptic strength.

Using multiple complementary approaches, such as chemogenetics, in vitro electrophysiology, in vivo optogenetics, in vivo calcium imaging, and a conditional knockout (cKO) strategy, we found that initial seizures not only increased MC and GC activity in vivo but also triggered a BDNF-dependent strengthening of MC-GC synaptic

Author contributions: K.N., M.A.F., Y.J.Y., J.T.G., and P.E.C. designed research; K.N., M.A.F., Y.J.Y., and S.P. performed research; Y.J.Y. contributed new reagents/analytic tools; K.N., M.A.F., Y.J.Y., S.P., and J.T.G. analyzed data; and K.N. and P.E.C. wrote the paper.

The authors declare no competing interest.

This article is a PNAS Direct Submission.



[1]To whom correspondence may be addressed. Email: kaoutsar.n@gmail.com or pablo.castillo@einsteinmed.edu.

This article contains supporting information online at http://www.pnas.org/lookup/suppl/doi:10.1073/pnas.2201151119/-/DCSupplemental.

Published August 5, 2022.

transmission. In addition, in vivo induction of MC-GC LTP was sufficient to promote convulsive seizures, whereas interfering with BDNF signaling and MC activity had an anticonvulsant effect. Our findings support a proepileptic role of MCs and BDNF in epileptogenesis and provide a potential causal link between MC-GC LTP and epilepsy.

## Results

**Chemogenetic Silencing of MCs Reduced Acute Kainic Acid–Induced Seizures.** To test the hypothesis that MC-GC LTP has a proconvulsant effect during early epilepsy, we first tested the prediction that silencing MCs should reduce the severity/susceptibility of experimental seizures induced by a single intraperitoneal (IP) injection of kainic acid (KA), a well-established experimental model that leads to later epilepsy (29, 30). A relatively high dose of KA (30 mg/kg) was used to induce strong seizures, which facilitates the detection of a potential decrease in seizure susceptibility/severity. To suppress MC output, the $G_i$ inhibitory designer receptor exclusively activated by a designer drug [hM4D($G_i$) or iDREADD] was selectively expressed in MCs. We bilaterally injected a Cre-recombinase–dependent virus expressing the iDREADD under the CaMKII promoter [adeno-associated virus (AAV)-CaMKII-DIO-hM4D($G_i$)-mCherry] into the DG of *Drd2*-Cre mice, whereas *Drd2*-Cre mice injected with AAV-CaMKII-DIO-mCherry served as control (Fig. 1*A*). Consistent

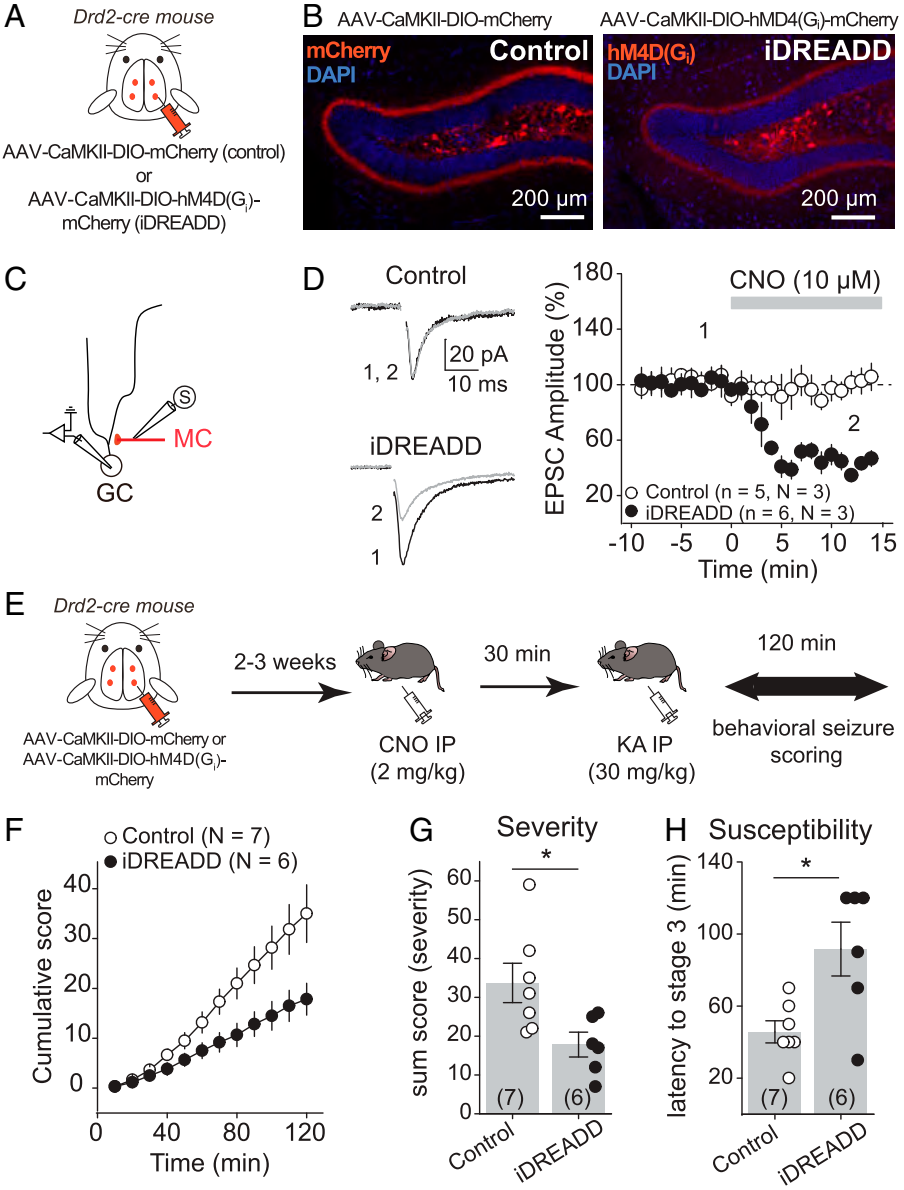


**Fig. 1.** Chemogenetic silencing of MCs reduced acute KA-induced seizures. (*A* and *B*) AAV expressing mCherry (control, AAV-CaMKII-DIO-mCherry) or the iDREADD hM4D($G_i$)-mCherry [AAV-CaMKII-DIO-hM4D($G_i$)-mCherry] were bilaterally injected into the ventral and dorsal DG of *Drd2*-cre mice. Confocal images of the DG show how the viral expression is selective for hilar MCs. Note the dense labeling of MC axons in the IML. (*C*) Schematic diagram illustrating the recording configuration. Evoked MC EPSCs were recorded from GC in response to MC axon stimulation in the IML. (*D*) Representative traces (*Left*) and time course plot (*Right*) showing that CNO significantly reduced EPSC amplitude in slices expressing iDREADD in MCs but not in controls. Here and in all figures, *n* indicates the number of cells and *N* indicates the number of animals. (*E*) Experimental timeline. Viral stereotaxic injections were performed in *Drd2*-cre mice to express control (AAV-CaMKII-DIO-mCherry) or iDREADD in MCs [AAV-CaMKII-DIO-hM4D($G_i$)-mCherry] 2 to 3 wk before assessing behavioral seizures (for 120 min). All animals were treated with CNO in vivo (2 mg/kg, IP) 30 min before seizures were acutely induced with a single KA IP injection (30 mg/kg). (*F–H*) Chemogenetic silencing of MCs reduced seizure severity and susceptibility. Scoring of seizures using a modified Racine scale for 120 min revealed significant decreases in the cumulative seizure score (*F*) and in the sum score (*G*) and a significantly increase in latency to convulsive seizures (*H*) when MCs were silenced as compared with control animals. Each number in parentheses indicates the number of animals. *$P < 0.5$. Data are presented as mean ± SEM. Here and in all figures, error bars indicate SEM.

with previous reports (5, 31), we found that the viral expression was selective to MCs (Fig. 1*B*). Next, we verified that iDREADD efficiently responded to the DREADD agonist clozapine *N*-oxide (CNO). Bath application of 10 μM CNO strongly inhibited MC activity in iDREADD-expressing cells (*SI Appendix*, Fig. S1) and significantly reduced the amplitude of evoked MC-GC excitatory postsynaptic currents (EPSCs) in acute slices obtained from *Drd2*-Cre mice injected with AAV-CaMKII-DIO-hM4D($G_i$)-mCherry but not with AAV-CaMKII-DIO-mCherry (Fig. 1 *C* and *D*) (iDREADD: 43.8 ± 4.3% of baseline, $n = 6$, $P = 0.0005$, paired *t* test; control: 100.6 ± 5.5% of baseline, $n = 5$, $P = 0.92$, paired *t* test). We then monitored and scored behavioral seizures induced by KA IP injection (30 mg/kg) for 2 h (see *Materials and Methods*) in both *Drd2*-Cre mice injected with AAV-CaMKII-DIO-hM4D($G_i$)-mCherry (iDREADD) or AAV-CaMKII-DIO-mCherry (control). The two groups were injected with CNO (2 mg/kg, IP) 30 min before KA administration (30 mg/kg, IP) (Fig. 1*E*). Consistent with a recent study using the pilocarpine model (5), we found that silencing MCs reduced seizure severity and susceptibility, as indicated by significant decreases in the total cumulative seizure score (Fig. 1*F*) [two-way ANOVA repeated measure (RM); AAV condition: $F(1,5) = 7.2$, $P = 0.04$; time: $F(1.1,5.6) = 71.7$, $P = 0.0002$; AAV condition × time: $F(1,5) = 88.1$, $P = 0.002$] and in the sum score (Fig. 1*G*) [control: 33.7 ± 5.1, $n = 7$; iDREADD: 17.8 ± 3.2, $n = 6$; control vs. iDREADD: $P = 0.02$, unpaired *t* test] and an increase in latency to stage 3 (Fig. 1*H*) (control: 45.7 ± 6.1, $n = 7$; iDREADD: 91.7 ± 14.9, $n = 6$; control vs. iDREADD: $P = 0.01$, unpaired *t* test). These results reinforce the notion that MC activity has a proconvulsant effect during initial drug-induced seizures.

**Initial Convulsive Seizures Potentiated MC-GC Transmission Presynaptically.** We hypothesized that early seizures may increase MC activity and thus induce MC-GC LTP in vivo. MC repetitive activity is sufficient to trigger a robust MC-GC LTP in acute brain slices obtained from healthy rodents (23). Furthermore, a recent in vivo study using a calcium indicator and fiber photometry reported that DG neuronal activity is increased during KA-induced seizures (32). However, the contribution of specific subtypes of neurons, including MCs and GCs, remains unknown. We therefore monitored MC and GC activity in vivo using calcium imaging during acutely induced seizures. To this end, we expressed the genetically encoded $Ca^{2+}$ indicator jRGECO1a selectively in DG excitatory neurons (*SI Appendix*, Fig. S2 *A–C*) by unilaterally injecting AAV-CaMKII-jRGECO1a into the DG of wild-type (WT) adult mice. The animals were then implanted with a chronic imaging window above the dorsal hippocampus, and MC and GC activity was visualized using head-fixed two-photon imaging before and during acute seizures (Fig. 2 *A* and *B*). After collecting basal activity, seizures were induced with a single KA IP injection (30 mg/kg). Neuronal activity was monitored during stage 3 of convulsive seizures, which was determined by the presence of forelimb clonus. Saline-injected mice served as a control. We found that during KA-induced convulsive seizures both MCs and GCs displayed robust calcium waves, which were absent from saline-injected mice (Fig. 2 *C–F*). In total, we recorded 117 MCs and 1,132 GCs from four saline-injected mice and 127 MCs and 1,162 GCs from five KA-injected mice (Fig. 2 and *SI Appendix*, Fig. S2 *D* and *E*). The convulsion-associated calcium waves were observed in almost all (~99%) recorded GCs and MCs and likely indicated strong, synchronized neural activity in GCs (Fig. 2*E*) (KA $\Delta F/F$ per cell = 2.226 ± 0.016, $P < 0.00001$, ANOVA; KA $\Delta F/F$ per mouse = 2.202 ± 0.181, $P = 0.0159$, Mann–Whitney *U* test) and MCs (Fig. 2*F*) (KA $\Delta F/F$ per cell = 1.756 ± 0.058, ANOVA; KA $\Delta F/F$ per mouse = 1.793 ± 0.071, $P = 0.0159$, Mann–Whitney *U* test). In addition, the seizure-associated calcium waves in GCs were significantly delayed compared with MCs, as indicated by a shift in changepoint (see *Materials and Methods*) (Fig. 2 *G–I*) ($GC_{changepoint} - MC_{changepoint}$ = 3.261 ± 1.170 s, $n = 5$ animals, $P = 0.049$, *t* test), suggesting that KA-induced MC activity precedes and may drive GCs.

We then tested whether initial KA-induced seizures, by increasing MC activity and inducing LTP, could strengthen MC-GC connections in vivo. We analyzed MC-GC synaptic transmission in both KA-injected and saline-injected mice. After a single KA injection (20 mg/kg, IP), the animals were monitored and killed humanely for acute hippocampal slice preparation once stage 3 of convulsive seizures was reached (Fig. 3*A*). Sham-injected mice were used as control. MC-GC synaptic function was assessed by activating MC axons while performing whole-cell voltage-clamp recordings from GCs. We found that MC-GC synaptic transmission was significantly strengthened, as indicated by an increase in the input/output function (Fig. 3*B*) [two-way ANOVA RM; IP injection: $F(1,9) = 6.5$, $P = 0.031$; stimulation intensity: $F(1.4,12.5) = 64.5$, $P < 0.001$; IP injection × stimulation intensity: $F(1,9) = 139.8$, $P < 0.001$], while both paired-pulse ratio (PPR) and coefficient of variation (CV) were significantly reduced in KA-injected as compared with saline-treated mice (Fig. 3*C*) (PPR: saline: 1.31 ± 0.08, $n = 10$; KA: 1.01 ± 0.06, $n = 10$; saline vs. KA: $P = 0.011$, unpaired *t* test; CV: saline: 0.44 ± 0.06, $n = 10$; KA: 0.28 ± 0.02, $n = 10$; saline vs. KA: $P = 0.026$, unpaired *t* test). These results strongly suggest that initial seizures, presumably by inducing presynaptic LTP, strengthened MC-GC synapses in vivo. If so, this plasticity should be occluded in hippocampal slices prepared from KA-injected mice. In support of this possibility, we found that both synaptically induced LTP by repetitive stimulation of MC axons (Fig. 3*D*) (saline: 155.5 ± 14.7% of baseline, $n = 6$, $P = 0.013$, paired *t* test; KA: 99.2 ± 3.8% of baseline, $n = 5$, $P = 0.85$, paired *t* test; saline vs. KA: $P = 0.011$, unpaired *t* test) and chemically induced LTP by transient application (50 μM for 10 min) of the adenylyl-cyclase activator forskolin (23) (Fig. 3*E*) (saline: 170.7 ± 7.6% of baseline, $n = 9$, $P < 0.001$, paired *t* test; KA: 114.3 ± 9.8% of baseline, $n = 6$, $P = 0.20$, paired *t* test; saline vs. KA: $P = 0.0005$, unpaired *t* test) were impaired in KA-injected mice as compared with control (Fig. 3 *D* and *E*). Altogether, our findings strongly suggest that early KA-induced seizures strengthened MC-GC synaptic transmission by inducing presynaptic MC-GC LTP in vivo.

We also examined whether KA-induced seizures could modify medial perforant path (MPP) to GC synaptic transmission (*SI Appendix*, Fig. S3*A*). We found an increase in input/output function and the ratio of α-amino-3-hydroxy-5-methyl-4-isoxazolepropionic acid receptor (AMPA) and N-methyl-D-aspartate receptor (NMDA) EPSCs (AMPA/NMDA ratio) but no change in PPR in KA-injected mice (*SI Appendix*, Fig. S3 *B–D*), suggesting that initial seizures strengthened MPP-GC synapses via a postsynaptic mechanism.

**Blocking Seizure-Induced MC-GC LTP Had an Anticonvulsant Effect.** BDNF/TrkB signaling is critical for MC-GC LTP. BDNF is released, by both MCs and GCs, upon repetitive presynaptic activity and is necessary and sufficient for the induction of MC-GC LTP (23, 24). To test whether BDNF is also

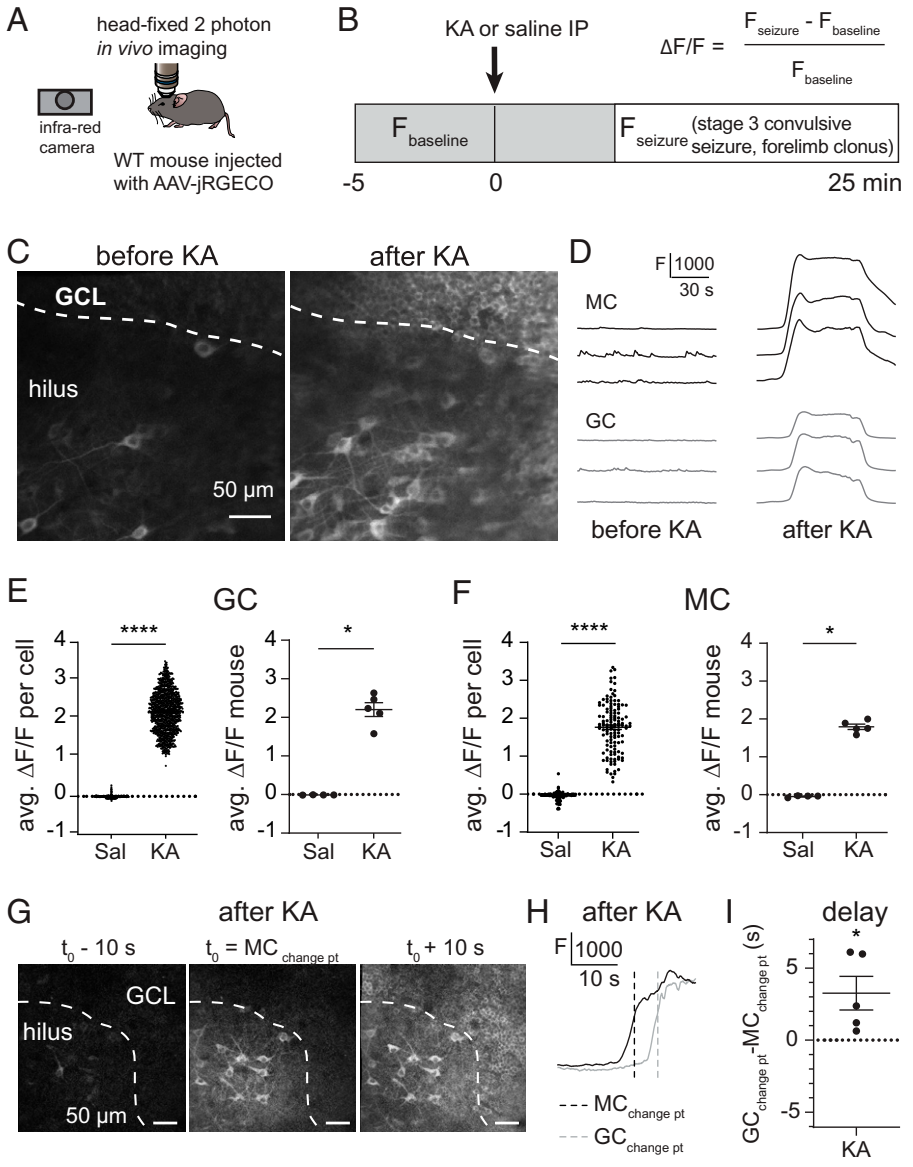


**Fig. 2.** Initial convulsive seizures increased MC and GC in vivo activity. (*A* and *B*) Schematic diagram showing the experimental apparatus (*A*). jRGECO1a-expressing MCs and GCs were imaged before and during KA (30 mg/kg)–induced convulsive seizures in head-fixed mice monitored with an infrared camera. Saline injections were used as control. (*C*) Mean image, acquired in vivo, of jRGECO1a-expressing MCs (hilus) and GCs (granule cell layer, GCL) before and after KA injection. (*D*) Representative fluorescence (*F*) traces of three individual MCs and GCs before and after KA injection. (*E* and *F*) Average ΔF/F (avg. ΔF/F) of recorded MCs and GCs after saline (Sal) or KA injection. Each data point corresponds to the average value per cell (*Left*) and per animal (*Right*). (*G*) Representative single-frame images acquired during MC activation [mean MC changepoint (change pt) $t_0$, *Middle*], as well as 10 s before and after (*Left* and *Right*), illustrating how the increase in MC activity, as measured by calcium signals, occurs a few seconds before the increase in GC activity during KA-induced convulsive seizures. (*H*) Representative *F* traces of individual MC (black trace) and GC (gray trace) activation during KA-induced convulsive seizures. Vertical dashed lines indicate changepoints for MC and GC. MCs were activated before GCs. (*I*) Summary plot showing the delay ($GC_{changepoint} - MC_{changepoint}$) in GC and MC activation, averaged by mouse. *$P < 0.5$, ****$P < 0.0001$. Data are presented as mean ± SEM.

involved in the seizure-induced strengthening of MC-GC synaptic transmission, occurring in vivo, we conditionally knocked out *Bdnf* from GCs, a manipulation that abolishes MC-GC LTP (24), and tested whether seizures can trigger MC-GC potentiation in absence of postsynaptic BDNF. Given that experimental seizures can be reduced in *Bdnf* KO mice (33, 34), we only injected 0.5 μL of AAV5.CaMKII.Cre-mCherry or AAV5.CaMKII.mCherry (control) into the DG upper blade of $Bdnf^{fl/fl}$ mice unilaterally (*SI Appendix*, Fig. S4 *A* and *B*) in order to prevent a potential failure in seizure induction when knocking out *Bdnf* from DG excitatory neurons. Mice were killed humanely 25 min after KA injection, which is the average time for reaching stage 3 convulsive seizure in WT control mice. We then prepared acute slices to monitor MC-GC synaptic function (Fig. 4*A*). While behavioral seizures were comparable in control and cKO mice (all animals reached stage 3 of convulsive seizures and no higher at 25 min postinjection), *Bdnf* deletion from GCs (Cre-mCherry$^+$ GCs) prevented seizure-induced MC-GC LTP, as KA IP injection failed to increase MC EPSC amplitude (Fig. 4*B*) [two-way ANOVA RM; IP injection: $F(1,6) = 0.003$, $P = 0.96$; stimulation intensity: $F(1.56,9.38) = 57.97$, $P = 0.0004$; IP injection × stimulation intensity: $F(1,6) = 287.4$, $P < 0.001$] or decrease PPR (Fig. 4*C*) (saline: 1.23 ± 0.01, $n = 7$; KA: 1.25 ± 0.1, $n = 7$; saline vs. KA: $P = 0.90$, unpaired *t* test) and CV (Fig. 4*C*) (saline: 0.40 ± 0.04, $n = 7$; KA: 0.42 ± 0.06, $n = 7$; saline vs. KA: $P = 0.79$, unpaired *t* test) as compared with saline-injected mice. The lack of KA-induced synaptic strengthening was not due to viral expression, since KA injection efficiently increased the input/output function (MC EPSC amplitude, Fig. 4*D*) [two-way ANOVA RM; IP injection:

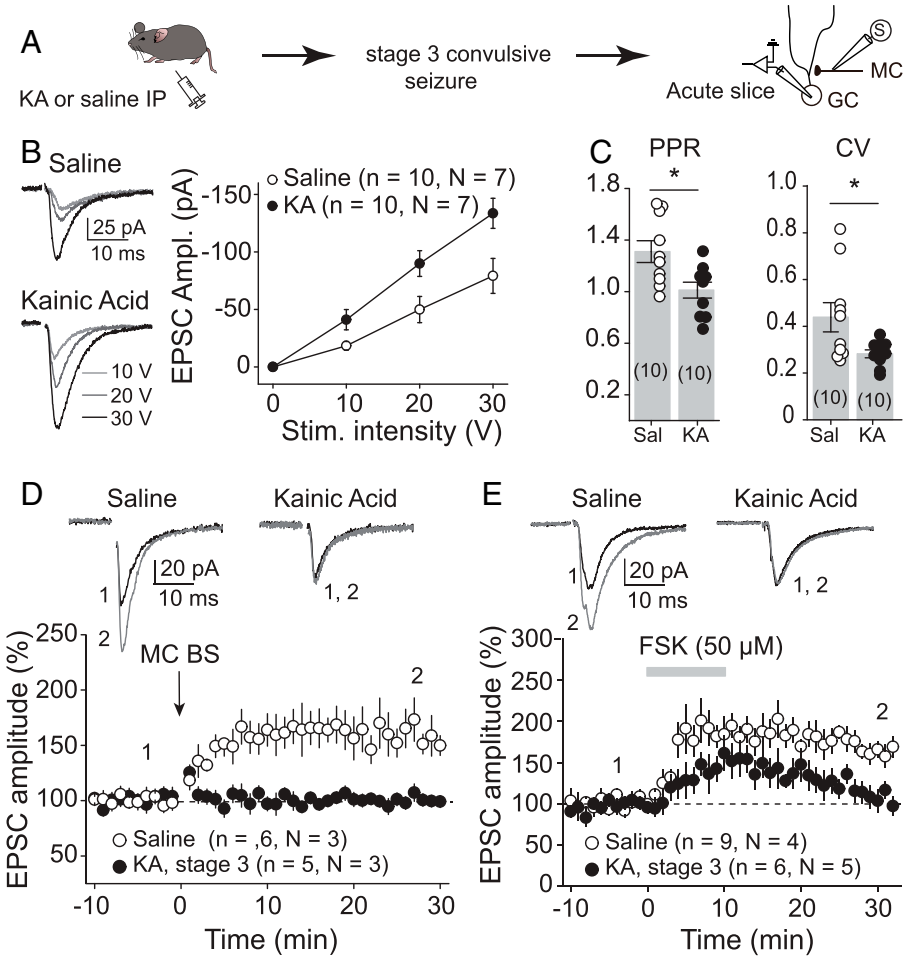


**Fig. 3.** Initial convulsive seizures increased MC-GC synaptic strength. (*A*) Seizures were acutely induced using KA IP (20 mg/kg). Mice were killed humanely after reaching stage 3 of convulsive seizures, and MC-GC synaptic function was accessed in acute hippocampal slices. Saline-injected mice were used as control. (*B*) Representative traces and summary plot showing how input/output function was increased in KA-injected mice. EPSC amplitude (Ampl.) vs stimulus (Stim.) intensity is plotted. (*C*) PPR and CV were both significantly decreased in KA-treated mice as compared with saline-injected mice. Each number in parentheses represents the number of cells. (*D* and *E*) Representative traces (*Top*) and time course summary plots (*Bottom*) showing that LTP at MC-GC synapses induced by either MC BS (five pulses at 100 Hz, repeated 50 times every 0.5 s, *D*) or 50 μM forskolin (FSK, *E*) application was impaired in KA-injected mice. *$P < 0.5$. Data are presented as mean ± SEM.

$F(1,4) = 23.6$, $P = 0.008$; stimulation intensity: $F(1.34,5.34) = 68.9$, $P = 0.0002$; IP injection × stimulation intensity: $F(1,4) = 537.0$, $P < 0.0001$] and reduced PPR (Fig. 4*E*) (saline: 1.34 ± 0.1, $n = 5$; KA: 0.98 ± 0.1, $n = 7$; saline vs. KA: $P = 0.014$, unpaired $t$ test) and CV (Fig. 4*E*) (saline: 0.39 ± 0.04, $n = 5$; KA: 0.27 ± 0.03, $n = 7$; saline vs. KA: $P = 0.031$, unpaired $t$ test) in mCherry$^+$ control GCs. Deleting *Bdnf* from GCs did not alter MC-GC synaptic function in saline-injected mice, as indicated by the fact that input/output function (Fig. 4 *B* and *D*) [saline: two-way ANOVA RM; AAV: $F(1,4) = 0.27$, $P = 0.63$; stimulation intensity: $F(1.48,5.94) = 75.57$, $P < 0.00001$; AAV × stimulation intensity: $F(1,4) = 174.09$, $P = 0.0002$], PPR (Fig. 4 *C* and *E*) (saline control: 1.34 ± 0.1, $n = 5$; saline cKO: 1.23 ± 0.01, $n = 7$; control vs. cKO: $P = 0.44$, unpaired $t$ test), and CV (Fig. 4 *C* and *E*) (saline control: 0.39 ± 0.04, $n = 5$; saline cKO: 0.40 ± 0.04, $n = 7$; control vs. cKO: $P = 0.91$, unpaired $t$ test) were similar in Cre$^+$ GCs (*Bdnf* cKO) as compared to mCherry$^+$ GCs (control). In contrast, KA-injected mice showed a significant reduction in input/output function (Fig. 4 *B* and *D*) [KA: two-way ANOVA RM; AAV: $F(1,6) = 10.84$, $P = 0.017$; stimulation intensity: $F(1.39,8.38) = 64.08$, $P = 0.00002$; AAV × stimulation intensity: $F(1,6) = 166.81$, $P = 0.00001$] and significant increase in both PPR (Fig. 4 *C* and *E*) (KA control: 0.98 ± 0.1, $n = 7$; KA cKO: 1.25 ± 0.1, $n = 7$; control vs. cKO: $P = 0.049$, unpaired $t$ test) and CV (Fig. 4 *C* and *E*) (KA control: 0.27 ± 0.03, $n = 7$; KA cKO: 0.42 ± 0.06, $n = 7$; control vs. cKO: $P = 0.044$, unpaired $t$ test) in *Bdnf* cKO mice as compared with control animals. GC membrane properties were similar among all of the different groups (*SI Appendix*, Fig. S5).

To directly address a potential confounding reduction of KA-induced seizures in *Bdnf* cKOs (33, 34), we also compared MC-GC synaptic function in Cre$^+$ (*Bdnf* cKO) with Cre$^-$ (control) GCs recorded from the same animal following KA administration (*SI Appendix*, Fig. S4 *A* and *B*). The amplitude of evoked EPSCs was significantly decreased (*SI Appendix*, Fig. S4*C*) and PPR was significantly increased in Cre-expressing GCs as compared with neighboring Cre-lacking GCs (*SI Appendix*, Fig. S4*D*), further supporting the BDNF requirement for the KA-induced MC-GC strengthening. Lastly, *Bdnf* deletion from GCs also reduced the KA-induced strengthening of MPP-GC transmission (*SI Appendix*, Fig. S6). Thus, while *Bdnf* cKO had no impact on basal MC-GC and MPP-GC synaptic transmission and GC membrane properties, it abolished KA-induced strengthening of both MC-GC and MPP-GC synaptic transmission.

Because protein kinase A (PKA) activity is required for MC-GC LTP downstream of BDNF/TrkB signaling (23, 24), we examined whether PKA activation could still induce LTP in

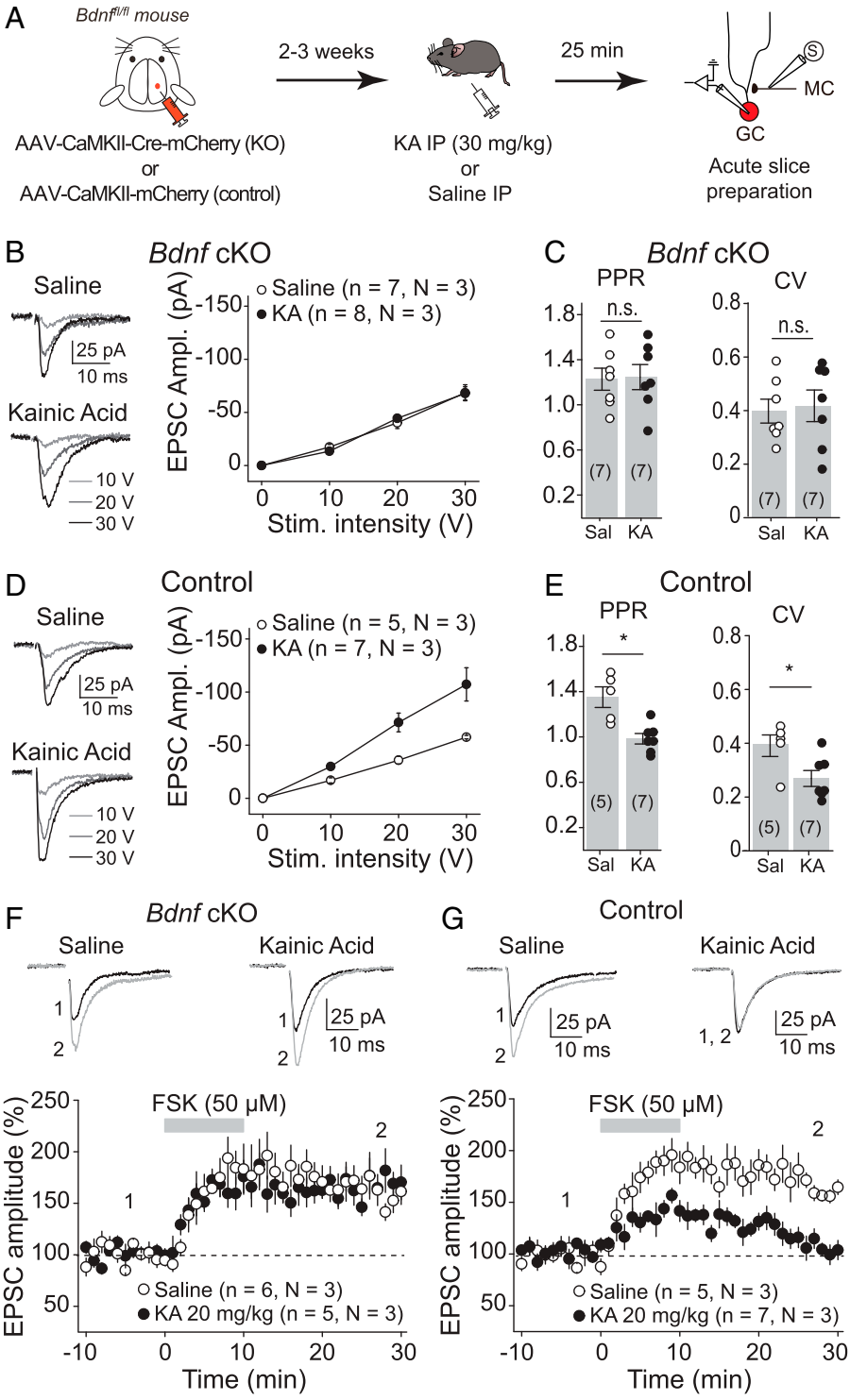


**Fig. 4.** Seizure-induced MC-GC synaptic strengthening required postsynaptic BDNF. (*A*) Experimental timeline. Control (AAV-CaMKII-mCherry) or Cre-expressing AAV (AAV-CaMKII-Cre-mCherry) were injected unilaterally into the dorsal blade of the DG of *Bdnf*$^{fl/fl}$ mice. Seizures were induced 2 to 3 wk later using KA IP (30 mg/kg), and acute hippocampal slices were prepared 25 min postinjection. Then, whole-cell recordings were performed from mCherry$^{+}$ GC, and synaptic responses were monitored in response to MC axon stimulation. (*B* and *C*) KA-induced seizure failed to increase MC-GC synaptic strength in GC-lacking BDNF. EPSC amplitude (*B*), PPR (*C*), and CV (*C*) were similar in Cre-mCherry$^{+}$ GCs obtained from KA vs. saline-injected mice. (*D* and *E*) Seizure induction increased MC-GC EPSC amplitude (*D*) and decreased PPR and CV (*E*) in control mice. (*F*) Representative traces and time course summary plots showing similar FSK-induced potentiation of evoked MC-GC EPSCs (50 μM FSK bath application for 10 min) recorded from *Bdnf* cKO GCs in KA- and saline-injected mice. (*G*) FSK-induced potentiation of MC-GC synaptic transmission in *Bdnf*$^{fl/fl}$ mice injected with a control virus (AAV-CaMKII-mCherry) was impaired in KA-injected mice (20 mg/kg) as compared with saline-treated mice. *$P < 0.05$; nonsignificant, n.s., $P > 0.05$. Data are presented as mean ± SEM.

BDNF-deficient GCs. Bath application of forskolin (50 μM for 10 min) triggered normal LTP in BDNF-deficient GCs (Cre-mCherry$^{+}$) obtained from both KA- and saline-injected mice in postsynaptic *Bdnf* cKOs (Fig. 4*F*) (saline: 162.9 ± 9.4% of baseline, $n = 6$, $P = 0.0011$, paired $t$ test; KA: 161.9 ± 5.7% of baseline, $n = 5$, $P = 0.0004$, paired $t$ test; saline vs. KA: $P = 0.85$, unpaired $t$ test), supporting the idea that postsynaptic *Bdnf* deletion prevented KA injection from inducing MC-GC LTP

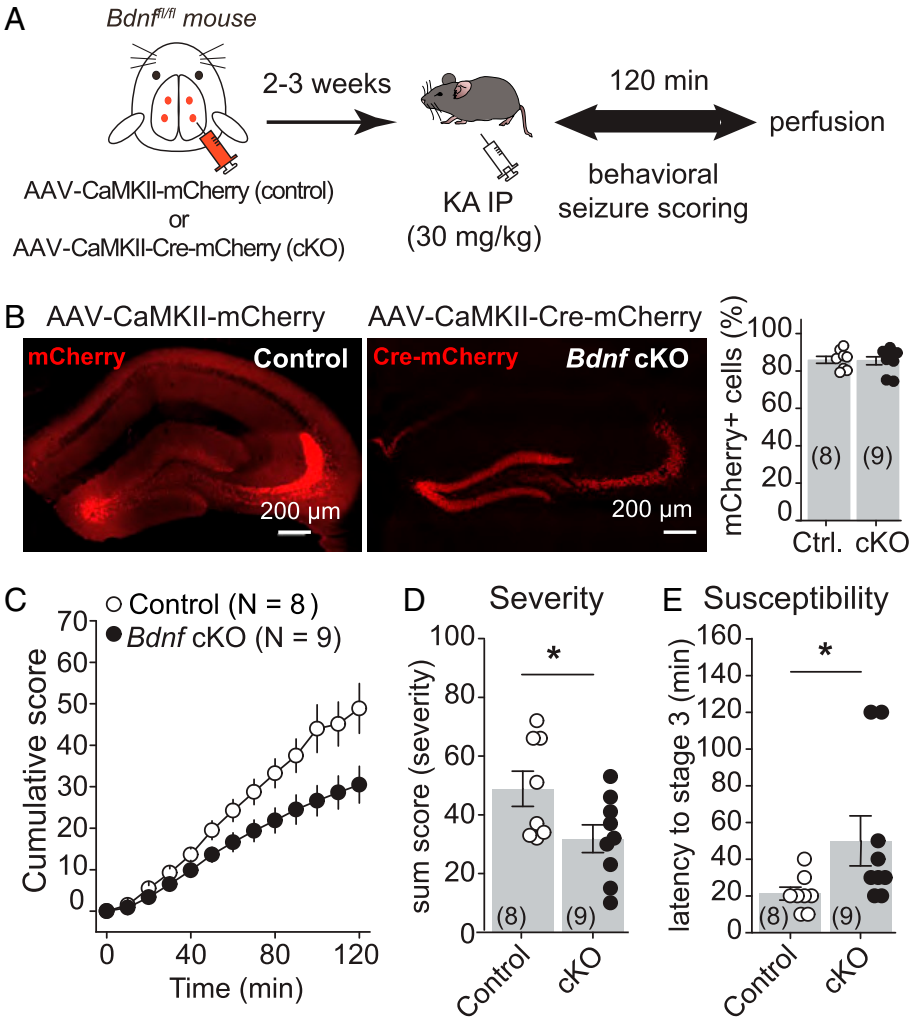


**Fig. 5.** Knocking out BDNF from hippocampal excitatory neurons reduced KA-induced seizures. (*A*) AAV-CaMKII-mCherry (control) or AAV-CaMKII-Cre-mCherry (cKO) was injected bilaterally into ventral and dorsal DG of *Bdnf*$^{fl/fl}$ mice. (*B*) Representative confocal images (*Left*) and quantification (*Right*) showing high viral expression in the DG. Control (Ctrl) vs cKO. (*C–E*) Deletion of BDNF from hippocampal excitatory neurons (*Bdnf*$^{fl/fl}$ mice injected with AAV-CaMKII-Cre-mCherry) induced significant decreases in the cumulative seizure score (*C*) and in the sum score (*D*) and a significantly increase in latency to convulsive seizures (*E*) as compared with controls (*Bdnf*$^{fl/fl}$ mice injected with AAV-CaMKII-mCherry). *$P < 0.05$. Data are presented as mean ± SEM.

in vivo. In contrast, and consistent with our previous results (Fig. 3*E*), forskolin failed to induce LTP in control GCs (mCherry$^{+}$) obtained from KA-injected mice but not from saline-injected mice (Fig. 4*G*) (saline: 171.5 ± 7.2% of baseline, $n = 5$, $P = 0.0006$, paired $t$ test; KA: 115.7 ± 8.1% of baseline, $n = 7$, $P = 0.10$, paired $t$ test; saline vs. KA: $P = 0.0006$, unpaired $t$ test). Altogether, these results reveal that initial seizures triggered MC-GC LTP in vivo via a BDNF-dependent mechanism and that such synaptic potentiation occluded subsequent induction of LTP in vitro.

Deleting *Bdnf* from DG excitatory neurons, a manipulation that abolishes MC-GC LTP both in vitro (24) or in vivo (Fig. 4 and *SI Appendix*, Fig. S4), could inhibit seizure induction. To test this possibility, we stereotaxically injected AAV-CaMKII-Cre-mCherry (cKO) or AAV-CaMKII-mCherry (control) into both dorsal and ventral DG of adult *Bdnf*$^{fl/fl}$ mice, bilaterally (Fig. 5*A*). We confirmed that the virus was highly expressed in the DG (Fig. 5*B*) (control: 85.9 ± 1.9% of DG neurons, eight mice; cKO: 85.5 ± 2.1% of DG neurons, nine mice; ∼1,000 analyzed neurons per animal) and that injection of AAV-CaMKII-Cre-mCherry into the hippocampus of *Bdnf*$^{fl/fl}$ mice strongly reduced *Bdnf* mRNA levels selectively in the hippocampus (*SI Appendix*, Fig. S7). *Bdnf* conditional deletion reduced seizure severity and susceptibility, as indicated by significant decreases in the total cumulative seizure score (Fig. 5*C*) [two-way ANOVA RM; AAV condition: $F(1,7) = 6.0$, $P = 0.044$; time: $F(1.26,8.87) = 150.4$, $P < 0.001$; AAV condition × time: $F(1,7) = 262.4$, $P < 0.001$] and in the sum score (Fig. 5*D*) (control: 48.9 ± 6.0, $n = 8$; cKO: 31.7 ± 4.7, $n = 9$; control vs. cKO: $P = 0.039$, unpaired $t$ test) and an increase in latency to stage 3 (Fig. 5*E*) (control: 21.2 ± 3.5, $n = 8$; cKO: 51.1 ± 13.4, $n = 9$; control vs. cKO: $P = 0.045$, Mann–Whitney $U$ test). Remarkably, c-Fos expression was significantly reduced in *Bdnf* cKO mice as compared with controls (*SI Appendix*, Fig. S8). Lastly, we found no significant changes in the amplitude and frequency of spontaneous EPSC (*SI Appendix*, Fig. S9) or in the amplitude of evoked MC-EPSCs (Fig. 4), MPP-EPSCs (*SI Appendix*, Fig. S6*C*), and lateral perforant path (LPP)–EPSCs (*SI Appendix*, Fig. S10) recorded from *Bdnf*-lacking GCs, showing that conditionally knocking out *Bdnf* from DG excitatory neurons did not modify the strength of basal excitatory inputs onto GCs. Altogether, these results indicate that seizure-induced MC-CG LTP accentuates the proconvulsant effects of KA.

**In Vivo Application of the MC-GC LTP Induction Protocol Promoted Behavioral Seizures.** We previously showed that optogenetic repetitive stimulation of MC axons triggers robust MC-GC LTP in vitro (23). We therefore tested whether in vivo

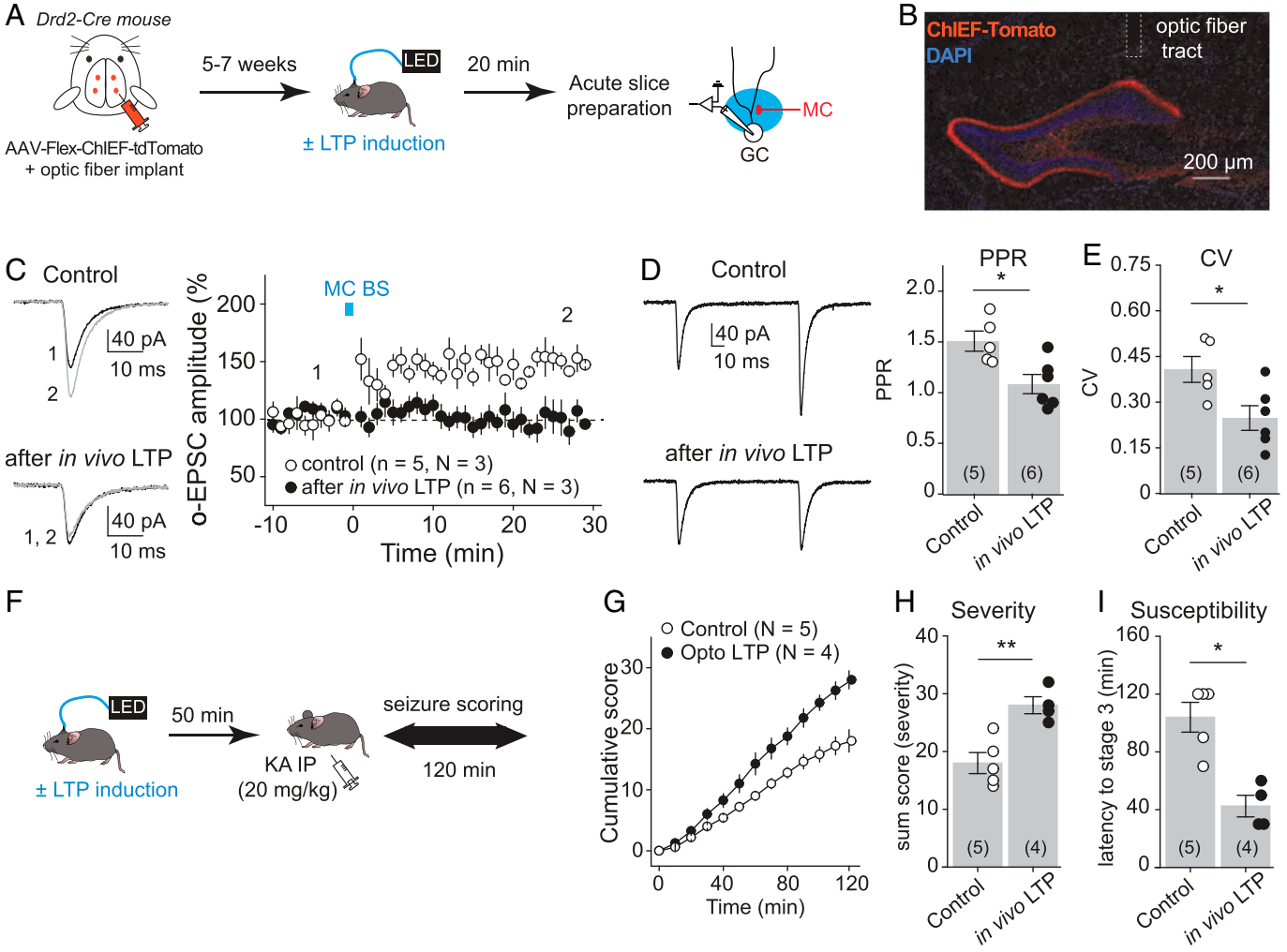


**Fig. 6.** In vivo induction of MC-GC LTP promoted seizures. (*A*) Experimental timeline. To selectively photostimulate MC axons in vivo, AAV-hSyn-ChIEF-tdTomato was bilaterally injected into ventral and dorsal DG of *Drd2*-cre mice, and an optical fiber was implanted above the IML of the DG. The LTP induction protocol (MC BS: five pulses at 30 Hz, repeated 50 times, every 0.5 s) was applied in vivo by delivering blue light through a patch cord cable connected to a fiber-coupled 470-nm light-emitting diode (LED) source 5 to 7 wk after surgery. Sham light was used as a control. Acute hippocampal slices were prepared 20 min later, and MC-GC synaptic properties were analyzed using whole-cell recordings of GCs and light stimulation of MC axons. (*B*) Representative confocal images showing the viral expression and the fiber tract location. (*C*) Optically evoked EPSCs (o-EPSCs) were recorded in GC in response to MC axon photostimulation. Representative traces (light) and time course summary plot (light) showing that in vivo application of MC BS prevented subsequent induction of LTP in vitro. (*D* and *E*) PPR (*D*) and CV (*E*) were both significantly decreased after in vivo application of the MC-GC LTP induction protocol as compared with the sham light (control) condition. Each number in parentheses indicates the number of cells. (*F*) Experimental timeline. The LTP induction protocol (MC BS: five pulses at 30 Hz, repeated 50 times, every 0.5 s) was delivered in vivo, while sham light was used as control. KA (20 mg/kg IP) was then administered 50 min after the optogenetic stimulation, and seizures were scored for 120 min. (*G–I*) Application of the MC-GC LTP induction protocol (optogenetically-induced LTP or Opto LTP) increased seizure severity and susceptibility, as indicated by significant increases in the cumulative seizure score (*G*) and in the sum score (*H*) and a significantly decrease in latency to convulsive seizures (*I*). $*P < 0.05$, $**P < 0.01$. Data are presented as mean ± SEM.

induction of LTP using optogenetic activation of MCs facilitated acutely evoked behavioral seizures. To this end, we selectively expressed the fast variant of channelrhodopsin ChIEF in MCs by bilaterally injecting the Cre-recombinase–dependent AAV-hSyn-DIO-ChIEF-tdTomato into the dorsal and ventral DG of *Drd2*-Cre mice (Fig. 6*A*). Blue light burst stimulation of MC axons (MC BS: five pulses of 5 ms at 30 Hz, repeated 50 times every 0.5 s) was delivered through an optic fiber placed above the dorsal DG inner molecular layer (IML) in vivo, and sham light (i.e., no light) was used as a control (Fig. 6 *A*, *B*, and *F*). Optic fiber location and selective viral expression in MCs were confirmed post hoc (Fig. 6*B*). We also verified that the light stimulation protocol induced MC-GC LTP in vivo. When it does, this plasticity should be occluded in hippocampal slices prepared after in vivo light stimulation. We found that repetitive light stimulation of MC axons failed to induce LTP in vitro when the LTP protocol was preapplied in vivo as compared with control slices (Fig. 6*C*) (after in vivo LTP: 96.1 ± 7.9% of baseline, $n = 6$, $P = 0.64$, paired $t$ test; control: 146.7 ± 4.9% of baseline, $n = 5$, $P = 0.0007$, paired $t$ test; in vivo LTP vs. control: $P < 0.001$, unpaired $t$ test). In addition, both PPR (Fig. 6*D*) (control: 1.51 ± 0.10, $n = 5$; in vivo LTP: 1.08 ± 0.09, $n = 6$; control vs. in vivo LTP: $P = 0.013$, unpaired $t$ test) and CV (Fig. 6*E*) (control: 0.41 ± 0.04, $n = 5$; in vivo LTP: 0.25 ± 0.04, $n = 6$; control vs. in vivo LTP: $P = 0.024$, unpaired $t$ test) were significantly reduced after in vivo photostimulation as compared with control mice (sham light). These results strongly suggest that in vivo MC BS (five pulses of 5 ms at 30 Hz, repeated 50 times every 0.5 s) induced presynaptic LTP at MC-GC synapses. We then tested whether in vivo induction of MC-GC LTP can promote behavioral seizures. In these experiments, to facilitate the detection of potential increase in seizure severity/susceptibility, seizures were induced with a lower dose of KA IP (20 mg/kg) 50 min after in vivo induction of LTP (Fig. 6*F*). Remarkably, we

found that in vivo application of a MC-GC LTP induction protocol significantly increased the severity and susceptibility of acutely evoked seizures induced by KA, as indicated by significant increases in cumulative seizure score (Fig. 6*G*) [two-way ANOVA RM; light: $F(1,3) = 100.7$, $P < 0.001$; time: $F(1.3,4.1) = 221.5$, $P < 0.001$; light × time: $F(1,3) = 109.3$, $P < 0.01$] and in the sum score (Fig. 6*H*) (control: 18.0 ± 1.8, $n = 5$; in vivo LTP: 28.0 ± 1.5, $n = 4$; control vs. in vivo LTP: $P = 0.0045$, unpaired $t$ test) and a significantly decrease in latency to convulsive seizures (Fig. 6*I*) (control: 104.0 ± 10.3, $n = 5$; in vivo LTP: 42.5 ± 7.5, $n = 4$; control vs. in vivo LTP: $P = 0.017$, Mann–Whitney $U$ test). While optogenetic activation of MCs could impact their basic membrane properties or synaptic inputs, we found that the stimulation protocol that triggers LTP in vivo did not significantly alter MC membrane resistance or the main excitatory synaptic drive, i.e., GC inputs, onto MC recorded in vitro (*SI Appendix*, Fig. S11) (see *Materials and Methods*). Taken together, these findings strongly suggest that in vivo induction of MC-GC LTP can worsen behavioral seizures.

## Discussion

In this study, we found that early seizures potentiate crucial hippocampal excitatory synapses, thereby facilitating further epileptic activity. KA-induced seizures not only increased MC and GC activity in vivo but also triggered a BDNF-dependent strengthening of MC-GC synaptic transmission that occluded subsequent induction of MC-GC LTP. In addition, blocking MC-GC LTP and silencing MCs selectively were both associated with significant decreases in seizure susceptibility and severity. Moreover, in vivo induction of MC-GC LTP was sufficient to worsen convulsive seizures subsequently triggered with KA. Overall, our findings strongly suggest that seizure-induced plasticity at MC-GC excitatory synapses may significantly contribute to the proconvulsant role of MCs during early stages of epilepsy.

**Initial Seizures Induce BDNF-Dependent Strengthening of MC-GC Synaptic Transmission.** Using in vivo two-photon imaging in awake behaving mice, we found that acutely induced seizures triggered a massive increase in both MC and GC calcium signals (Fig. 2), indicating a robust increase in neuronal activity. Our findings are consistent with a recent study reporting in vivo epileptiform calcium signals detected with fiber photometry in the DG following KA administration (32). While these signals likely reflect the synchronized activity of a large population of neurons, including interneurons, we could assess calcium activity of individual MCs and GCs (Fig. 2 and *SI Appendix*, Fig. S2 *D* and *E*) by combining selective expression of a calcium indicator in DG excitatory neurons and two-photon live imaging. It has been reported that dorsal GCs are mainly activated by ventral MCs (31), which we were not able to confirm given the limited access to the ventral hippocampus of our head-fixed two-photon imaging approach. However, imaging of the dorsal hippocampus revealed that MC activation during convulsion seizures precedes GCs (Fig. 2 *G*–*I*). We therefore hypothesize that KA administration activates MCs, which in turn engage GCs. In support of this idea, we have recently reported that MCs express functional extrasynaptic kainate receptors whose activation with submicromolar concentrations of KA can drive MC activity in vitro, whereas GCs show comparatively much less sensitivity (at least one order of magnitude) to KA application (35). While interneurons (36) and CA3 pyramidal cells also express kainate receptors (37, 38), it is unlikely that activation of these neurons could directly drive GCs, although CA3 pyramidal cells could contribute indirectly by activating MCs (39). Furthermore, MCs show higher activity in vivo in contrast to GCs (40–42), making them more likely to be engaged during epileptic activity, regardless the nature of the chemoconvulsant. This last notion is also supported by the fact that MC silencing not only reduced KA-induced seizures (Fig. 1) but also prevents pilocarpine-induced epilepsy (5). Although MCs also excite inhibitory interneurons (16), the anticonvulsant effect of MC silencing (Fig. 1) suggests that MC silencing during initial seizures has a stronger impact on the activity of GCs than interneurons (5). Besides inducing synaptic plasticity, the KA-induced increase in MC and GC intracellular calcium concentration (Fig. 2) may also contribute to excitotoxicity and cell death. Altogether, our findings demonstrate that MCs and GCs are highly active during initial experimental seizures, suggesting that sustained activation of MCs contributes to GC recruitment.

We gathered multiple lines of evidence indicating that initial convulsive seizures induce presynaptically expressed MC-GC LTP in vivo. MC-GC synaptic strength was increased in KA-treated mice as compared with sham-injected animals, and this strengthening was associated with a significant reduction in both PPR and CV (Fig. 3 *B* and *C*), suggesting a presynaptic mechanism. Moreover, induction of MC-GC LTP in vitro was occluded after convulsive seizures (Fig. 3 *D* and *E*), indicating a common step. The KA-induced strengthening of MC-GC synaptic transmission in vivo was likely induced by the increase in MC activity (35), consistent with the observation that repetitive MC activity triggers robust MC-GC LTP in acute rodent hippocampal slices (23). Although in vitro epileptic activity was associated with a rise in the net excitatory drive between MCs and GCs (5), it is unclear whether this effect results from disinhibition or direct MC-GC synaptic strengthening. Our findings show that both in vivo optogenetic activation of MCs (Fig. 6) and acute seizures (Fig. 3) were sufficient to trigger presynaptic MC-GC LTP.

Several studies indicate that seizures can increase both BDNF levels (43–46) and TrkB activation in the hippocampus (25, 47). In addition, BDNF is necessary and sufficient for MC-GC LTP (23), and it can be released from both MCs and GCs following MC repetitive activity in vitro (24). It is therefore likely that by releasing BDNF, MC and GC activity induces MC-GC LTP in vivo. In support of this mechanism, we found that genetic removal of *Bdnf* from GCs abolished seizure-induced MC-GC LTP (Fig. 4 and *SI Appendix*, Fig. S4), while it did not affect basal MC-GC synaptic (Fig. 3) or GC membrane properties in sham-injected mice (*SI Appendix*, Fig. S5). Of note, we did not observe any failure of seizure induction when *Bdnf* was sparsely knocked out. Altogether, our findings indicate that BDNF mediates in vivo seizure-induced strengthening of MC-GC excitatory synapses.

**Seizure-Induced LTP at MC-GC Synapses is Proconvulsant.** Our results strongly suggest that activity-dependent strengthening of MC-GC synapses promotes acute seizures. While MCs innervate GCs and inhibitory interneurons, MC repetitive activity that induces MC-GC LTP, at least in vitro, has no effect on feedforward inhibition onto GCs (23), and such repetitive activity does not induce plasticity at GC-MC synapses (*SI Appendix*, Fig. S11). LTP-induced worsening of seizures (Fig. 6) is supported by the extensive MC projection onto the proximal dendrites of GCs (16) and the powerful MC-GC excitatory drive reported both in vitro (23) and in vivo (31). Given that a single MC innervates as much as 75% of the septotemporal axis of the hippocampus (48), broad induction of MC-GC LTP can be detrimental,

underscoring a link between uncontrolled LTP at the hippocampal excitatory synapse and seizures. Conversely, blocking activity-dependent strengthening of MC-GC synapses in vivo reduced induced seizure severity. PKA and BDNF signaling pathways are both necessary and sufficient for activity-dependent LTP at MC-GC synapses (23, 24). Both MC silencing using $G_i$ iDREADD (Fig. 1) and knocking out *Bdnf* from hippocampal excitatory neurons (Fig. 5) reduced acute KA-induced seizure severity. However, MC silencing not only prevents MC-GC LTP induction but also reduces basal MC-GC synaptic transmission (Fig. 1) and MC output activity. Although *Bdnf* cKO had no effect on MC-GC basal transmission (Fig. 4) and GC membrane properties (*SI Appendix*, Fig. S5), we cannot discard an effect on other synapses. In fact, we found that deleting *Bdnf* from GCs did not alter MPP- and LPP-GC synaptic transmission (*SI Appendix*, Figs. S6, S9, and S10) but prevented KA-induced MPP-GC strengthening (*SI Appendix*, Fig. S6). A potential role of MC-GC LTP in this strengthening cannot be discarded. *Bdnf* deletion reduced c-Fos expression in the DG of KA-injected mice (*SI Appendix*, Fig. S8), suggesting that BDNF/TrkB signaling contributes to seizure-induced opening of the DG gate, likely by strengthening MC-GC synapses. Consistent with this scenario, optogenetic induction of MC-GC LTP in vivo was sufficient to worsen convulsive seizures. Notably, type 1 cannabinoid receptors, which are highly expressed at MC terminals (49), tonically suppress MC-GC transmission and also dampen the induction of MC-GC LTP (50) in an activity-dependent manner. By suppressing excitatory drive, these receptors could be a potential target to prevent epilepsy (14, 51–53). In agreement with recent findings using the pilocarpine model (5), our results strongly support a proconvulsant role of MCs during early epilepsy. In contrast, in a chronic mouse model of TLE induced by KA intrahippocampal administration, MCs are reportedly antiepileptic (4), suggesting that the role of MCs may differ significantly with the disease stage. A change in MC connectivity that leads to a reduced excitatory/inhibitory drive of GCs could underlie the antiepileptic role of surviving MCs in chronic epilepsy (54).

Compelling evidence indicates that BDNF and its high-affinity receptor TrkB promote worsening of TLE (25, 33, 34, 55–59), but the precise mechanisms and specific contributions of different cell types are not entirely clear. Here we identified two reciprocally connected excitatory neurons in the DG, MCs and GCs, that can mediate the BDNF proconvulsant effects via BDNF-dependent MC-GC LTP. Interfering with BDNF/TrkB signaling in different ways reduced epilepsy—i.e. heterozygous deletion of *Bdnf* (33), neuronal deletion of *Bdnf* or *TrkB* (34), chemogenetic blockade of TrkB kinase activity in $TrkB^{F616A}$ mutant mice (58), and a mutant mouse that uncouples TrkB from its downstream phospholipase Cγ1 signaling (56). Importantly, based on our previous (23) and present (Figs. 4 and 6) findings, these manipulations could also prevent seizure-induced MC-GC LTP and the associated facilitation of epileptic activity. Conversely, overexpression of BDNF in the brain (59) and local infusion of BDNF into the hippocampus (55) worsen epileptic seizures. BDNF is sufficient to induce MC-GC LTP in vitro (23), raising the possibility that in vivo infusion of BDNF promotes seizures by inducing MC-GC LTP broadly. Of note, exogenous BDNF delivery into the hippocampus of chronically epileptic rats can have antiepileptic and neuroprotective effects (60), suggesting that BDNF action might differ with epilepsy stages.

Altogether, our findings uncover a potential mechanism implicated in the early stages of epilepsy before brain damage becomes irreversible. We highlighted how initial seizures can shape an important hippocampal excitatory synapse in a BDNF-dependent manner, and how broad, uncontrolled induction of LTP can be detrimental and promote subsequent induction of seizures. Manipulations that suppress LTP induction and BDNF signaling at MC-GC synapses may be a strategy for the treatment of epilepsy.

## Materials and Methods

C57BL/6, *Bdnf* floxed ($Bdnf^{fl/fl}$), or *Drd2*-cre (B6.FVB(Cg)-Tg(*Drd2*-cre)ER44Gsat/Mmucd, MMRRC 032108-UCD) mice (2 to 3.5 mo old, both males and females) were used in this study. All animals were group housed in a standard 12:12 h light:dark cycle and had free access to food and water. Animal handling, breeding, and use followed a protocol approved by the Animal Care and Use Committee of the Albert Einstein College of Medicine, in accordance with NIH guidelines. Experimental procedures, involving hippocampal slice preparation, electrophysiology, in vivo two-photon imaging, *Bdnf* conditional KO (cKO), MC silencing, in vivo induction of MC-GC LTP with optogenetics, seizure induction and monitoring, immunohistochemistry, fluorescent in situ hybridization, and adeno-associated virus vector construction, were detailed in *SI Appendix, Supplementary Materials and Methods*. Image acquisition, quantification, data, and statistical analysis are also included in *SI Appendix, Supplementary Materials and Methods*.

For more details, refer to *SI Appendix, Supplementary Materials and Methods*.

**Data Availability.** All study data are included in the article and/or *SI Appendix*. Original code was uploaded to GitHub (https://github.com/GoncalvesLab/Nasrallah-et-al-PNAS-2022-Collab) (61). Plasmids generated for this study have been deposited on AddGene (190240, 190241) (62, 63).

**ACKNOWLEDGMENTS.** We thank the members of the P.E.C. laboratory for constructive feedback, especially Coralie Berthoux and Czarina Ramos for critical reading of the manuscript. We also thank Pascal Kaeser (Harvard University) for sharing an AAV-hSyn-Flex-ChIEF-tdTomato plasmid and Lisa Monteggia (Vanderbilt University) for sharing $Bdnf^{fl/fl}$ mice. This research was supported by the NIH grants R01-NS113600, R01-MH125772, R01-NS115543 and R01-MH116673 to P.E.C., and R21-MH120496 to Y.J.Y.; the Fondation pour la Recherche Médicale (Postdoctoral Fellowship for research abroad), the Fondation Bettencourt Schueller award (Prix pour les Jeunes Chercheurs 2016), and the American Epilepsy Society Postdoctoral Research Fellowship (2020) to K.N.; the Einstein Training Program in Stem Cell Research from the Empire State Stem Cell Fund through New York State Department of Health Contract C34874GG to M.A.F.; and a Whitehall Foundation Research Grant (2019-05-71) to J.T.G. Confocal images were obtained at the Einstein Imaging Core (supported by the Rose F. Kennedy Intellectual Disabilities Research Center, NIH Shared Instrument Grant 1S10OD25295 to Konstantin Dobrenis), and fluorescent in situ hybridization in brain slices was performed using a PerkinElmer P250 high-capacity slide scanner (Shared Instrument Grant 1S10OD019961) at the Einstein Analytical Imaging Facility (supported by Cancer Center Support Grant P30 CA0133330).

Author affiliations: [a]Dominick P. Purpura Department of Neuroscience, Albert Einstein College of Medicine, Bronx, NY 10461; [b]Gottesman Institute for Stem Cell Biology and Regenerative Medicine, Albert Einstein College of Medicine, Bronx, NY 10461; [c]Department of Anatomy and Structural Biology, Albert Einstein College of Medicine, Bronx, NY 10461; and [d]Department of Psychiatry & Behavioral Sciences, Albert Einstein College of Medicine, Bronx, NY 10461

1. R. S. Fisher *et al.*, ILAE official report: A practical clinical definition of epilepsy. *Epilepsia* **55**, 475–482 (2014).
2. M. Bialer *et al.*, Progress report on new antiepileptic drugs: A summary of the Thirteenth Eilat conference on new antiepileptic drugs and devices (EILAT XIII). *Epilepsia* **58**, 181–221 (2017).
3. H. E. Scharfman, The enigmatic mossy cell of the dentate gyrus. *Nat. Rev. Neurosci.* **17**, 562–575 (2016).
4. A. D. Bui *et al.*, Dentate gyrus mossy cells control spontaneous convulsive seizures and spatial memory. *Science* **359**, 787–790 (2018).
5. J. J. Botterill *et al.*, An excitatory and epileptogenic effect of dentate gyrus mossy cells in a mouse model of epilepsy. *Cell Rep.* **29**, 2875–2889.e6 (2019).
6. B. S. Chang, D. H. Lowenstein, Epilepsy. *N. Engl. J. Med.* **349**, 1257–1266 (2003).

7. S. Jinde *et al.*, Hilar mossy cell degeneration causes transient dentate granule cell hyperexcitability and impaired pattern separation. *Neuron* **76**, 1189–1200 (2012).
8. Ad. Ratzliff, V. Santhakumar, A. Howard, I. Soltesz, Mossy cells in epilepsy: Rigor mortis or vigor mortis? *Trends Neurosci.* **25**, 140–144 (2002).
9. I. Blümcke *et al.*, Loss of hilar mossy cells in Ammon's horn sclerosis. *Epilepsia* **41** (suppl. 6), S174–S180 (2000).
10. J. H. Margerison, J. A. Corsellis, Epilepsy and the temporal lobes. A clinical, electroencephalographic and neuropathological study of the brain in epilepsy, with particular reference to the temporal lobes. *Brain* **89**, 499–530 (1966).
11. L. Seress *et al.*, Survival of mossy cells of the hippocampal dentate gyrus in humans with mesial temporal lobe epilepsy. *J. Neurosurg.* **111**, 1237–1247 (2009).
12. B. E. Swartz *et al.*, Hippocampal cell loss in posttraumatic human epilepsy. *Epilepsia* **47**, 1373–1382 (2006).
13. P. S. Buckmaster, A. L. Jongen-Rêlo, Highly specific neuron loss preserves lateral inhibitory circuits in the dentate gyrus of kainate-induced epileptic rats. *J. Neurosci.* **19**, 9519–9529 (1999).
14. Y. Sugaya *et al.*, Crucial roles of the endocannabinoid 2-arachidonoylglycerol in the suppression of epileptic seizures. *Cell Rep.* **16**, 1405–1415 (2016).
15. R. K. Wong, R. D. Traub, R. Miles, Cellular basis of neuronal synchrony in epilepsy. *Adv. Neurol.* **44**, 583–592 (1986).
16. P. S. Buckmaster, H. J. Wenzel, D. D. Kunkel, P. A. Schwartzkroin, Axon arbors and synaptic connections of hippocampal mossy cells in the rat in vivo. *J. Comp. Neurol.* **366**, 271–292 (1996).
17. D. G. Amaral, H. E. Scharfman, P. Lavenex, The dentate gyrus: Fundamental neuroanatomical organization (dentate gyrus for dummies). *Prog. Brain Res.* **163**, 3–22 (2007).
18. D. A. Henze, L. Wittner, G. Buzsáki, Single granule cells reliably discharge targets in the hippocampal CA3 network in vivo. *Nat. Neurosci.* **5**, 790–795 (2002).
19. A. J. Pernía-Andrade, P. Jonas, Theta-gamma-modulated synaptic currents in hippocampal granule cells in vivo define a mechanism for network oscillations. *Neuron* **81**, 140–152 (2014).
20. M. Diamantaki, M. Frey, P. Berens, P. Preston-Ferrer, A. Burgalossi, Sparse activity of identified dentate granule cells during spatial exploration. *eLife* **5**, e20252 (2016).
21. E. Krook-Magnuson *et al.*, In vivo evaluation of the dentate gate theory in epilepsy. *J. Physiol.* **593**, 2379–2388 (2015).
22. D. Hsu, The dentate gyrus as a filter or gate: A look back and a look ahead. *Prog. Brain Res.* **163**, 601–613 (2007).
23. Y. Hashimotodani *et al.*, LTP at Hilar Mossy cell-dentate granule cell synapses modulates dentate gyrus output by increasing excitation/inhibition balance. *Neuron* **95**, 928–943.e3 (2017).
24. C. Berthoux, K. Nasrallah, P. E. Castillo, BDNF-induced BDNF release mediates long-term potentiation. bioRxiv [Preprint] (2021). https://doi.org/10.1101/2021.1230.474558. Accessed 30 December 2021.
25. T. W. Lin, S. C. Harward, Y. Z. Huang, J. O. McNamara, Targeting BDNF/TrkB pathways for preventing or suppressing epilepsy. *Neuropharmacology* **167**, 107734 (2020).
26. J. A. French *et al.*, Characteristics of medial temporal lobe epilepsy: I. Results of history and physical examination. *Ann. Neurol.* **34**, 774–780 (1993).
27. M. Raspall-Chaure, R. F. Chin, B. G. Neville, R. C. Scott, Outcome of paediatric convulsive status epilepticus: A systematic review. *Lancet Neurol.* **5**, 769–779 (2006).
28. A. Pitkänen, K. Lukasiuk, Mechanisms of epileptogenesis and potential treatment targets. *Lancet Neurol.* **10**, 173–186 (2011).
29. M. Lévesque, M. Avoli, The kainic acid model of temporal lobe epilepsy. *Neurosci. Biobehav. Rev.* **37**, 2887–2899 (2013).
30. E. Rusina, C. Bernard, A. Williamson, The kainic acid models of temporal lobe epilepsy. *eNeuro* **8**, ENEURO.0337-20.2021 (2021).
31. F. Fredes *et al.*, Ventro-dorsal hippocampal pathway gates novelty-induced contextual memory formation. *Curr. Biol.* **31**, 25–38.e5 (2021).
32. X. Zhang *et al.*, Stereotypical patterns of epileptiform calcium signal in hippocampal CA1, CA3, dentate gyrus and entorhinal cortex in freely moving mice. *Sci. Rep.* **9**, 4518 (2019).
33. M. Kokaia *et al.*, Suppressed epileptogenesis in BDNF mutant mice. *Exp. Neurol.* **133**, 215–224 (1995).
34. X. P. He *et al.*, Conditional deletion of TrkB but not BDNF prevents epileptogenesis in the kindling model. *Neuron* **43**, 31–42 (2004).
35. C. Ramos *et al.*, Activation of extrasynaptic kainate receptors drives hilar mossy cell activity. *J Neurosci.* **42**, 2872–2884 (2022).
36. M. Frerking, R. C. Malenka, R. A. Nicoll, Synaptic activation of kainate receptors on hippocampal interneurons. *Nat. Neurosci.* **1**, 479–486 (1998).
37. P. E. Castillo, R. C. Malenka, R. A. Nicoll, Kainate receptors mediate a slow postsynaptic current in hippocampal CA3 neurons. *Nature* **388**, 182–186 (1997).
38. C. Mulle *et al.*, Altered synaptic physiology and reduced susceptibility to kainate-induced seizures in GluR6-deficient mice. *Nature* **392**, 601–605 (1998).
39. H. E. Scharfman, The CA3 "backprojection" to the dentate gyrus. *Prog. Brain Res.* **163**, 627–637 (2007).
40. N. B. Danielson *et al.*, In vivo imaging of dentate gyrus mossy cells in behaving mice. *Neuron* **93**, 552–559.e4 (2017).
41. D. GoodSmith *et al.*, Spatial representations of granule cells and mossy cells of the dentate gyrus. *Neuron* **93**, 677–690.e5 (2017).
42. Y. Senzai, G. Buzsáki, Physiological properties and behavioral correlates of hippocampal granule cells and mossy cells. *Neuron* **93**, 691–704.e5 (2017).
43. J. C. Lauterborn *et al.*, Differential effects of protein synthesis inhibition on the activity-dependent expression of BDNF transcripts: Evidence for immediate-early gene responses from specific promoters. *J. Neurosci.* **16**, 7428–7436 (1996).
44. C. Humpel *et al.*, Monitoring release of neurotrophic activity in the brains of awake rats. *Science* **269**, 552–554 (1995).
45. D. H. Lowenstein, M. S. Seren, F. M. Longo, Prolonged increases in neurotrophic activity associated with kainate-induced hippocampal synaptic reorganization. *Neuroscience* **56**, 597–604 (1993).
46. D. K. Binder, S. D. Croll, C. M. Gall, H. E. Scharfman, BDNF and epilepsy: Too much of a good thing? *Trends Neurosci.* **24**, 47–53 (2001).
47. D. K. Binder, M. J. Routbort, J. O. McNamara, Immunohistochemical evidence of seizure-induced activation of trk receptors in the mossy fiber pathway of adult rat hippocampus. *J. Neurosci.* **19**, 4616–4626 (1999).
48. D. G. Amaral, M. P. Witter, The three-dimensional organization of the hippocampal formation: A review of anatomical data. *Neuroscience* **31**, 571–591 (1989).
49. I. Katona *et al.*, Molecular composition of the endocannabinoid system at glutamatergic synapses. *J. Neurosci.* **26**, 5628–5637 (2006).
50. K. R. Jensen, C. Berthoux, K. Nasrallah, P. E. Castillo, Multiple cannabinoid signaling cascades powerfully suppress recurrent excitation in the hippocampus. *Proc. Natl. Acad. Sci. U.S.A.* **118**, e2017590118 (2021).
51. G. Marsicano *et al.*, CB1 cannabinoid receptors and on-demand defense against excitotoxicity. *Science* **302**, 84–88 (2003).
52. K. Monory *et al.*, The endocannabinoid system controls key epileptogenic circuits in the hippocampus. *Neuron* **51**, 455–466 (2006).
53. I. Katona, Cannabis and endocannabinoid signaling in epilepsy. *Handb. Exp. Pharmacol.* **231**, 285–316 (2015).
54. C. R. Butler, G. L. Westbrook, E. Schnell, Adaptive mossy cell circuit plasticity after status epilepticus. *J. Neurosci.* **42**, 3025–3036 (2022).
55. H. E. Scharfman, J. H. Goodman, A. L. Sollas, S. D. Croll, Spontaneous limbic seizures after intrahippocampal infusion of brain-derived neurotrophic factor. *Exp. Neurol.* **174**, 201–214 (2002).
56. X. P. He, E. Pan, C. Sciarretta, L. Minichiello, J. O. McNamara, Disruption of TrkB-mediated phospholipase Cgamma signaling inhibits limbic epileptogenesis. *J. Neurosci.* **30**, 6188–6196 (2010).
57. C. Heinrich *et al.*, Increase in BDNF-mediated TrkB signaling promotes epileptogenesis in a mouse model of mesial temporal lobe epilepsy. *Neurobiol. Dis.* **42**, 35–47 (2011).
58. G. Liu *et al.*, Transient inhibition of TrkB kinase after status epilepticus prevents development of temporal lobe epilepsy. *Neuron* **79**, 31–38 (2013).
59. S. D. Croll *et al.*, Brain-derived neurotrophic factor transgenic mice exhibit passive avoidance deficits, increased seizure severity and in vitro hyperexcitability in the hippocampus and entorhinal cortex. *Neuroscience* **93**, 1491–1506 (1999).
60. C. Falcicchia *et al.*, Seizure-suppressant and neuroprotective effects of encapsulated BDNF-producing cells in a rat model of temporal lobe epilepsy. *Mol. Ther. Methods Clin. Dev.* **9**, 211–224 (2018).
61. K. Nasrallah *et al.*, Data from "Seizure-induced strengthening of a recurrent excitatory circuit in the dentate gyrus is proconvulsant." GitHub. https://github.com/GoncalvesLab/Nasrallah-et-al-PNAS-2022-Collab. Deposited 21 July 2022.
62. K. Nasrallah *et al.*, Plasmid from "Seizure-induced strengthening of a recurrent excitatory circuit in the dentate gyrus is proconvulsant." AddGene. http://www.addgene.org/search/advanced/?q=190240. Deposited 3 August 2022.
63. K. Nasrallah *et al.*, Plasmid from "Seizure-induced strengthening of a recurrent excitatory circuit in the dentate gyrus is proconvulsant." AddGene. http://www.addgene.org/search/advanced/?q=190241. Deposited 3 August 2022.

**Title:**

# Delayed formation of neural representations of space in aged mice

**Authors:**

Kelsey D. McDermott, M. Agustina Frechou, Jake T. Jordan, Sunaina S. Martin, J. Tiago Gonçalves*

*Corresponding author. Email: tiago.goncalves@einsteinmed.edu

**Affiliations:**

Dominick P. Purpura Department of Neuroscience and Gottesmann Institute for Stem Cell Biology and Regenerative Medicine, Albert Einstein College of Medicine, Bronx, NY

**Teaser:**

Representations of space in the aged mouse hippocampus are initially disrupted in novel environments, but improve once environments become familiar.

**Abstract:**

Aging is associated with cognitive deficits, with spatial memory being very susceptible to decline. The hippocampal dentate gyrus (DG) is important for processing spatial information in the brain and is particularly vulnerable to aging, yet its sparse activity has led to difficulties in assessing changes in this area. Using *in vivo* two-photon calcium imaging, we compared DG neuronal activity and representations of space in young and aged mice walking on an unfamiliar treadmill. We found that calcium activity was significantly higher and less tuned to location in aged mice, resulting in decreased spatial information encoded in the DG. However, with repeated exposure to the same treadmill, both spatial tuning and information levels in aged mice became similar to young mice, while activity remained elevated. Our results show that spatial

representations of novel environments are impaired in the aged hippocampus and gradually improve with increased familiarity. Moreover, while the aged DG is hyperexcitable, this does not disrupt neural representations of familiar environments.

**Main Text:**

## Introduction

As the world's population ages, it becomes more important to understand the cognitive effects of aging and to develop therapeutic strategies for the aging brain. While healthy aging has milder cognitive effects than neurodegenerative states, several aspects of cognitive function exhibit decline (*1*). Memory deteriorates with age, with spatial memory being particularly susceptible to deficits in older humans and animals (*2*–*4*). Older adults show orientation deficits (*5*, *6*), although they tend to perform better in familiar locations or tasks than in novel ones (*7*–*9*). This aging-related decay is thought to be caused by vulnerabilities in the hippocampal circuits that mediate spatial memory (*10*, *11*). The dentate gyrus (DG) is one of the hippocampal subregions that are most vulnerable to aging (*12*–*14*), and the inputs from the entorhinal cortex to DG are a main area of dysfunction in both Alzheimer's Disease (AD) patients and AD mouse models (*15*). During aging, there are reduced synaptic contacts from both the medial and lateral entorhinal cortex (*16*) onto DG neurons, as well as reduced synaptic plasticity of these inputs (*17*). However, the is very limited data about how DG activity changes with aging, primarily because neuronal activity in this region tends to be too sparse for *in vivo* electrophysiological recordings (*18*).

Here we investigated whether aging is associated with impaired DG activity and spatial representations, which could account for the spatial memory deficits seen in aged individuals. Since the DG is upstream of other hippocampal areas, changes in this region could help elucidate

the causes of aging-related changes in neuronal activity (*19–22*) and neural representations of space (*19*, *23*, *24*) found in some areas of the hippocampus but not in others. Using *in vivo* two-photon microscopy we imaged calcium activity in a large population of DG neurons of young and aged mice as the animals walked head-fixed on a treadmill to which they had never been exposed. We found that aged mice have increased DG single-cell calcium activity and disrupted neural representations of space upon their first exposure to the treadmill setting. However, further imaging sessions on subsequent days showed that spatial representations become similar to those of young mice as the animals familiarize themselves with the treadmill, whereas single-cell activity remains elevated. Our results highlight the importance of novelty and familiarity to spatial encoding in aged animals.

## Results

To record neuronal activity in DG excitatory neurons, we injected young (3-4 month old) and aged (21-26 month old) C57Bl6 mice with an AAV encoding the calcium indicator jRGECO1a (*25*) under the CaMKII promoter (Fig. 1A). We then implanted the mice with a hippocampal imaging window above the DG (*26*, *27*) to enable *in vivo* two-photon calcium imaging in this region (Fig. 1A,B). After waiting 3-4 weeks to allow for viral expression and recovery from surgery, we imaged mice on four consecutive days. During each imaging session the mice ran head-fixed along a treadmill containing tactile cues with four distinct segments (Fig. 1A,C) that was manually moved (Fig. S1). We recorded 10 minute videos of calcium activity and identified the regions corresponding to active cells using Suite2p software (Fig. 1D). Previous studies found that hippocampal activity in area CA3 becomes elevated during aging (*19*, *28*). We determined single-cell calcium activity by measuring the area under the curve of transients and normalizing to the distance run by each mouse (*29*) (Fig. 1E-G). We found that the aged group had higher activity levels than the young group (Fig. 1E, p=0.00463, nested bootstrap), which aligns with previous reports of hyperactivity. We also estimated the fraction of active neurons during each imaging session and found no

changes between groups (Fig. S2). We next investigated whether there were differences between the spatial representations of young and aged DG neurons. Both young and aged DG neurons have a variety of spatial responses, including place cells that only respond to a specific location and neurons whose activity shows low spatial preference (Fig. 2A,B). We determined the spatial

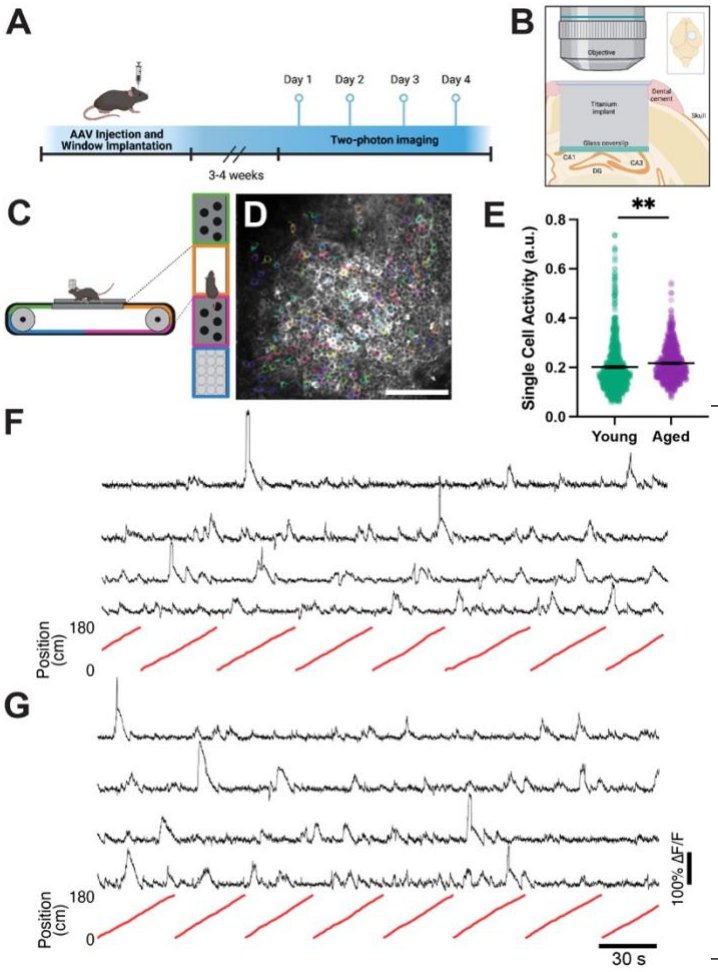


**Figure 1. DG is hyperactive in aged animals.** A) Experimental timeline, including AAV injection, window implantation, and two-photon imaging. B) Diagram of chronic window implant over the right hemisphere of the DG. C) Diagram of imaging setup, with side view (left) and top view (right) of mouse head-fixed to treadmill with multiple tactile zones. D) Example field of view with regions of interest of active cells shaded in color. Scale bar = 100 µm. E) Mean single cell calcium activity. F) Example calcium traces (black) and corresponding treadmill positions (red) from young mice. G) Example calcium traces (black) and corresponding treadmill positions (red) from aged mice. a.u.= arbitrary units. Young N=8 mice, n=910 cells; Aged N=8 mice, n=699 cells. **p<0.01

selectivity of neuronal activity using a previously described spatial tuning index (see methods). DG neurons in aged mice had significantly lower tuning indices than those in young mice (Fig. 2C, $p<0.0001$, nested bootstrap). This difference indicates that the activity of DG neurons in aged mice was not as place-specific as that of young DG neurons, suggesting an aging-related degradation of the spatial code. We also computed single-cell Fisher Information (FI), as a measure of how much spatial information was encoded by individual DG neurons. By plotting whole-recording calcium activity raster plots for neurons in the 10$^{th}$ percentile of FI we verified that

neurons with high spatial information behave like 'place cells' (*30*) in both young and aged animals, as their activity is concentrated at a single location on the treadmill (Fig. 2D,E). This place-specific response was present across laps as neurons in both cohorts of mice largely kept the same place response in both even and odd laps. Aged mice encoded less spatial information than young mice as denoted by a significant decrease in FI (Fig. 2F, p=0.00005, nested bootstrap).

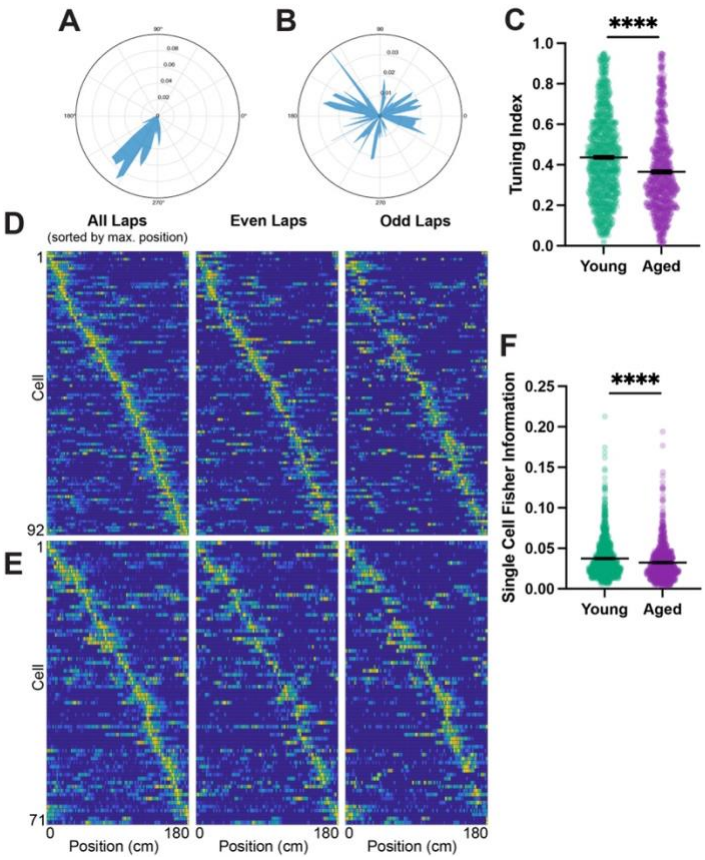


**Figure 2. DG representations of space are impaired in aged mice.** A) Tuning vector polar plots representing a highly spatially tuned cell and B) a cell with low spatial tuning. C) Spatial tuning index. D) Raster plots of tuning vectors of young mouse neurons in 10$^{th}$ percentile Fisher Information, sorted by the position of activity maximum for whole recording (All Laps). Raster plots of partial recording (Even Laps and Odd Laps) keeping same sorting used for whole recording. E) Same raster plots for aged mice. C) Single cell Fisher information. Statistics done with nested bootstrap analysis. Bars represent mean +/- SEM. Young N=8 mice, n=910 cells; Aged N=8 mice, n=699 cells. *p<0.05, **p<0.01, ***p<0.001, ****p<0.0001. See also supplemental figures 1 and 2.

To confirm that the changes in spatial representations in aged mice corresponded to a change in spatial memory, mice underwent behavioral testing using an object placement paradigm. This test takes advantage of a mouse's natural preference for novelty to assess how well animals can remember the location of objects in space, a behavior that is thought to be hippocampus-dependent (*31*). We allowed mice to explore an arena with visual cues and two novel and identical objects during a training trial. We then displaced one object to another location in the arena and

again allowed the mice to explore during a test trial (Fig. S3A). Young mice had a preference for the novel object that was significantly above chance (p= 0.0017, One sample Wilcoxon test) whereas aged mice did not score above chance (Fig S3B-C, p=0.6355, One sample Wilcoxon test). Additionally, significantly more aged mice than young mice failed the test (Fig. S3D, p=0.0393, Chi squared test). This change in preference can also be seen in the exploration times per objects, in which young mice spend more time engaged with the displaced object, while aged mice spend about an even amount of time between objects (Fig. S3E, p=0.0205 , Two-way ANOVA with Sidak multiple comparisons test). These data confirm earlier findings of spatial memory deficits in aged mice, which we now show is accompanied by impaired neural representations of space in the DG.

Older individuals are better able to distinguish places in an environment that they are familiar with than in a novel environment (*7*, *8*), so we asked how the representations of space in the DG changed across four consecutive days of imaging, as the treadmill belt became more familiar to the mice. Single-cell calcium activity remained elevated in aged mice through all recording days, even though this difference was not significant in days 2 and 3 (Fig. 3A, nested bootstrap with Bonferroni correction). While in young mice there was a slight but significant decrease in activity (p=0.00005) across days, in aged mice activity increased over time (p<0.0001) (Fig. 3B-C, nested bootstrap). In contrast to activity, the differences in tuning index and FI were erased over the four days of imaging, as young and aged groups converged. The spatial tuning index of young mice remained approximately constant over the course of all imaging sessions (p=0.19772), whereas the tuning of aged mice underwent an increase so that the differences between both groups were no longer significant in days 3 and 4 (p=0.00005). (Fig. 3D-F, nested bootstrap, Bonferroni corrected in 3D). FI rose in both young and aged groups over the four imaging days, but the increase was more pronounced in aged animals so that the differences between young and aged

animals were no longer significant in days 3 and 4 (Fig. 3G-I, nested bootstrap, Bonferroni corrected in 3G). These data suggest that representations of space in aged animals can be rescued by repeated exposure to the same environment.

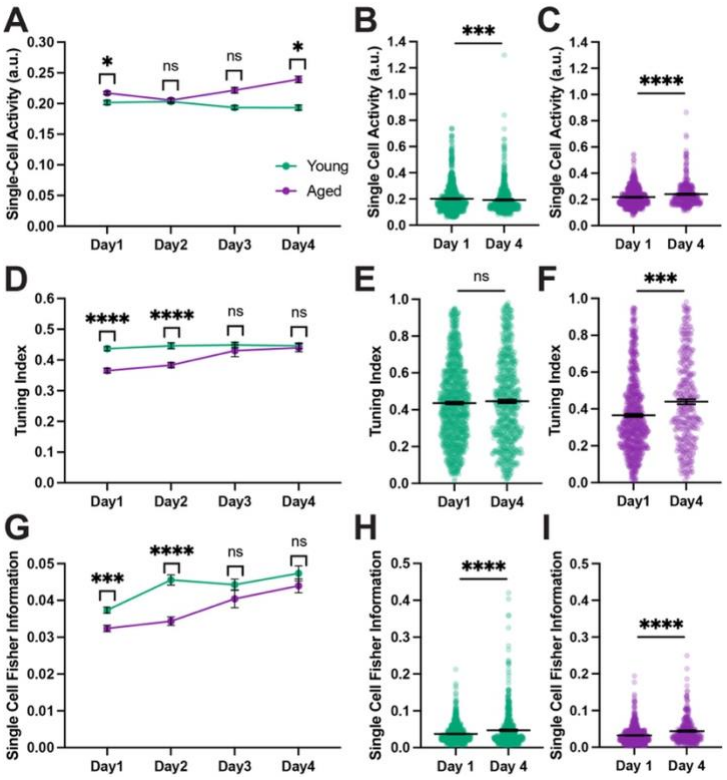


**Figure 3. Deficits in aged spatial representations are rescued with increased familiarity.** A) Mean single cell calcium activity across days. B) Single cell activity in young mice on day 1 versus day 4. C) Single cell activity in aged mice on day 1 versus day 4. D) Mean tuning index across days. E) Tuning index in young mice on day 1 versus day 4. F) Tuning index in aged mice on day 1 versus day 4. G) Mean single cell Fisher Information across days. H) Fisher Information in young mice on day 1 versus day 4. I) Fisher Information in aged mice on day 1 versus day 4. Statistics done with a nested bootstrap analysis. Bars represent mean +/- SEM. a.u.= arbitrary units. Young: day 1 N=8 , n=910; day 2 N=7, n=694; day 3 N=7, n=623; day 4 N=7, n=610; Aged: day 1 N=8, n=699; day 2 N=8, n=619; day 3 N=5, n=147; day 4 N=6, n=331. ns=not significant, *p<0.05, **p<0.01, ***p<0.001, ****p<0.0001.

Previous studies found the stability of neural representations of space was altered in aged animals (*32*, *33*). We therefore tracked the activity of individual neurons across days to investigate the stability of the active cell ensemble (Fig. 4A-C). We first asked whether cells that were active in the initial imaging session were reactivated on subsequent days. Surprisingly, we found no difference between groups, suggesting that both DG neurons in young and aged mice have similar reactivation rates (Fig. 4D, mixed effects model with Sidak multiple comparisons test). We went on to compare the activity in the cells that were active both on day 1, when the treadmill was novel, and day 4, when it had become familiar. The single-cell activity of matched cells increased across days in the young mice (p= 0.00234, nested bootstrap) but not in the old mice (p=0.15981, nested bootstrap) (Fig. 4E-F). This may reflect a ceiling for activity since the aged mice already

had higher activity on day 1. While the tuning index did not differ in either group across days (Fig. 4G-H, p=0.07626, p=0.21341), both groups saw higher spatial information, as FI was significantly increased in reactivated cells on day 4 (Fig. 4I-J, p=0.00015, p=0.00024), which may simply reflect the fact that FI increases sharply for the entire population across the four days. We then asked whether the reactivated cells had a distinct profile compared to those neurons that were not active across days. In day 1, cells that were to be reactivated did not differ from other cells in single cell activity levels. Whether cells were reactivated or not, their activity levels were higher in the aged mice on day 1, which recapitulates the pattern seen in the general population (Fig. 4K). These effects were gone by day 4, again reflecting the trend in the general population (Fig. 4L). In the aged group, cells that were reactivated showed higher tuning levels than other cells on day 1 (Fig. 4M), but this effect was also absent on day 4 (Fig. 4N). Reactivated cells had significantly higher FI than other neurons in both the young and aged groups on both day 1 and day 4 (Fig. 4O-P). This suggests that higher spatial information is a predictor of whether neurons will be reactivated over several days. Overall, we did not see evidence any changes in the stability of coding ensembles in aged animals, when compared with the young cohort. However, since reactivated neurons initially have higher tuning and spatial information than non-reactivated cells in aged animals, and increase their FI over time, it's possible that they contribute to the improvement of spatial representations in aged mice improve over the four days of imaging.

In summary, we have found that, in aged animals, DG neurons are hyperexcitable and impaired in their encoding of spatial features in novel environments. Our results highlight how the defects in spatial representations in the DG are specific to the first introduction to a novel context and can be rescued by increasing familiarity with a given environment.

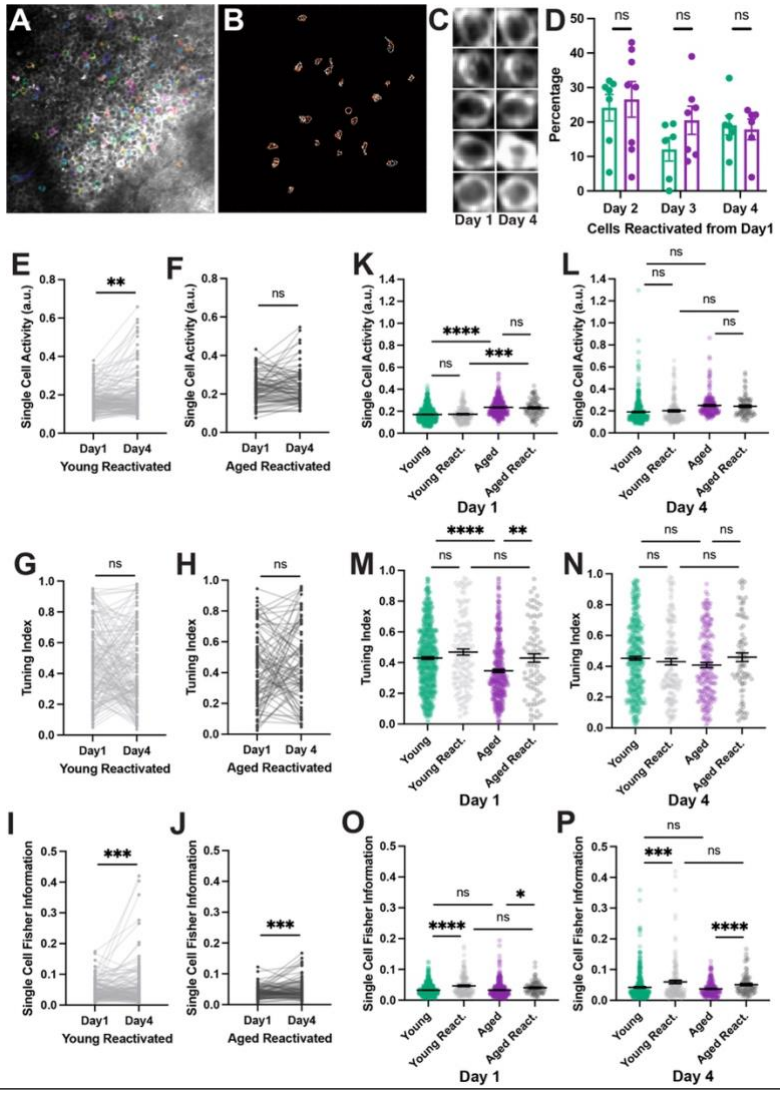


**Figure 4. Reactivated cells do not have a distinct profile in aged animals.** A) Example field of view used to match cells across days. Neurons that were active during recording session are shaded in color. B) Matched regions of interest from the field of view in panel A, red and white contours represent cells active on day 1 and 4. C) Examples of matched cells on day 1 and 4. D) Reactivation rate of neurons that were active on day 1. Percentages are based on imaging day versus day 1, regardless of whether the cell was active on other days. E-F) Matched single cell calcium activity in reactivated cells in young (E) and aged (F) mice. G-H) Matched tuning index in reactivated cells in young (G) and aged (H) mice. I-J) Matched single cell Fisher Information in reactivated cells in young (I) and aged (J) mice. K-L) Single cell activity of reactivated and non-reactivated cells on day 1 (K) and day 4 (L). M-N) Tuning of reactivated and non-reactivated cells on day 1 (M) and day 4 (N). O-P) Single cell Fisher Information of reactivated and non-reactivated cells on day 1 (O) and day 4 (P). Statistics done with nested bootstrap analysis. Bars represent mean +/- SEM. a.u.= arbitrary units. Young: N=6; day 1 n=617; day 1 react. n=140; day 4 n=396; day 4 react. n=140; Aged: N=5; day 1 n=375; day 1 react. n=80; day 4 n=196; day 4 react. n=80. ns=not significant, *p<0.05, **p<0.01, ***p<0.001, ****p<0.0001.

## Discussion

Aging is associated with cognitive decline in spatial memory in healthy aged humans and rodents (*2–4*). In this study we asked whether aged mice have impaired representations of space in the DG circuits that mediate spatial memory, which could account for the memory deficits seen in aged individuals.

Several studies have found that neuronal activity is elevated in the hippocampus of aged animals specifically in hippocampal area CA3 (*19–22*). Human studies using fMRI in older and younger adults have generally confirmed the hyperexcitability findings in the DG-CA3 axis (*5*, *14*), although fMRI does not have the resolution to distinguish between areas DG and CA3. This aging-related hyperexcitability phenotype is thought to contribute to the memory deficits seen in aged individuals (*34*, *35*). In order to understand the causes of the aging-related hyperexcitability it would be important to record neuronal activity from the DG, as this region provides the main inputs to CA3.

We used *in vivo* two-photon calcium imaging to record activity from young and aged DG neurons. This allowed us to image a large population of cells and therefore have a better chance capturing active cells in a sparsely active population. Additionally, using an imaging-based approach allowed us to study the same group of cells across time. We have found that single-cell calcium activity is indeed increased in aged DG neurons, when compared to young controls (Fig. 1E).

We also found that during the initial exposure to the treadmill, there is a significant reduction in spatial information and tuning in aged DG neurons, as compared to their young counterparts (Fig. 2B-C). By using untrained mice for our experiments we were able to capture the very first neuronal representations of a novel environment. We found that during the course of four consecutive imaging days, spatial information and tuning in the aged mice converged with those of young mice, which leads us to conclude that aged mice require additional exposure to a novel

191 environment in order to form adequate neural representations of space. It can therefore be said
192 that the spatial encoding defects seen in aged mice are specific to novel environments. This is in
193 agreement with previous reports that found that spatial representations in CA1 were disrupted
194 when novel environmental cues were introduced during a navigation task (*33*, *36*). Interestingly,
195 both young and aged groups saw an increase in spatial information through the four days of
196 imaging, whereas spatial tuning increased in aged mice but was not significantly different in young
197 mice. We did not find a convergence in single-cell calcium activity levels between aged and young
198 groups, meaning that the hyperexcitability is no impediment to aged mice eventually forming
199 accurate spatial representations. There are several interesting parallels between our findings and
200 human data showing that aged individuals are better able to navigate familiar environments than
201 novel ones (*8*) leading them to avoid taking novel routes in favor of navigating familiar routes.

202

203 To verify that aged mice have impairments in spatial memory, we used an object placement test
204 that is not physically tasking and does not involve an aversive component. Our behavior data
205 confirmed that aged mice are more likely to fail at an object placement task than their younger
206 counterparts. This goes along with studies analyzing similar spatial memory tasks that have found
207 deficits in aged animals (*37*, *38*). Our results also highlight the well-described heterogeneity
208 present during normal aging, as about half of aged mice were still able to pass the test (*39*, *40*).

209 In order to better compare our data to previous studies of DG activity using IEG labelling, we
210 determined the percentage of active cells in our imaging fields but found no difference in the
211 number of active cells between young and aged animals. This may be due to differences in the
212 activation of ensembles based on the experimental designs. However, there are also some
213 caveats to our experimental data that must be kept in mind: we calculate the total number of cells
214 from mean projections of whole calcium imaging movies, which can introduce several biases, for
215 example active cells will tend to be brighter and therefore more visible. We found a correlation

between the percentage of active cells and the total number of cells in the imaging field (Fig. S2B), as fields of view with fewer detected cells had much higher variance of the fraction of active cells. Fields with more total cells generally had more cells that were dimmer and less active but were still counted in the total. In contrast, in fields with few cells due to areas of lower viral expression or obscured by blood vessels, there are likely more cells present than can be quantified in the mean projection image. These differences in imaging fields across animals makes it difficult to calculate exact percentages, limiting the usefulness of this approach.

Previous studies have found that increased hippocampal excitability contributes to aging-related cognitive impairments. Our experimental design did not allow us to determine whether hyperexcitability contributes to the deficits in spatial information seen in the novel environment during the first day of imaging, but our results suggest that instead dysfunction in the plasticity mechanisms that underlie spatial selectivity may be to blame. Spatial selectivity can develop very fast in CA1 hippocampal neurons through a mechanism termed behavioral timescale synaptic plasticity (*41*) that is mostly active in novel contexts, leading to the development and stabilization of spatial tuning within the first few minutes of exposure to a new environment (*42*). While less is known about the dynamics of spatial selectivity in the DG, spatially tuned cells also seem to emerge and stabilize within the first few minutes of exposure to a novel environment, with further refinement as the animals are re-exposed to the same environment over the following days (*43*). This is in line with our finding that spatial information increases over several days both in young and aged animals. Previous literature has shown that aging is associated with plasticity deficits in the hippocampus (*17*, *44*, *45*), namely in long term potentiation and depression. Given that these plasticity mechanisms are likely most active as mice map out new environments (*42*) we speculate that this may explain the protracted development of spatial selectivity that we see in aged mice. Expression of some IEGs, such as *Arc* and *Egr1,* which are thought to be regulators of neuronal

plasticity, is reduced in the DG of aged animals. Deficits in the expression of these genes following neuronal activity could be at the origin of plasticity defects in aged animals. The increased excitability of aged DG neurons could therefore also be seen as a compensation mechanism for both the reduced synaptic input from the entorhinal cortex, and the reduced expression of IEGs. Another factor potentially contributing to the delayed formation of spatial representations in the aged DG is a reduction of adult neurogenesis. Adult-born neurons are known to enhance DG neuronal plasticity (*46*, *47*) but their numbers fall to almost zero in aged animals (*48*).

Aging-associated memory deficits have also been associated with changes in the stability of spatial representations as some previous studies have found that the aged hippocampal spatial code undergoes larger changes over different sessions than in young mice (*32*), whereas others have found that spatial representations are more rigid (*24*, *33*). We did not see changes in the reactivation of cells from one session to another between groups (Fig. 4D). This is in contrast to data showing that more distinct dentate populations express the IEG *Arc* when aged mice are re-exposed to the same environment (*49*), which could be due to age-related changes in DNA methylation rather than changes in neuronal excitability (*50*). In order to further investigate the properties of cells in the aged DG over time, we matched cells that were active in our imaging fields across days. We did not find major differences in the reactivated cells in any measures between young and aged groups, suggesting that ensembles of neurons follow the same basic mechanisms in the aged DG. When comparing reactivated neurons to the remainder of the population, we found that reactivated cells had significantly higher spatial information (Fig. 4 O,P), indicating that this may be a marker of whether a neuron will contribute to spatial representations over time.

To summarize, our data shows that new DG spatial representations are initially impaired and take longer to form in aged mice. These data expand our knowledge of the network activity and spatial representations in the aged hippocampus and suggest that aging-associated hippocampal

hyperactivity is not an impediment to the formation of rich spatial representations. The protracted refinement of spatial representations suggests that the plasticity mechanisms responsible for the development of spatial selectivity are impaired in aged animals and are likely to be a relevant therapeutic target for ameliorating the memory deficits associated with aging.

**Acknowledgements**

We thank Dr. Carolyn Pytte for the generous gift of aged mice from her laboratory at Queens College. We thank Dr. Maria Gulinello, the director of the behavior core facilities at Einstein, for her training and technical advice on behavior experiments. We thank Dr. Alberto Cruz-Martín for helpful feedback and discussions.

**Funding:**

The Einstein Training Program in Stem Cell Research from the Empire State Stem Cell Fund through New York State Department of Health Contract C34874GG (KDM, MAF), Whitehall Foundation Research Grant 2019-05-71 (JTG), National Institutes of Health NINDS R01NS125252-01A1 (JTG)

**Author contributions:**

Conceptualization: KDM, JTG; Methodology: KDM, MAF, JTJ, JTG; Investigation: KDM, SSM, JTG; Visualization: KDM, JTG; Supervision: JTG; Writing—original draft: KDM, JTG; Writing—review & editing: KDM, JTG

**Competing interests:**

The authors have no competing interests.

**Data availability:**

The analysis code used in this study is openly available at https://github.com/GoncalvesLab/McDermott-et-al-aging. All imaging data, consisting of calcium traces for every active cell and the position of the mouse on the treadmill, will be made openly available on a repository site before final publication. Due to their large size, raw calcium imaging movies will be made available upon request.

## Methods

**Animals** – Aged mice were 21-26 months old C57Bl6J females originally from Jackson Labs and kindly gifted by Dr. Carolyn Pytte of Queens College. Young mice were 3-4 months old C57Bl6J females purchased from Jackson Labs. All mice were housed in standard conditions with a 14/10 hour light/dark cycle. Mice were provided food and water ad libitum. All procedures were done during the light part of the cycle and in accordance with the Einstein Institutional Animal Care and Use Committee (Protocol #00001197).

**Viral injections** – Mice were anesthetized (induction: 5%, maintenance 0.5% isoflurane in $O_2$ vol/vol). Following anesthetization, mice were attached to a stereotactic apparatus and the right hemisphere of the dentate gyrus (DG) was injected with 1µl of a DJ-serotype AAV vector encoding the red-shifted calcium indicator jRGECO1a (*25*) under the CamKII promoter at $10^{12}$ GC/ml titer. Viral injections were done with a pulled glass pipette using a Nanoject III microinjector (Drummond) at previously described coordinates (*51*).

**Window implantation** – Following viral injection, dexamethasone (1 mg/kg) was administered via subcutaneous injection to minimize brain swelling. Optibond (Kerr Dental) adhesive was applied to the skull and cured to help secure the implant once attached. A 3mm diameter

craniotomy was made over the right dorsal DG and the overlaying tissue was removed by aspiration down to the hippocampal fissure where a custom-built cylindrical titanium implant with a glass coverslip on the bottom was inserted over the dorsal surface of the DG (*27*). The implant and a titanium bar for head-fixation were attached to the skull with dental cement. All mice were given carprofen (5 mg/kg, subcutaneous) as a post-surgery analgesic.

**Two-photon Imaging** – *In vivo* calcium imaging movies were acquired with a custom two-photon laser scanning microscope (based on Thorlabs Bergamo) using a femtosecond-pulsed laser (Coherent Fidelity 2, 1070 nm) and a 16x water immersion objective (0.8 NA, Nikon). Imaging sessions were started 3-4 weeks after surgery to allow for recovery and for optimal viral expression. During imaging sessions, mice were head-fixed to the microscope with a titanium headbar and the microscope stage was adjusted so that the hippocampal window was perpendicular to the axis of the objective for optimal imaging conditions. Mice were awake and walking on a manually rotated treadmill belt throughout imaging. The treadmill contained four zones with different textures as previously described (*52*). Ten-minute videos were acquired at 15.253 fps with a 343.6 x 343.6 µm field of view. Treadmill data was acquired using National Instruments analog-to-digital converter and synchronized with the imaging data using Thorsync software. To track the same field of view, the initial location was noted on the first imaging day using a coordinate system and by taking an image of the field. During following sessions, the coordinates and initial field image were used to match as close as possible to the same field.

**Data Analysis**– The open-source Suite2p software (version 10.0) was used to register and motion correct videos, for cell detection and spike deconvolution (*53–55*). Regions of interest corresponding to active neurons were identified by Suite2p and further manually curated in order to identify all active cells in the field of view. The ROIMatchPub (*56*) was used to identify and match cells in the same field of view across imaging sessions. Matched ROIs were manually confirmed after automated detection.

Single-cell calcium activity was determined as previously described (*29*). Briefly, ΔF/F data was filtered with a zero phase shift, third order Butterworth lowpass filter. This filtered ΔF/F was thresholded to 2 standard deviations($\sigma$) above a rolling-mean baseline. Single cell activity was determined as the cumulative sum of the thresholded trace for each cell. This was then normalized to the total distance traveled by each mouse.

Tuning indices were using deconvolved calcium traces, which were thresholded to 2$\sigma$ above the baseline. Any point not significantly above that noise threshold was set to zero. Videos were cut to only include periods of movement >1s in duration. The treadmill band was segmented into 100 position bins, and transients were mapped to these bins according to the location of the mice on the treadmill in order to generate a tuning vector for each cell (*26*).The mean of the thresholded activity at each location was calculated for every neuron and normalized to the time the mouse spent at that position. The tuning index was defined as the modulus of this normalized tuning vector.

Single-cell Fisher Information (FI) was calculated as previously described (*29*, *57*). A bias-corrected signal to noise ratio was computed using the unfiltered ΔF/F fluorescence data for each individual cell, where the signal is the square of the difference of the mean activity at two locations on the treadmill, and the noise is the average variance of the activity at each location. Position data was segmented into 20 bins.

**Behavior** – Object Placement –A square-shaped arena 42x42x30 (LxWxH) was set up with visual cues along the walls and with two novel and identical objects on the floor. Mice were individually placed in the arena for a 4 minute training trial. Following a 45 minute retention period, one object was displaced to another location in the arena and the mice were placed again for a 4 minute test trial. Exploration of the objects was quantified by an experimenter and confirmed with computer tracking.

**Statistics** – Nested bootstrap analysis – When pooling cell data from different mice into a single experimental group, significance testing was done using a muti-level bootstrapped approach as previously described (*29*). To assess whether differences between two experimental groups are significant, a null surrogate distribution was constructed for each mouse in each group by resampling with substitution from the pool of all imaged cells. The difference between the null distributions generated for each group was calculated and the previous steps repeated to generate 100,000 bootstrap estimates of the difference between two groups' null distributions. The empirically observed value of the difference between conditions was then compared to the null distribution values with a statistical significance level ($\alpha$) set at 0.05. If the empirical group differences fall outside of the 95$^{th}$ percentile of the 100,000 bootstrap estimates of the difference between the null distributions, then it is considered to be a statistically significant difference. The p-value is the proportion of bootstrap different estimates that are larger than the empirical difference between groups (or smaller, if the difference is negative). Whenever comparing more than two groups, Bonferroni's correction for multiple comparisons was applied.

- Mixed-effects models with Geisser-Greenhouse correction for matched values were used to compare mean values by mouse across imaging days. Sidak's multiple comparisons test was used to compare groups on each imaging day.

- Nonparametric one sample Wilcoxon tests were used to determine if group medians were significantly above chance levels in behavior experiments.

- A two-sided Chi squared test with 95% confidence interval was used to compare pass/fail rates in behavior experiments.

## References


1. W. Jagust, Vulnerable neural systems and the borderland of brain aging and neurodegeneration. *Neuron*. **77**, 219–234 (2013).
2. C. A. Barnes, Aging and the physiology of spatial memory. *Neurobiol Aging*. **9**, 563–568 (1988).
3. C. Techentin, D. Voyer, S. D. Voyer, Spatial abilities and aging: a meta-analysis. *Exp Aging Res*. **40**, 395–425 (2014).
4. K. Konishi, S. Mckenzie, N. Etchamendy, S. Roy, V. D. Bohbot, Hippocampus-dependent spatial learning is associated with higher global cognition among healthy older adults. *Neuropsychologia*. **106**, 310–321 (2017).
5. N. Diersch, J. P. Valdes-Herrera, C. Tempelmann, T. Wolbers, Increased Hippocampal Excitability and Altered Learning Dynamics Mediate Cognitive Mapping Deficits in Human Aging. *J. Neurosci.* **41**, 3204–3221 (2021).
6. S. D. Moffat, Aging and Spatial Navigation: What Do We Know and Where Do We Go? *Neuropsychol Rev*. **19**, 478–489 (2009).
7. K. C. Kirasic, Spatial cognition and behavior in young and elderly adults: implications for learning new environments. *Psychol Aging*. **6**, 10–18 (1991).
8. V. Muffato, M. Della Giustina, C. Meneghetti, R. De Beni, Age-related differences in pointing accuracy in familiar and unfamiliar environments. *Cogn Process*. **16 Suppl 1**, 313–317 (2015).
9. N. A. Merriman, J. Ondřej, E. Roudaia, C. O'Sullivan, F. N. Newell, Familiar environments enhance object and spatial memory in both younger and older adults. *Exp Brain Res*. **234**, 1555–1574 (2016).
10. W. B. Scoville, B. Milner, Loss of recent memory after bilateral hippocampal lesions. *J. Neurol. Neurosurg. Psychiatr.* **20**, 11–21 (1957).
11. R. G. M. Morris, P. Garrud, J. N. P. Rawlins, J. O'Keefe, Place navigation impaired in rats with hippocampal lesions. *Nature*. **297**, 681–683 (1982).
12. S. A. Small, M. K. Chawla, M. Buonocore, P. R. Rapp, C. A. Barnes, Imaging correlates of brain function in monkeys and rats isolates a hippocampal subregion differentially vulnerable to aging. *Proc Natl Acad Sci U S A*. **101**, 7181–7186 (2004).
13. G. W. Small, What we need to know about age related memory loss. *BMJ*. **324**, 1502–1505 (2002).
14. M. A. Yassa, A. T. Mattfeld, S. M. Stark, C. E. L. Stark, Age-related memory deficits linked to circuit-specific disruptions in the hippocampus. *PNAS*. **108**, 8873–8878 (2011).
15. H. Moreno, W. E. Wu, T. Lee, A. Brickman, R. Mayeux, T. R. Brown, S. A. Small, Imaging the Abeta-related neurotoxicity of Alzheimer disease. *Arch Neurol*. **64**, 1467–1477 (2007).
16. S. N. Burke, C. A. Barnes, Senescent synapses and hippocampal circuit dynamics. *Trends in Neurosciences*. **33**, 153–161 (2010).
17. D. J. Froc, B. Eadie, A. M. Li, K. Wodtke, M. Tse, B. R. Christie, Reduced Synaptic Plasticity in the Lateral Perforant Path Input to the Dentate Gyrus of Aged C57BL/6 Mice. *Journal of Neurophysiology*. **90**, 32–38 (2003).
18. D. GoodSmith, X. Chen, C. Wang, S. H. Kim, H. Song, A. Burgalossi, K. M. Christian, J. J. Knierim, Spatial Representations of Granule Cells and Mossy Cells of the Dentate Gyrus. *Neuron*. **93**, 677-690.e5 (2017).
19. I. A. Wilson, S. Ikonen, M. Gallagher, H. Eichenbaum, H. Tanila, Age-associated alterations of hippocampal place cells are subregion specific. *J Neurosci*. **25**, 6877–6886 (2005).
20. Y. H. El-Hayek, C. Wu, H. Ye, J. Wang, P. L. Carlen, L. Zhang, Hippocampal excitability is increased in aged mice. *Experimental Neurology*. **247**, 710–719 (2013).
21. D. Simkin, S. Hattori, N. Ybarra, T. F. Musial, E. W. Buss, H. Richter, M. M. Oh, D. A. Nicholson, J. F. Disterhoft, Aging-Related Hyperexcitability in CA3 Pyramidal Neurons Is

Mediated by Enhanced A-Type K+ Channel Function and Expression. *J Neurosci*. **35**, 13206–13218 (2015).

22. H. Lee, Z. Wang, S. L. Zeger, M. Gallagher, J. J. Knierim, Heterogeneity of Age-Related Neural Hyperactivity along the CA3 Transverse Axis. *J. Neurosci.* **41**, 663–673 (2021).
23. C. A. Barnes, B. L. McNaughton, J. O'Keefe, Loss of place specificity in hippocampal complex spike cells of senescent rat. *Neurobiology of Aging*. **4**, 113–119 (1983).
24. H. Tanila, M. Shapiro, M. Gallagher, H. Eichenbaum, Brain Aging: Changes in the Nature of Information Coding by the Hippocampus. *J. Neurosci.* **17**, 5155–5166 (1997).
25. H. Dana, B. Mohar, Y. Sun, S. Narayan, A. Gordus, J. P. Hasseman, G. Tsegaye, G. T. Holt, A. Hu, D. Walpita, R. Patel, J. J. Macklin, C. I. Bargmann, M. B. Ahrens, E. R. Schreiter, V. Jayaraman, L. L. Looger, K. Svoboda, D. S. Kim, Sensitive red protein calcium indicators for imaging neural activity. *eLife*. **5**, e12727 (2016).
26. N. B. Danielson, P. Kaifosh, J. D. Zaremba, M. Lovett-Barron, J. Tsai, C. A. Denny, E. M. Balough, A. R. Goldberg, L. J. Drew, R. Hen, A. Losonczy, M. A. Kheirbek, Distinct Contribution of Adult-Born Hippocampal Granule Cells to Context Encoding. *Neuron*. **90**, 101–112 (2016).
27. J. T. Gonçalves, C. W. Bloyd, M. Shtrahman, S. T. Johnston, S. T. Schafer, S. L. Parylak, T. Tran, T. Chang, F. H. Gage, In vivo imaging of dendritic pruning in dentate granule cells. *Nat Neurosci*. **19**, 788–791 (2016).
28. M. A. Yassa, S. M. Stark, A. Bakker, M. S. Albert, M. Gallagher, C. E. L. Stark, High-resolution structural and functional MRI of hippocampal CA3 and dentate gyrus in patients with amnestic Mild Cognitive Impairment. *NeuroImage*. **51**, 1242–1252 (2010).
29. M. A. Frechou, S. S. Martin, K. D. McDermott, Ş. Gökhan, W. A. Tomé, R. Coen-Cagli, J. T. Gonçalves, Adult neurogenesis improves spatial information encoding in the mouse hippocampus (2022), p. 2022.11.30.518622, , doi:10.1101/2022.11.30.518622.
30. J. O'Keefe, J. Dostrovsky, The hippocampus as a spatial map. Preliminary evidence from unit activity in the freely-moving rat. *Brain Research*. **34**, 171–175 (1971).
31. J. Haettig, Y. Sun, M. A. Wood, X. Xu, Cell-type specific inactivation of hippocampal CA1 disrupts location-dependent object recognition in the mouse. *Learn Mem*. **20**, 139–146 (2013).
32. C. A. Barnes, M. S. Suster, J. Shen, B. L. McNaughton, Multistability of cognitive maps in the hippocampus of old rats. *Nature*. **388**, 272–275 (1997).
33. I. A. Wilson, S. Ikonen, I. Gureviciene, R. W. McMahan, M. Gallagher, H. Eichenbaum, H. Tanila, Cognitive aging and the hippocampus: how old rats represent new environments. *J Neurosci*. **24**, 3870–3878 (2004).
34. J. Jiménez-Balado, T. S. Eich, GABAergic dysfunction, neural network hyperactivity and memory impairments in human aging and Alzheimer's disease. *Seminars in Cell & Developmental Biology*. **116**, 146–159 (2021).
35. R. P. Haberman, A. Branch, M. Gallagher, Targeting Neural Hyperactivity as a Treatment to Stem Progression of Late-Onset Alzheimer's Disease. *Neurotherapeutics*. **14**, 662–676 (2017).
36. H. Tanila, P. Sipilä, M. Shapiro, H. Eichenbaum, Brain Aging: Impaired Coding of Novel Environmental Cues. *J Neurosci*. **17**, 5167–5174 (1997).
37. M. E. Wimmer, P. J. Hernandez, J. Blackwell, T. Abel, Aging impairs hippocampus-dependent long-term memory for object location in mice. *Neurobiol Aging*. **33**, 2220–2224 (2012).
38. S. Yanai, T. Tago, J. Toyohara, T. Arasaki, S. Endo, Reversal of spatial memory impairment by phosphodiesterase 3 inhibitor cilostazol is associated with reduced neuroinflammation and increased cerebral glucose uptake in aged male mice. *Frontiers in Pharmacology*. **13** (2022) (available at https://www.frontiersin.org/articles/10.3389/fphar.2022.1031637).

39. A. M. Hamieh, E. Camperos, A. M. Hernier, V. Castagné, C57BL/6 mice as a preclinical model to study age-related cognitive deficits: Executive functions impairment and inter-individual differences. *Brain Res*. **1751**, 147173 (2021).
40. A. J. Gower, Y. Lamberty, The aged mouse as a model of cognitive decline with special emphasis on studies in NMRI mice. *Behav Brain Res*. **57**, 163–173 (1993).
41. K. C. Bittner, A. D. Milstein, C. Grienberger, S. Romani, J. C. Magee, Behavioral time scale synaptic plasticity underlies CA1 place fields. *Science*. **357**, 1033–1036 (2017).
42. J. B. Priestley, J. C. Bowler, S. V. Rolotti, S. Fusi, A. Losonczy, Signatures of rapid plasticity in hippocampal CA1 representations during novel experiences. *Neuron*. **110**, 1978-1992.e6 (2022).
43. S. Kim, D. Jung, S. Royer, Place cell maps slowly develop via competitive learning and conjunctive coding in the dentate gyrus. *Nat Commun*. **11**, 4550 (2020).
44. S. N. Burke, C. A. Barnes, Neural plasticity in the ageing brain. *Nature Reviews Neuroscience*. **7**, 30–40 (2006).
45. C. M. Norris, D. L. Korol, T. C. Foster, Increased susceptibility to induction of long-term depression and long-term potentiation reversal during aging. *J Neurosci*. **16**, 5382–5392 (1996).
46. J. S. Snyder, N. Kee, J. M. Wojtowicz, Effects of Adult Neurogenesis on Synaptic Plasticity in the Rat Dentate Gyrus. *Journal of Neurophysiology*. **85**, 2423–2431 (2001).
47. F. Massa, M. Koehl, T. Wiesner, N. Grosjean, J.-M. Revest, P.-V. Piazza, D. N. Abrous, S. H. R. Oliet, Conditional reduction of adult neurogenesis impairs bidirectional hippocampal synaptic plasticity. *Proceedings of the National Academy of Sciences*. **108**, 6644–6649 (2011).
48. H. G. Kuhn, H. Dickinson-Anson, F. H. Gage, Neurogenesis in the dentate gyrus of the adult rat: age-related decrease of neuronal progenitor proliferation. *J. Neurosci.* **16**, 2027–2033 (1996).
49. D. F. Marrone, E. Satvat, M. J. Shaner, P. F. Worley, C. A. Barnes, Attenuated long-term Arc expression in the aged fascia dentata. *Neurobiology of Aging*. **33**, 979–990 (2012).
50. M. R. Penner, T. L. Roth, M. K. Chawla, L. T. Hoang, E. D. Roth, F. D. Lubin, J. D. Sweatt, P. F. Worley, C. A. Barnes, Age-related changes in Arc transcription and DNA methylation within the hippocampus. *Neurobiology of Aging*. **32**, 2198–2210 (2011).
51. C. Zhao, E. M. Teng, R. G. Summers, G. Ming, F. H. Gage, Distinct Morphological Stages of Dentate Granule Neuron Maturation in the Adult Mouse Hippocampus. *J. Neurosci.* **26**, 3–11 (2006).
52. J. T. Jordan, K. D. McDermott, M. A. Frechou, M. Shtrahman, J. T. Gonçalves, Treadmill-based task for assessing spatial memory in head-fixed mice. *STAR Protoc*. **2**, 100770 (2021).
53. M. Pachitariu, C. Stringer, M. Dipoppa, S. Schröder, L. F. Rossi, H. Dalgleish, M. Carandini, K. D. Harris, Suite2p: beyond 10,000 neurons with standard two-photon microscopy. *bioRxiv*, 061507 (2017).
54. M. Pachitariu, C. Stringer, K. D. Harris, Robustness of Spike Deconvolution for Neuronal Calcium Imaging. *J. Neurosci.* **38**, 7976–7985 (2018).
55. J. Friedrich, P. Zhou, L. Paninski, Fast online deconvolution of calcium imaging data. *PLoS Comput Biol*. **13**, e1005423 (2017).
56. ransona, ransona/ROIMatchPub (2023), (available at https://github.com/ransona/ROIMatchPub).
57. I. Kanitscheider, R. Coen-Cagli, A. Kohn, A. Pouget, Measuring Fisher information accurately in correlated neural populations. *PLoS Comput Biol*. **11**, e1004218 (2015).

535 **Figure legends:**

536 **Figure 1. DG is hyperactive in aged animals.** A) Experimental timeline, including AAV injection,
537 window implantation, and two-photon imaging. B) Diagram of chronic window implant over the
538 right hemisphere of the DG. C) Diagram of imaging setup, with side view (left) and top view (right)
539 of mouse head-fixed to treadmill with multiple tactile zones. D) Example field of view with regions
540 of interest of active cells shaded in color. Scale bar = 100 μm. E) Mean single cell calcium activity.
541 F) Example calcium traces (black) and corresponding treadmill positions (red) from young mice.
542 G) Example calcium traces (black) and corresponding treadmill positions (red) from aged mice.
543 a.u.= arbitrary units. Young N=8 mice, n=910 cells; Aged N=8 mice, n=699 cells. **p<0.01

544 **Figure 2. DG representations of space are impaired in aged mice.** A) Tuning vector polar
545 plots representing a highly spatially tuned cell and B) a cell with low spatial tuning. C) Spatial
546 tuning index. D) Raster plots of tuning vectors of young mouse neurons in 10$^{th}$ percentile Fisher
547 Information, sorted by the position of activity maximum for whole recording (All Laps). Raster plots
548 of partial recording (Even Laps and Odd Laps) keep same sorting used for whole recording. E)
549 Same raster plots for aged mice. C) Single cell Fisher information. Statistics done with nested
550 bootstrap analysis. Bars represent mean +/- SEM. a.u.= arbitrary units. Young N=8 mice, n=910
551 cells; Aged N=8 mice, n=699 cells. *p<0.05, **p<0.01, ***p<0.001, ****p<0.0001. See also
552 supplemental figures 1 and 2.

553 **Figure 3. Deficits in aged spatial representations are rescued with increased familiarity.** A)
554 Mean single cell calcium activity across days. B) Single cell activity in young mice on day 1 versus
555 day 4. C) Single cell activity in aged mice on day 1 versus day 4. D) Mean tuning index across
556 days. E) Tuning index in young mice on day 1 versus day 4. F) Tuning index in aged mice on day
557 1 versus day 4. G) Mean single cell Fisher Information across days. H) Fisher Information in young
558 mice on day 1 versus day 4. I) Fisher Information in aged mice on day 1 versus day 4. Statistics
559 done with a nested bootstrap analysis. Bars represent mean +/- SEM. a.u.= arbitrary units. Young:

day 1 N=8 , n=910; day 2 N=7, n=694; day 3 N=7, n=623; day 4 N=7, n=610; Aged: day 1 N=8, n=699; day 2 N=8, n=619; day 3 N=5, n=147; day 4 N=6, n=331. ns=not significant, *p<0.05, **p<0.01, ***p<0.001, ****p<0.0001.

**Figure 4. Reactivated cells do not have a distinct profile in aged animals.** A) Example field of view used to match cells across days. Neurons that were active during recording session are shaded in color. B) Matched regions of interest from the field of view in panel A, red and white contours represent cells active on day 1 and 4. C) Examples of matched cells on day 1 and 4. D) Reactivation rate of neurons that were active on day 1. Percentages are based on imaging day versus day 1, regardless of whether the cell was active on other days. E-F) Matched single cell calcium activity in reactivated cells in young (E) and aged (F) mice. G-H) Matched tuning index in reactivated cells in young (G) and aged (H) mice. I-J) Matched single cell Fisher Information in reactivated cells in young (I) and aged (J) mice. K-L) Single cell activity of reactivated and non-reactivated cells on day 1 (K) and day 4 (L). M-N) Tuning of reactivated and non-reactivated cells on day 1 (M) and day 4 (N). O-P) Single cell Fisher Information of reactivated and non-reactivated cells on day 1 (O) and day 4 (P). Statistics done with nested bootstrap analysis. Bars represent mean +/- SEM. a.u.= arbitrary units. Young: N=6; day 1 n=617; day 1 react. n=140; day 4 n=396; day 4 react. n=140; Aged: N=5; day 1 n=375; day 1 react. n=80; day 4 n=196; day 4 react. n=80. ns=not significant, *p<0.05, **p<0.01, ***p<0.001, ****p<0.0001.

**Figure S1. Velocity and laps run during two photon imaging.** A) Average velocity of mice walking along treadmill belt. B) Average number of laps run per imaging session. Statistics done with mixed effects model. Each point represent an individual animal. Bars represent mean +/- SEM. ns=not significant.

583 **Figure S2. No difference in active cell number between young and aged mice.** A) Percentage
584 of cells active out of the total cells in a field of view, by mouse. Statistics done with mixed effects
585 model. Bars represent mean +/- SEM. ns=not significant. B) Correlation of percentage active cells
586 versus the total number of cells pooled from all imaging days. Data are shown by mouse.

587 **Figure S3. Aged mice show a deficit in a spatial memory task.** A) Schematic of the object
588 placement behavioral paradigm. B) Novelty preference of mice measured by percentage of total
589 time spent exploring the novel object. C) Discrimination index calculated by dividing the difference
590 in exploration time between objects by the total exploration time [(novel-familiar)/(novel+familiar)].
591 D) Pass/fail rate of task, where passing was defined as at least a 53% preference for novel object.
592 E) Exploration time dedicated to each object. Statistics in B and C were done with one sample
593 Wilcoxon tests, D with Chi squared test and E with mixed effects model. Bars represent mean +/-
594 SEM. Young N=13, Aged N=13. ns=not significant, *p<0.05, **p<0.01.

595

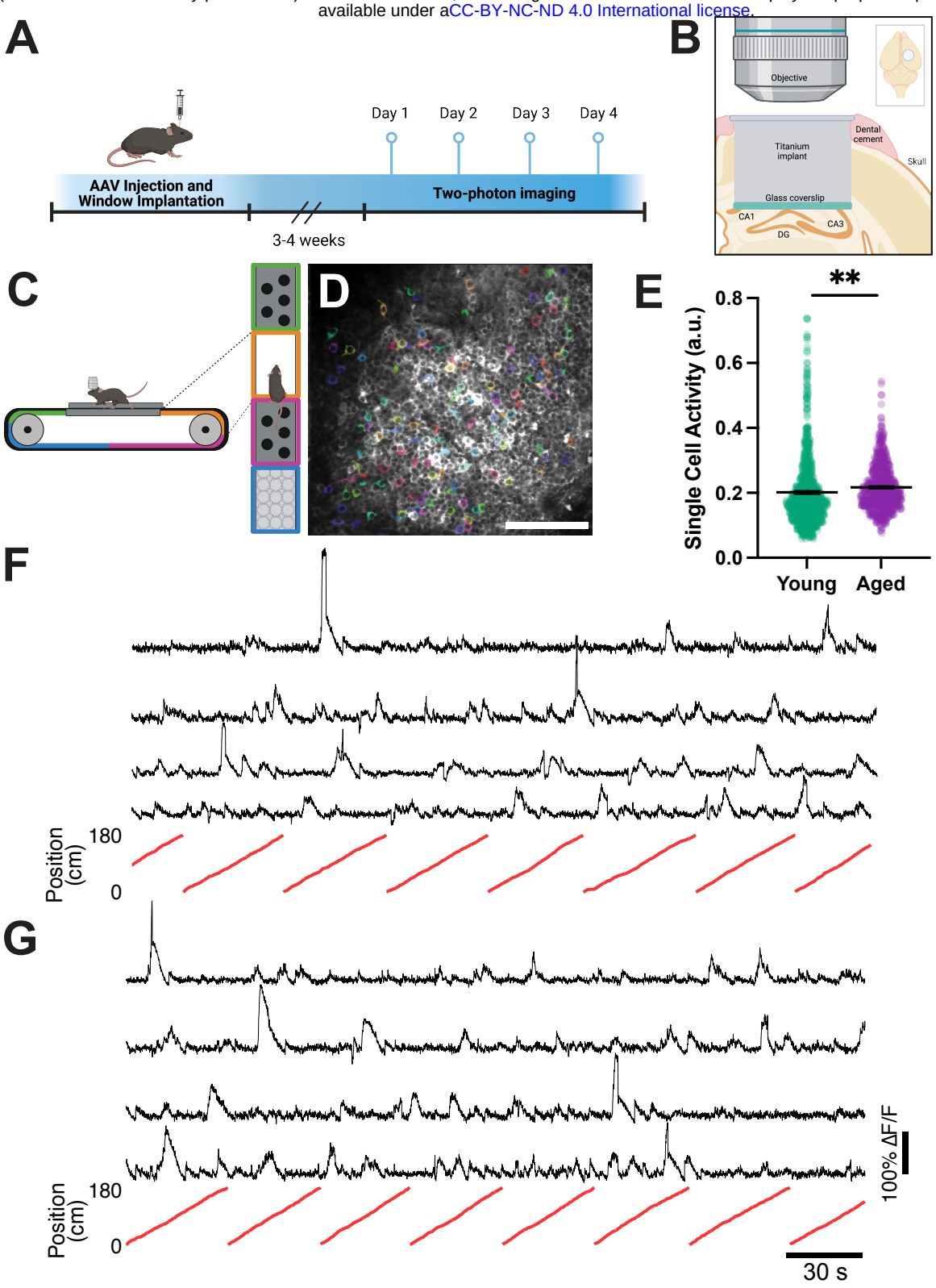


**Figure 1**

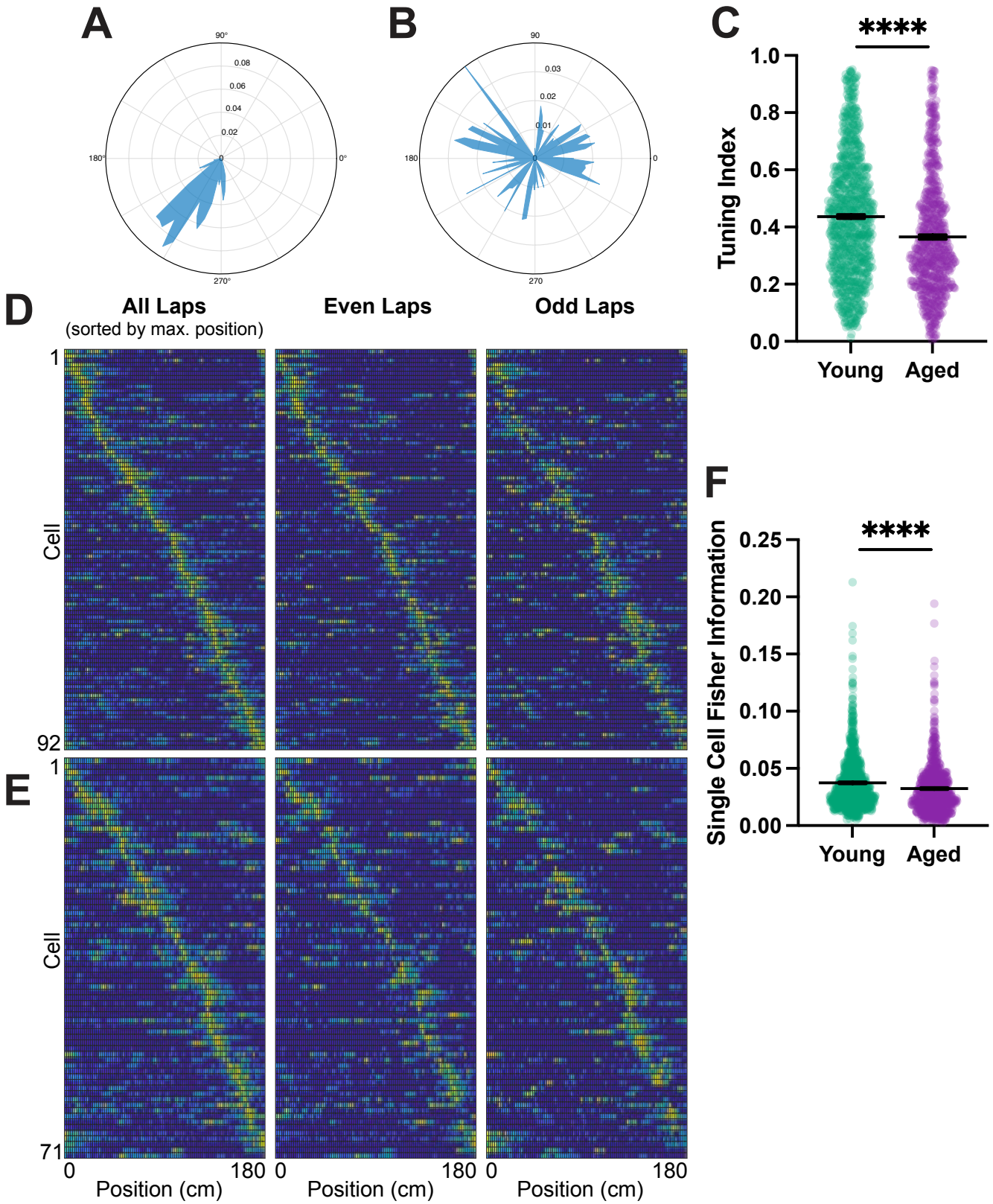
A
B
C
D
E
F
All Laps
(sorted by max. position)
Even Laps
Odd Laps
Cell
Position (cm)
Tuning Index
Young
Aged
****
Single Cell Fisher Information

Figure 2

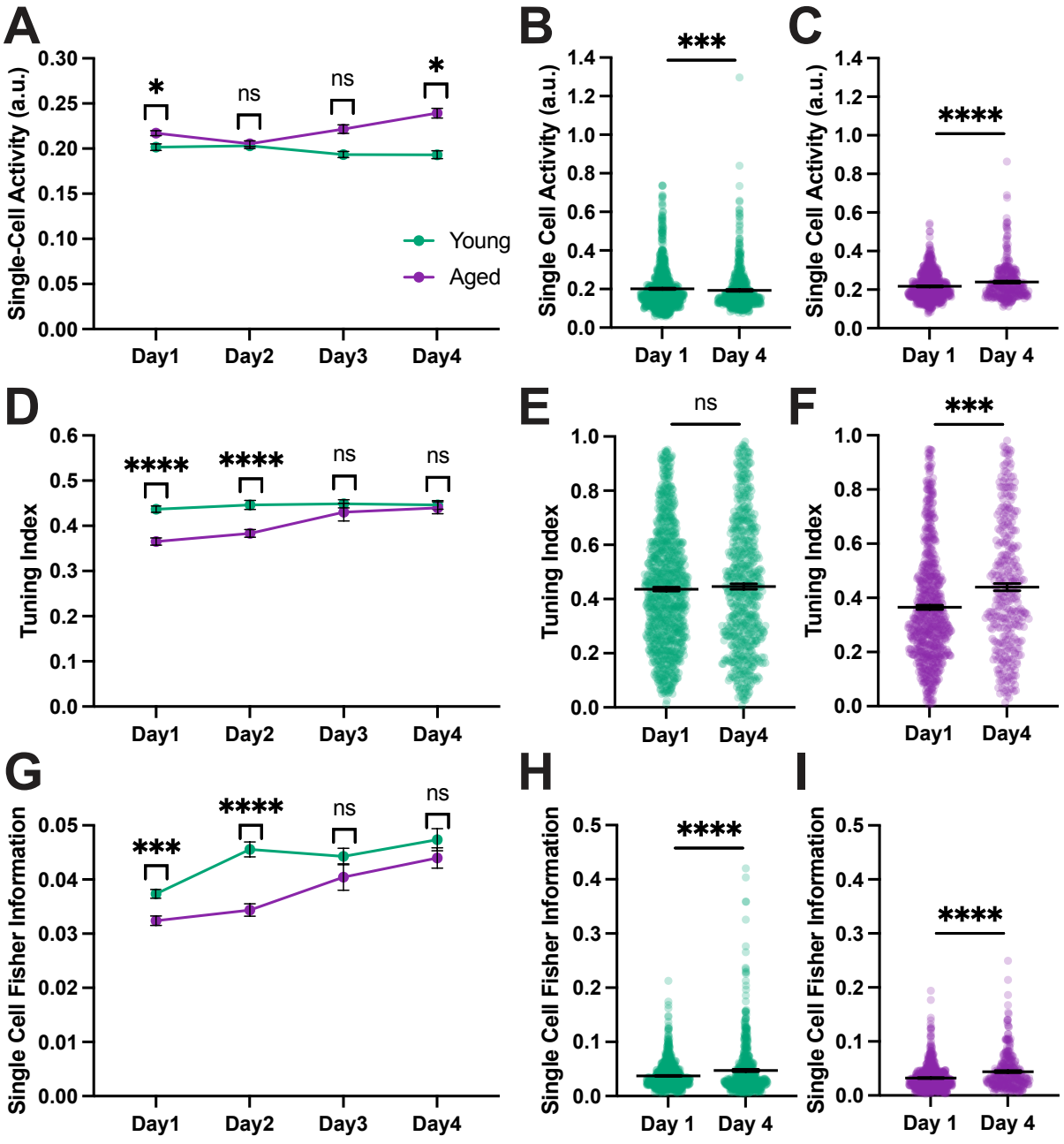


# Figure 3

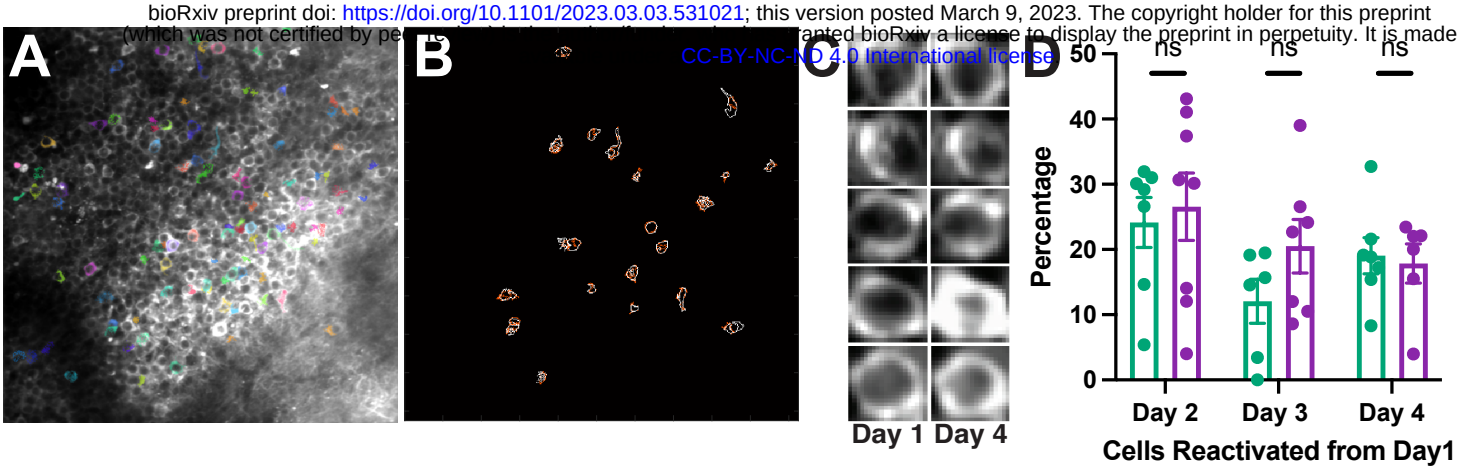


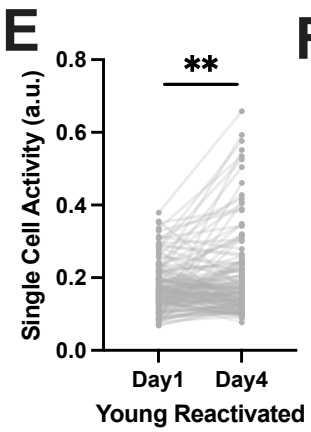


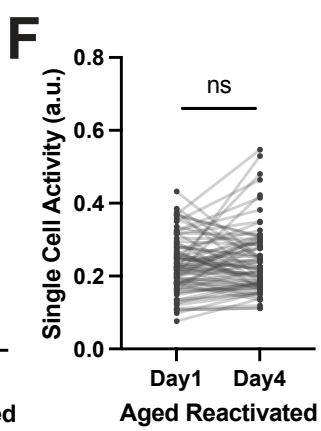


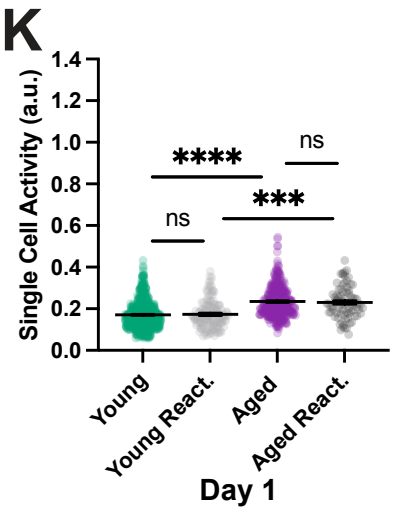


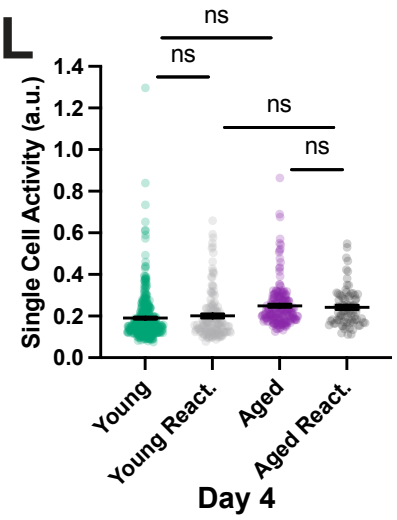


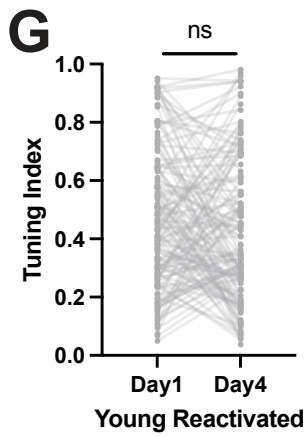


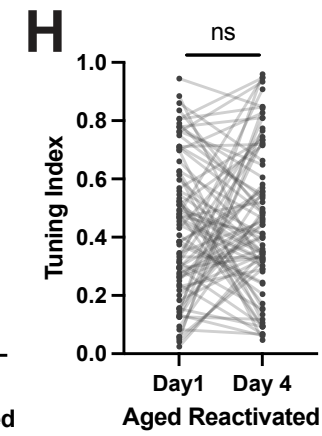


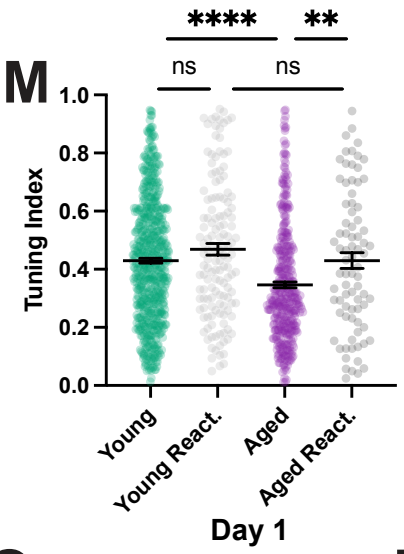


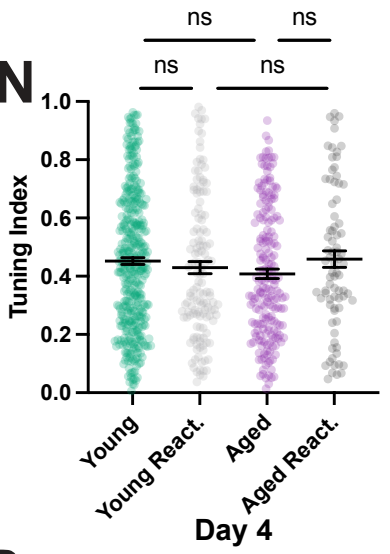


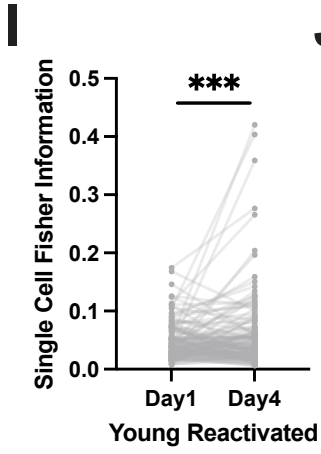


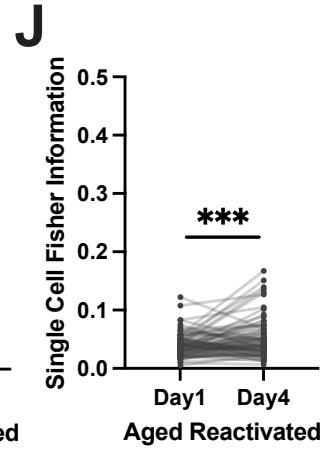


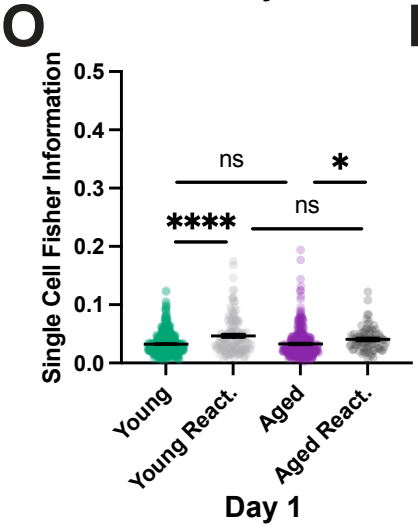


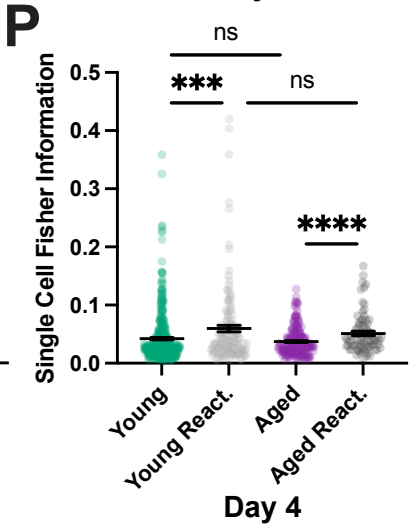


# Figure 4

STAR Protocols

CellPress
OPEN ACCESS

Protocol

# Treadmill-based task for assessing spatial memory in head-fixed mice

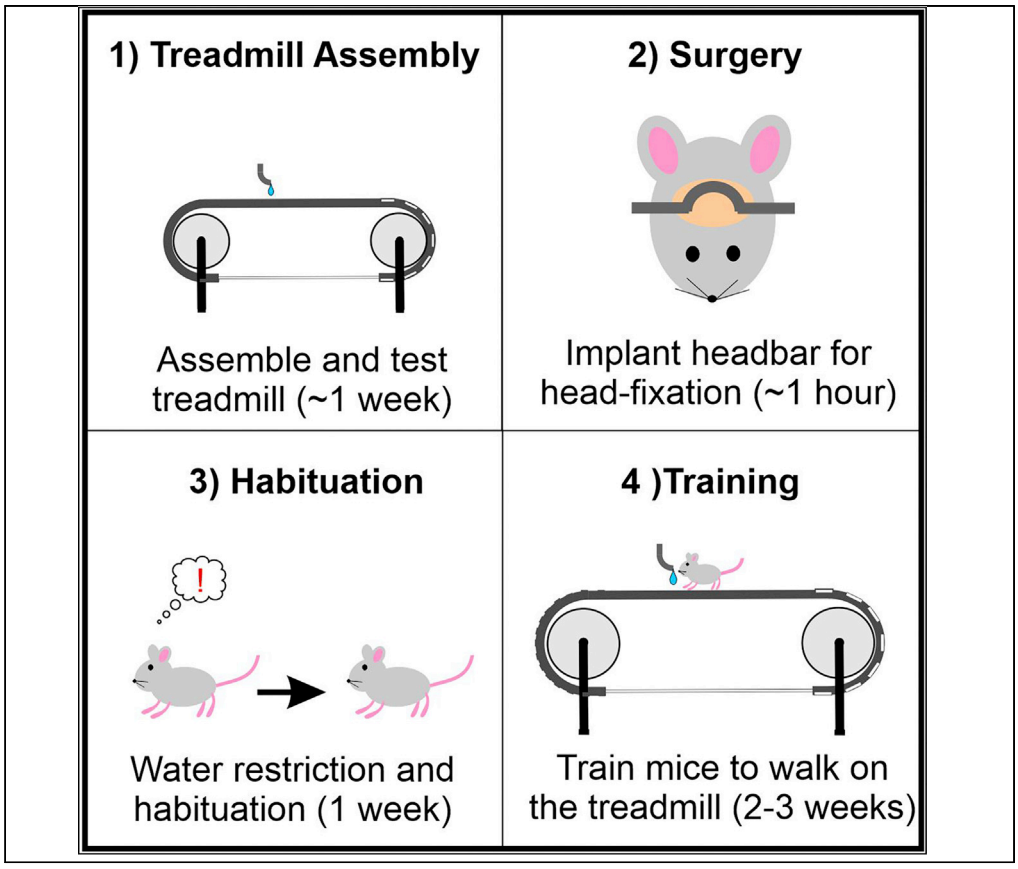


Several mouse *in vivo* neuronal recording techniques require head fixation. Head-fixed treadmill walking can be used to design tasks that enable the study of neural activity in the context of behavior. Here, we provide a detailed protocol for constructing a treadmill with tactile spatial cues, training mice on a rewarded behavioral task, and analyzing behavioral data. We discuss common problems and solutions we have developed to optimize training. Finally, we demonstrate how to test spatial memory performance using this task.

Jake T. Jordan, Kelsey D. McDermott, M. Agustina Frechou, Matthew Shtrahman, J. Tiago Gonçalves

jake.jordan@einsteinmed.org (J.T.J.)
tiago.goncalves@einsteinmed.org (J.T.G.)

## Highlights

Protocol for a rewarded head-fixed treadmill task for mice

Assembly of treadmill and overview of a surgical procedure

Training of mice on head-fixed, rewarded spatial memory tasks

Analysis of reward search by spatial analysis of lick behavior along a treadmill

Jordan et al., STAR Protocols *2*, 100770
September 17, 2021 
https://doi.org/10.1016/j.xpro.2021.100770

STAR Protocols

CellPress
OPEN ACCESS

Protocol

# Treadmill-based task for assessing spatial memory in head-fixed mice

Jake T. Jordan,[1,3,*] Kelsey D. McDermott,[1] M. Agustina Frechou,[1] Matthew Shtrahman,[2] and J. Tiago Gonçalves[1,4,*]

[1]Dominick P. Purpura Department of Neuroscience and Gottesman Institute for Stem Cell Biology and Regenerative Medicine, Albert Einstein College of Medicine, Bronx, NY 10461, USA

[2]Department of Neurosciences, University of California San Diego, La Jolla, CA 92093, USA

[3]Technical contact

[4]Lead contact

*Correspondence: jake.jordan@einsteinmed.org (J.T.J.), tiago.goncalves@einsteinmed.org (J.T.G.)
https://doi.org/10.1016/j.xpro.2021.100770

## SUMMARY

**Several mouse *in vivo* neuronal recording techniques require head fixation. Head-fixed treadmill walking can be used to design tasks that enable the study of neural activity in the context of behavior. Here, we provide a detailed protocol for constructing a treadmill with tactile spatial cues, training mice on a rewarded behavioral task, and analyzing behavioral data. We discuss common problems and solutions we have developed to optimize training. Finally, we demonstrate how to test spatial memory performance using this task.**

## BEFORE YOU BEGIN

Prior to beginning, obtain institutional animal use approval and follow legal and ethical guidelines for animal care and use throughout.

The protocol was developed using male and female C57Bl6J mice bred in house and aged 12–13 weeks at the time of surgery were used for these experiments. It can also be used with other strains of mice and has been successfully tested using 18-month-old mice. Animals were housed on a 14/10 h light-dark cycle with experiments performed during the light phase. Laboratory chow was available *ad libitum*. Except during citric acid water treatment, tap water was available *ad libitum*. All procedures were approved by the Institutional Animal Care and Use Committee (protocol #: 00001197).

This protocol describes steps for assembling a head-fixed, animal-driven treadmill for mouse behavior (Royer et al., 2012; Danielson et al., 2016) as well as instructions for training the mice and analyzing their behavior. Although similar set-ups that use virtual reality (VR) environments exist, this task in particular is non-visual, relatively easy to learn and can thus be used to train mice with visual or mild cognitive impairments, such as aged or certain transgenic mice. The treadmill consists of a fabric belt wrapped around two foam wheels on ball bearings. Four radio frequency identification (RFID) tags are attached at regularly spaced intervals along the belt and an optical rotary encoder measures the spin of one of the treadmill wheels. The position of the mouse is determined by converting the output voltage of the rotary encoder to the mouse's velocity between RFID reads. The treadmill belt can occasionally slip on the wheels, introducing an error in the estimation of the position but using several RFID tags at different points along the belt will ensure that this error does not accumulate. Placing RFID tags at transition points between tactile zones also allows for comparisons of behavior and/or neural activity across zones as well as at transition points. An additional

RFID tag is placed at a location along the belt where the mouse will receive a reward of sweetened water. These water rewards are dispensed from a lick port equipped with a sensor to measure licking behavior. Spatial learning and memory can be assessed by analyzing the spatial distribution of licking behavior.

### 3D-printing and machining of custom parts

Timing: 1–2 days

Detailed information on the design and assembly of each component is available on the lab GitHub Page: https://github.com/GoncalvesLab/HeadFixedTreadmill.

1. 3D print the platform used to hold the mouse up during treadmill walking.
2. Custom-made titanium headbars are implanted on the mouse's skull to hold it in place during recordings. They can be laser-cut from ~1–1.5 mm thickness titanium sheet stock and re-used indefinitely.
3. The head-restraint assembly is made from metal components for maximum stability and durability. Custom metal components (head plate, brackets, etc.) should be cut by an experienced machinist.
4. The treadmill wheels are made from an exercise roller cut into 9 cm-wide cylinders.
   a. As precisely as possible, drill a hole through the center (~4.5 cm from the edge) and insert one of the axle rods through the center. The wheel (foam roller segment) should be in the middle of the axle rod.
   b. To prevent slippage of the foam wheel against the axle, apply cyanoacrylate glue to the sides of the wheel where the rod is protruding out.

### Treadmill assembly

Timing: 1 week

The treadmill apparatus consists of several electrical components used to collect data about mouse movement on the treadmill and licking behavior as well as to trigger and administer water rewards (Figures 1 and 2).

5. Setup the data acquisition computer. Experiments are controlled by a PC equipped with a data acquisition card (National Instruments PCIe-6323).
   a. Be sure that the computer used has MATLAB (version 2020a or newer) installed with the scripts RunTreadmill.m and OpenTreadmillFile.m stored in a directory listed in the path variable.

   *Note:* We are acquiring treadmill data and controlling reward administration using NI hardware and MATLAB software, however other data acquisition systems can also be used, including open-source alternatives based on eg. Raspberry Pi.

6. Insert axle rods into the ball bearings (Figure 3).
   a. One axle will require the wheel of the optical rotary encoder to be attached before it is inserted into the ball bearings.
      i. To do this, gently remove the wheel and encoder from the plastic casing so as not to damage the wheel or encoder (the plastic casing can be damaged and discarded).
      ii. The encoder will then be attached to custom ball bearings plate with matching screw holes.
7. Assemble the treadmill wheels.
   a. For our purposes, we have extruded 1-inch aluminum rails attached vertically to an air table (Figure 2). These rails form the frame that is used to suspend the wheels, axles and ball bearing plates as well as the platform and RFID reader.

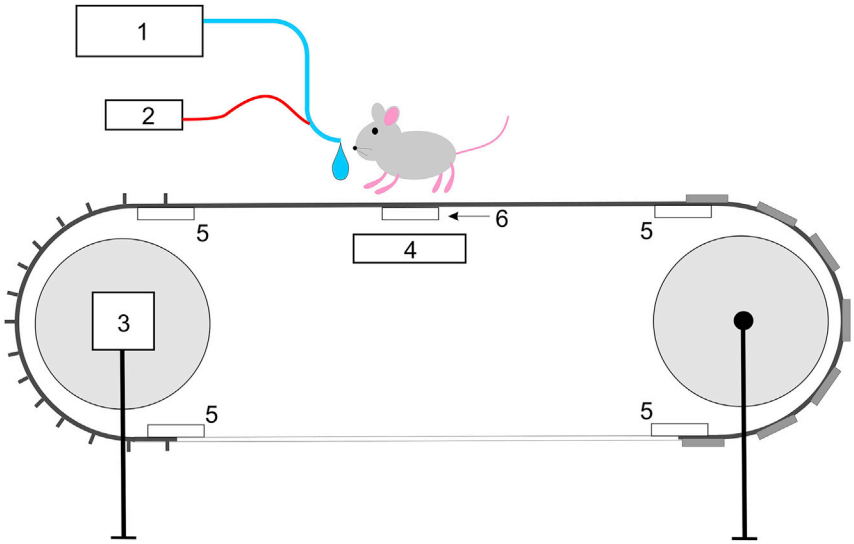


**Figure 1. Electronic components of head-fixed treadmill apparatus**

b. The two rails used to suspend each wheel should be spaced approximately as far apart as the two ball bearings plates on either side of the axles assembled in step 6.
c. The two suspended wheels should be spaced approximately 50 cm apart from each other with the platform in the middle.

8. Assemble the platform with RFID scanner attached.
   a. We affix the RFID scanner to the bottom of the platform using heavy duty electrical tape directly under where the mouse will be walking.
      i. The wires to the RFID scanner should be soldered and individually isolated with heat-shrink tubing, as the vibrations caused by mouse walking can lead to short-circuiting and malfunction.
   b. The height of the platform should be slightly (~0.5 cm) lower than the top of the two wheels.
9. Attach the head plate to the head plate brackets and attach the brackets to a pair of rails so that the head plate is approximately 2.5 cm above the platform.

⚠ CRITICAL: (Step 9): Mice may have difficulty running on a surface that is too smooth or be distracted by a surface that is very soft. Pay attention to how mice react when you begin their training, and reassess the quality of the belt and its texture if they have trouble pulling the belt or tend to remain in one area instead of walking (after some training).

10. For the treadmill belt, cut the velvet fabric into 7.5 cm-wide strips. The total length of our belt is 180 cm which can be made from four 45 cm-long strips of velvet appended together. This can be done quickly by stapling the strips together, but they may also be sewn together. Do not close the belt into a ring until it wrapped around both wheels (see step c below).
    a. The mouse needs to be able to grip the belt early in training to begin walking. This can be done by using variable tactile cues (e.g., for a spatial memory task) or uniform tactile cues (e.g., if studying non-spatial memory). Sandpaper circles of different grit or stripes made with a hot glue gun can serve this function.
    b. Attach the RFID tags to the underside of the belt with a piece of duct tape.
       i. We use 5 tags: 4 for tactile zone transitions and 1 for a reward site.

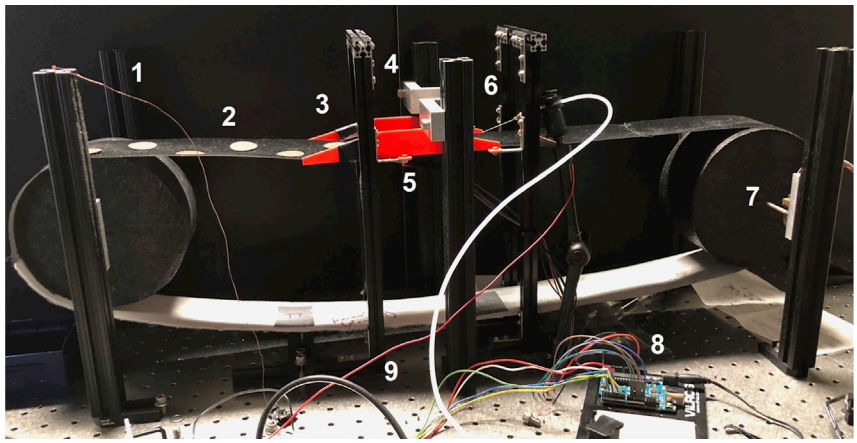


**Figure 2. Assembled treadmill with a 180-cm-long belt**

1 – Grounding copper wire; 2 – treadmill belt; 3 – mouse platform; 4 – head plate; 5 – RFID scanner affixed to the bottom of the platform; 6 – reward port; 7 – optical rotary encoder; 8 – RFID Arduino; 9 – red cable is input from reward port to the lick counter (not pictured). Positioning of all Arduinos, lick counter, pump and NI box is not critical and can be determined by the experimenter's preference.

c. Wrap the belt around the treadmill wheels and platform and append the ends of the treadmill belt together (stapled or sewn).

11. Solder a wire to a metal gavage needle. This wire will be plugged into the lick counter. Add the reward port by assembling the gavage needle, tubing and 10 mL syringe. Place the syringe in the clamp on the microinfusion pump and follow manufacturer instructions to program 10 µL pulses. Use a flexible arm clamp to place the reward port near where the mouse will be walking such that it can be near the mouse's snout during trial but moved away for ease of access when attaching or removing mice.
12. The rotary encoder and RFID reader are operated with Arduino microcontrollers. Plug wires and BNC cables into the appropriate components following the instructions on our Github (https://github.com/GoncalvesLab/HeadFixedTreadmill).
13. Test the treadmill by running a short (~1 min) test session using the RunTreadmill.m program in MATLAB. Confirm that water rewards are being administered and run the OpenTreadmillFile.m script and follow the instructions at the top of that code to confirm that data from all treadmill components are being correctly acquired.
    a. Do this at the beginning of every training day or immediately after changing treadmill belts or reward locations.
14. For synchronizing the movement, lick and reward data with neuronal recordings (imaging or electrophysiology), generate a transistor-transistor logic (TTL) signal from the recording apparatus and record it by running the wire to an input of the National Instruments data acquisition hardware at the beginning and end of each recording session, or for each frame. For example, many microscopes can output a "FrameOut" signal for each recorded video frame. This signal can be used to synchronize the behavioral data with neural recordings.

*Note:* The treadmill belt does not necessarily need to be made of the same material listed in the key resources table. Whichever material is used will need to be light enough to be easily pulled by the mouse, but must also not slip on the foam wheels. Belt slippage (i.e. when the belt and wheel are not turning at the same rate) will cause an error in estimating the position of the mouse using the output of the optical rotary encoder.

## Preparation for surgery

Timing: <1 hour

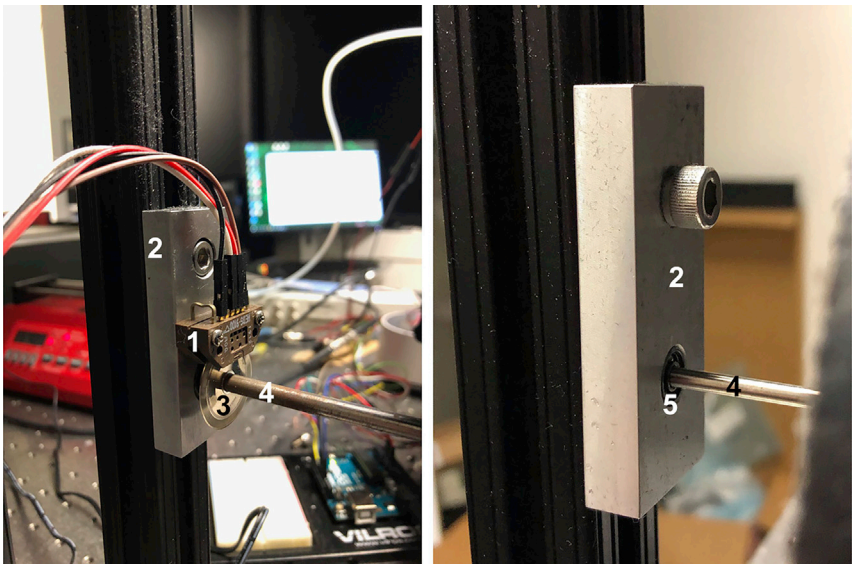


**Figure 3. Assembly of wheel axle with ball bearings plates**

Left: The optical rotary encoder (1) is attached to one of the custom plates (2). The encoder disk (3) is attached to an axle (4) which is inserted into the ball bearings. Right: An axle inserted into the ball bearings (5) on the three other custom plates.

15. If using the Janelia lick counter, mice will need to be implanted with a grounding pin soldered to a small tungsten wire.
    a. To assemble, clamp the gold pin in a helping hand alligator clamp. Insert a tungsten wire into the shallow hole of the flat end of the pin. Solder and then snip the wire approximately 1 mm from the pin. Likewise, solder a female connector to a long piece of wire (long enough to connect the mouse's implanted pin to the lick counter) to ground the mouse. Licks will be sensed when a grounded mouse contacts the lick port, closing the circuit.
16. Prepare the surgery area using sterile techniques. For this surgery, in addition to the headbar and grounding pin, you will need:
    a. Scalpel
    b. Forceps
    c. Dental curing light for Optibond and Flow-It Accelerated Light Cure (ALC) composite adhesives.

*Note:* Although the Comparator Dual Port Lick Detector requires a grounding pin, not all lick counting systems require this, a possible alternative is to use an optical lick counter. We chose to use the Comparator Dual Port Lick detector because we had previous experience with this system.

## KEY RESOURCES TABLE

| REAGENT or RESOURCE | SOURCE | IDENTIFIER |
|---|---|---|
| Chemicals, peptides, and recombinant proteins | | |
| Artificial sweetener | Splenda | n/a |
| Citric acid | Milliard | MIL-CTRCACD-5-A |
| Isoflurane, USP | Covetrus | 11695-6777-2 |
| Carpofen | Zoetis | 1041283 |
| Optibond | Kerr | 33381 |

(*Continued on next page*)

*Continued*

| REAGENT or RESOURCE | SOURCE | IDENTIFIER |
|---|---|---|
| Flow-It ALC Flowable Dental Composite | Pentron | N11H |
| Dental cement powder | Lang Dental | 1330 |
| Dental cement liquid | Lang Dental | 1306 |
| Deposited data | | |
| All code and sample data are available on our GitHub page | Gonçalves Lab GitHub | n/a |
| Experimental models: Organisms/strains | | |
| C57BL6J mice | Jackson Laboratory | 000664 |
| Software and algorithms | | |
| MATLAB | MathWorks | 2020a |
| Arduino IDE | Arduino | 1.8.12 |
| RFID library for Arduino | Arduino | MRFC-522 Library |
| Other | | |
| Computer | Dell | Optiplex 7080 |
| Arduino Uno | Arduino | A000066 |
| Arduino Due | Arduino | A000062 |
| Data acquisition card | National Instruments | PCIe-6323 |
| Breakout box | National Instruments | BNC 2090A |
| Data cable | National Instruments | SHC68-68-EPM |
| Microinfusion pump | Braintree Scientific | Braintree Scientific BS-8000 |
| Lick port | Janelia Research Campus | Comparator Dual Port Lick Detector |
| Optical rotary encoder | Digi-Key | HEDS-5500#A05 |
| RFID scanner | SunFounder | RC522 |
| RFID tags (5) | Amazon | ISO14443A |
| Wires | Amazon | 120 piece kit |
| BNC cables (3) | Amazon | MC2791 |
| Heat-shrink tubing | Amazon | 560 piece set |
| Flexible arm (to hold and move lick port): Articulating Magic Arm (11 inch long) | Amazon | Mmo-PN-329618834 |
| Gold pin (1 per mouse) | a-msystems.com | 520200 |
| Gold pin connector | a-msystems.com | 520100 |
| Copper wire | | |
| Velvet textured treadmill material | McMaster-Carr | 88015K1 |
| Custom mouse platform | See GitHub | n/a |
| Custom headbar (1 per mouse; reusable) | See GitHub(laser-cut by IMH products IMH.com) | n/a |
| Custom head plate | See GitHub | n/a |
| Custom head plate brackets (2; 1 left, 1 right) | See GitHub | n/a |
| Custom ball bearing plates (3) | See GitHub | n/a |
| Custom ball bearing plates with encoder screw holes (1) | See GitHub | n/a |
| Exercise roller (cut into 3.5 inch cylinders) | ProsourceFit | High density cylindrical roller 18" (L) x6" (diam.) |
| Axles (2) | McMaster-Carr | 60355K501 |
| Ball bearings (4) | McMaster-Carr | 1257K86 |
| 10 mL Syringe (20G x 1.5") (at least 3) | Becton Dickinson | 309604 |
| Gavage needle (for lick port) | Pet Surgical | 2018-08 |
| Tubing | CM Scientific | R-3603 |
| T-slotted aluminum rails (6; 30.5 cm) | McMaster-Carr | 47065T503 |
| T-slotted framing fasteners (6) | McMaster-Carr | 47065T142 |
| Headbar screws (2) | McMaster-Carr | 92196A052 |
| Forceps | Fisher Scientific | 08-953C |
| Scalpel (No. 3 handle) | Fisher Scientific | 13-812-234 |
| Sterile scalpel blades | Fisher Scientific | 22-079-684 |

## STEP-BY-STEP METHOD DETAILS

### Surgery

Timing: <1 h for headbar implant only, 1–2 days if including a viral injection and cranial window implant

Here, we describe how to attach the headbar to the mouse skull as well as implant a grounding pin for lick counting. For details on intracranial viral injections and/or cranial window implants, which should be done prior or simultaneously to headbar implantation, see Mizrahi et al. (2004) and Dombeck et al. (2007).

1. Anesthetize the mouse in accordance with IACUC-approved protocols.
2. Once anesthetized and unresponsive to touch, maintain anesthesia with 1%–2% isoflurane and 0.5 L/min $O_2$ with the mouse on a heating pad.
3. Clean scalp with betadine and 70% ethanol. Use a scalpel to make a longitudinal incision about 5–6 mm long, exposing the skull.
4. Using scalpel, thoroughly etch the surface of the skull to enhance the bonding of the Optibond and dental cement to the surface of the skull. Then, apply a layer of Optibond dental adhesive over the exposed surface of the skull. If necessary, pull the skin back with forceps to avoid getting Optibond on the skin. Cure the Optibond using blue light.
   a. If injecting virus and/or implanting electrodes or a cranial window, follow that procedure now and then return to this protocol.
5. If necessary, sterilize grounding pin and implant on the back of the skull, over the cerebellum.
   a. Prepare a smooth portion of the back of the skull by trimming away neck muscle and then drill a small (~1 mm) craniotomy.

   ⚠ CRITICAL: The muscle has a tendency to bleed, so carefully scrape away the connective tissue where the muscle connects to the skull with a scalpel to minimize bleeding.

   b. Using forceps with a steady hand, insert the tungsten wire end of the gold pin into the craniotomy and hold as still as possible. With the other hand, apply Flow-It ALC around the base of the pin and then cure with blue light.

   ⚠ CRITICAL: Make sure to implant the pin at an angle (Figure 4) that will not interfere with the treadmill setup when you attach it to the mouse or with the objective if you are imaging.

The blue light used to cure the composite dental adhesives may irritate the mouse's skin (e.g., ears) when exposed. Aim the light away from it, or cover up any exposed skin when curing.

6. Implant the headbar using dental cement.
   a. Apply a thin layer of dental cement over the entire surface of the skull. This layer should have a low viscosity (determined by relative amounts of dental cement powder and dental cement liquid mixed together) to allow it to spread easily.
   b. After 2–3 min, apply a small amount of thick dental cement to the back of the skull. Immediately place the headbar in the middle of this thick spot of cement so that the wings of the headbar are perpendicular to the long axis of the mouse's body. Be sure to balance the headbar before the cement dries fully so that the mouse will not be at an angle while head-fixed.
   c. Apply one last coat of dental cement over the back of the headbar and spread around to the rest of the skull with care not to cover the wings of the headbar.
7. Allow the dental cement 5–10 min to dry.

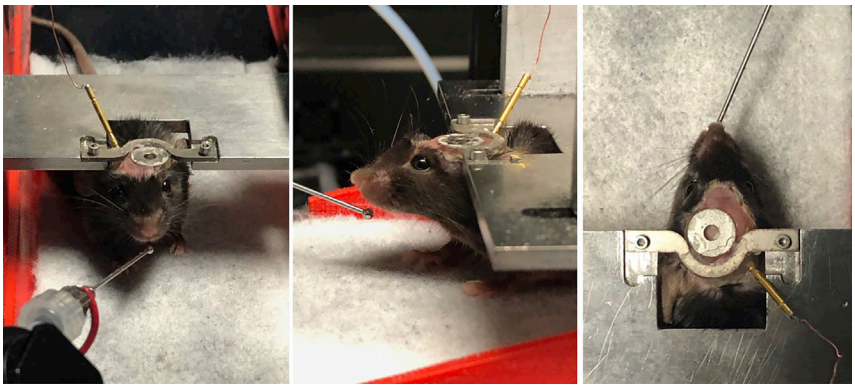

**Figure 4. Three views of a mouse with a surgically implanted cranial window and headbar, head-fixed to a custom head plate**

Note the lick port positioned by the spout and a grounding wire connected to an implanted pin.

8. Inject the mouse subcutaneously with 5 mg/kg of carpofen dissolved in saline (at a concentration of 1 mg/mL)and remove from anesthesia.
9. Mice should begin to recover from anesthesia within minutes and will be fully responsive in approximately one hour.

### Water restriction and habituation

Timing: 1 week

In order to ensure mice are sufficiently motivated to walk on the treadmill for water rewards, water consumption must be restricted in some way that follows IACUC-approved water deprivation protocols. We replace homecage water with 2% citric acid water, which reduces water intake and is a safer alternative to removing homecage access to water completely (Reinagel, 2018; Urai et al., 2021).

10. Replace homecage water with 2% citric acid water.
    a. Weigh mice prior to citric acid water treatment (baseline) and then every day for 5 days and then once per week after treatment has begun.

⚠ CRITICAL: Ensure that animal weight does not drop below 85% of the baseline weight. If this does happen, immediately allow access to 1 mL of clean water. If a mouse continues to be below this threshold, remove from experiments.

11. During the first week of citric acid water treatment, habituate mice to handling by the experimenter in the room in which experiments will be conducted. Do this for at least 3 min per day for 3 days (does not need to be consecutive).
12. Prior to starting any behavior session, ensure that there is sufficient water in the syringe and that all treadmill data is being acquired.
    a. To test whether all data are being acquired, run a test session
13. One week after the beginning of citric acid water administration, begin training.

### Treadmill training

Timing: ~2–3 weeks

Mice will vary in the amount of training sessions needed to walk well on the treadmill. Begin with 20-min training sessions, and reduce the training time as mice improve walking by 5 min per session until training session are 10 min long. Define the number of laps you will need for your experimental purposes, and train mice until the entire cohort has reached that level or has been excluded.

14. Run the program RunTreadmill.m and enter all the relevant information in the GUI.
    a. Do not start the data acquisition until the animal is head-fixed.
15. Affix the headbar to the head plate (Figure 4).
    a. If the mouse turns so that its rear legs are to the side or nearly in front of the head, gently tug the treadmill belt until the mouse is in a walking position. Some mice may continue to do this during the first couple of days of training, but it will diminish over time.

⚠ CRITICAL: When placing mice on and off the treadmill, take care not to stress them as this will impair performance. Quickly transfer mice from the cage to the treadmill platform and avoid dangling them by the tail. Do not overly force the mouse into head-fixation. Place the mouse behind the head-fixation stage. Many mice naturally duck their heads under the head-fixation stage to investigate. When they do this, simply pull the belt forward lightly so that the headbar is now near the fixation point and hold the headbar in place while screws are inserted. This minimizes the degree to which you have to force the mouse in place. Over training they will become more used to this process and tend to voluntarily walk to the head-fixation position.

16. On day 1, train the animal to lick the reward spout by administering a free 10 μL reward (10% Splenda in water) and touching it to their snout.
    a. Only do this once per day at the beginning of the training session for the first 2–3 days.
17. Run the session from the MATLAB command line.
18. Start a timer for the duration of the session. Turn off the room lights and come back when the timer has gone off.
19. Unscrew the headbar and gently place the mouse back in the homecage.
20. Check the performance on the task (e.g., rewards earned, licking behavior, etc.) by running the OpenTreadmillFile.m program.

*Note:* Reward volumes vary in the literature (4–20 μL). Although we use a 10 μL reward, others may decide to vary this amount based on their specific experimental needs.

*Note:* For sanitary purposes, clean the syringe containing sweetened water regularly (once per week) by flushing with 70% ethanol and tap water to avoid mold growth. Regularly clean the area of mouse feces and replace treadmill belts when they become soiled. This will vary based on frequency and volume of use, but is usually around once every 1–2 months.

## EXPECTED OUTCOMES

The recorded data structure contains the output of the rotary encoder (Treadmill belt movement), licking behavior and reward triggers (Figure 5) as well as scans of each RFID tag.

Mice should learn the task in around 2–3 weeks, with the majority of licking occurring at or near the reward zone. Completed laps per session and overall lick rate will generally be low in the beginning of training and will gradually increase. Trained mice have ranged from 2–26 laps per 10-min session. Some experiments may require mice to run a certain number of laps within a certain amount of time and therefore some sessions may fail to reach this threshold, however, this number is likely to vary across experiments and, if applicable, neural recording techniques (see Figure 6 for performance of an example cohort from the beginning of training).

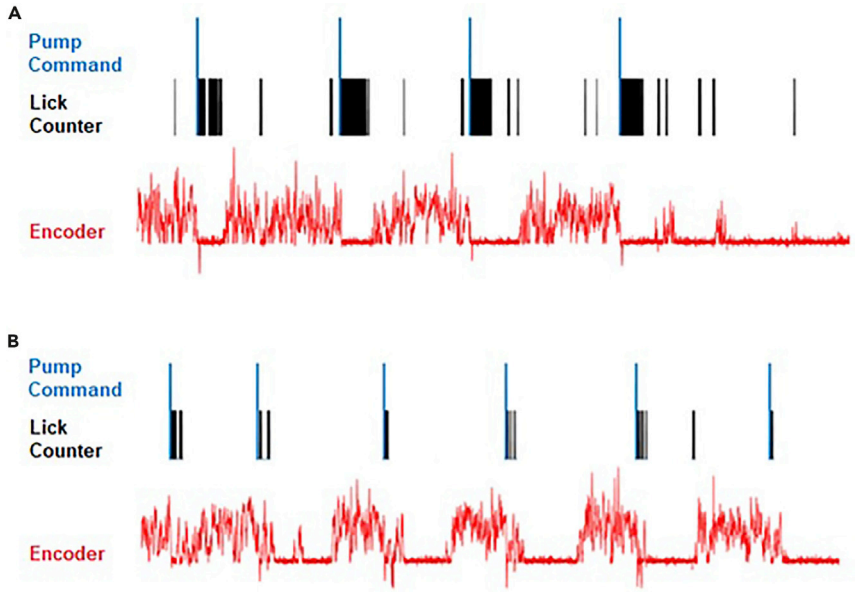


**Figure 5. Example treadmill output data**

Data from example sessions of a well-trained mouse receiving sucrose water at the reward site (A) and the same mouse during a probe trial in which reward was omitted (B). Blue traces represent the voltage input commands that would normally trigger reward (pump is disconnected during probe trials, black ticks represent licks, and red traces represent the output of the rotary encoder.

## QUANTIFICATION AND STATISTICAL ANALYSIS

Analysis of spatial licking behavior can be done using our custom software. Typically, learning can be demonstrated by a gradual increase in the fraction of the total licks occurring in the rewarded quadrant of the belt. "Lick maps" can also be computed to help visualize the spatial specificity of lick behavior by dividing the belt into bins of a certain length (e.g., 3 cm) and computing the fraction of all licks occurring in each bin (Figure 7).

Spatial memory can be tested by conducting a probe session in which reward is omitted. This removes the possibility that the presence of water in the lick port or any sounds from the reward pump is indicating to the mouse where a reward may be administered. Thus, mouse must rely on memory of the rewarded location to direct licking behavior. To conduct a probe trial, switch off the reward pump and then run a session as you normally would. Overall lick rates will decrease sharply during these sessions as the mice do not get rewards. However, licking behavior will still be concentrated near the reward zone. An alternative to probe trials is to make the reward administration contingent on the detection of licking within the reward location.

## LIMITATIONS

Our head-fixed system prohibits studying the contribution of head movement to neuronal activity, although a new device has recently been developed to overcome this limitation (Bakhurin et al., 2020). This is an important limitation to consider for hippocampal studies that may want to analyze head-direction cells and other similar cell types.

Probe sessions, in which the pump is off and no reward is given (Figure 7), can be used to measure lick preference for reward locations. However, these sessions can only be performed 1–2 times per cohort before animals give up on the task entirely.

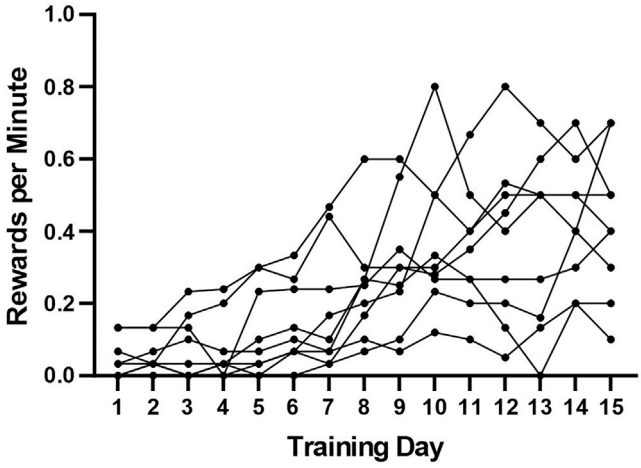


**Figure 6. Example of 9 mice trained on the treadmill task for 5 days per week for 3 weeks**

## TROUBLESHOOTING

### Problem 1

Mouse movement can be enough to cause issues such as false lick detection from the lick counter or disconnection of the RFID scanner. If the scanner is temporarily disconnected, it will malfunction and shut off mid-session (steps 18 and 10).

### Potential solution

To prevent false lick detection, we reduced the sensitivity of the lick counter by soldering a 47 nF capacitor at pins IN1 or IN2 and GND (on the bottom of the board). To prevent scanner disconnection, we soldered all wires to the scanner and then carefully insulated each wire with heat shrink tubing at the soldering site.

### Problem 2

Early on in training, some mice will grab the lick port with their front paws as they lick. This will yield a very long pulse that (using our analysis software) will be counted as a single lick, despite many licks occurring (steps 18 and 20).

### Potential solution

This behavior usually goes away with training. If it becomes a recurrent issue, the experimenter may want to put a barrier around the lick port to prevent grabbing. It is always good practice to check the lick data after each session to screen for these types of issues and potentially exclude animals.

### Problem 3

Mice that are small in size due to age or genetic line may have more difficulty pulling the treadmill belt. This could lead to them learning the task more slowly, or result in fewer laps (step 18).

### Potential solution

If possible, use adult mice that are $\geq$20 grams so that they can pull the belt easily. If smaller mice are necessary, we recommend trying out different textures to find ones that are easiest for the mice to grip (sandpaper and felt have worked well for us). Additionally, the level between head fixation and belt can be adjusted so that smaller mice have better posture and do not have to stretch.

### Problem 4

Mice do not perform many laps, even with weeks of training (steps 16–20).

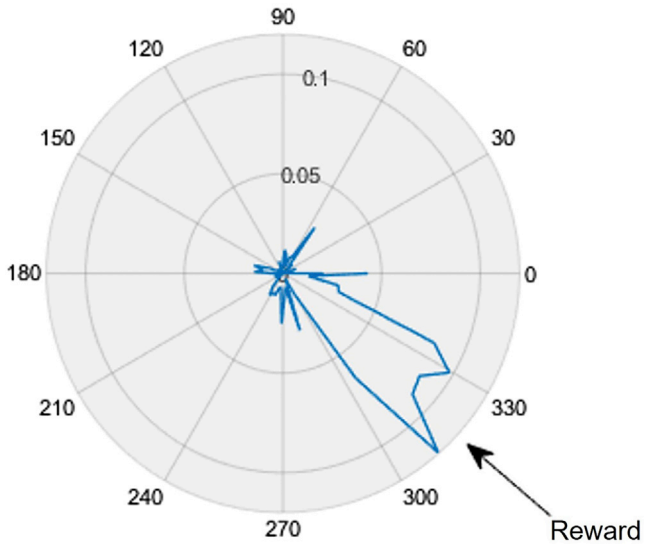


**Figure 7. A normalized lick rate map of a session run on a 180 cm treadmill**

The blue trace indicates the fraction of licks occurring in 3 cm wide bins. A clear preference is shown to lick in vicinity of the reward location.

### Potential solution

In addition to habituation by the experimenter prior to training, it is recommended that the experimenters avoid stressing mice as much as possible. For instance, chronic drug administration with repeated restraint and injections should be avoided and alternative strategies for drug administration should be followed. Mice should be handled as gently as possible to avoid stress.

If headbars are implanted at an angle so that the mouse's head is fixed at an unnatural angle during walking, it will likely not ever perform the task. During surgery, ensure that the headbar is attached at an angle consistent with the mouse's natural head angle during walking.

### Problem 5

Lap sizes computed by the custom analysis software are inconsistent (step 20).

### Potential solution

This is usually caused by the mechanics of the treadmill, e.g., slippage of the belt on the wheel with the optical decoder. If the belt and decoder are not rotating together, then distance computed for each lap (demarked by RFID scans) will be inconsistent and can affect spatial analysis of behavior or neural activity. Make sure that the belt is not wrapped too loose around both wheels. There should be some slack of the belt on the underside of the treadmill, but it should not be dragging on the table. Another possible source is resistance in wheel axles. Check the axles by spinning the wheels and ensure that the rotate smoothly. If not, realign the axle and ball bearings until there is no resistance.

### Problem 6

Mice walk backwards or move the belt back and forth rapidly to trigger water rewards (step 18).

### Potential solution

Older systems have used single reward tags which when scanned, trigger a reward. Mice can "cheat" this system by moving the single tag over the scanner rapidly, triggering many rewards without having to complete laps. Our system is designed to prevent this from occurring by requiring a preceding RFID tag to be scanned prior to the reward RFID tag being scanned to trigger reward. I.e., the mouse has to run forward through the reward zone in order to trigger the reward.

### Problem 7

RunTreadmill.m is freezing and/or rewards are being delivered many seconds after the reward RFID tag is scanned (step 17).

### Potential solution

This has occurred when using version 2019b of MATLAB. Switching to version 2020a resolved this issue.

## RESOURCE AVAILABILITY

### Lead contact

Further information and requests for resources and reagents should be directed to and will be fulfilled by the lead contact, Tiago Gonçalves (tiago.goncalves@einsteinmed.org).

### Materials availability

No new reagents were used for this study.

### Data and code availability

Custom code is available on the Gonçalves lab GitHub Page: https://github.com/GoncalvesLab/HeadFixedTreadmill.

## ACKNOWLEDGMENTS

J.T.J. was funded by an NIH T32 training grant (5 T32 HD098067-03) and would like to thank the Intellectual and Developmental Disabilities Research Center for its support (1 P50 HD105352-01; support for the Rose F. Kennedy IDDRC). K.D.M. and M.A.F. were funded by The Einstein Training Program in Stem Cell Research from the Empire State Stem Cell Fund through New York State Department of Health Contract C34874GG. M.S. was funded by a NINDS K08 grant (NS093130) and a NIBIB R21 Trailblazer Award (EB029139-01). Whitehall Foundation Research Grant (2019-05-71) was provided to J.T.G. We would like to thank Ehsan Sabri, Eliezyer Fermino De Oliveira, Luke Sjulson, and Renata Batista-Brito for technical advice and assistance.

## AUTHOR CONTRIBUTIONS

Conceptualization, J.T.J. and J.T.G.; methodology, J.T.J., K.D.M., M.A.F., M.S., and J.T.G.; investigation and visualization, J.T.J.; writing – original draft, J.T.J. and K.D.M.; writing – review and editing, J.T.J., K.D.M., M.A.F., and J.T.G.; supervision, J.T.G.

## DECLARATION OF INTERESTS

The authors declare no competing interests.

## REFERENCES

Bakhurin, K.I., Hughes, R.N., Barter, J.W., Zhang, J., and Yin, H.H. (2020). Protocol for recording from ventral tegmental area dopamine neurons in mice while measuring force during head-fixation. STAR Protoc. *1*, 100091.

Danielson, N.B., Zaremba, J.D., Kaifosh, P., Bowler, J., Ladow, M., and Losonczy, A. (2016). Sublayer-specific coding dynamics during spatial navigation and learning in hippocampal area CA1. Neuron *91*, 652–665.

Dombeck, D.A., Khabbaz, A.N., Collman, F., Adelman, T.L., and Tank, D.W. (2007). Imaging large-scale neural activity with cellular resolution in awake, mobile mice. Nat. Neurosci. *56*, 43–57.

Mizrahi, A., Crowley, J.C., Shtoyerman, E., and Katz, L.C. (2004). High-resolution in vivo imaging of hippocampal dendrites and spines. J. Neurosci. *24*, 3147–3151.

Reinagel, P. (2018). Training rats using water rewards without water restriction. Front. Behav. Neurosci. *12*, 84.

Royer, S., Zemelman, B.V., Losonczy, A., Kim, J., Chance, F., Magee, J.C., and Buzsáki, G. (2012). Control of timing, rate and bursts of hippocampal place cells by dendritic and somatic inhibition. Nat. Neurosci. *15*, 769–775.

Urai, A.E., Aguillon-Rodriguez, V., Laranjeira, I.C., Cazettes, F., International Brain Laboratory, Mainen, Z.F., and Churchland, A.K. (2021). Citric acid water as an alternative to water restriction for high-yield mouse behavior. eNeuro *8*, ENEURO.0230-20.2020.